`

The Development of Nanomedicine Formulations for the Treatment of Sudden Preterm Birth

Thesis submitted in accordance with the requirements of the University of Liverpool for the degree of Doctor in Philosophy by:

Jessica May Taylor MCHEM

June 2021

`

Acknowledgements

Firstly, I would like to say a huge, sincere thank you to Dr. Tom McDonald for giving me the opportunity to carry out the research presented in this thesis. Tom, you have given me the capacity to prove myself as a scientist and I will be forever grateful. I would also like to thank Prof Steve Rannard. Thank you for always believing in me and giving me your full support. Your words of encouragement and wisdom have meant a great deal to me. Thank you to you both for all of the knowledge, ideas and direction you have given me over the past four years.

Secondly, I would like to thank all of my colleagues who are part of the Functional Materials Team. Thank you to everyone for always encouraging me both personally and scientifically. I would like to say a personal thank you to Steph for the limitless coffees and laughs; and not to forget Helen and Jay for their quick thinking tactics and first aid skills- who knew a litre of vodka in an open wound would lead to a lifelong scar down my leg?! That's something I'll never quite forget.

I would like to say a special thank you to Andy Dwyer. Andy- "Dr Inspo", you have made a lasting impression on me, larger than you could ever imagine. Your ability as a scientist, your advice, your passion and your ambition. You really have inspired me from day one. I will be eternally grateful for the influence you have had on my career so far.

Thirdly, I would like to say thank you to everyone that helped me get to this point. The academic staff, research staff, domestic staff and student support staff in the Department of Chemistry. Peter, Gita, Debs, John and Sam- thank you for everything! I would also like to say a special thank you to Adele Fitchett, my GCSE and A Level chemistry teacher. Without her passion for chemistry and an inspirational talent as a teacher, I would never have made it here today. Thank you all for everything.

The next thank you is for the girls. Jess, Beck, Vic, Soph and Hol. Where do I start?! You have all been on the very same roller-coaster with me for the past 8 years. You have all seen the extreme highs and lows throughout the course of this PhD (& my life) and I will always

remember the support you have given me. You are all indispensable to me and I cannot wait to make more memories in our sisterhood! To the girls who have been with me since our high school days; thanks for you for everything. I am truly grateful for you all and your support.

To Tom- thank you for being with me every step of the way for the past eight years. You are the best and I can't wait to build a life in our new home together (with no PhD stress!). Thank you also to Tom's mum and dad, Ann & Colin, for all of your support.

Finally, a special thank you to my family. To my mum and dad, I would've never have gotten here without you. You both know how passionate I am about the cause for this PhD and desire to make a difference to families struggling with pregnancy related implications; and for that I will always be grateful for all of your support. Dad, look where those late night chemistry lessons have got me now… I suppose you deserve some credit! Thank you both for everything, I hope this achievement has made you both proud.

To my Nan, thank you for being my number one fan. I love you the world and I wouldn't be who I am today without you. To Auntie Joan, Auntie Lisa, Uncle Billy and Uncle Peter. Thank you! It humbles me to know how proud you all are of me. I really mean it when I say, I appreciate each and every one of you!

Finally, a special thank you to my gramps, our big john and Sue. Three people who I have lost in the past year. Although they are not with us anymore, I know how much the completion of this PhD would've meant to them. My grandad was my biggest advocate, supporter and fan and for that, this thesis is dedicated to him.

I will be forever grateful for this experience and the opportunity to complete this PhD. To all of you mentioned above, and more, thank you!

`

Gramps, this one's for you!

`

Abbreviations

ADME	Absorption, Distribution, Metabolism, Elimination
AOT	Sodium Bis(2-ethylhexyl) sulfosuccinate
API	Active Pharmaceutical Ingredient
ATO	Atosiban
ATO-LIP	Atosiban targeted liposomes
BCS	Biopharmaceutical Classification System
BPD	Bronchopulmonary Dysplasia
CAC	Critical Aggregation Concentration
$CDCl_3$	Deuterated chloroform
CDER	Centre for Drug Evaluation and Research
CMC	Critical Micelle Concentration
COMP	Compritol 888 ATO
COMP-SLNs	Compritol 888 ATO Solid Lipid Nanoparticles
COX	Cycloexygenase
DCC	Dicyclohexylcarbodiimide
DCM	Dichloromethane
DCU	Dicyclohexylurea
DI	Deionised
DLS	Dynamic Light Scattering
DMAP	4-dimethylamiinopyridine
DSC	Differential Scanning Calorimetry
DSPC	1,2 Diasteroyl-*sn*-glycero-phosphocholine
D_z	Z average
EMA	European Medicine Agency
ETFD	Emulsion Templated Freeze Drying
EtOAc	Ethyl Acetate
EtOH	Ethanol
FDA	Food and Drug Administration
HLB	Hydrophilic Lipophilic Balance
HPLC	High performance liquid chromatography
HPMC	Hydroxypropyl methylcellulose
HP-β-CD	Hydroxylpropyl β-Cyclodextrin
IND	Indomethacin
IND-NLCS	Indomethacin Nanostructured Lipid Carriers
IND-SLNS	Indomethacin Solid Lipid Nanoparticles
IPA	Isopropanol
IR	Infrared
ITC	Isothermal Titration Calorimetry
IV	Intravenous
LIP	Liposomes
mPEG-*b*-PCL	methoxypolyethylene glycol-polycaprolactone
MW	Molecular weight
MWCO	Molecular Weight Cut Off
NC	Nanocapsules

NDC	Sodium Deoxycholate
NE	Nanoemulsion
NEC	Necrotizing Enterocolitis
NLC	Nanostructured Lipid Carrier
NMR	Nuclear Magnetic Resonance
NS	Nanospheres
NSAID	Non-Steroidal Anti-Inflammatory
o/w	Oil in water
OR	Oxytocin Receptor
ORA	Oxytocin Receptor Antagonist
ORA-LIP	Oxytocin Receptor Antagonist targeted liposomes
OR-LIP	Oxytocin receptor targeted liposomes
PCL	ε-Polycaprolactone
PdI	Polydispersity Index
PEG	Polyethylene glycol
PEG-*co*-PLGA	Polyethylene glycol-*co*-(polylactic-b-glycolic) acid
PEO	Polyethylene Oxide
PK	Pharmacokinetic
PLA	Polylactide
PLE	Porcine Liver Esterase
PPO	Polypropylene Oxide
PVA	Polyvinyl alcohol
PVP	Polyvinyl Pyrrolidone
PXRD	Powder X-Ray Diffraction
Py-COMP-SLN	Pyrene loaded Compritol 888 ATO Solid Lipid Nanoparticles
RDS	Respiratory Distress Syndrome
SDN	Solid Drug Nanoparticle
SIM	Solvent Injection Method
SLN	Solid Lipid Nanoparticle
TGA	Therapeutic Goods Administration
THF	Tetrahydrofuran
T_m	Melting point
TPGS	d-α tocopheryl polyethylene glycol 1000 succinate
UV/Vis	Ultraviolet Visible spectroscopy
w/o	Water in oil
WHO	World Health Organisation

Abstract

Preterm birth is an ongoing clinical issue causing threat to both maternal and fetal health. Current therapeutic agents for the prevention of preterm suffer from high and repetitive dosage requirements, predominantly due to poor aqueous solubility and unwanted accumulation. Throughout this thesis, efforts to formulate indomethacin (IND) into several different types of nanocarrier systems; both lipid derived and non-lipid derived, has been thoroughly explored.

Firstly, IND-SLN systems at 3 wt% IND containing Compritol 888 ATO (COMP) solid lipid and binary combinations of Pluronic® F68: Tween 80 and Pluronic® F127: Tween 80 as appropriate stabilisers were investigated. The impact the different Pluronic® stabilisers had on the COMP lipid core were probed though investigating changes observed in the polarity of the lipid core. The internal core microenvironment was determined through the implementation of pyrene as a fluorescent probe. A range of commonly used Pluronics® (F68, F127, L64 and P105) where used to identify a relationship between the physical characteristics and impact on the internal lipid core. It was highlighted that the molecular weight (MW) of the polypropylene oxide (PPO) block dominates the polarity of the microenvironment. Further work showed that the polarity of the microenvironment can therefore be tuned through blending different Pluronic® stabilisers of different MW PPO block lengths. This finding was of significant importance as tuning the environment through the use of successful stabilisers may enhance drug loadings of specific actives, dependent on their own polarity.

The consequent investigations explored the implementation of five different liquid lipids, namely mineral oil, castor oil, safflower oil, sunflower oil and soybean oil. Successful investigation showed two formulations containing IND. 10wt% IND-NLCs were formed using sunflower and safflower oil, stabilised by Pluronic® F127 and using COMP as a solid lipid. Further work showed that the removal of 1-propanol disrupted the stability of the dispersions. As a result, 5 wt% IND-NEs were produced using acetone as a volatile organic solvent. This reduced the necessity to mechanically remove the organic solvent from the

dispersions. Optimal samples contained safflower, sunflower and soybean oil as suited liquid lipids.

Finally, investigations into the development of IND solid drug nanoparticles (SDNs) were explored. The development of IND-SDNs were unsuccessful and therefore esterified analogues of increasing hydrophobicity were formed. The relationship between the physical characteristics of molecules and their ability to successfully form SDNs was developed. The hexyl ester analogue proved to be the most stable over a 24 hour period with the ability to be reconstituted after eight weeks.

In summary, work presented throughout this thesis has investigated the formation of lipid derived and non-lipid derived nanosystems as carriers of the therapeutic agent, indomethacin. Several optimal formulations may be further explored, with the potential to aid clinical developments for the prevention of preterm birth.

`

Contents

`

CHAPTER 1

Introduction

Chapter 1

1.0 Introduction

1.1 Pregnancy

Pregnancy, clinically known as gestation, is the process by which offspring develop inside the uterus of a female.[1] The full-term gestation period in humans is approximately 40 weeks and is commonly separated in to three stages known as trimesters. The first trimester occurs from weeks 0-12, the second from weeks 13-26 and the third from weeks 27-40.[2] The trimesters are used to track the fetal development throughout the gestational period, from conception to the birth of the neonate.[3]

1.1.1 Labour

Labour, or parturition, is a complex physiological process that is initiated *via* a cascade of cellular activity changes in response to hormonal changes in both the mother and fetus.[4,5] These in-depth physiological processes do not need to be understood for the work presented in this thesis, however they will be discussed briefly below. To maintain a healthy pregnancy, the ovaries and placenta are responsible for the production of two fundamental hormones; oestrogen and progesterone (Figure 1.1). Both hormones work through binding to the promotor regions of specific steroid hormone receptors that then enables the regulation of the transcription of specific genes required for the development and function of the uterus.

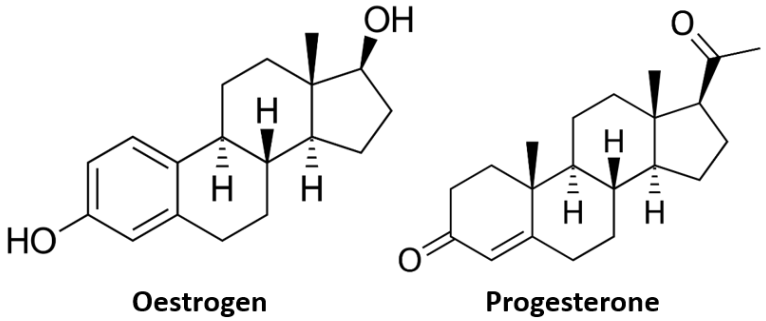

Figure 1.1**:** The chemical structure of oestrogen and progesterone, two fundamental hormones for regulating pregnancy and initiating labour.

Briefly, in the initial stages of pregnancy, oestrogen prepares the uterus lining for implantation of the blastocyst (a cluster of cells developed after fertilisation) and aids placental formation.[6] The role of oestrogen in later pregnancy is to increase the expression of a hormone receptor, the oxytocin receptor (OR), on the surface of the uterus as discussed later in this section.[7] Progesterone inhibits the smooth muscle cells of the uterus, named the myometrium (Figure 1.2), from contracting in early pregnancy.[8] The concentration of progesterone decreases when the pregnancy reaches full term to allow contractility to occur, thereby allowing labour to proceed.[9]

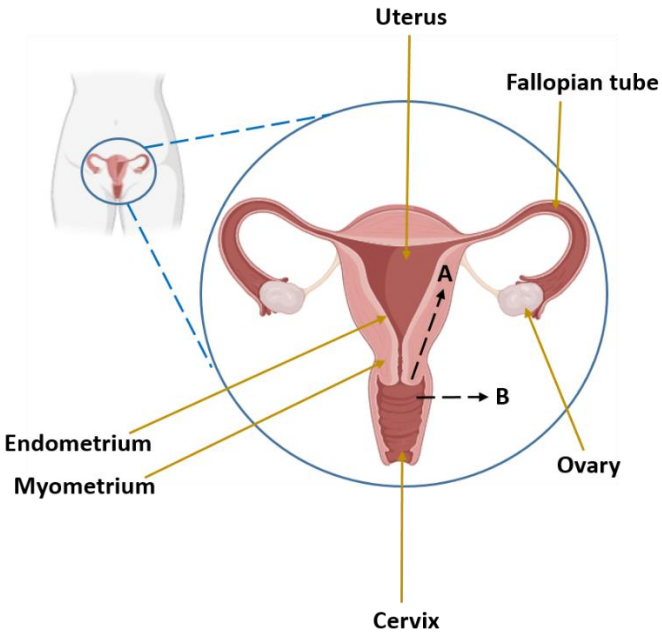

Figure 1.2: Progesterone inhibits early contractions in the myometrium, whilst oestrogen aids placental formation in the earlier, embryonic stage of pregnancy. (A) Indicates the contraction movement upwards of the myometrium in labour. The endometrium is the lining of the uterus that thickens during pregnancy. (B) Indicates the cervical widening and dilation during labour.

On the onset of labour, cortisol- the 'stress hormone,' increases. This causes a simultaneous decrease in the concentrations of both progesterone and oestrogen, and stimulates prostaglandin production. Prostaglandins are lipophilic compounds that cause the myometrium and endometrium to contract upwards (Figure 1.2, arrow A) and the cervix to dilate (Figure 1.2, arrow B), initiating phasic contractions in the uterus.[10–12] The contractions upregulate the production of oxytocin (Figure 1.3).

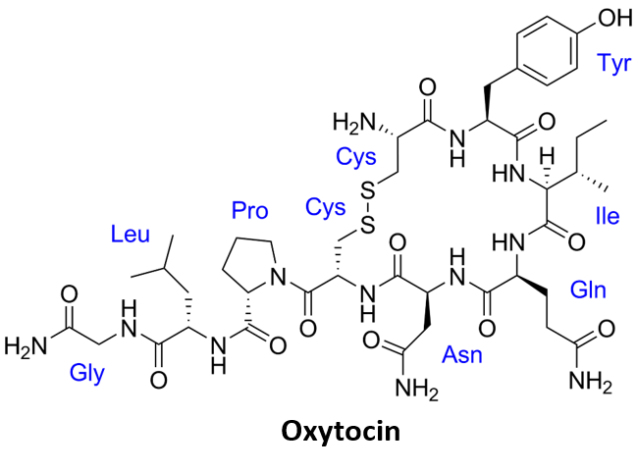

Figure 1.3**:** The chemical structure of oxytocin.

Oxytocin is a hormone that increases throughout pregnancy and is released in pulses from the maternal pituitary gland during labour, to prepare the cervix for dilatory responses.[11,12] As the expression of ORs is upregulated in later pregnancy, as the oxytocin is released, it can successfully bind to the ORs. In turn, the frequency and intensity of contractions is also increased.[11,12] The physiological initiation of uterine contractions also involves increasing intracellular calcium levels causing frequent electrical changes in myometrial tissue; however the true full mechanism of cellular changes during labour is unknown.[11,12] The role of oestrogen and oxytocin in labour is summarised below in Figure 1.4.

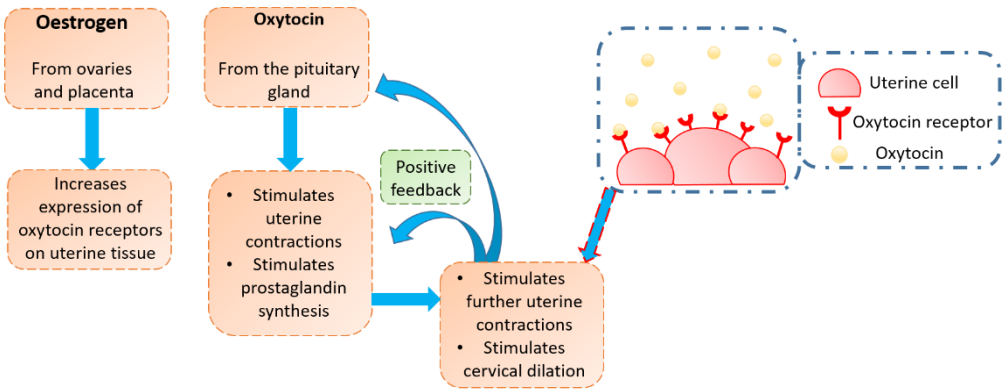

Figure 1.4: A diagrammatic summary of the initiation of labour and the role of hormones cortisol, oestrogen and oxytocin.

For premature births, this process happens earlier on in the pregnancy when the fetus is not fully developed, therefore increasing the probability of multiple medical complications. The

early onset of labour can be initiated for several reasons and will be discussed later in section 1.3.1.

1.2 What is premature birth?

Premature, or preterm, birth is defined as the birth of a child prior to 37 weeks of gestational age. According to the 2018 report from the World Health Organisation (WHO), preterm birth globally affects up to 15 million babies each year, with a total of 1 million infant mortalities.[13,14] This translates to more than 1 in 10 infants born prematurely per year, accounting for 7.3% of live births in the UK alone.[15] Throughout recent decades, prematurity has received increasing amounts of interest from both researchers and clinicians. This is due to the rising number of cases and severity of health implications for both the mother and the neonate. The gestational age of the neonate is the most critical factor that directly influences the health, survival and neonatal development. Therefore, each case is categorised into three gestational time divisions as follows; extremely preterm (< 28 weeks), very preterm (28-32 weeks) and moderate to late preterm (32 to 37 weeks); where the latter stage accounts for 70% of cases.[16] For infants born at 22 weeks or with a birth weight of $\leq$500 g, they are classed as the lower viability limit with some studies experiencing no survival of neonates in this category.[17,18] However, as gestation time increases so does survival rates, with an increase in neonatal viability commonly classed from 24 weeks. According to a study conducted by Truffet *et al*. neonates born at 24 weeks had an increased survival rate at 31%, followed by 78% at 28 weeks and 97% at 32 weeks.[19] Although the largest concern linked to premature birth is immediate maternal-fetal mortality; non-immediate effects and long term morbidity includes neurodevelopmental delay, cerebral palsy, chronic lung disease and mental health implications.[20]

1.3 Risk factors and potential causes of premature birth

1.3.1 Pre-empted prematurity cases

The definitive causes of up to 40% of preterm births are unknown.[21] In less than 25% of cases, premature births are pre-planned by obstetricians; primarily because the mother or the fetus

are suffering from a potentially life-threatening condition.[15] This can often occur when the fetus is suffering from growth restriction or olgio or poly hydraminos, conditions characterised by too little or too much amniotic fluid (Figure 1.5, sections (i)-(iii)). Alternatively, planned preterm birth can occur if the mother suffers from short cervix, gestational diabetes, placenta previa or preeclampsia (Figure 1.5, sections (iv)-(vii)). In all of the above cases, if the medical condition is known, the mother and fetus are monitored routinely to identify changes throughout the pregnancy. More significantly, multiple gestations i.e. twins, triplets account for more than 50% of preterm birth complications and 10-12% of all fetal deaths.[22–24] The occurrence of multiple gestations has increased by over 19% in the US alone since 1995, and such pregnancies propose a higher risk to perinatal morbidity and mortality.[23] This due the increased risk of maternal health effects followed by low birth weight of neonates; especially those linked to intrauterine growth restriction.[25,26] In these situations, obstetricians can induce birth at 37 weeks if they can justify the advantage of early labour based on maternal fetal considerations.[15,27]

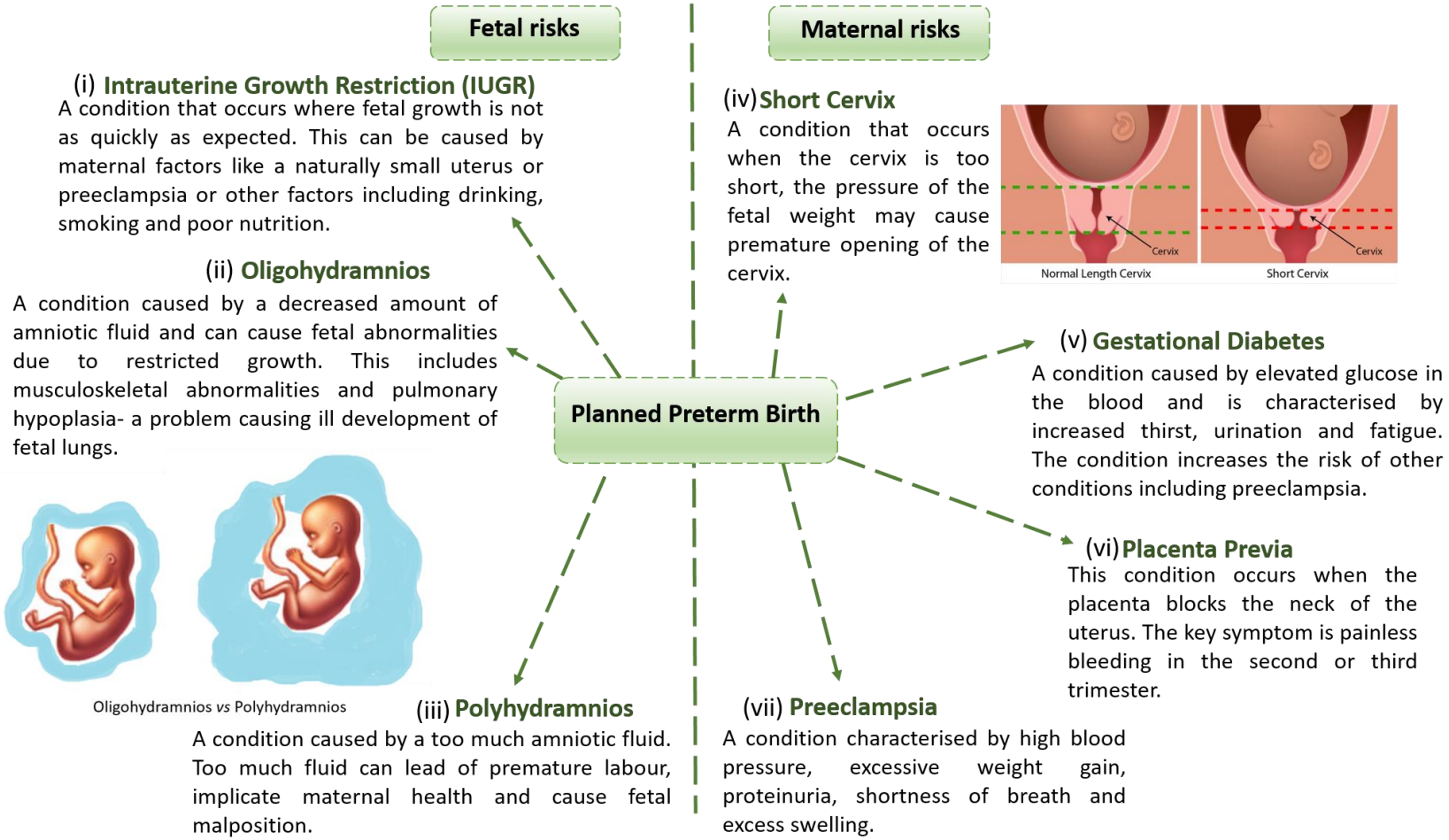

Figure 1.5**:** Summary of conditions resulting in potentially planned prematurity which may lead to planned prematurity cases including (i) Intrauterine growth restriction, (ii) Oligohydraminos, (iii) Polyhydraminos, (iv) Short cervix, (v) Gestational diabetes, (vi) Placenta previa and (vii) Preeclampsia. The illustration for (iv) short cervix was adapted from Varier *et al.* [28].

1.3.2 Sudden prematurity cases

The majority of preterm births, over 75% of cases, are unplanned; 40% of which are linked to premature rupture of membranes i.e. "waters breaking".[29] Treatment options are limited to anti-contraction (tocolytic) treatments will be discussed in more detail later in section 1.5. The increase in prematurity cases globally has attracted significant attention for further research and development for increased understanding of more effective and clinically available treatment options. In order to understand potential risk factors leading to sudden preterm birth, researchers have shown that there are links between maternal lifestyle, genetic and environmental factors which may directly influence the fate of maternal-fetal health.[30] It is also known that a significant number of unplanned cases are consequences of an unexpected emergency; which may include a placental abruption (separation of the placenta from the uterus), an infection, undiagnosed pre-eclampsia (high blood pressure) or a prolapsed cord (where the umbilical cord drops through cervix).[31,32]

Maternal age is often a key indication to the potential risks that could occur on the journey between conception and birth. Pregnancies at a young age (≤19 years) or an advanced maternal age (≥35 years) are two imperative high-risk categories. The argument of why young adolescents are at a greater risk of preterm birth is somewhat controversial, with many arguments supporting biological immaturity as a risk factor.[33–35] As a result of biological immaturity, it has previously been shown that they are at risk of preterm premature rupture of membranes and spontaneous preterm births.[36] On the other hand, advanced maternal age increases the chances of placental abruption, where the placental lining separates from the uterus of the mother. These conditions are more common in those ≥35 years.[37] Furthermore, advanced maternal age comes with more potential for underlying health implications including gestational diabetes, preeclampsia and obesity, all of which are huge risk factors for preterm birth complications.[38,39] As discussed in section 1.3.1, these conditions are often monitored and if clinically necessary, are planned prematurity cases. However, if the condition is unknown and therefore left untreated, then spontaneous preterm birth and further

complications become an unexpected morbidity risk. A summary of conditions related to sudden preterm complications are highlighted in Figure 1.6 (next page).

1.4 Side effects of preterm birth

Premature birth is coupled with both physical health and mental wellbeing implications. The side effects may physically implicate the mother, unborn fetus or the newborn, and both parents may also suffer notable drawbacks in their mental wellbeing from the experience.

1.4.1 Parental side effects

Maternal death during pregnancy accounts for an estimated 500,000 women globally, with up to 25% of cases occurring after labour from postpartum haemorrhage (PPH).[41] This is a condition described by the loss of ≥500 mL of blood from vaginal delivery or ≥1000 mL following caesarean delivery and can occur between 24 hours and 12 weeks after giving birth.[42,43] It can occur as a result of pregnancy complications *e.g.* polyhydramnios (too much amniotic fluid) and hypertension disorders or complications during labour *e.g.* prolonged/obstructed labour or malposition of the fetus.[42] However, the most frequent maternal side effects of premature birth are primarily linked to psychological complications, with literature providing evidence of mental health conditions lasting up to 7 years postpartum.[40,44,45]

(i) **Multiple Gestations**
Multiple gestations accounts for pregnancies of more than one child e.g. twins or triplets. This can lead to further problems associated with intrauterine growth restriction (IUGR).

(ii) **Maternal Age**
Complications can occur at maternal age on <19 years or >35 years. Younger maternal age is particularly associated with preterm premature rupture of membranes (PPROM). Advanced maternal age is associated with placental abruption or perineal laceration. Nevertheless, either age groups could experience a large range of complications.

(iii) **Placental Abruption**
This is a condition where the uterus separates from the placenta and can cause vaginal bleeding and abdominal pain.

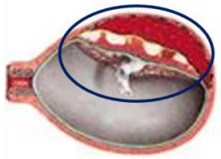

(iv) **Perineal laceration**
This is a tear in the perineum

(viii) **Obesity**
Obesity is a risk factor in unplanned preterm births as it increases the risk of gestational diabetes and preeclampsia. If these conditions are not known or treated throughout pregnancy then the result is an unplanned preterm birth.

Unplanned Preterm Birth

(v) **Intrauterine Infection**
This is an infection un the womb that can be caused by Streptococcus B, E-Coli, HIV, Bacterial Vaginosis or STI's. It causes the amniotic fluid (chlorioamnioitis) or umbilical cord (funisitis) to become infected and inflamed.

(vii) **Antiphospholipid Syndrome (APS)**
This is an autoimmune condition that increases the likelihood of thrombosis.
APS can cause pregnancy complications where one risk factor is an unplanned preterm birth. APS is treatable and wouldn't likely cause severe complications if monitored and treated appropriately.

(vi) **Prolapsed Cord**
A prolapsed cord is when the umbilical cord is exposed from the uterus before the baby and causes a potential reduction in blood circulation in the fetus.

Figure 1.6: Summary of conditions leading to sudden preterm birth Conditions or factors that increase the risk of sudden prematurity are (i) Multiple gestations, (ii) Maternal age, (iii) Placental abruption, (iv) Perineal laceration, (v) Intrauterine infection, (vi) Prolapsed cord, (viii) Antiphospholipid syndrome and (viii) Obesity.

1.4.2 Neonatal side effects of preterm birth

There are a number of health complications that can be determined immediately upon preterm birth and also developmental conditions that can only be detected once the baby reaches full term or later in life. Table 1.1 shows several potential conditions that are reported due to premature birth.

Table 1.1: Overview of neonatal side implications due to premature birth

Organ effected	Implication
Lung	Respiratory Distress Syndrome (RDS)
	Chronic Lung Disease
	Bronchopulmonary Dysplasia
	Pulmonary Hypertension
Gastrointestinal tract	Necrotizing enterocolitis (NEC) ± perforation
Brain	Intraventricular Hemorrhage
	Periventricular Leukomalacia
	Periventricular hemorrhagic infarction
Heart	Patent Ductus Arteriosus
Eyes	Retinopathy of prematurity (ROP)
Systemic	Nosocomial Infections

A significant concern with sudden prematurity is the mortality caused by the incomplete development of fetal organs. The most commonly diagnosed condition that increases neonatal mortality rates is respiratory distress syndrome (RDS); a condition characterised by a collapsed lung.[49] This syndrome is as a result of immaturity of the respiratory system causing structural issues and a decrease in pulmonary surfactant causing the lungs to stick together (Figure 1.7). [50,51]

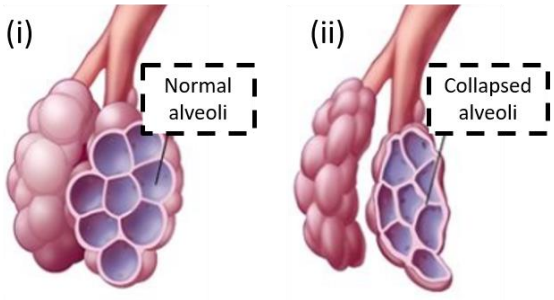

Figure 1.7: (A) The structures of alveoli in a (i) normal lung *vs* (ii) an infant with RDS, often treated with steroidal betamethasone or dexamethasone.

This increases the risk of inflammation and scarring on the neonatal lung.[52] The prognosis of this disorder is dependent on gestational age and affects up to 50% of neonates born prior to 28 weeks.[53] Clinicians will often administer corticosteroids, for example epimeric dexamethasone or betamethasone (Figure 1.8) for the prenatal prevention of RDS.

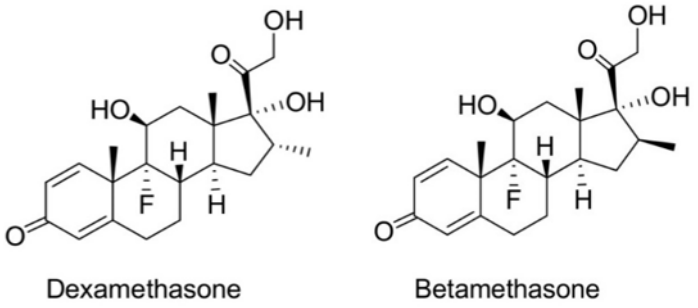

Figure 1.8: The chemical structure of steroids dexamethasone and betamethasone

These steroids are a group of synthetic hormones and have shown to vastly improve lung maturation through the increased production of the phospholipids, phosphatidyl choline, to reduce surface tension thus preventing a collapsed lung (Figure 1.7).[50,51] If the neonate still shows symptoms of RDS at birth, a large number will go on to experience chronic lung disease as a longer term effect and can lead to bronchopulmonary dysplasia (BPD). BPD is diagnosed when a preterm neonate is still oxygen dependent 36 weeks.[54] BPD results in physiological complications that leads to a decrease in surface area for gaseous exchange, decreased angiogenesis (formation of blood vessels) and decreased alveolarization (formation of alveoli).[55] The use of dexamethasone and betamethasone after birth has proven more controversial than prenatal usage due to studies showing a reduction in antenatal weight and changes to the heart or breathing patterns. These side effects can be attributed to the broad spectrum uses provided by the corticosteroid treatment.[56] On the contrary, other studies have shown that the single use of steroids has proven beneficial with only recurrent use posing a threat and therefore the use of these steroids are still widely used in obstetrics today.[56]

Furthermore, this steroidal treatment has also been efficacious in the reduction of threatening intestinal infection cases in preterm infants *e.g.* necrotizing enterocolitis (NEC) - an inflammatory disorder of the gastrointestinal tract caused by bacteria.[57] This causes part of the

bowel tissue to die, at which point the infant needs surgical intervention. If left untreated with corticosteroids it can cause gastrointestinal bleeding and septic shock.[58,59]

Additionally, due to the complexity of the fetal brain, there are several morbidities that can influence antenatal health and are heavily dependent on gestational age. For example, periventricular leukomalacia is a brain condition common in neonates born before 32 weeks gestation and the incidence decreases with an increase in gestational age.[60] It is characterised by the necrosis (death) of ventricular white matter (nerve fibres) in the brain causing a softening in the ventricular tissue that can lead to cerebral palsy.[61] Cerebral Palsy induces further comorbidities including developmental delay, mental retardation, epilepsy, vision and hearing impairments and functional ability.[62,63] For all morbidities and chronic conditions caused through preterm birth complications, the child faces a lifelong battle with illness or medical implications with large pill burdens and treatment is often limited due to poor efficacy. Therefore, there is a stark need for new clinical treatment options to increase gestation time and reduce both maternal and neonatal mortality and morbidity rates. Treatment options for planned and sudden prematurity are discussed in the following section.

1.5 Clinically available treatment options for premature birth

The appropriate clinical treatment in each case is dependent on whether prematurity is predicted or sudden. In cases where prematurity is potentially damaging to maternal or fetal health, there are treatment plans available to mitigate risks and will be further discussed in section 1.5.1. For sudden prematurity cases there are also various treatments available including tocolytics, oxytocin receptor antagonists (ORAs), steroidal treatment and so forth; with many research groups dedicated to further understanding their mechanism of actions and structure property relationships between the different drugs and tissue physiology.[11,12,64,65] Nevertheless, the cases of prematurity are on the increase, and there are severe clinical drawbacks with all the therapeutic treatments proposed and will be discussed in section 1.5.2.

1.5.1 Pre-empted prematurity: treatment options

As outlined previously, 25% of all cases of preterm birth are planned for.[15] This occurs when the safety of the mother or baby is at risk if the pregnancy reaches full term gestation.[66] For women who have had previous premature births and are therefore at higher risk in subsequent pregnancies, or those with physiological implications such as a short cervix are often provided with progesterone supplementation.[67] The natural role of progesterone in preterm birth is well studied, from its importance to implantation in early pregnancy, to maintaining uterine activity dormancy during pregnancy.[68,69] The versatility and importance of progesterone throughout the gestation period, therefore made it an ideal therapeutic agent to study for its potential to reduce the occurrence of preterm birth.

As of 2011, the Food and Drug Administration (FDA) approved the use of hydroxyprogesterone caproate, the first new drug for use during pregnancy in 15 years (Figure 1.9).[70]

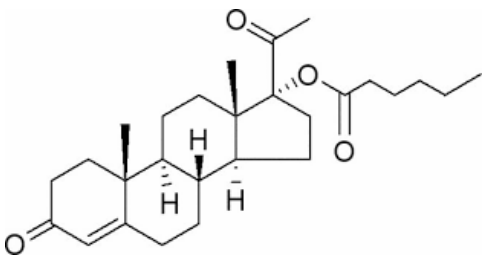

Figure 1.9: The chemical structure of hydroxyprogesterone caproate

Further studies, up to January 2020, have also promoted progesterone uses with suspected prevention of over 8,000 miscarriages in the UK alone.[71] Nevertheless, it is also important to understand that no therapeutic treatment is 100% effective, nor has an exact mirrored effect in every pregnancy scenario. Consequently, there are some contradictory arguments suggesting that progesterone supplementation is not hugely beneficial in all cases, and is less successful in multiple gestation pregnancies.[72,73] This may be due to different pathophysiology in multiple gestations, including increased risk of intrauterine infections and inflammation, hormonal disorders or cervical dysfunction.[24]

A second treatment option for women with an inherent weak cervix is a cervical cerclage. This is a stich placed at the opening of the womb to provide strength and support to decrease the risk of cervical shortening or widening prematurely; a condition that has often led to late miscarriage in the second trimester (Figure 1.10).[74]

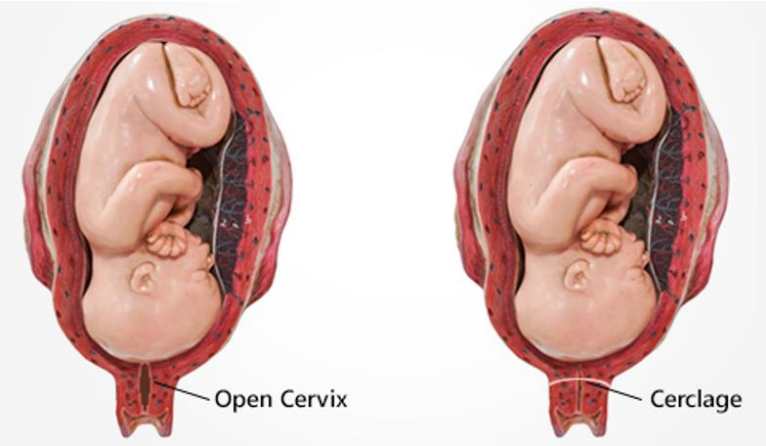

Figure 1.10**:** Illustration showing the method of cervical cerclage stitching to reduce the cases of preterm birth.

This method may be favourable in women who have previously experienced late miscarriages, cervical diseases or those who have experience cervical trauma from previous surgical termination.[75,76] Nonetheless as a cervical cerclage does not address the physiological cervical softening that occurs in premature birth. This treatment also bares the risk of unpredictable failure that may occur in the latter stages of pregnancy.[77]

1.5.2 Sudden prematurity: treatment options

To clinically address sudden premature labour, a class of drugs called tocolytics are used. Tocolytics are subdivided into several categories including calcium channel blockers (nifedipine, magnesium sulfate), oxytocin receptor antagonists (atosiban, retosiban), beta minimetics (tertbutaline, salbutamol) and prostaglandin inhibitors (indomethacin).[78,79] All tocolytics aim to inhibit uterine contractions and can be effective in prolonging gestation for up to 7 days, with average delays of 48-72 hours.[80,81] Although there appears to be a range of clinically suitable drugs, fundamental drawbacks include restricted repeated dosages for 48 continuous hours and they have negligible effect on improving the fetal prognosis.[10,80,82]

Therefore, tocolytics are predominantly used to delay gestation in order to co-administer corticosteroids such as betamethasone and dexamethasone. The clinical aim of this co-therapy is to increase gestation time, whilst enhancing lung maturation of the fetus to reduce fetal morbidity from conditions such as respiratory distress syndrome as discussed previously in section 1.4.2.

In addition to the timely constraints faced clinically with each of these therapeutics, there are a number of potential side effects that must be considered. From a maternal perspective, side effects are predominantly transient; such as headache, hypotension, tachycardia, anxiety, nausea/ vomiting, dizziness and flushing.[83,84] A study by Guclu *et al.*, has reiterated that the use of beta mimetics and calcium channel blockers as tocolytics are associated with a number of these acute, and potentially severe maternal side effects.[85] However, drugs that are lipophilic, non-polar and of a low molecular weight can cross the placental barrier, into the fetal circulation and cause severe side effects and life changing fetal morbidities. This commonly occurs with prostaglandin inhibitor, indomethacin, as discussed below.

1.6 Indomethacin as a target tocolytic

Indomethacin is a non-steroidal anti-inflammatory (NSAID) and as well as a tocolytic has multiple other clinical uses including for gout, as an anti-pyretic and reducing swelling from inflammation. As a tocolytic agent, indomethacin falls into the category of prostaglandin inhibitor tocolytics (Figure 1.11). It has been continuously shown to inhibit myometrial contractions, however is clinically restricted due to its physicochemical properties that allow it to cross the placental barrier and implicate fetal health.[86]

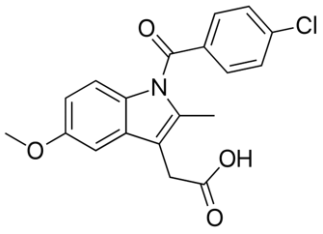

Figure 1.11: Chemical structure of Indomethacin, a tocolytic agent.

1.6.1 Mechanism of Action

Indomethacin is a non-selective prostaglandin inhibitor. Prostaglandins are lipophilic molecules that promote contractility in the myometrium and endometrium tissue in the uterus with their production upregulated upon the onset of labour.[87] Prostaglandins are produced from a substrate called arachidonic acid *via* cyclooxygenase 1 and 2 (COX) enzymes, producing a series of prostaglandin metabolites (Figure 1.12).[87]

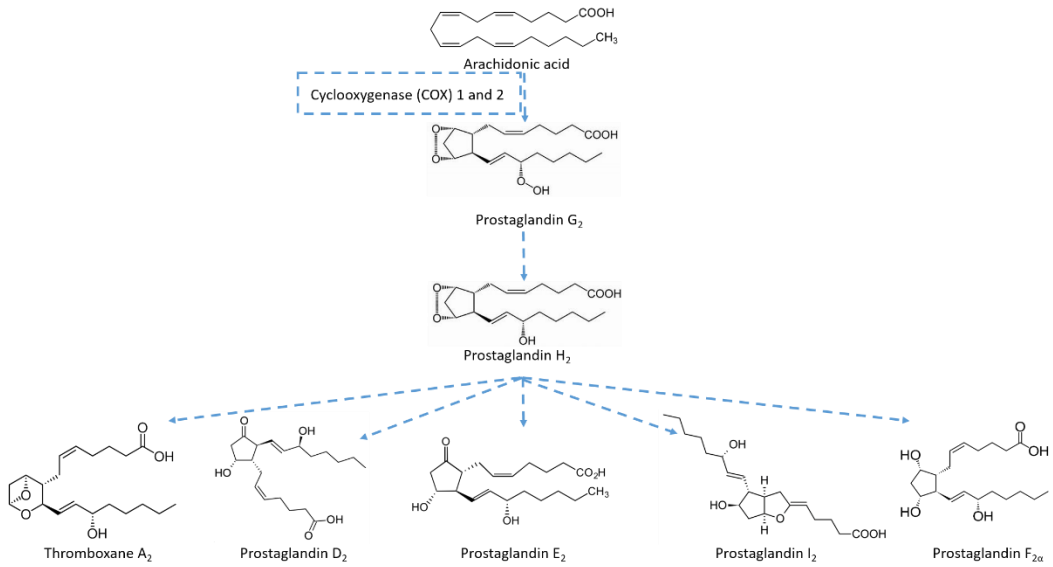

Figure 1.12: The production of prostaglandin bioactive compounds from arachidonic acid, catalysed by cyclooxygenase enzymes

As indomethacin inhibits COX -1 and -2, the pathway of prostaglandin synthesis in inhibited in the initial step, preventing the cascade of prostaglandin G_2 and H_2 production and conversion to prostaglandin subtypes which would normally lead to increased contractions (Figure 1.13).

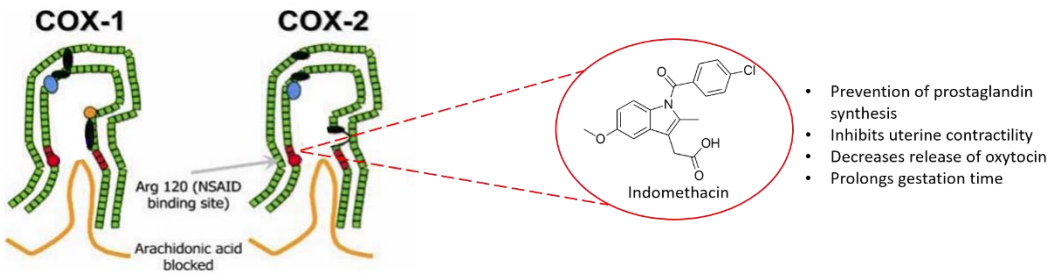

Figure 1.13: The inhibition of COX-1 and COX-2 *via* Indomethacin. The simplified structure of COX 1 and 2 enzymes was adapted from Meek *et al.*[88]

This treatment was thought to be particularly successful as COX-2 enzyme expression is upregulated at the onset of labour and therefore administration of a COX inhibitor reduces the production of prostaglandin metabolites, thereby decreasing contractility.[10,87] Therefore, as uterine contractility is inhibited, the gestation time is increased; a key clinical aim for a new generation of tocolytics.

1.6.2 Clinical restrictions of indomethacin

1.6.2.1 Drawbacks of indomethacin use

Indomethacin's physicochemical characteristics; low molecular weight (358 g/mol), moderate-high lipophilicity (ClogP= 3.5), poor aqueous solubility (0.95 mg/L) and ability to diffuse across the placenta into fetal circulation, means this drug poses a significant risk to both maternal and fetal health. Maternal considerations of indomethacin usage include peptic ulceration, gastrointestinal bleeding, thrombocytopenia, postpartum haemorrhage, hypertension or renal failure.[89–91] However, the use of indomethacin poses a much more significant risk to the development of fetal complexities due to its ability to diffuse across the placental barrier. The combination of indomethacin's physicochemical considerations and its high affinity to bind to albumin in the blood plasma, a higher dosage is required to produce a tocolytic effect. The higher dosage requirements are also coupled with enhanced fetal transfer and accumulation, leading to an increased probability of side effects. Examples include patent ductus arteriosus, oligohydramnios, necrotizing enterocolitis, intracranial haemorrhage and pulmonary hypertension.[86,91] Further research has also shown that the side effects of indomethacin are mainly irreversible if administered after 32 weeks of gestation, hence a further drawback for the safety and efficacy of the treatment.[92] This is thought to be a result of the much longer $t_{1/2}$ of indomethacin in fetal circulation, in comparison to maternal circulation (>14 hours *vs* > 2hours), particularly when administered orally.[93] The severity of the side effects is therefore due to the inability of the fetus to hepatically metabolise the drug quickly enough prior to the next required maternal dosage to prolong a tocolytic pharmacological effect.[93]

There are a number of clinically viable tocolytic agents currently used, however many are dosage restricted due to their physicochemical properties; poor aqueous solubility, high dosage requirements, poor targeting and unwanted accumulation in fetal or maternal organs. This therefore means there is clinical need for the development of a drug delivery system that combines high drug loading with specific treatment targeting while maintaining high aqueous solubility.

1.6.2.2 Indomethacin dosage regimes

The dosage requirements of indomethacin depend heavily on the route of administration. For example, for rectal administration a dosage of 100 mg is administered and repeated every one to two hours thereafter.[94] Conversely, oral administration enables a faster absorption route and therefore requires an initial dosage of 25 mg, followed by additional 25 mg dosage forms every 6 hours, up to a maximum of 48 hours. [94] Furthermore, the most rapid absorption route is achieved through intravenous (IV) administration. Alvan *et al.* explored initial IV dosages of 25 mg indomethacin, that reached increased bioavailability.[95] The most rapid and efficient administration route is required for the prevention of sudden preterm birth, rendering IV indomethacin as the potentially optimal route.

1.6.3 Advancing indomethacin formulations

Due to the drawbacks of indomethacin as a bulk material as discussed previously, there is a strong need for a chemical intervention for a new treatment of sudden preterm birth. As indomethacin has poor aqueous solubility and lipophilic characteristics, reformulating the small molecule into a more hydrophilic vehicle would be of significant clinical benefit. Therefore, the encapsulation of indomethacin to a nanoformulation may enhance physicochemical properties of the molecule whilst maintaining, or improving, the pharmacological effect would be an extraordinary clinical development for sudden preterm birth.

1.7 Introduction to Nanomedicine

Nanomedicine is a rapidly evolving field that has bridged chemistry, pharmacology and biomedical science, with a mutual aim to improve clinical translation of new materials from benchtop research to the frontline of the healthcare system. The application of nanotechnology to medicine has enabled a rapid growth over the last 25 years of novel diagnostic, therapeutic and imaging tools synthesised from carefully defined materials in the nanometre range of 1-1000 nm (Figure 1.14).[96,97] Although the IUPAC definition of the nanometre range for therapeutics is between 1-100 nm; this is somewhat controversial within the field and for the purpose of this thesis the former range of 1-1000 nm is appropriate.

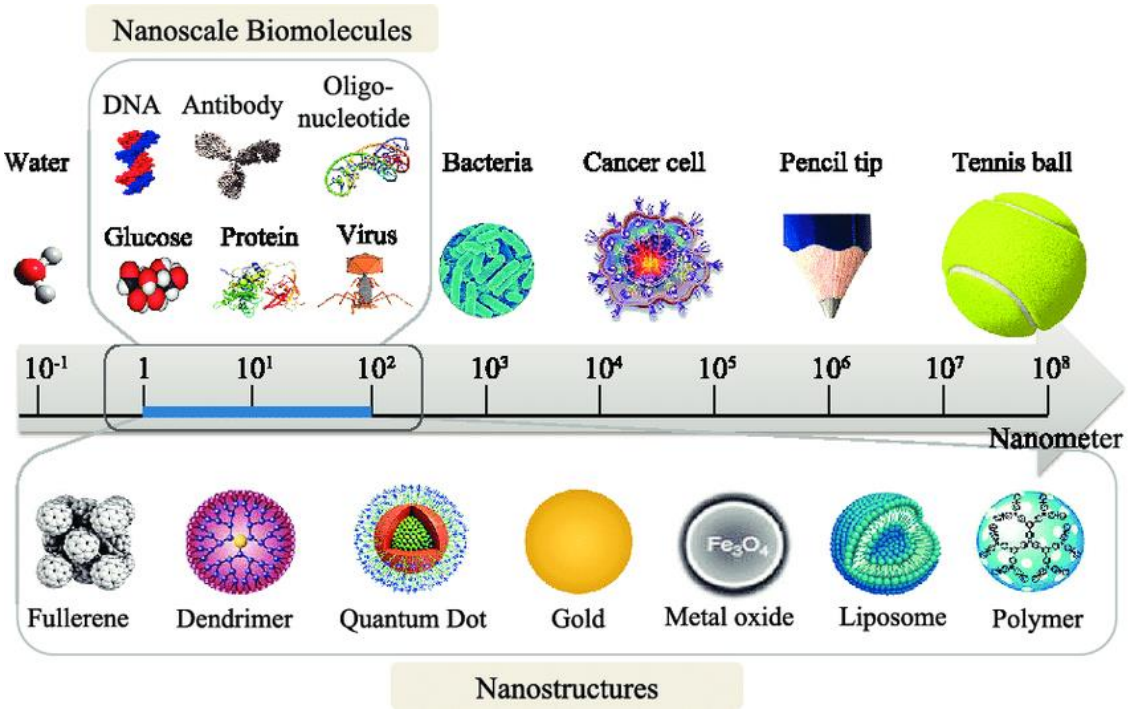

Figure 1.14: A general schematic overview of the nanoscale. The area of the scale highlighted in blue indicates nanoscale biomolecules (top) and different subdivisions of nanomaterials commonly used in nanomedicine (bottom). Illustration adapted from:Saallah *et al.* [97]

1.7.1 Pharmacological benefits of nanomedicines vs conventional treatments

The common focus for nanomedicine interventions is typically for enhancement of pharmacokinetic (PK) profiles and biodistribution properties of poorly performing small molecule drugs. Subsequently, the modification of PK profiles benefits the treatment of chronic conditions that suffer from high pill burdens, repetitive dosing, poor patient adherence

and illnesses with problematic resistance to currently available treatments. Unfortunately, the biological complexity of many conditions means that current small molecule treatment is not therapeutically effective and suffers from poor pharmacokinetic parameters. The pharmacokinetic profiles of drugs dictate their therapeutic safety and efficacy through their absorption, distribution, metabolism and elimination (ADME) profiles. However, an estimated 40% of existing drug compounds and 70-90% of new small molecule candidates are limited by their physicochemical properties, leading to poor permeability and low aqueous solubility.[98,99] These parameters are summarised using the Biopharmaceutical Classification System (BCS) shown in Figure 1.15, where class II and class IV are characterised by a mutual low aqueous solubility; a fundamental drawback for pharmacokinetic efficacy and safety.[98,100]

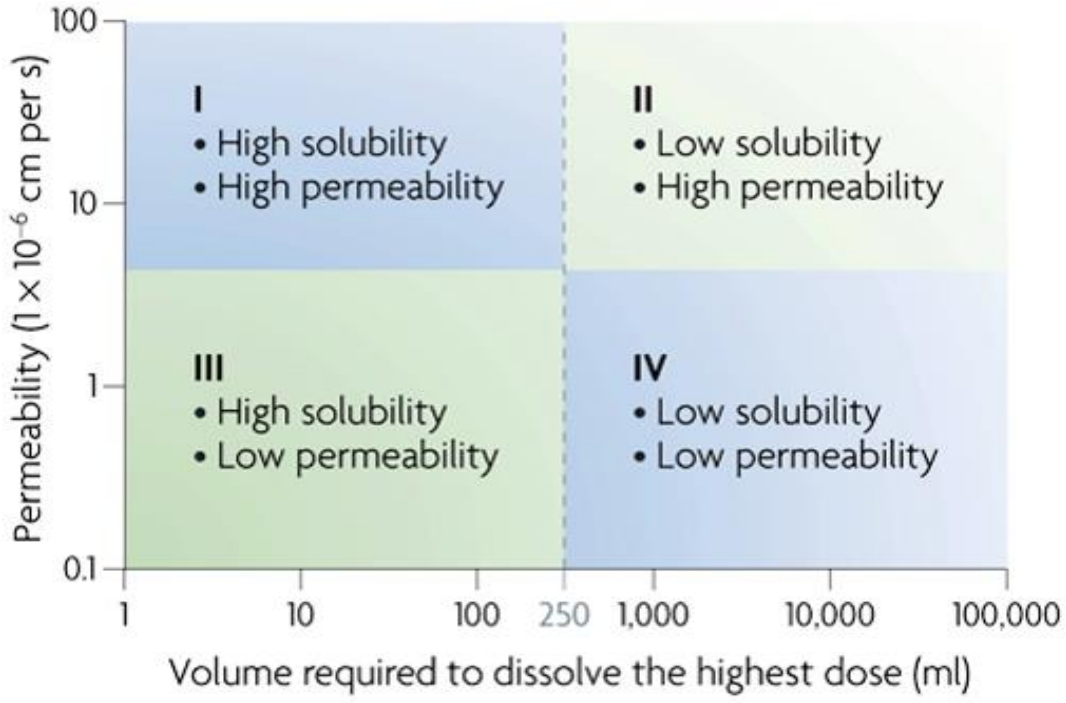

Figure 1.15: A graphical representation of the Biopharmaceutical Classification System (BCS). Class I (blue, top left) and III (green, bottom left) drugs have high aqueous solubility and differing permeability. Class II (green, top right) and IV (blue, bottom right) drugs have low aqueous solubility and differing permeability properties.[101]

Poorly soluble entities, often due to the high lipophilicity (LogP) of the molecules, require higher dosing which leads to toxicity risks and adverse effects and/or more frequent dosing, therefore increasing the risk of poor patient adherence.[102] Poor adherence is ill compliance of patients to abide by recommended dosing, and leads to the drug not exerting its therapeutic

effect with potential to build resistance and pharmacological implications towards any future treatment. Through formulating bulk materials, in particular, from categories II and IV into nanomedicines, it is possible to alter the chemical properties to change the PK profiles.[103] Indomethacin as a key tocolytic of choice falls into the class II category and has been used as a class II model drug previously.[104] Fortunately, due to the precisely engineered properties of nanomaterials, it is possible to maintain or improve the therapeutic effect of the pre-existing drug. Nanomedicine research has been driven to understand nanoparticle-biological relationships, to therefore improve nanoparticle design to promote pharmacological advances over generic bulk materials.[105]

1.8 Types of Nanomedicines

Nanomedicines are subdivided into several categories as shown in Figure 1.16.

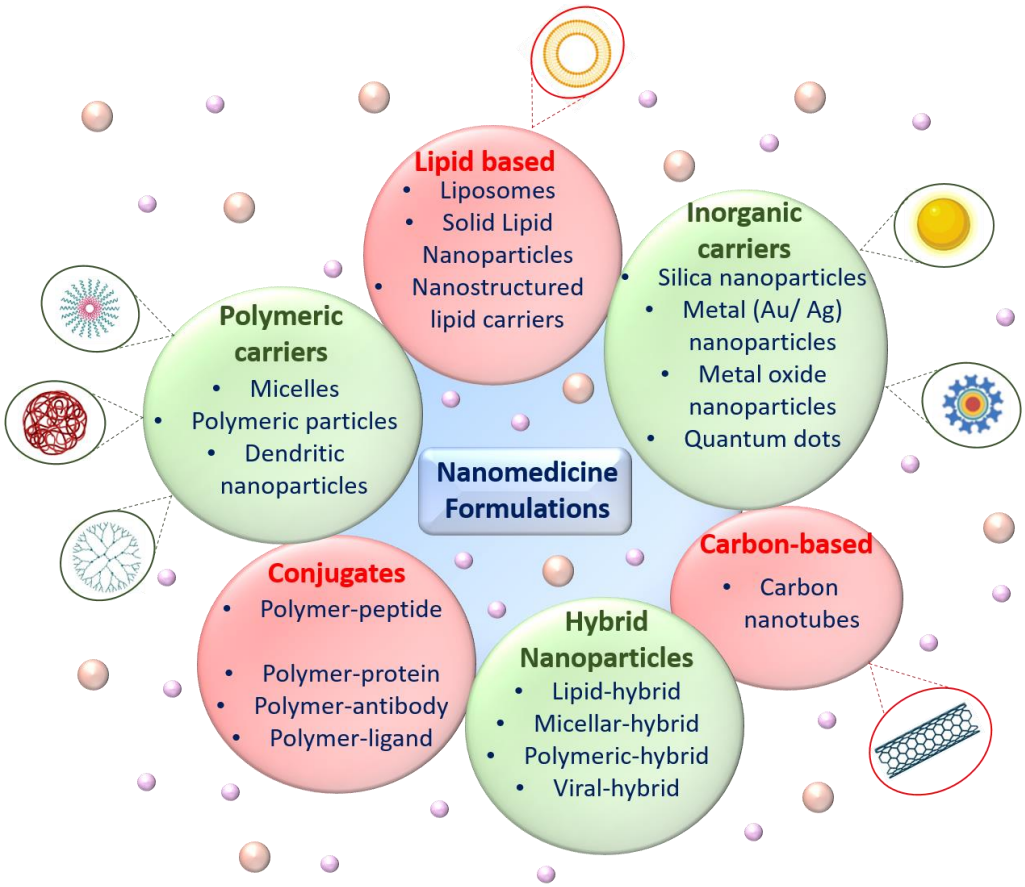

Figure 1.16**:** Illustration representing the variety of functionality design that can be incorporated into nanomedicines.

The scope of nanomedicine design has been increasing over the past few decades with different generations of materials being identified to improve key drawbacks of older generation formulations.[106] For example, polymeric particles have branched out from generic AB block micelles into complex and diverse polymeric structures of different architectures giving rise to polymer-protein or polymer-drug conjugates and polymeric prodrugs (Figure 1.17).[107–110]

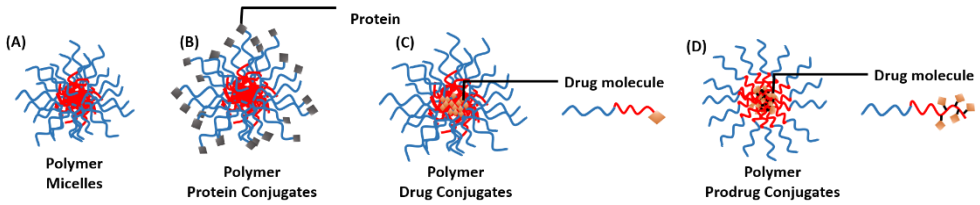

Figure 1.17: Illustration showing the (A) Polymeric micelles, (B) Polymer protein conjugates, (C) Polymer drug conjugates and (D) Polymer prodrug conjugates as examples of different derivatives of polymeric nanomaterials

Another subtype of polymeric derived stabilisers are solid drug nanoparticles (SDNs) and have been applauded for their hugely beneficial PK improvements. SDNs are of significant importance within this thesis and therefore a summary of SDN formulations is provided in the following section.

1.8.1 Solid Drug Nanoparticles

SDNs are colloids consisting of an active pharmaceutical ingredient (API) that is stabilised by a mixture of surfactant and polymeric excipients (Figure 1.18).[111] SDNs differ largely from polymeric nanoparticles and are not considered as typical nanocarrier systems.[111,112]

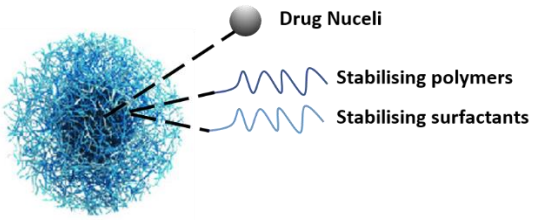

Figure 1.18**:** The generic structure of solid drug nanoparticles

The fundamental drawback that SDNs combat in comparison to other formulations, is their ability to increase the aqueous solubility of APIs with a consequent improvement in

bioavailability.[113–115] SDNs have been applauded for sustained release and improvement of circulation times, reducing dosage requirements and with the potential to reduce the clinical burden on patients.[116,117] Additionally, the ETFD method is rapid and easily scalable which address common scale-up experimental issues found with other bottom up nanoparticle preparations.[118] Successes for SDN formulations have been of paramount importance in new developments for anti-retroviral treatment. For example, SDNs containing the anti-retroviral drugs maraviroc (70 wt%), efavirenz (70 wt%) and lopinavir (70 wt%) in addition to dual component SDNs of lopinavir and ritonavir (56:14 wt%) have been successfully synthesised and translated for further immunological testing.[114,119,120] In addition, an alternative therapy using the therapeutic agent, maraviroc, had a successful drug loading of 70 wt% in SDN formulations containing polyvinyl alcohol (PVA) and sodium bis (2-ethylhexyl) sulfosuccinate (AOT) as the polymer and surfactant respectively. This formulation led to a respective 2.5-fold increase in *in vivo* bioavailability, from 58.71 ng.h ml^{-1} to 145.33 ng.h ml^{-1}.[119] Nevertheless, the versatility of SDN formulations has also been highlighted through the development of anti-malarial prophylaxis SDNs using therapeutic atovaquone, reaching successful drug loading of 80 wt%.[121]

1.8.1.1 Excipients for SDN formulations

A further advantage of SDNs is that the excipients commonly used are from the Food and Drug Administration Centre of Drug Evaluation and Research (FDA-CDER) list. This means that the polymer and surfactant excipients are already excipients in pre-approved clinical formulations and therefore reduces the risk of unexpected pharmacological implications in future formulations. Examples of commonly used polymers and surfactants are listed below in Table 1.2

Table 1.2: Polymers and surfactants from the FDA-CDER list that are excipients in existing and approved clinical formulations.

Polymers	Surfactants
Polyethylene glycol (PEG)	d-α-tocopheryl polyethylene glycol 1000 succinate (TPGS)
Pluronic® F68	Tween 20
Pluronic® F127	Tween 80
Polyvinyl pyrrolidine (PVP)	Sodium deoxycholate (NDC)
Hydroxylpropyl methyl cellulose (HPMC)	Dioxytl sulfosuccinate sodium salt (AOT)
Polyvinyl alcohol (PVA)	Polyethylene glycol(15)-hydroxyl stearate (Solutol)

There are several ways to synthesise SDNs including nanoprecipitation, nanomilling, and homogenisation methods.[121] Nevertheless, for this particular research, advances in the emulsion templated freeze drying (ETFD) method has become of significant importance due to its versatility and scalability of the process. The ETFD process is explained in the section below.

1.8.1.2 The synthesis of SDNs: The ETFD approach

The EFTD method involves forming an oil in water (o/w) emulsion using volatile organic solvent, often dichloromethane or chloroform. A mixture of water-soluble polymers and surfactants are dissolved in the continuous aqueous phase.[114] The two phases are added together, sonicated and immediately frozen prior to lyophilisation. Upon the addition of the two phases, the drug is contained within droplets of the organic solvent and the polymers and surfactants arrange at the interface between the two phases (Figure 1.19A). The rapid cooling of the mixture causes supersaturation of the excipients in both solvent systems and drives phase separation between the organic and aqueous phase crystals of the pure solvents form and the drug crystallises in small compartments within the mixture (Figure 1.19B). Upon the removal of the organic solvent and water in the lyophilisation process, the monolith product contains nanosized crystals of drug in a porous scaffold of polymers and surfactants (Figure 1.19C). As the sample is reconstituted the nanoparticles are released (Figure 1.19D).[114]

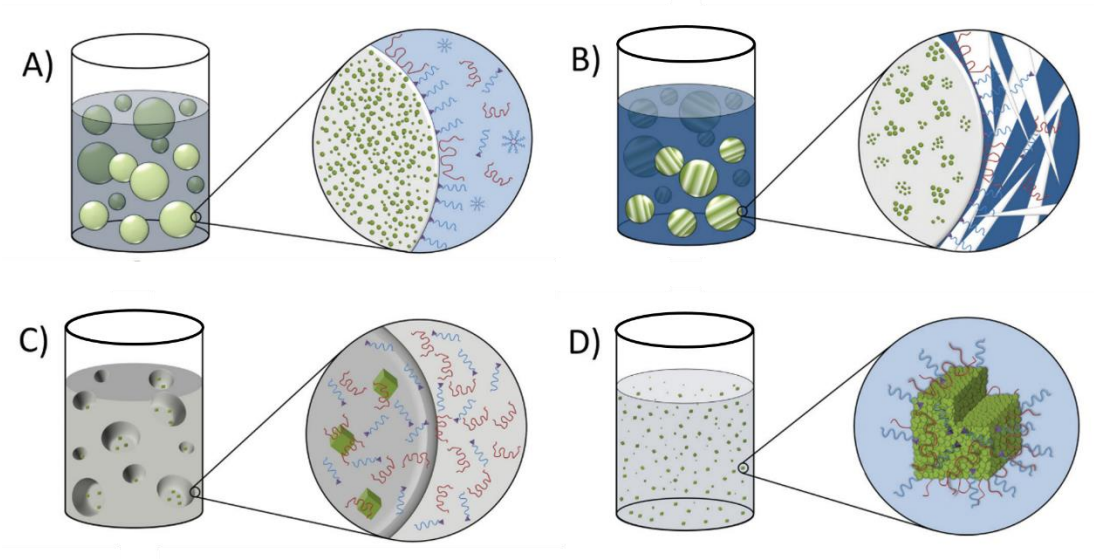

Figure 1.19: Illustration of the ETFD process. A) Dissolution of drug molecules in pockets of a chlorinated solvents stabilised by polymers and surfactants in the aqueous phase. B) Rapid cooling in liquid nitrogen leads to crystal formation of ice, causing supersaturation and phase separation of drug and stabilisers. C) Lyophilisation of the emulsion generates a porous monolith containing drug nanoparticles and a polymer-surfactant scaffold. D) Reconstituting the monolith in appropriate media forms a dispersion of drug nanoparticles stabilised by polymers and surfactants. Figure adapted from: McDonald *et al*.[114]

Consequently, as a result of previous successes with poorly aqueous soluble entities, there is a large scope for using this approach for other poorly water-soluble compounds. Although SDN systems formulated by ETFD have been a significant advancement within the field, drawbacks such as uncontrolled or premature release profiles have been reported, particularly if there are drug molecules also bound on the surface of the particles.[122] Alternative nanosystems that can combat this drawback are systems containing lipid excipients. Lipid derived nanoparticles are discussed in the following section.

1.8.2 Lipid Derived Nanoparticles

An alternative route for beneficial nanomedicines has become apparent through the use of lipid derived nanoparticles. The development of lipid derived carriers, in particular with liposomes at the forefront of recent improvements, has addressed several biological implications of other subtypes of nanomaterials. In addition to the greater controlled release profiles mentioned in the section above, they are also associated with enhanced biocompatibility, stability and biodegradability of excipients used within the

formulations.[123,124] Moreover, more recent advances of liposomes have included the development of solid lipid nanoparticles (SLNs) and nanostructured lipid carriers (NLCs) (Figure 1.20).[125–127]

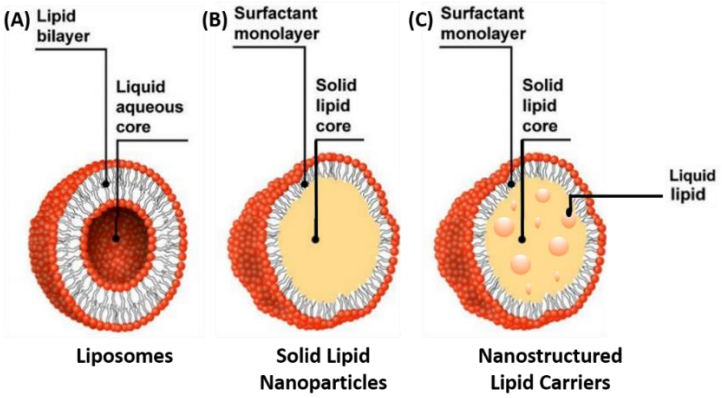

Figure 1.20: Illustration of (A) Liposomes, (B) SLNs and (C) NLCs as examples of more recent lipid derived nanoparticles. Diagram adapted from Balamurugan *et al.*[128]*:*

1.8.2.1 Solid Lipid Nanoparticles

SLNs were introduced as a new potential nanocarrier system in 1991, however they sparked further interest within the nanomedicine field following a publication by Muller *et al.* in 2000, that successfully highlights the opportunities amongst SLN systems for pharmaceutical translation.[129] These nanocarrier systems consist of three fundamental excipients: a physiological solid lipid, a compatible API and a stabilising polymer as shown in Figure 1.21.

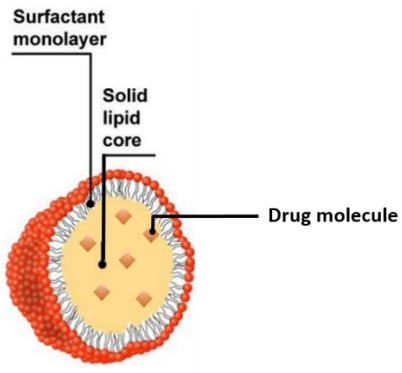

Figure 1.21: The generic structure of SLNs. Diagram adapted from: Balamurugan *et al.*[128]

SLNs were developed to combine the advantages of liposomes such as high chemical and physical stability, biocompatibility, specific targeting capabilities and sustained release.[130–132] Moreover, their composition of physiologically compatible excipients affords other

pharmacological benefits such as improvement of bioavailability and GI absorption, decreased toxicity with a simultaneous increase in efficacy for comparable dosages to non-formulated entities.[133,134] SLNs have been extremely successful at encapsulating a range of therapeutic agents for a variety of conditions, including, benzodiazepines oxazepam and diazepam, anticancer agent's doxorubicin, idarubicin and paclitaxel and hormones such as progesterone and so forth.[129 135,136]

1.8.2.2 Drawbacks of SLNs

Firstly, SLNs suffer from poor drug loading as the majority of the stabilised hydrophobic mass is the bulk solid lipid vehicle. This means that experimentally, there has to be a balance between achieving a drug loading significant enough to support clinical translation, whilst still formulating stable nanoparticles with optimum physical and pharmacological characteristics to provide targeted, sustained release profiles.

Secondly, solid lipids within SLNs often undergo polymorphic transitions that occur from an unstable high energy crystalline matrix to a more stable, highly ordered lattice (Figure 1.22).[137] Polymorphic transitions occur with many lipid cores, particularly with mixtures of mono- di- and triglyceride lipids which naturally exist in several different crystalline polymorphs. In many cases polymorphic transitions within the nanoparticle structures leads to drug expulsion upon storage and consequent drug precipitation, thus decreasing shelf life and viability for clinical translation (Figure 1.22).[137,138]

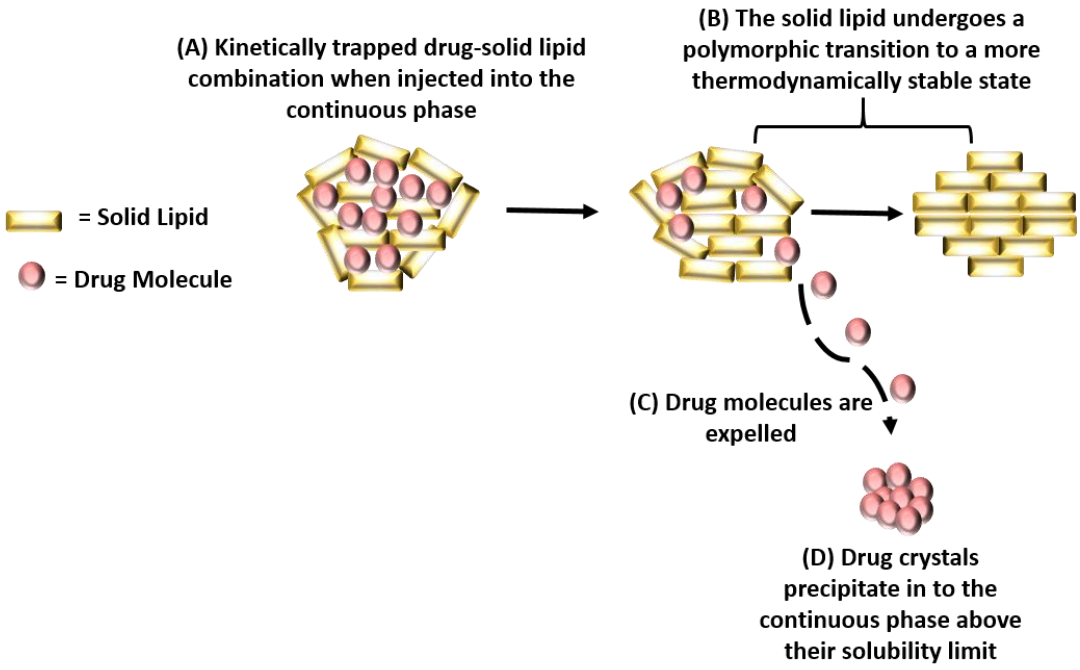

Figure 1.22: Illustration showing how polymorphic transitions cause drug expulsion and precipitation upon storage. (A) Drug molecules are kinetically trapped in an imperfect crystalline matrix of solid lipid molecules. (B) The solid lipid undergoes a polymorphic transition to a more ordered, thermodynamically stable state. (C) Drug molecules are expelled and (D) Insoluble drug crystals precipitate into the aqueous continuous phase.

Although the drawbacks associated with SLNs seem to be a significant challenge from a materials chemistry approach, this does not diminish the huge scope for SLN formulations. The biological and pharmacological advantages of SLNs provide unique opportunities for development within the field.

1.8.2.3 NLC Development

A population of 'second generation' lipid nanoparticles were developed, known as nanostructured lipid carriers (NLCs). Their development was inspired to combat the drawbacks associated with SLN formulations as discussed in section 1.8.2.2.[139] NLC formulations are very closely linked to SLNs in terms of their composition, however with an additional liquid lipid in the core of the carrier (Figure 1.23).[140] NLCs have analogous advantages to SLNs, such as chemical stability and decreased toxicity, biodegradability and scalability in comparison to alternative non-lipid (polymeric, inorganic nanoparticles) and lipid derived (liposomal) nanosystems.[139,141]

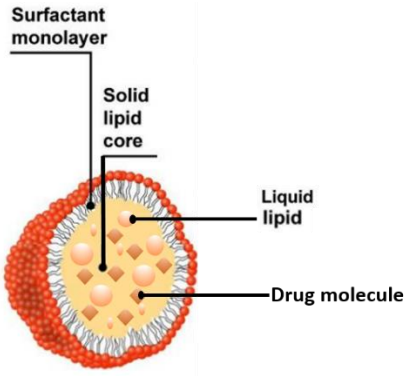

Figure 1.23: The generic structure of NLCs. Diagram adapted from: Balamurugan *et al*. [128]

Moreover, NLCs are often associated with higher drug loading within samples due to the addition of the liquid lipid within the core matrix which helps to solubilise hydrophobic drugs.[138,142] The addition of the liquid lipid accentuates significant other advantages such as enhancing controlled drug release profiles and stability over time, increased drug permeability and bioavailaibility.[143,144] The methods of production of NLCs and SLNs are also comparable and are discussed in the following section.

1.8.2.4 Methods of Preparation of SLNs and NLCs

SLN/NLC preparation methods vary greatly, from those requiring high mechanical stress such as, high pressure or hot homogenisation, ultrasonic emulsion evaporation and spray drying that have multiple advantages, particularly for scale up purposes.[131] However, more favourable, less costly, low mechanical stress methods often utilise nanoprecipitation techniques for their synthesis. Methods of production underpinned by nanoprecipitation includes the solvent diffusion method, solvent injection method (SIM), solvent evaporation and co-nanoprecipitation.[142,145] The SIM as a synthetic method to formulate nanoparticles is used throughout this thesis and is discussed in the section below.

1.8.2.5 Solvent injection method

For the SIM, the lipid core excipients and drug are dissolved in an organic, water miscible phase which is rapidly injected into the polymer containing aqueous phase through a needle (Figure 1.24). [152,155] It is important to note that the lipid excipients and the drug must be fully dissolved in the organic phase, which is often a problem for high melting point solid lipids,

which are relatively insoluble in most organic media.[156] Therefore for the injection of the hydrophobic material, the lipid must be heated ~10 °C above its melting point, in order to form a homogeneous, low viscosity mixture with the drug and organic solvent prior to injection.[131] This method of synthesis for SLNs/NLCs is illustrated in Figure 1.24.

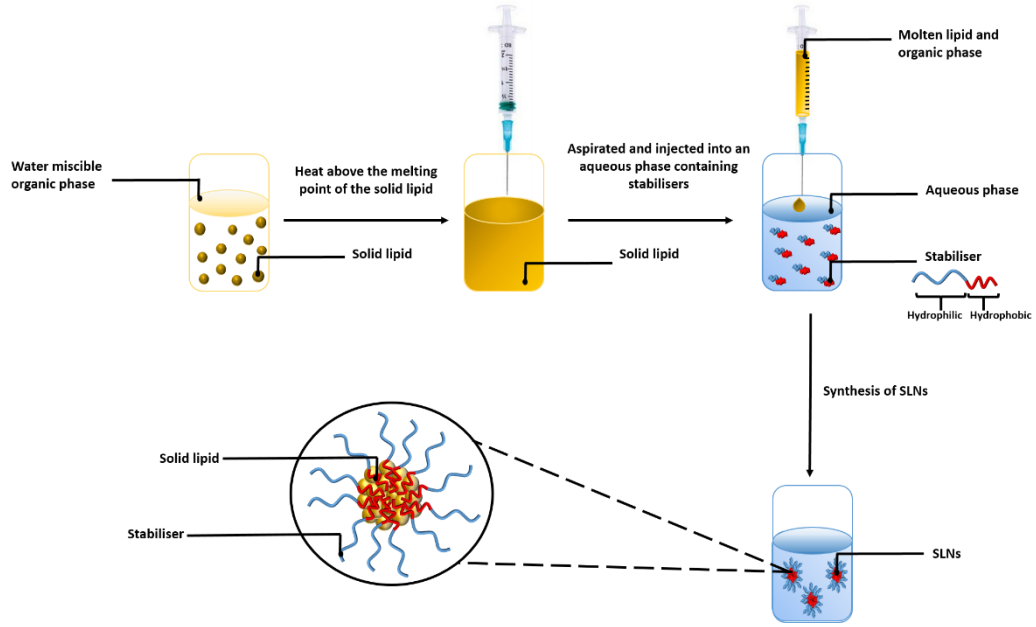

Figure 1.24: Solvent injection method for COMP-SLNs and COMP-NLCs

Upon injection of the hydrophobic material, the organic solvent droplets readily diffuse into the miscible aqueous phase, thereby causing lipid nuceli precipitation and the formation of SLNs/NLCs through the diffusion of stabilisers onto the lipid core.[155] The solvent can then be removed from the dispersion *via* several methods however, the most commonly used are dialysis, freeze drying, spray drying or centrifugation and washing. The choice of excipients for SLNs and NLCs are comparable with regards to their solid lipid and choice of stabiliser, with the only significant difference being the choice of the additional liquid lipids in NLCs. The commonly chosen excipients are discussed in the following section.

1.8.2.6 Solid Lipids for SLNs and NLCs

Lipid cores in SLN and NLC formulations allow for the solubilisation of a hydrophobic drug, as well as transportation and release of the drug molecule, before degrading into non-toxic excipients for clearance. Since the development of SLNs and NLCs, the most commonly used

solid lipids are triglycerides, with the general structure shown in Figure 1.25 and a list of common solid lipids are highlighted in Table 1.3.

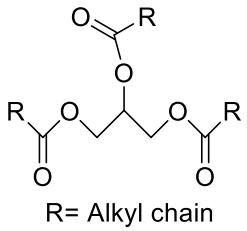

Figure 1.25: General structure of triglyceride solid lipids

Table 1.3: Solid lipid commonly used in SLN and NLC formulations

Brand name	**Solid Lipid**
	Glyceryl monostearate (C18)
Compritol 888 ATO	Mixture of mono, di and triglycerides of glyceryl behenate
Precirol ATO 5	Glyceryl distearate
-	Stearic acid (C18)
	Glyceryl tripalmitate (C16)
Gelot 64	Mixture of glyceryl monostearate and PEG-75 stearate
Emulcire 61	Mixture of cetyl lalcohol and ethoxylated fatty alcohols
Gelicure 44/14	Lauryl (C12) polyoxyl-32-glycerides, glycerol, polyethylene glycol-33 (PEG-33)
Geleol	Mixtures of mono, di and triesters of palmitic (C16) and stearic (C18) acids
Dynasan 116/ 118	Glyceryl trimyristate (C14) / Glyceryl tristearate (C18)

Compritol 888 ATO (COMP), a mixture of mono (12-18 %), di (52-54 %) and triglycerides (28-32 %) of behenic acid (Figure 1.26) and has proven to be one of the most common and compatible solid lipids for hydrophobic drug molecules.[137] COMP is advantageous over other solid lipids explored for drug delivery, predominantly due to its attractive sustained release properties. An example of this is given in a study reported by R Kumar *et al.*, highlighting the successful encapsulation of ketoprofen, a multi- use anti-inflammatory, in COMP-SLNs. This formulation showed a sustained release profile over a 72-hour time period, contrary to the recommended repetitive dosing of 3- or 4-times daily dependent on the condition treated.[157,158]

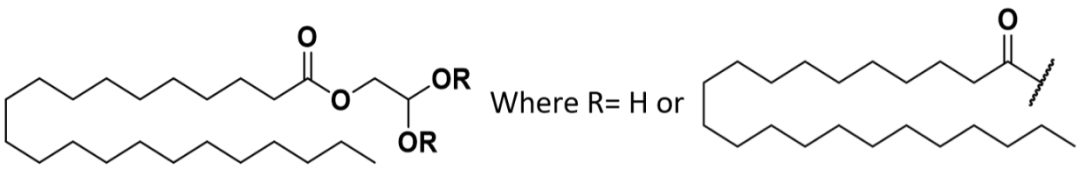

Figure 1.26: Structure of Compritol 888 ATO (COMP).

The solid lipid chosen for a particular SLN system is often predicted through a drug-lipid screening process. The aim of this process is to screen a range of several solid lipids with the drug of choice, in order to identify the physical mixture with optimum properties. These include decreased crystallinity of a drug-lipid mixture to identify the greatest degree of compatibility before formulations can be progressed.

1.8.2.7 Liquid Lipids excipients for NLCs

As previously stated, the addition of a liquid lipid for NLC formulations increases the capability to improve drug loading; firstly by increasing drug solubility and secondly by reducing drug expulsion.[159,160] Therefore, the choice of the liquid lipid is of paramount importance for the formulation development. Liquid lipids that are chosen for NLCs are decided through a compatibility screen to assess the solubility of the drug in the liquid lipid and the miscibility of the liquid and solid lipid, particularly when the solid lipid is molten as this is the physical state often used in NLC synthesis. There are a range of several liquid lipids commonly used shown below in Table 1.4.

Table 1.4: Liquid lipids commonly used in NLC formulations

Branded Liquid Lipid	**Liquid Lipid**
Miglyol 808, 812, 840	Medium chain triglycerides (C6-12)
Triolein	Glyceryl trioleate
Lauroglycol 90	Propylene glycol monolaurate
Capryol 90	Propylene glycol monocaprylate
Labrasol	PEG-8-caprylic/capric glycerides
-	Soybean oil- palmitic and stearic acid glycerides
-	Mineral oil- paraffins, napthalenes, hydrocarbons and aromatic compounds
-	Safflower oil- oleic, linoleic, palmitic and stearic acid glycerides
-	Sunflower oil oleic, linoleic, palmitic and stearic acid glycerides
-	Castor oil- ricinoleic acid
-	Oleic acid

Similarly, to the solid lipid excipients, liquid lipids are often derived from natural sources and therefore do not present unpredictable toxicity or biocompatibility setbacks at later stage of the formulation development, therefore aiding a more translatable formulation for clinical benefit. Examples of successful lipid derived and non-lipid derived nanomaterials used clinically are discussed in the following section.

1.9 Clinically approved nanoparticle therapeutics

In order for legal usage of new therapeutic materials, a regulatory body such as the US Food and Drug Administration (FDA), Therapeutic Goods Administration (TGA) or European Medicine Agency (EMA) must approve the material before being registered for commercial and human use.[166,167] The liposomal formulation, Doxil, was an early approved nanomedicine by the FDA in 1995, for the treatment of ovarian cancer with further approval for metastatic breast and multiple myeloma cancers and for Kaposki's sarcoma in HIV patients.[168,169] Doxil consisted of zwitterionic phospholipids and cholesterol to create oligolamellar liposomes to encapsulate doxorubicin and improve its pharmacokinetic parameters. In comparison to Doxil, the administered free doxorubicin was subject to extensive clearance, in particular by the liver and spleen, causing decreased circulation time and of limited therapeutic benefit.[169] By adopting polyethylene glycol (PEG) on the surface of the liposome, the circulation time of Doxil was increased. In turn, this allowed for sufficient concentrations to accumulate in the tumour site and extravasate within the tumour vasculature through the enhanced permeation and retention of the nanoparticles and in turn heavily reduced cardiotoxicity in patients.[169]

Since then, continual developments within the field have progressed and now nearly 40% of the current approved nanomedicines are either protein-polymer conjugates or liposomes.[168] Examples of approved materials are summarised by Anselmo *et al.* and are shown below in Table 1.4.[170]

Table 1.5**:** Examples of clinically approved nanomedicine formulations. [170]

Name	**Particle Type**	**Approved indication**	**Approval (Year)**
Doxil/ Caelyx	Liposomal doxorubicin (PEGylated)	Ovarian cancer , Metastatic breast cancer HIV associated Kaposki's sarcoma , Multiple myeloma	FDA (1995) EMA (1996)
DaunoXome	Liposomal daunorubicin (non-PEGylated)	HIV associated Kaposki's sarcoma	EMA (1996)
Myocet	Liposomal doxorubicin (non PEGylated)	Metastatic breast cancer	EMA (2000)
Abraxane	Albumin particle bound paclitaxel	Advanced nonsmall cell lung cancer Metastatic breast cancer, Metastatic pancreatic cancer	FDA (2005) EMA (2009)
Marqibo	Liposomal vincristine (non PEGylated)	Philidelphia chromosome negative actue lymphoblastic leukemia	FDA (2012)
MEPACT	Lipsoomes mifamurtide (non PEGy;ated)	Osteosarcome	EMA (2009)
Onivyde MM-398	Lipsoomal irinotecan (PEGylated)	Metastatic pancreatic cancer	FDA (2015)
ComoFer/INFeD/Ferrisat DexFerrum/DexIron	Iron dextran colloid Iron dextran colloid	Iron deficient anaemia Iron deficient anaemia	FDA (1992) FDA (1996)
Feragene/Rienso/Feumoxytol	Iron polyglucose sorbitol carboxymethylether colloid	Iron deficiency in patients with chronic kidney disease	FDA (2009)
Ferrlecit	Iron gluconate colloid	Iron replacement for anaemia treatment in patients with chronic kidney disease	FDA (1999)
Venofer	Iron sucrose colloid	Iron replacement for anaemia treatment in patients with chronic kidney disease	FDA (2000)
Injectafter/ Ferinject	Iron carboxymaltose colloid	Iron deficient anaemia	FDA (2013)
AmBisome	Lipsoomal amphortercin B	Cryptococcal Menningitis in HIV infected patients	FDA (1997)
Diprivan	Liposomal propofol	Induction and maintence of sedation or anesthesia	FDA (1989)

1.10 Nanomedicines for preterm birth

As previously stated, nanomedicine interventions are often employed for chronic conditions to improve current treatment options, decrease pill burdens and encourage prolonged release with specific cell targeting.[171] However, its uses for acute conditions such as preterm birth are not as extensively studied. There has been ongoing research into the development of liposomal formulations for preterm birth, some encapsulating indomethacin. As discussed in section 1.6.2, there are clear clinical drawbacks preventing the routine use of indomethacin due to its potential damaging effects on fetal health, despite its ability to prevent myometrial contractions. The recent development in liposomal formulations for preterm birth are discussed below.

1.10.1 Liposomal formulations for preterm birth

Liposomes, in addition to being the first FDA approved nanomedicine, attracted scientific attention due to their advantages over other nanomedicine formulations.[169] Liposomal development is now hugely diverse with formulations with surface conjugation to proteins, antibodies, targeting ligands or PEG, in order to increase cellular uptake (Figure 1.27).[172]

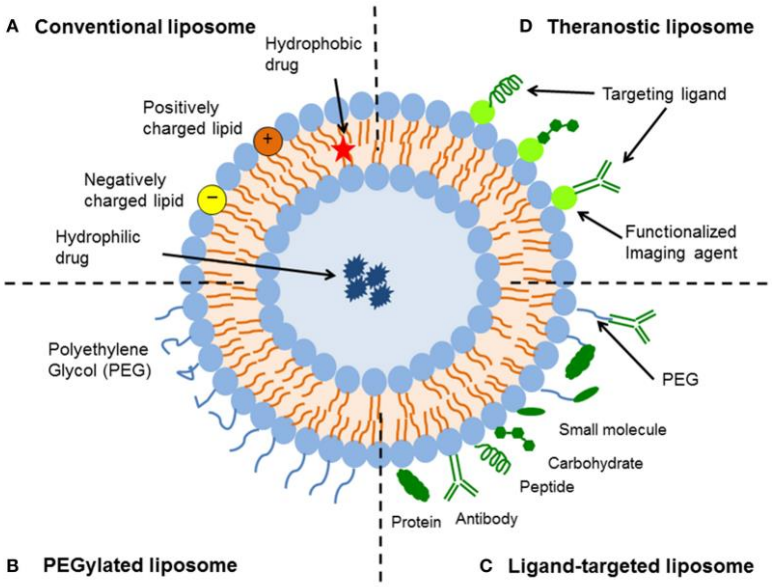

Figure 1.27**:** Illustration of the chemistry able to modify liposomal formulations to control physicochemical and pharmacokinetic parameters. Diagram adapted by Sercombe *et al.*[172]

To the best of our knowledge, the first reported indomethacin liposomal formulation for the prevention of preterm birth was published by J. Refuerzo *et al.* in 2015.[174] The group developed fluorescently labelled multilamellar liposomes (150-200 nm) synthesised from phosphatidylcholine and cholesterol *via* the lipid hydration-extrusion technique and contained 3.7 wt% indomethacin.[174] The fluorescently labelled particles were imaged to identify particle accumulation, which showed predominant uterine accumulation and minimal evidence of liposomal transfer throughout the placental barrier in a pregnant mouse model.[174] The liposomes were shown to decrease fetal indomethacin concentrations by 7.6 fold in comparison to the free drug when administered at 1 mg/kg, suggesting great potential to reduce the severity of fetal side effects.[174] J. Refuerzo *et al.* then published a further study in 2016 showing the development of uterine targeted liposomal formulations, denoted LIP-IND-ORA.[175] In comparison to the previous study, the same components were used to synthesise the liposomes, however a natural oxytocin receptor antagonist (ORA), atosiban, was added. The addition of this ligand adds targeting capabilities to the liposome and was added through conjugation of a PEG linker on the exterior of the liposome as shown in Figure 1.28.

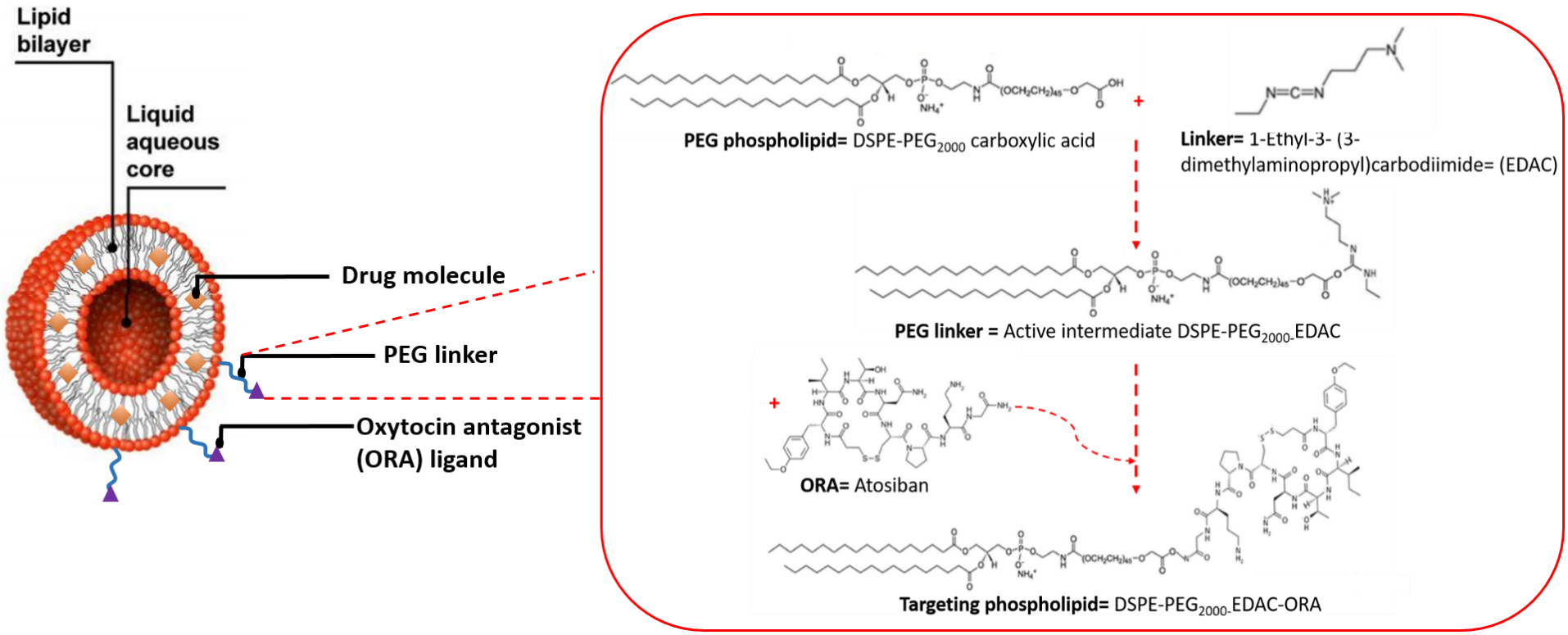

Figure 1.28: Illustration to show the chemical components of targeted Indomethacin liposomes reported by Refuerzo *et al.*[175]

This study focused on the difference between LIP-IND-ORA *vs* bulk indomethacin. They successfully showed that targeted LIP-IND-ORA formulations doubled the concentration of indomethacin reaching the uterus, coupled with a three-fold increase in concentration of LIP-IND-ORA in the uterus in comparison to the liver, placenta or the fetus.[175] Nevertheless, they did not compare non-targeted indomethacin liposomes *vs* targeted LIP-IND-ORA on their ability to prevent preterm birth *in vivo*.[175] Paul *et al.* then reported uterine targeted liposomes containing tocolytic nifedipine, salbutamol, rolipram and indomethacin in 2017.[176] Liposomes contained excipients cholesterol and the phospholipid 1-2 distearoyl-sn-glycero-phosphocoline (DSPC), as adopted from a method developed by Hua *et al*. in 2011 for the development of antibody conjugated liposomes.[177] In order to add a myometrial targeting functionality, 1,2-diastearoyl-*sn*-glycero-3-phospho-ethanolamine-N-(PEG_{2000})-malemide (DSPE) was used as a PEG-linker and conjugated to an anti-oxytocin receptor antibody and the resulting liposomes were synthesised by high pressure extrusion.[176] Their key findings showed that nifedipine, salbutamol and rolipram oxytocin receptor (OR) targeted liposomes were able inhibit human myometrial contractility. [176] Nevertheless, indomethacin loaded OR targeted liposomes were the most effective in reducing preterm birth rates to 18% in an inflammatory mouse model. However, non-targeted liposomes had no significant effect and remained at a preterm birth rate percentage of 58%.[176] As of 2019, further studies were published by Hua *et al.* containing tocolytic agent nifedipine or salbutamol hemisulfate.[178] This study aimed to explore the *in vitro* mechanisms of cellular uptake, internalization and toxicity profiles of the liposomal materials, rather than *in vivo* assessment of preterm contractility inhibition as conducted by Paul *et al.*[176,178] In agreement with the previous studies by Refuerzo *et al.* and Paul *et al.*, this study showed that the incorporation of ORA ligands enhanced cellular interactions with myometrial tissue, with potential to increase tocolytic efficacy and decrease dosage profiles.[175,176,178] Hua *et al.* later explored the effect of different oxytocin receptor targeting ligands, on the same liposomes containing salbutamol hemisulfate or nifedpine.[179] This study revealed that regardless of the targeting ligand (either an anti-ORA monoclonal antibody (ORA-LIP) or atosiban (ATO-LIP)), the quantity and mechanism of

cellular uptake and effect on cell viability remained comparable in all cases. Additionally, both sets of targeting ligands enhanced myometrial cellular internalisation from conventional liposomes from 4% to 82% (OR-LIP) and 86% (ATO-LIP).[179] This study also highlights further versatility in treatment for ORA targeted liposomes in endometrium adenocarcinoma, neuroblastoma, breast cancer and glioma as these cancers have upregulated expression of OTR receptors.[179]

1.10.2 Pre-existing nanoformulations of Indomethacin

Indomethacin is a drug with versatile uses with indications other than preterm birth. As such, has been incorporated into other available nanomedicine formulations. As an NSAID, it has multiple clinical benefits due to its anti-inflammatory, anti-pyretic and analgesic properties.[135] Although it is most commonly used within the obstetric field, there are also reported cases for postoperative uses, such as after reversing permanent muscle shortening surgeries, osteoarthritis, gout and chronic ocular inflammatory diseases.[180–182]

There are multiple reports of polymeric derived nanomaterials containing indomethacin, with most frequent literature references incorporating the polymer Ɛ-polycaprolatcone (PCL). Elmowafy *et al.*, compared the synthesis of indomethacin loaded nanospheres (NS) containing drug embedded into a solid polymer matrix and nanocapsules (NC) with drug embedded into a hollow or liquid polymer matrix and protected by a polymeric vesicle (Figure 1.29). Both formulation subtypes were used PCL or hydroxylpropyl β-cyclodextrin (HP β-CD) and Tween 80 for the formation of a topical transdermal drug delivery system, with NC's containing Miglyol 812 as the liquid oil for the capsule core.[183]

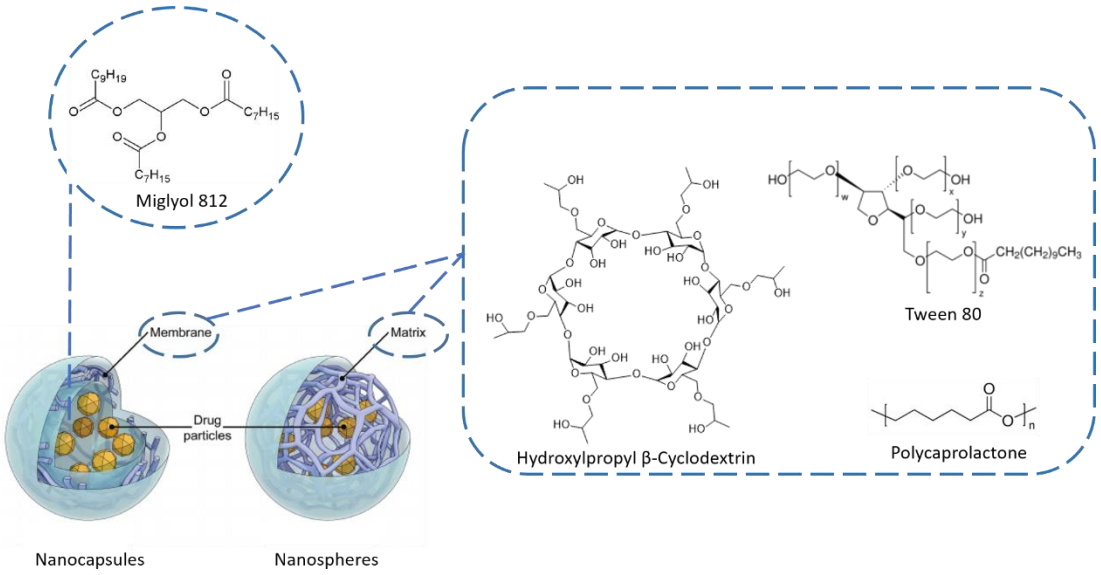

Figure 1.29**:** Schematic showing Indomethacin loaded nanospheres (NS) and nanocapsules (NCs) as formulated by *Elmowafy et al.* [183]

This group successfully synthesised NS (137-142 nm) and NC (185-193 nm) loaded with 1 wt% of indomethacin and showed successful encapsulation efficiencies ranging from 93-98%. Moreover, consequent gel formulations made using methylcellulose had improved *in vitro* release profiles in comparison to commercially available gel, Indotopic®, as well as having a comparable 1 wt% of indomethacin.[183] Consequently, the NC formulations had significantly better analgesic and anti-inflammatory properties than NS formulations.[183] Furthermore, a recent paper published by Styliari *et al.* highlights the frequent use of AB block copolymer methoxy polyethylene glycol-polycaprolactone (mPEG-*b*-PCL) polymer to stabilise indomethacin crystals (Figure 1.30).[99]

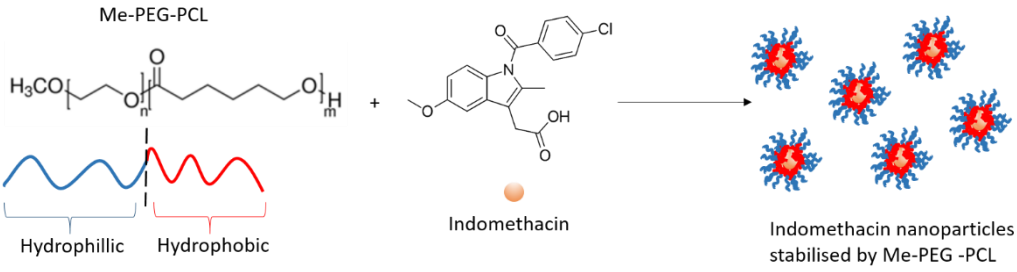

Figure 1.30**:** Structure of methyoxy polyethylene glycol- polycaprolactone AB block copolymer used to successfully encapsulate Indomethacin.

Interestingly, Shin *et al*. reported that the nanoprecipitation of mPEG-*b*-PCL was able to encapsulate indomethacin and develop a trend showing that as the repeating units of PCL were

increased, higher indomethacin loading efficiencies were achieved, however with slower release over time.[184,185] This behaviour can be attributed to the strong hydrophobic affinities between indomethacin and Ɛ-caprolactone chains.[185] There is a theoretical potential for this to be of pharmacokinetic benefit, with slower release allowing prolonged time for the formulation to remain intact and thus increase circulation time, or in preventing burst release. Nevertheless, experiments would have to be carried out in order to support this hypothesis and were not explored in this study.

In addition to PCL, other indomethacin loaded polymeric nanoparticles have included the use of polyvinylpyrrolidine (PVP), polyethylene glycol-*b*-polylactic-*co*-glycolic acid (PEG-*b*-PLGA) and polylactide (PLA) (Figure 1.31).[186–189]

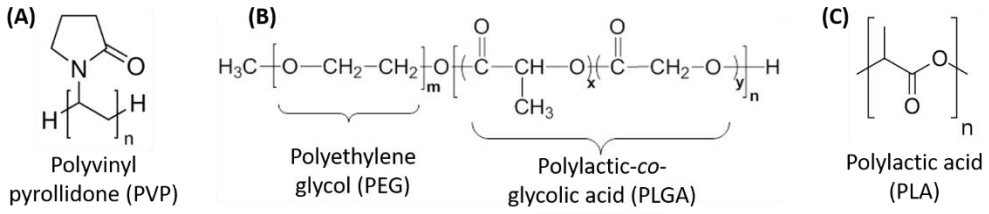

Figure 1.31**:** Chemical structures of (A) PVP (B) PEG-*co*-PLGA and (C) PLA as example stabilisers previously used in Indomethacin loaded nanoformulations

The use of PVP in nanoparticle synthesis has been heavily adopted due to its ability to act as a surface stabiliser, a dispersant and a reducing agent, whereas PEG-PLGA and PLA polymers benefit from biocompatibility and degradability and thus been found in previous FDA approved formulations.[190–192]

On the contrary to polymeric materials, lipid derived carriers other than liposomes (SLNs, NLCs, and lipid-polymer hybrids) have become of high importance within the nanomedicine field due to their advantageous pharmacological compatibility. In 2013, Hippalgoanker *et al.* developed indomethacin loaded SLNs for the treatment of chronic ocular inflammation.[135] The SLNs were synthesised through a hot homogenisation technique to produce 1.87 wt% Indomethacin SLNs with a Z average (D_z) of 140 ± 5 nm. The SLN formulation was compared directly against Indocollyre®- commercially available indomethacin eye drops containing 0.1

wt% of drug.[135] The results showed that the indomethacin SLN formulation increased corneal permeation (Figure 1.32) without effecting corneal integrity. This therefore suggests that SLNs may improve the safety and efficacy for the treatment of ocular inflamation.[135]

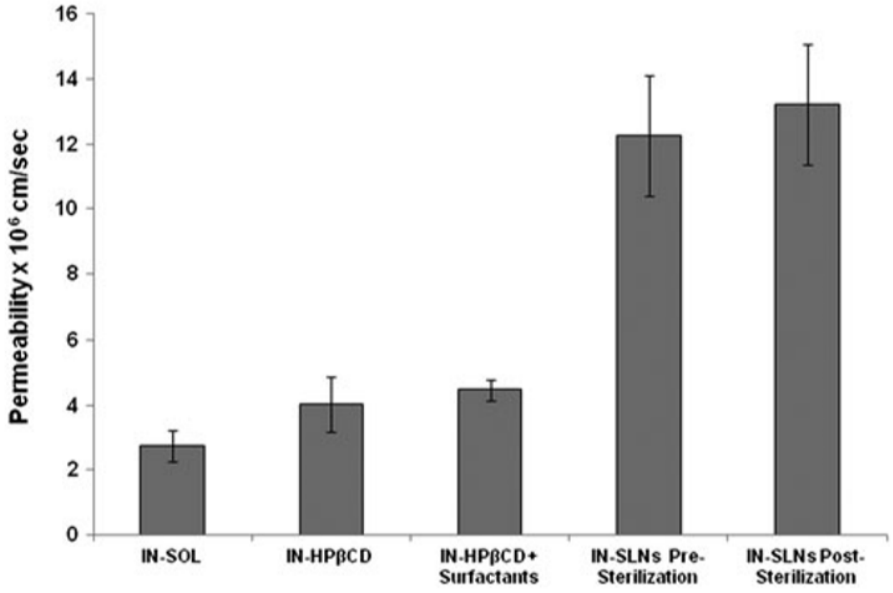

Figure 1.32: Hippalgaonkar *et al.* showed that indomethacin SLNs (IN-SLNs) demonstrated the highest corneal permeability for the treatment of ocular inflammation.[193]

Balguri *et al*. then published a secondary study to assess the delivery of indomethacin SLNs to the posterior segment ocular tissues for the treatment of conditions such as macular edema and ocular inflammation.[136] Balguri *et al*. used the same excipients as described by Hippalgoanker *et al.* for SLN formation, functionalised with chitosan chloride to enhance ocular tissue penetration, forming particles with D_z values of 265 ± 8 nm.[136] Further in-depth studies from their work show that the addition of a liquid lipid, Miglyol 812 or 829, formed monomodal NLCs (227 ± 11 nm) with a 5 fold higher concentration of indomethacin to the ocular tissues than chitosan chloride functionalised SLNs.[136] This leads to the aim of this thesis, to develop on the current literature to advance current indomethacin loaded formulations for the prevention of preterm birth.

1.11 Thesis outline and aims

The research described in this thesis investigates different nanomedicines for the delivery of indomethacin with future applications in the treatment of preterm birth. The thesis is made up of four experimental chapters, each chapter includes a brief introduction to prime the reader with the underpinning literature and background. It is evident from the current literature, that liposomal formulations are the main focus of research into new treatments for prematurity as demonstrated by Refuerzo, Paul and Hua.[175,176,178] Liposomal development is the subject of much interest due to their general success within the nanomedicine field, as accredited by the regulatory approved formulations, and their biological advances that they possess over other nanomedicines.[172,173] Nevertheless, as with all nanomedicines there are disadvantages of liposomes including poor encapsulation efficiencies of therapeutics, poor release profiles and lower successes for *in vivo* targeting.[194] As a result, this thesis investigates other nanomedicine derivatives for the encapsulation and delivery of indomethacin as a tocolytic agent. Solid lipid nanoparticles, nanostructured lipid carriers, nanoemulsions and solid drug nanoparticles as potential candidates are briefly discussed below.

Chapter 2 explores the development of SLNs as potential indomethacin carriers. The development of indomethacin SLNs has previously shown benefits for bioavailability and pharmacokinetic advances for the treatment of ocular inflammation.[193] The information gathered from the research by Hippalgaonkar *et al*. was used as an initial platform for formulation development for SLNs for preterm birth prevention.[193] Throughout Chapter 2 a range of experimental parameters were optimised. These included the solid lipid choice, solid lipid mass, solvent: antisolvent ratios, stabiliser choice and stabiliser concentrations. The use of analytical techniques including differential scanning calorimetry (DSC) and powder X ray diffraction (PXRD) were implemented. These techniques were used to test the hypothesis that the thermograms and diffraction patterns can identify favourable and unfavourable interactions between two different bulk excipients. The final formulation enabled

encapsulation of indomethacin with a drug loading of 3 wt%. The successes and drawbacks of the formulation are thoroughly discussed throughout the Chapter 2.

Chapter 3 explores the relationship between Pluronic® stabilisers and their ability to tune the polarity of the core lipid environment in SLNs. From Chapter 2, the successful development of indomethacin SLNs was strongly dependent on the Pluronic® stabiliser that was used. Therefore, Chapter 3 probes the relationship between Pluronic® stabiliser properties, their ability to colloidally stabilise SLNs and their ability to tune the polarity microenvironment. It was hypothesised that the stability of SLNs was dependent on the affinity of the interaction between the Pluronic® stabilisers and the lipid core. The different affinities result in changes in the lipid core polarity, as the non-polar region of the Pluronic® stabiliser adsorbs to different extents with the non-polar lipid core. The changes in polarity were monitored *via* the implementation of pyrene as a small molecule fluorescent probe. Pyrene was chosen due to its extensive use in monitoring core polarity of polymeric materials and polymer properties.[195–197]

Chapter 4 investigates the formation of indomethacin NLCs in comparison to SLN formulations. NLCs are comparable formulations to SLNs with respect pharmacological advantages and within their scope for targeted/ non-targeted drug delivery systems.[198] However, a fundamental advantage observed with NLCs is their significantly increased ability to enhance drug loading within the formulations.[136] This is attributed to the addition of a liquid lipid within the core of the particles, in comparison to a sole solid lipid in SLN formulations. The aim of Chapter 4 was to increase the drug loading of indomethacin SLNs formed in Chapter 2. The liquid lipids employed were soybean, mineral, safflower, sunflower and castor oil due to their low cost, abundance and previous success in NLC formulations.[144,199–202] The successes and drawbacks of indomethacin NLCs formed at 10 wt% drug loading are discussed and the subsequent development of indomethacin nanoemulsions at 5 wt% were discovered.

Chapter 5 explores the development of indomethacin SDNs as an alternative formulation subtype to lipid derived nanoparticles. The experimental investigation of SDNs was initiated

due to an increased ability of SDNs to accommodate higher drug loadings than lipid derived nanoparticles.[114,119] Therefore, this rendered SDNs a more translatable formulation for indomethacin due to the clinical dosage required for preterm birth prevention (dosage regimes discussed in section 1.6.2.2). The experimental optimisation to reach SDN formulations containing 30 wt% of several indomethacin analogues are discussed throughout Chapter 5.

1.12 References

1 A. M. Jukic, D. D. Baird, C. R. Weinberg, D. R. Mcconnaughey and A. J. Wilcox, *Hum. Reprod.*, 2013, **28**, 2848–2855.

2 D. Briscoe, H. Nguyen, M. Mencer, N. Gautam and D. B. Kalb, *Am. Fam. Physician*, 2005, **71**, 1935–1941.

3 Y. Rofé, M. B. Littner and I. Lewin, *J. Clin. Psychol.*, 1993, **49**, 3–12.

4 V. Hundley, S. Downe and S. J. Buckley, *Best Pract. Res. Clin. Obstet. Gynaecol.*, 2020, **67**, 4–18.

5 L. Dixon, J. Skinner and M. Foureur, *New Zeal. Coll. Midwives J.*, 2013, **48**, 15–23.

6 M. De and G. W. Wood, *J. Endocrinol.*, 1990, **126**, 417.

7 G. Dante, V. Vaccaro and F. Facchinetti, *Facts, views Vis. Obstet. Gynaecol.*, 2013, **5**, 66–71.

8 G. Di Renzo, I. Giardina, G. Clerici, E. Brillo and S. Gerli, *Horm. Mol. Biol. Clin. Investig.*, 2016, **27**, 35–48.

9 A. C. Turnbull, A. P. F. Flint, J. Y. Jeremy, P. T. Patten, M. J. N. C. Keirse and A. B. M. Anderson, *Lancet*, 1974, **303**, 101–104.

10 A. Livshits and D. S. Seidman, *Pharmaceuticals*, 2010, **3**, 2082–2088.

11 S. Arrowsmith, A. Kendrick and S. Wray, *Obstet. Gynaecol. Reprod. Med.*, 2010, **20**, 241–247.

12 S. Arrowsmith and S. Wray, *J. Neuroendocrinol.*, 2014, **26**, 356–369.

13 World Health Organization (WHO), New global estimates on preterm birth, https://www.who.int/reproductivehealth/global-estimates-preterm-birth/en/, (accessed 28 May 2020).

14 L. Liu, S. Oza, D. Hogan, Y. Chu, J. Perin, J. Zhu, J. E. Lawn, S. Cousens, C. Mathers and R. E. Black, *Lancet*, 2016, **388**, 3027–3035.

15 National Institute for Health and Care Excellence (NICE), *Preterm labour and birth*, 2016.

16 W. A. Engle, K. M. Tomashek, C. Wallman, A. R. Stark, D. H. Adamkin, D. G. Batton, E. F. Bell, V. K. Bhutani, S. E. Denson, G. I. Martin, K. L. Watterberg, W. Engle, K. J. Barrington, G. D. V. Hankins, T. N. K. Raju and J. Couto, *Am. Acad. Pediatr.*, 2007, **120**, 1390–1401.

17 S. Al-Alaiyan, *Ann. Saudi Med.*, 2008, **28**, 1–3.

18 P. I. Macfarlane, S. Wood and J. Bennett, *Arch. Dis. Child. Fetal Neonatal Ed.*, 2003, **88**, 199–202.

19 P. T. B Larroque, G Breart, M Kaminski, M Dehan, M Andre, A Burguet, H Grandjean, B Ledesert, C Leveque, F Maillard, J Matis, J Roze, *Arch. Dis. Child. Fetal Neonatal Ed.*, 2004, **89**, 139–144.

20 J. Chatterjee, J. Gullam, M. Vatish and S. Thornton, *Arch. Dis. Child. Fetal Neonatal Ed.*, 2007, **92**, 88–93.

21 R. F. Lamont, *BJOG An Int. J. Obstet. Gynaecol.*, 2003, **110**, 71–75.

22 F. M. Ubaldi, D. Cimadomo, A. Vaiarelli, G. Fabozzi, R. Venturella, R. Maggiulli, R. Mazzilli, S. Ferrero, A. Palagiano and L. Rienzi, *Front. Endocrinol. (Lausanne).*, 2019, **10**, 1–18.

23 K. S. Montgomery, S. Cubera, C. Belcher, D. Patrick, H. Funderburk, C. Melton and M. Fastenau, *J. Perinat. Educ.*, 2005, **14**, 26–35.

24 F. Fuchs and M. V. Senat, *Semin. Fetal Neonatal Med.*, 2016, **21**, 113–120.

25 G. Puccio, M. Giuffré, M. Piccione, E. Piro, V. Malerba and G. Corsello, *Ital. J. Pediatr.*, 2014, **40**, 1–7.

26 B. S. Muhlhausler, S. N. Hancock, F. H. Bloomfield and R. Harding, *Pediatr. Res.*, 2011, **70**, 117–122.

27 L. Lightstone, *Pregnancy*, 2015, **43**, 550–555.

28 M. Choudhary, Preterm Risk Prediction Tests Not Suitable as Routine Screens, https://www.medindia.net/news/healthinfocus/preterm-risk-prediction-tests-not-

suitable-as-routine-screens-168587-1.htm.
29 L. nan Zeng, L. li Zhang, J. Shi, L. ling Gu, W. Grogan, M. M. Gargano and C. Chen, *Taiwan. J. Obstet. Gynecol.*, 2014, **53**, 443–451.
30 S. Vause and T. Johnston, *Arch. Dis. Child. Fetal Neonatal Ed.*, 2000, **83**, 79–85.
31 R. L. Goldenberg, J. F. Culhane, J. D. Iams and R. Romero, *Lancet*, 2008, **371**, 75–84.
32 M. E. Griese and S. A. Prickett, *Princ. Pract.*, 2001, **22**, 311–315.
33 M. L. Hediger, T. O. Scholl, J. I. Schall and P. M. Krueger, *Ann. Epidemiol.*, 1997, **7**, 400–406.
34 A. A. M. Da Silva, V. M. F. Simões, M. A. Barbieri, H. Bettiol, F. Lamy-Filho, L. C. Coimbra and M. T. S. S. B. Alves, *Paediatr. Perinat. Epidemiol.*, 2003, **17**, 332–339.
35 O. Demirci, E. Yılmaz, Ö. Tosun, P. Kumru, A. Arınkan, D. Mahmutoğlu, S. Selçuk, Z. N. Dolgun, R. Arısoy, E. Erdoğdu and N. Tarhan, *Balkan Med. J.*, 2016, **33**, 344–349.
36 M. L. Hediger, T. O. Scholl, J. I. Schall and P. M. Krueger, *Ann. Epidemiol.*, 1997, **7**, 400–406.
37 S. Cnattingius, *Am. J. Epidemiol.*, 1997, **145**, 319–323.
38 B. N. Jahromi and Z. Husseini, *Taiwan. J. Obstet. Gynecol.*, 2008, **47**, 318–321.
39 S. Y. Chu, W. M. Callaghan, S. Y. Kim, C. H. Schmid, J. Lau, L. J. England and P. M. Dietz, *Pathophysiol. Complicat.*, 2007, **30**, 2070–2076.
40 C. Carson, M. Redshaw, R. Gray and M. A. Quigley, *BMJ Open*, , DOI:10.1136/bmjopen-2015-007942.
41 M. M. Edhi, H. M. Aslam, Z. Naqvi and H. Hashmi, *BMC Res. Notes*, 2013, **6**, 1–6.
42 B. A. Kebede, R. A. Abdo, A. A. Anshebo and B. M. Gebremariam, *PLoS One*.
43 E. Chandraharan and A. Krishna, *BMJ*.
44 K. Treyvaud, K. J. Lee, L. Q. Doyle and P. J. Anderson, *J. Pediatr.*, 2014, **164**, 515–521.
45 A. R. Misund, P. Nerdrum and T. H. Diseth, *BMC Pregnancy Childbirth*, 2014, **14**, 1–8.
46 C. Blackburn and M. Harvey, *Early Child Dev. Care*, 2020, **190**, 296–309.
47 C. Ionio, C. Colombo, V. Brazzoduro, E. Mascheroni, E. Confalonieri, F. Castoldi and G. Lista, *Eur. J. Psychol.*, 2016, **12**, 604–621.
48 A. Bry and H. Wigert, *BMC Psychol.*, 2019, **7**, 1–12.
49 C. Course and M. Chakraborty, *Sci. Rep.*, 2020, **10**, 1–7.
50 G. Saccone and V. Berghella, *Br. Med. J.*, 2016, **355**, 1–17.
51 P. O. Nkadi, T. A. Merritt and D. M. Pillers, *Mol. Genet. Metab.*, 2009, **92**, 95–101.
52 D.-A. M. P. Paul O. Nkadi, T. Allen Merritt, *Natl. Inst. Heal.*, 2010, **97**, 95–101.
53 J. Dyer, *P&T Community*, 2019, **44**, 12–14.
54 C. Anderson and N. H. Hillman, *Mo. Med.*, 2019, **116**, 117–122.
55 H. C. Glass, A. T. Costarino, S. A. Stayer, C. Brett, F. Cladis and P. J. Davis, *Anesthsia Analg.*, 2015, **120**, 1337–1351.
56 O. Olaloko, R. Mohammed and U. Ojha, *Int. J. Gen. Med.*, 2018, **11**, 265–274.
57 J. Pietz, B. Achanti, L. Lilien, E. C. Stepka and S. K. Mehta, *Pediatrics*.
58 R. M. Ward and J. C. Beachy, *BJOG An Int. J. Obstet. Gynaecol.*, 2003, **110**, 8–16.
59 W. E. BERDON, H. GROSSMAN, D. H. BAKER, A. MIZRAHI, O. BARLOW and W. A. BLANC, *Radiology*, 1964, **83**, 879–887.
60 K. Ahya and P. Suryawanshi, *Res. Reports Neonatalogy*, 2017, **8**, 1–8.
61 K. . Ahya and P. Suryawanshi, *Res. Reports Neonatol.*, 2017, **8**, 1–8.
62 M. M. S. Jan, *Ann. Saudi Med.*, 2006, **26**, 123–132.
63 H. K. Graham, P. Rosenbaum, N. Paneth, B. Dan and J. Lin, *Nat. Rev. Dis. Prim.*, 2016, **2**, 1–25.
64 S. Arrowsmith, P. Keov, M. Muttenthaler and C. W. Gruber, *J. Vis. Exp.*, 2018, **2018**, 1–12.
65 A. Sarah, N. James, B. Leanne and W. Susan, *Reprod. Sci.*, 2016, **23**, 98–111.
66 Pathways-NICE, *Natl. Inst. Heal. Care Excell.*, 2019, 1–12.
67 R. Romero, A. Conde-Agudelo, E. Da Fonseca, J. M. O'Brien, E. Cetingoz, G. W.

Creasy, S. S. Hassan and K. H. Nicolaides, *Am. J. Obstet. Gynecol.*, 2018, **218**, 161–180.
68 G. C. Di Renzo, A. Rosati, A. Mattei, M. Gojnic and S. Gerli, *Int. J. Obstet. Gynaecol.*, 2005, **112**, 57–60.
69 J. M. Dodd and C. A. Crowther, *Int. J. Womens. Health*, 2009, **1**, 73–84.
70 E. R. Norwitz and A. B. Caughey, *Rev. Obstet. Gynecol.*, 2011, **4**, 60–72.
71 Royal College of Obstetricians and Gynaecologists, Progesterone could prevent 8,450 miscarriages a year, finds new research, https://www.rcog.org.uk/en/news/progesterone-could-prevent-8450-miscarriages-a-year-finds-new-research/.
72 D. Jm, G. Rm, O. Cm and D. Ar, *Cochrane Database Syst. Rev.*, 2019, 1–3.
73 S. Wood, S. Ross, S. Tang, R. Sauve and R. Brant, *J. Perinat. Med.*, 2012, **40**, 593–599.
74 Z. Alfirevic, T. Stampalija and N. Medley, *Cochrane Database Syst. Rev.*, , DOI:10.1002/14651858.CD008991.pub3.www.cochranelibrary.com.
75 M. Chandiramani and A. H. Shennan, *Obs. Gynaecol.*, 2008, **10**, 99–106.
76 R. Simcox and A. Shennan, *Int. J. Surg.*, 2007, **5**, 205–209.
77 B. Koullali, A. R. Westervelt, K. M. Myers and M. D. House, *Semin. Perinatol.*, 2018, **41**, 505–510.
78 D. M. Haas, D. M. Caldwell, P. Kirkpatrick, J. J. McIntosh and N. J. Welton, *Br. Med. J.*, 2012, **345**, 1–16.
79 M. Hanley, L. Sayres, E. Reiff, A. Wood, C. Grotegut and J. Kuller, *Obstet. Gynecol. Surv.*, 2019, **74**, 50–55.
80 D. G. Waller and A. P. Sampson, in *Medical Pharmacology and Therapeutics (Fifth Edition)*, 2018, pp. 513–529.
81 H. Van Geijn, in *Drugs During pregnancy and Lactation (Second Edition)*, 2007, pp. 368–380.
82 A. Carlin, J. Norman, S. Cole and R. Smith, *Br. Med. J.*
83 R. Gáspár and J. Hajagos-tóth, *Pharmaceuticals*, 2013, **6**, 689–699.
84 S. Songthamwat and C. N. Nan, *Int. J. Womens Heal.*, 2018, **10**, 317–323.
85 S. Guclu, M. Gol, U. Saygili, N. Demir, O. Sezer and A. A. Baschat, *Ultrasound Obstet. Gynecol.*, 2006, **27**, 403–408.
86 R. Brusseau, *Fetal Intervention and the EXIT Procedure*, Elsevier Inc., Sixth Edit., 2019.
87 K. J. Sales and H. N. Jabbour, *Reproduction*, 2009, **126**, 559–567.
88 I. L. Meek, M. A. F. J. van de Laar and H. E. Vonkeman, *Pharmaceuticals*, 2010, **3**, 2146–2162.
89 R. T. Taylor, E. C. Huskisson, G. H. Whitehouse, F. D. Hart and D. H. Trapnell, *Br. Med. J.*, 1968, **4**, 734–737.
90 Royal College of Obstetricians and Gynaecologists, Indomethacin, https://elearning.rcog.org.uk/preterm-labour/management/tocolysis/indomethacin.
91 H. Shehata, *Drugs and drug therapy*, Elsevier Ltd, Fourth Edi., 2010.
92 C. D. Cuppett and S. N. Caritis, *Uterine Contraction Agents and Tocolytics*, Elsevier Inc., 2013.
93 G. J. Anger and M. Piquette-Miller, *Pharmacokinetics in pregnancy*, Elsevier Inc., 2017.
94 A. Beverly and M. D. Von Der Pool, *Am. Fam. Physician*, 1998, **57**, 2457–2464.
95 G. Alvan, M. Orme, L. Bertilsson, R. Ekstrand and L. Palmer, *Clin. Pharmacol. Ther.*, 1975, **18**, 364–373.
96 G. H. Hawthorne, M. P. Bernuci, M. Bortolanza, A. C. Issy and E. Del-Bel, *Clinical Developments in Antimicrobial Nanomedicine: Toward Novel Solutions*, Elsevier Inc., 2017.
97 S. Saallah and I. W. Lenggoro, *KONA Powder Part. J.*, 2018, **2018**, 89–111.
98 A. Charalabidis, M. Sfouni, C. Bergström and P. Macheras, *Int. J. Pharm.*, 2019, **566**, 264–281.

99 I. D. Styliari, V. Taresco, A. Theophilus, C. Alexander, M. Garnett and C. Laughton, *RSC Adv.*, 2020, **10**, 19521–19533.
100 J. Rautio, H. Kumpulainen, T. Heimbach, R. Oliyai, D. Oh, T. Järvinen and J. Savolainen, *Nat. Rev. Drug Discov.*, 2008, **7**, 255–270.
101 G. . Amidon, H. Lennernas, V. . Shah and J. . Crison, *Am. Assoc. Pharm. Sci.*, 2014, **16**, 894–898.
102 A. Dahan, J. M. Miller and G. L. Amidon, *AAPS J.*, 2009, **11**, 740–746.
103 L. Arms, D. W. Smith, J. Flynn, W. Palmer, A. Martin, A. Woldu and S. Hua, *Front. Pharmacol.*, 2018, **9**, 1–17.
104 A. ElShaer, S. Khan, D. Perumal, P. Hanson and A. R. Mohammed, *Curr. Drug Deliv.*, 2011, **8**, 363–372.
105 Z. Li, C. Xiao, T. Yong, Z. Li, L. Gan and X. Yang, *Chem. Soc. Rev.*, 2020, **49**, 2273–2290.
106 C. Fornaguera and C. Solans, *J. Pers. Med.*, 2017, **7**, 1–16.
107 G. Chen, Y. Wang, R. Xie and S. Gong, *Adv. Drug Deliv. Rev.*, 2019, **130**, 58–72.
108 R. Duncan, *Curr. Opin. Biotechnol.*, 2011, **22**, 492–501.
109 N. Larson and H. Ghandehari, *Chem. Mater.*, 2012, **24**, 840–853.
110 A. Xie, S. Hanif, J. Ouyang, Z. Tang, N. Kong, N. Y. Kim, B. Qi, D. Patel, B. Shi and W. Tao, *EBioMedicine*, 2020, **56**, 102821.
111 H. Zhang, D. Wang, R. Butler, N. L. Campbell, J. Long, B. Tan, D. J. Duncalf, A. J. Foster, A. Hopkinson, D. Taylor, D. Angus, A. I. Cooper and S. P. Rannard, *Nat. Nanotechnol.*, 2008, **3**, 506–511.
112 M. Siccardi, P. Martin, D. Smith, P. Curley, T. Mcdonald, M. Giardiello, N. Liptrott, S. Rannard and A. Owen, *J. Interdiscip. Nanomedicine*, 2016, **1**, 110–123.
113 B. Deschamps, N. Musaji and J. A. Gillespie, *Int. J. Nanomedicine*, 2009, **4**, 185–192.
114 T. O. Mcdonald, M. Giardiello, P. Martin, M. Siccardi, N. J. Liptrott, D. Smith, P. Roberts, P. Curley, A. Schipani, S. H. Khoo, J. Long, A. J. Foster, S. P. Rannard and A. Owen, *Adv. Healthc. Mater.*, 2014, **3**, 400–411.
115 S. Weir, R. Torkin and H. R. Henney, *Curr. Med. Res. Opin.*, 2013, **29**, 1627–1636.
116 M. N. Samtani, A. Vermeulen and K. Stuyckens, *Clin. Pharmacokinet.*, 2009, **48**, 585–600.
117 L. Baert, G. van 't Klooster, W. Dries, M. François, A. Wouters, E. Basstanie, K. Iterbeke, F. Stappers, P. Stevens, L. Schueller, P. Van Remoortere, G. Kraus, P. Wigerinck and J. Rosier, *Eur. J. Pharm. Biopharm.*, 2009, **72**, 502–508.
118 U. Wais, A. W. Jackson, Y. Zuo, Y. Xiang, T. He and H. Zhang, *J. Control. Release*, 2016, **222**, 141–150.
119 A. C. Savage, L. M. Tatham, M. Siccardi, T. Scott, M. Vourvahis, A. Clark, S. P. Rannard and A. Owen, *Eur. J. Pharm. Biopharm.*, 2019, **138**, 30–36.
120 M. Giardiello, N. J. Liptrott, T. O. Mcdonald, D. Moss, M. Siccardi, P. Martin, D. Smith, R. Gurjar, S. P. Rannard and A. Owen, *Nat. Commun.*, 2016, **7**, 1–10.
121 R. P. Bakshi, L. M. Tatham, A. C. Savage, A. K. Tripathi, G. Mlambo, M. M. Ippolito, E. Nenortas, S. P. Rannard, A. Owen and T. A. Shapiro, *Nat. Commun.*, 2018, **9**, 1–8.
122 S. A. A. Rizvi and A. M. Saleh, *Saudi Pharm. J.*, 2018, **26**, 64–70.
123 B. García-Pinel, C. Porras-Alcalá, A. Ortega-Rodríguez, F. Sarabia, J. Prados, C. Melguizo and J. M. López-Romero, *Nanomaterials*, 2019, **9**, 1–23.
124 X. Yan, M. Zhou, S. Yu, Z. Jin and K. Zhao, *Vaccine*, 2020, **38**, 1096–1104.
125 F. Tamjidi, M. Shahedi, J. Varshosaz and A. Nasirpour, *Innov. Food Sci. Emerg. Technol.*, 2013, **19**, 29–43.
126 B. Sarangi, U. Jana, N. N. Palei, G. P. Mohanta and P. K. Manna, *Eur. J. Pharm. Med. Res.*, 2018, **5**, 225–236.
127 V. Dave, R. B. Yadav, K. Kushwaha, S. Yadav, S. Sharma and U. Agrawal, *Bioact. Mater.*, 2017, **2**, 269–280.
128 K. Balamurugan and P. Chintamani, *Pharma Innov. J.*, 2018, **7**, 779–789.
129 R. H. Muller, K. Mader and S. Gohla, *Eur. J. Pharm. Biopharm.*, 2000, **50**, 161–177.
130 C. Pardeshi, P. Rajput, V. Belgamwar, A. Tekade, G. Patil, K. Chaudhary and A. Sonje,

Acta Pharm., 2012, **62**, 433–472.
131 S. Mukherjee, S. Ray and R. S. Thakur, *Indian J. Pharm. Sci.*, 2009, **71**, 349–358.
132 P. Ekambaram, A. A. H. Sathali and K. Priyanka, *Sci. Rev. Chem. Commun.*, 2018, **2**, 80–102.
133 K. D. Jyotsana R Madan, Priyanka A Khude, *Int. J. Pharm. Investig.*, 2014, **4**, 60–64.
134 R. Shtay, C. Ping and K. Schwarz, *J. Food Eng.*, 2018, **231**, 30–41.
135 K. Hippalgaonkar, G. R. Adelli, K. Hippalgaonkar, M. A. Repka and S. Majumdar, *J. Ocul. Pharmacol. Ther.*, 2013, **29**, 216–228.
136 S. P. Balguri, G. R. Adelli and S. Majumdar, *Eur. J. Pharm. Biopharm.*, 2016, **109**, 224–235.
137 E. B. Souto, W. Mehnert and R. H. Müller, *J. Microencapsul.*, 2006, **23**, 417–433.
138 P. A. Makoni, K. W. Kasongo and R. B. Walker, *Pharmaceutics*, , DOI:10.3390/pharmaceutics11080397.
139 P. Ghasemiyeh and S. Mohammadi-Samani, *Res. Pharm. Sci.*, 2018, 13.
140 B. Gaba, M. Fazil, S. Khan, A. Ali, S. Baboota and J. Ali, *Bull. Fac. Pharmacy, Cairo Univ.*, 2015, **53**, 147–159.
141 A. Gordillo-Galeano and C. E. Mora-Huertas, *Eur. J. Pharm. Biopharm.*, 2018, **133**, 285–308.
142 V. Mishra, K. K. Bansal, A. Verma, N. Yadav and S. Thakur, 2018, 1–21.
143 P. Ghasemiyeh and S. Mohammadi-Samani, *Rsearch Pharm. Sci.*, 2018, **13**, 288–303.
144 P. Kraisit and N. Sarisuta, *Molecules*, 2018, **23**, 6–8.
145 P. Ganesan and D. Narayanasamy, *Sustain. Chem. Pharm.*, 2017, **6**, 37–56.
146 H. Fessi, F. Puisieux, J. P. Devissaguet, N. Ammoury and S. Benita, *Int. J. Pharm.*, 1989, **55**, 1–4.
147 K. S. Yadav and K. K. Sawant, *AAPS PharmSciTech*, 2010, **11**, 1456–1465.
148 S. Schubert, J. T. Delaney and U. S. Schubert, *Soft Matter*, 2011, **7**, 1581–1588.
149 J. Tao, S. F. Chow and Y. Zheng, *Acta Pharm. Sin. B*, 2019, **9**, 4–18.
150 S. Salatin, J. Barar, M. Barzegar-Jalali, K. Adibkia, F. Kiafar and M. Jelvehgari, *Res. Pharm. Sci.*, 2017, **12**, 1–14.
151 S. K. Kannan, D. Duraisamy and Y. Sudhakar, *Int. J. Curr. Res.*, 2018, **10**, 64131–64141.
152 C. C. M.-G. M.A. Schubert, *Eur. J. Pharm. Biopharm.*, 2003, **55**, 125–131.
153 S. Batzri and E. D. Korn, *Biochim. Biophys. Acta*, 1973, **298**, 1015–1019.
154 J. Tang, M. Weston, R. P. Kuchel, F. Lisi, K. Liang and R. Chandrawati, *Mater. Adv.*, 2020, **1**, 1745–1752.
155 V. A. Duong, T. T. L. Nguyen and H. J. Maeng, *Molecules*, 2020, **25**, 1–36.
156 Gattefosse, Developing Sustained Release Tablets with Compritol ® 888 ATO Formulation Guidelines, https://www.pharmaexcipients.com/wp-content/uploads/2020/03/Compritol-888_ATO_Formulation_Guideline_pdf.pdf.
157 R. Kumar, A. Singh and N. Garg, *ACS Omega*, 2019, **4**, 13360–13370.
158 B.-E. S. Aburahma MH, *Expert Opin. Drug Deliv.*, 2014, **11**, 1865–1883.
159 N. Poonia, R. Kharb, V. Lather and D. Pandita, *Futur. Sci. Open Access*, , DOI:10.4155/fsoa-2016-0030.
160 A. D'Souza and R. Shegokar, *Curr. Drug Deliv.*
161 Z. Shen, A. Fisher, W. K. Liu and Y. Li, *PEGylated 'stealth' nanoparticles and liposomes*, Elsevier Ltd, 2018.
162 S. Y. Fam, C. F. Chee, C. Y. Yong, K. L. Ho, A. R. Mariatulqabtiah and W. S. Tan, *Nanomaterials*, 2020, **10**, 1–18.
163 F. El Mohtadi, R. D'Arcy, X. Yang, Z. Y. Turhan, A. Alshamsan and N. Tirelli, *Int. J. Mol. Sci.*, 2019, **20**, 1–14.
164 N. Popov, L. W. Honaker, M. Popova, N. Usol'tseva, E. K. Mann, A. Jákli and P. Popov, *Materials (Basel).*, 2017, **11**, 14–17.
165 A. Gordillo-Galeano and C. E. Mora-Huertas, *Eur. J. Pharm. Biopharm.*, 2018, **133**, 285–308.
166 V. Sainz, J. Conniot, A. I. Matos, C. Peres, E. Zupančič, L. Moura, L. C. Silva, H. F.

Florindo and R. S. Gaspar, *Biochem. Biophys. Res. Commun.*, 2015, **468**, 504–510.
167 S. Soares, J. Sousa, A. Pais and C. Vitorino, *Front. Chem.*, 2018, **6**, 1–15.
168 V. Tambe, R. Maheshwari, Y. Chourasiya, H. Choudhury, B. Gorain and R. K. Tekade, *Clinical aspects and regulatory requirements for nanomedicines*, Elsevier Inc., 2018.
169 Y. Barenholz, *J. Control. Release*, 2012, **160**, 117–134.
170 A. C. Anselmo and S. Mitragotri, *Bioeng. Transl. Med.*, 2016, **1**, 10–29.
171 A. Z. Mirza and F. A. Siddiqui, *Int. Nano Lett.*, , DOI:10.1007/s40089-014-0094-7.
172 L. Sercombe, T. Veerati, F. Moheimani, S. Y. Wu, A. K. Sood and S. Hua, *Front. Pharmacol.*, 2015, **6**, 1–13.
173 S. Manchanda, N. Das, A. Chandra, S. Bandyopadhyay and S. Chaurasia, *Fabrication of advanced parenteral drug-delivery systems*, Elsevier Inc., 2019.
174 M. Leon, M. Longo and B. Godin, *Am. J. Obstet. Gynecol.*, 2015, **212**, 508.e1-508.e7.
175 J. S. Refuerzo, F. Leonard, N. Bulayeva, D. Gorenstein, G. Chiossi, A. Ontiveros, M. Longo and B. Godin, *Sci. Rep.*, 2016, **6**, 1–12.
176 J. W. Paul, S. Hua, M. Ilicic, J. M. Tolosa, T. Butler, S. Robertson and R. Smith, *Obstetrics*, 2017, **216**, 283.e1-283.e14.
177 S. Hua, H.-I. Chang, N. M. Davies and P. J. Cabot, *J. Liposome Res.*, 2011, **21**, 95–105.
178 S. Hua, *J. Liposome Res.*, 2019, **29**, 357–367.
179 S. Hua and B. Vaughan, *Int. J. Nanomedicine*, 2019, **14**, 2191–2206.
180 J. Sanchez-Sotelo, *Elbow Stiffness: Rehabilitation After Surgical Contracture Release*, Elsevier Inc., Fifth Edit., 2018.
181 Y. Sharav and R. Benoliel, in *Orofacial Pain and Headache*, 2008, pp. 349–376.
182 A. Russo, C. Costagliola, L. Delcassi, F. Parmeggiani, M. R. Romano, R. Dell'Omo and F. Semeraro, *Mediators Inflamm.*, 2013, **2013**, 1–11.
183 M. Elmowafy, A. Samy, A. E. Abdelaziz, K. Shalaby, A. Salama, M. A. Raslan and M. A. Abdelgawad, *Beni-Suef Univ. J. Basic Appl. Sci.*, 2017, **6**, 184–191.
184 I. G. Shin, S. Y. Kim, Y. M. Lee, C. S. Cho and Y. K. Sung, *J. Control. Release*, 1998, **51**, 1–11.
185 S. Y. Kim, I. G. Shin, Y. M. Lee, C. S. Cho and Y. K. Sung, *J. Control. Release*, 1998, **51**, 13–22.
186 W. Badri, K. Miladi, R. Eddabra, H. Fessi and A. Elaissari, *J. Nanomater.*, 2015, **2015**, 1–9.
187 A. Rezaei Mokarram, A. Kebriaee zadeh, M. Keshavarz, A. Ahmadi and B. Mohtat, *DARU, J. Pharm. Sci.*, 2010, **18**, 185–192.
188 K. M. Pustulka, A. R. Wohl, H. S. Lee, A. R. Michel, J. Han, T. R. Hoye, A. V. McCormick, J. Panyam and C. W. Macosko, *Mol. Pharm.*, 2013, **10**, 4367–4377.
189 V. Závišová, M. Koneracká, O. Štrbák, N. Tomašovičová, P. Kopčanský, M. Timko and I. Vavra, *J. Magn. Magn. Mater.*, 2007, **311**, 379–382.
190 K. M. Koczkur, S. Mourdikoudis, L. Polavarapu and S. E. Skrabalak, *Dalt. Trans.*, 2015, **44**, 17883–17905.
191 R. Bakhaidar, J. Green, K. Alfahad, S. Samanani, N. Moollan, S. O'Neill and Z. Ramtoola, *Pharmaceutics*, 2019, **11**, 1–14.
192 B. K. Lee, Y. Yun and K. Park, *Adv. Drug Deliv. Rev.*, 2016, **107**, 176–191.
193 K. Hippalgaonkar, G. R. Adelli, K. Hippalgaonkar, M. A. Repka and S. Majumdar, *J. Ocul. Pharmacol. Ther.*, 2013, **29**, 216–228.
194 M. Rahman, S. Beg, A. Verma, F. Anwar, A. Samad and V. Kumar, *Liposomal-Based Therapeutic Carriers for Vaccine and Gene Delivery*, Elsevier Inc., 2017.
195 J. Varshosaz, F. Hassanzadeh, H. Sadeghi-aliabadi, Z. Larian and M. Rostami, *Chem. Eng. J.*, 2014, **240**, 133–146.
196 G. S. Kwon, M. Naito, K. Kataoka, M. Yokoyama, Y. Sakurai and T. Okano, *Colloids Surfaces B Biointerfaces*, 1994, **2**, 429–434.
197 R. D. Pensack, R. J. Ashmore, A. L. Paoletta and G. D. Scholes, *J. Phys. Chem. C*, 2018, **122**, 21004–21017.
198 A. Khosa, S. Reddi and R. N. Saha, *Biomed. Pharmacother.*, 2018, **103**, 598–613.

199 N. Kumar and C. Chaiyasut, *Int. J. Pharm. Pharm. Sci.*, 2015, **7**, 252–257.
200 F. Pinto, D. P. C. de Barros and L. P. Fonseca, *Ind. Crops Prod.*, 2018, **118**, 149–159.
201 M. J. Abla and A. K. Banga, *Int. J. Cosmet. Sci.*, 2014, **36**, 239–246.
202 V. Rodriguez-Ruiz, J. Á. Salatti-Dorado, A. Barzegari, A. Nicolas-Boluda, A. Houaoui, C. Caballo, N. Caballero-Casero, D. Sicilia, J. B. Venegas, E. Pauthe, Y. Omidi, D. Letourneur, S. Rubio, V. Gueguen and G. Pavon-Djavid, *Molecules*, 2018, **23**, 1–12.

CHAPTER 2

The Development of Indomethacin loaded Solid Lipid Nanoparticles

Chapter 2

2.1 Introduction

2.1.1 SLNs

Solid Lipid Nanoparticles (SLNs) are a subset of nanoparticle formulations that consist of a solid lipid, a drug and a range of stabilising polymers that are predominantly recruited from pre-existing FDA approved formulations.[1,2] The solid lipid is often a bulk crystalline lipid, that acts as a carrier vehicle for a hydrophobic drug molecule. The successes and drawbacks of SLNs have been thoroughly discussed in Chapter 1, section 1.8.2. However the key advantages that inspired SLNs containing indomethacin (IND) as a therapeutic treatment for preterm birth, are discussed briefly in the following section.

2.1.1.1 Advantages of SLNs for the treatment of preterm birth

SLNs are formulations with key advantages over alternative non-lipid (polymeric, inorganic nanoparticles) and lipid derived (liposomal) nanosystems. Their advantages are predominantly due to the inclusion of a bulk crystalline solid lipid that increases the stability of particle structures and has potential to enhance controlled release profiles.[3] Additional advantages that are particularly attractive for SLN uses in preterm birth, include the biocompatibility and biodegradability of the excipients and decreased toxicity profiles of SLN formulations *vs* the small molecule active ingredient.[1,2,4] Furthermore, there has been claims to suggest that SLNs provide better protection over drug molecule degradation in comparison to liposomes *in vivo*, with a reduction is drug leakage as a key advantage.[5] This may be attributed to the high melting point of the lipid core, preventing temperature disruption at physiological body temperature. Additionally, this may provide protection of the encapsulated drug from enzymes, pH and other factors that could cause premature drug molecule degradation before the exertion of a therapeutic effect. The materials optimisation of SLNs for indomethacin encapsulation are discussed throughout this chapter.

2.1.2 Chapter Aims

Throughout this chapter we aim to understand how preliminary analytical techniques can be implemented to understand the scientific design to aid the selection of optimal excipients for SLN formulations, with respect to the active ingredient. The use of DSC and PXRD was implemented to explore the use of several solid lipids and their compatibility with IND. Experimental parameters were then explored to understand how varying experimental conditions can influence the formation and stability of SLNs. The optimisation of solvents, anti-solvents and hydrophobic masses, as well as different types and concentrations of stabilisers were all investigated. The optimal formulation was taken forward to assess the success of the IND loading ability. The drawbacks and experimental developments for IND-SLNs are discussed thoroughly throughout this chapter.

2.2 Results and Discussion

2.2.1 DSC thermal analysis to determine optimal drug: solid lipid combinations

Differential Scanning Calorimetry (DSC) measurements of drug-lipid melts allows the determination of the melting points (T_m) of the compounds which can be correlated back to the individual bulk materials. Any thermodynamic changes observed within the thermograms can be attributed to morphological changes within the drug-lipid melts, as the bulk materials contain different melting points and crystallinity.[6,7] Ultimately, a change in the thermogram aids a logical prediction of whether the drug-lipid core would be unfavourably crystalline or develop an imperfect crystal structure allowing drug incorporation when combined together. If the melting transitions of drug and lipid two remain unchanged upon the mixing of the two compounds, it can be assumed that there is negligible inclusion of the drug within the solid lipid structure. This implies that the drug and lipid would coexist as two separate entities, rather than a favourable co-nucleation for SLN development. However, a distinct change in the thermograms may support the theory of an increased number of lattice defects between the two naturally crystalline materials and thus indicates the inclusion of the drug within the solid lipid lattice.[6] Commonly this can be identified in DSC through a decrease in the expected T_m of a material. This occurs because an increase in crystal distortion causes a weakening of intermolecular Van Der Waals interactions, thus decreasing the energy required to melt the material.[7] Importantly, DSC also

provides information on whether there are different polymorphic forms produced upon mixing of the two compounds, which can be identified through different T_m values that are characteristic of different polymorphs. For example, IND has two most common polymorphic forms, denoted form I and form II with respective T_m of 161 °C and 155 °C and less readily isolated forms III and IV with T_m's of 134°C and 148°C. [8,9] As each of the different polymorphs have different stability profiles (I-IV with respective decreasing stability), identification of a less stable drug polymorph within a drug lipid melt suggests that there is poorer drug-lipid compatibility. This is concluded as the presence of a more unstable polymorph would increase the likelihood of IND to undergo polymorphic transitions to its more thermodynamically stable state. In turn, this results in the potential for drug expulsion and formulation destabilisation upon storage. Therefore, samples identified with highly unstable polymorphs are often excluded from further testing. The solid lipids selected for testing are shown below in Table 2.1.

Table 2.1: Solid lipids tested for compatibility with IND.

Branded Solid Lipid	**Solid Lipid**
Compritol 888 ATO	Mixture of mono, di and triglycerides of glyceryl behenate
Precirol ATO 5	Glyceryl distearate
Gelot 64	Mixture of glyceryl monostearate and PEG-75 stearate
Gelicure 44/14	Lauryl (C12) polyoxyl-32-glycerides, glycerol, polyethylene glycol-33 (PEG-33)
Geleol	Mixtures of mono, di and triesters of palmitic (C16) and stearic (C18) acids

Briefly, to form the drug-lipid melts, the solid lipid (500 mg) and IND (500 mg) were heated 10 °C above the melting point of the lipid for 5 minutes before being left to cool down at room temperature overnight and analysed by DSC. Analysis of the thermograms shown in Figure 2.1A-E, allows the IND and lipid curves to be directly compared to the thermograms observed with the combined melt.

`

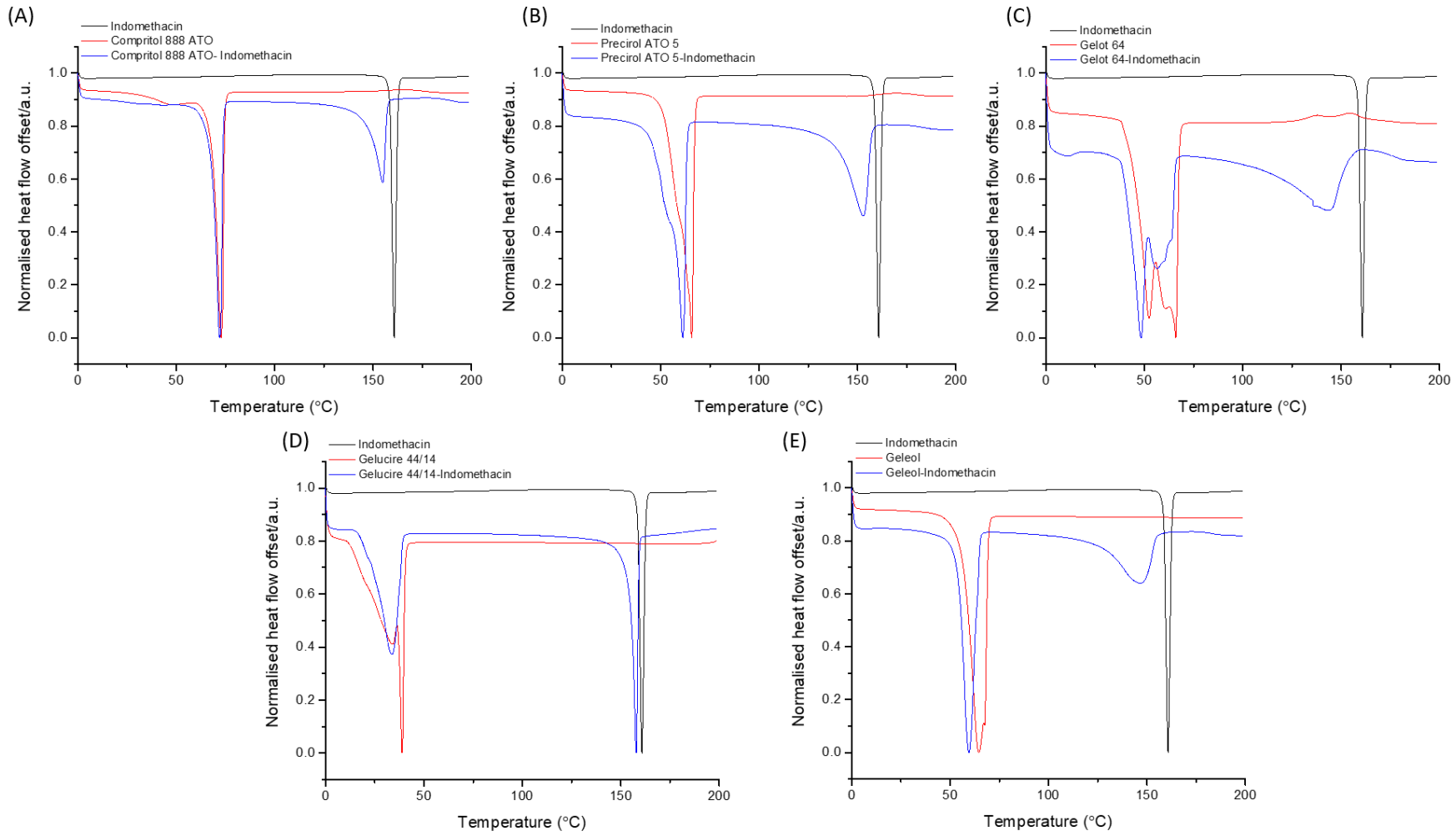

Figure 2.1: DSC thermograms obtained for drug-solid lipid melts using (A) Compritol 888 ATO (B) Precirol ATO 5 (C) Gelot 64 (D) Gelucire 44/14 and (F) Geleol. IND (black line), the solid lipid (red line) and the drug-lipid melts (blue line) and shown in each thermograms. All thermograms represented are from the first heat cycle. All samples were heated from 0°C to 200°C with a heat rate of 5°C/ min.

`

2.2.1.1 Analysis of the DSC thermograms obtained for the drug-solid lipid melts

The thermograms were analysed to assess changes in the intensity or broadening in the T_m peaks to qualitatively assess changes in crystallinity between bulk IND and the solid lipids *vs* the drug lipid melts (Figure 2.1). Figure 2.1A, B, C and E all show a significant reduction in the intensity of the IND T_m, indicating that there was notable solubility and increased homogeneity within the drug-lipid melts. Further analysis of Gelot 64 (Figure 2.1C) and Geleol (Figure 2.1E) samples showed significant broadening of the T_m peak. This suggests that a reduction in crystallinity of the IND crystals within these samples was possible, therefore implying an enhanced dissolution of IND within these particular melts. However, Figure 2.1D shows no significant difference to the intensity of the IND T_m. This indicates the presence of a strongly crystalline IND rather than a solubilised homogeneous mixture. Therefore, solely from analysis of the thermogram curves it was predicted that all solid lipids excluding Gelucire 44/14 were potential, appropriate solid lipids for SLN development. Nevertheless, further analysis of the polymorphic forms obtained for all drug lipid melts is discussed in the following section.

2.2.1.2 Analysis of the IND polymorph in drug-solid lipid melts

With regards to assessing the IND polymorph formed, the drug lipid melts were analysed for a shift in the T_m values and correlated to the characteristic T_m's of the different polymorphic forms. As previously stated, the polymorphic form obtained predict solid lipids with a probability to maintain a thermodynamically stable drug-lipid melt over time. This is attributed to unstable polymorphs being more susceptible to undergo spontaneous polymorphic transitions, thus causing drug expulsion. Table 2.2 highlights the range of T_m values obtained for the individual bulk materials and for the lipid and drug within the drug-lipid melt, alongside the predicted polymorphs present. It is also important to state that a shift in the T_m value is assumed to be as a result of different IND polymorphs for the purpose of this experiment. However, it is also possible that there are other influencing factors such as reduction in IND crystal size and/or particle size that can also be represented by a shift in the T_m value.

Table 2.2: T_m of IND and individual solid lipids before and after the formation of drug-lipid melts. The polymorphic form of the drug-lipid melts is also highlighted.

Chemical	T_m bulk material (°C)	T_m of lipid in each drug-lipid melt (°C)	T_m of drug in each drug-lipid melt (°C)	Predicted IND polymorphic form
IND	160.7	-	-	I
Compritol 888 ATO	72.0	71.6	154.7	II
Precirol ATO 5	64.9	60.7	153.0	II
Gelot 64	52.1, 65.4	47.9, 57.3	143.8	IV
Gelucire 44/14	33.8, 38.3	33.2	157.4	II
Geleol	65.0	59.0	149.0	IV

From Table 2.2, it was suggested that all drug-lipid melts may have induced a change in the IND polymorph from the thermodynamically favoured form I lattice (T_m= 161°C) supported by a consistent decrease in IND T_m shown. This may be attributed to the heating process involved, as previous reports from Atef *et al.* have consciously produced the metastable IND form II *via* heating in ethanol at 60 °C followed by precipitation into distilled water.[10] From this assumption, the T_m values for Compritol 888 ATO, Precirol ATO 5 and Gelicure 44/14 suggest that in these samples the IND was in the metastable form II (T_m= ~155-157 °C). Conversely, Gelot 64 and Geleol samples may have contained a less thermodynamically stable, lower melting point polymorph. Consequently, it was predicted that samples containing IND as the most stable polymorph, the metastable form II polymorph, identified using Compritol 888 ATO, Precirol ATO 5 or Gelicure 44/14 could be most suited for SLN development.

From the analysis of the DSC thermograms curves and the polymorphic forms combined, it was therefore concluded that Compritol 888 ATO and Precirol ATO 5 would be the optimal solid lipids for further formulation development. This was concluded from the decrease in the intensity of the T_m peaks supporting a decreased quantity of IND crystals, coupled with the predicted identification of the metastable form II polymorph present in these drug- lipid melts. This information can be further compared to the crystallinity analysis using powder X ray diffraction (PXRD) and is discussed in the following section.

2.2.1.3 PXRD crystallinity analysis

An additional technique used for drug-lipid melt analysis is PXRD. PXRD uses X-ray scattering of atoms to obtain a diffraction pattern to provide information on the crystallinity of the materials. A change in the diffraction pattern correlates to a change in the fundamental crystal structure, thus can identify structural changes in drug-lipid melts and detect the occurrence of polymorphic transitions.[7,10,11] The drug-lipid melts where qualitatively analysed by PXRD and the results are presented in Figure 2.2. All the data has been normalised with respect to IND, and the y axis for graphs B to E has been scaled between 0-0.3 in order to allow a clearer visual comparison.

From Figure 2.2 it was determined that the crystallinity of the drug in the drug lipid melts was significantly reduced *vs* bulk IND (Figure 2.2A). This was concluded from the decreased frequency and intensity of IND peaks, particularly at $2\theta \sim 11.5°$, 16.7° and 26.5°. However, there were no obvious shifts in the PXRD peaks to correspond to a particular polymorphic form of IND (Appendix Figure A2). Nevertheless, all drug-lipid melts still presented a degree of crystallinity that was associated with either solid lipid or drug. Figure 2.2B represents the drug-lipid melt using Compritol 888 ATO and showed a significant reduction in the intensity of the drug and of the lipid. This was contrary to Figure 2.2C (Precriol ATO 5), Figure 2.2D (Gelot 64) and Figure 2.2E (Geleol), that have showed an increase in crystallinity in the drug-lipid melt *vs* the bulk lipid. This can be concluded from Figure 2.2 C-E where the drug-lipid melt peaks (red traces) exceed the intensity of the bulk lipid material (black traces) when incorporating the same masses of material. The increased intensity of the drug lipid melt traces are highlighted in Figure 2.2 C-E by the black arrows. The increase in crystallinity from the bulk lipid to the drug-lipid melt suggests that there was residual crystalline IND within the sample and therefore not forming a complete miscible drug-lipid melt. The potential presence of crystalline IND indicates that the solid lipids C-E may exacerbate drug expulsion, thus proposing a problem for SLN formulation development. From the collated DSC and PXRD data it was concluded that Compritol 888 ATO was the most appropriate solid lipid for IND-SLN formulation development. Herein, Compritol 888 ATO is denoted as COMP.

`

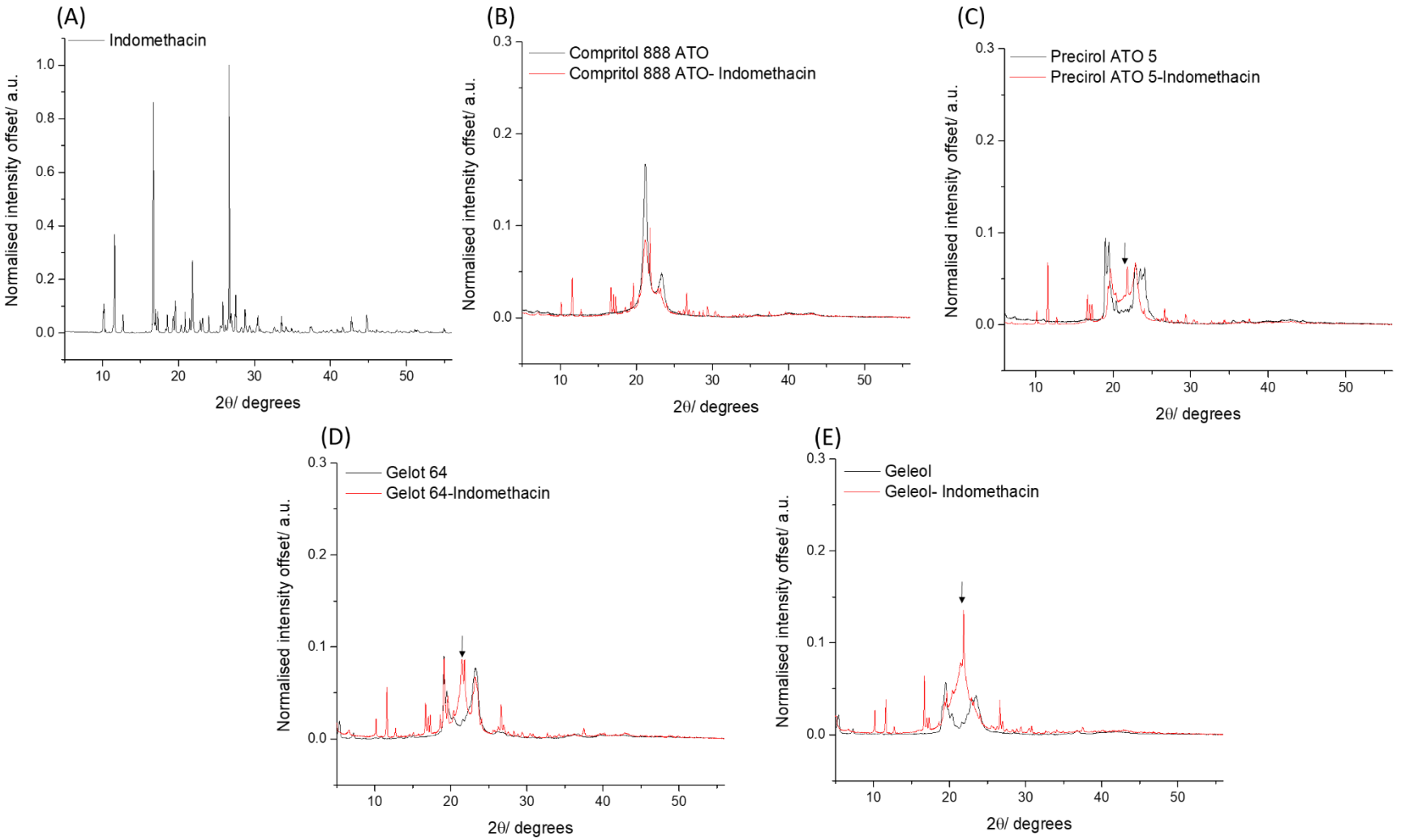

Figure 2.2: PXRD diffractograms obtained from (A) IND, (B) IND-Comprtiol 888 ato, (C) IND- Precirol ATO 5, (D) IND-Gelot 64 and (E) IND-Geleol. The black arrow on (C), (D) and (E) represents the greater increase in crystallinity seen for the drug-lipid melts in comparison to the individual bulk solid lipid.

`

2.2.1.4 Preliminary formation of SLNs with COMP vs less optimal solid lipids

As the drug lipid melt containing COMP showed the presence of the metastable IND polymorph, supported by a shift in the T_m to 154.7°C, and was the only solid lipid to form a melt exhibiting a decreased crystallinity in the diffraction pattern, it was considered the optimal lipid for SLN development. However, in order to prove that the DSC/PXRD screening process was indicative for SLN formulation, two of the alternative lipids were chosen for a proof of concept screen. Gelot 64 and Geleol were chosen based on their prior 'poor' properties, primarily the significant shift in the T_m in the DSC thermograms suggesting the production of unfavourable polymorphs. Additionally, both these lipids have comparable triglyceride derived structures to COMP, as shown in Figure 2.3. The synthesis of the SLNs were carried out through the solvent injection method (SIM). For further details on the SIM refer to Chapter 1, section 1.8.2.5.

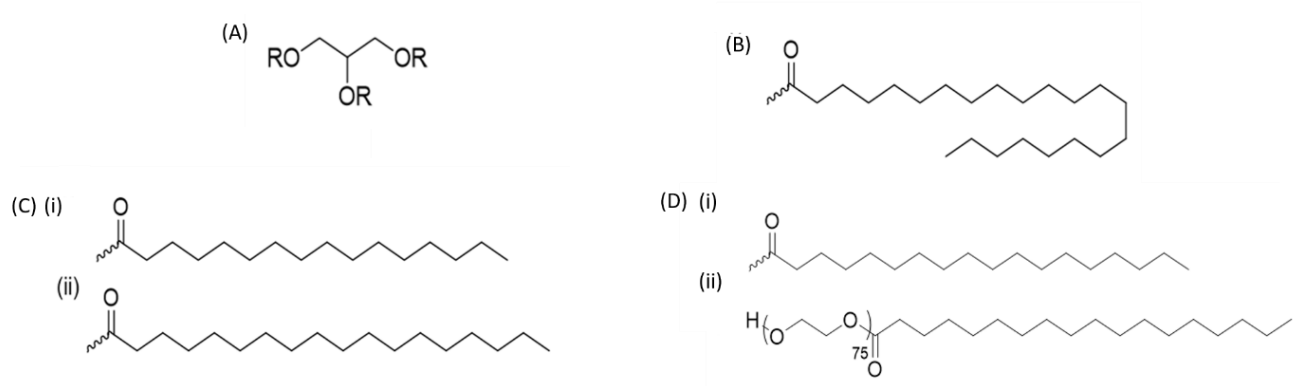

Figure 2.3: (A) Generic structure of triglycerides where the R group varies dependent on the solid lipid. (B) COMP: R group= esters of behenic acid (B) Gelot 64: R group= esters of (i) palmitic and (ii) stearic acid and (C) Geleol: R group= (i) glyceryl monostearate (ii) PEG_{75} stearate.

Experimentally the solid lipid (4 mg) was heated in 1-propanol (4 mL) for 2 minutes to form a homogeneous melt and was then rapidly injected into an aqueous dispersion containing deionised water (20 mL) and Pluronic® F68 as a polymeric stabiliser (5 mg/mL). These parameters were chosen as they were common starting points for nanoprecipitation methods previously developed within the research group. The COMP-SLN dispersion was determined visually to be the only stable formulation as determined by its slightly turbid appearance shown in Figure 2.4A, with no creaming or precipitation.

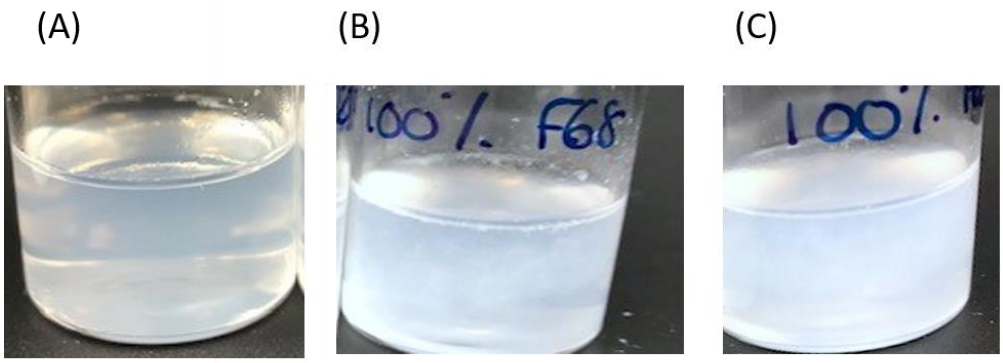

Figure 2.4: Visual appearance of SLN dispersions using (i) COMP, (ii) Gelot 64 and (iii) Geleol.

Conversely, Figure 2.4 B and C shows that immediate precipitation of material occurs with both Gelot 64 and Geleol respectively. This was confirmed visually through the 'shimmer-like' effect. This visual appearance is characteristic of non-spherical particle formation causing the light to diffract at multiple different angles.[7,10,11] Therefore, the data obtained from the DSC and PXRD analysis was considered appropriate to determine the optimal solid lipid and thus COMP was employed for all further studies. The following section discusses stabiliser compatibility with COMP-SLNs.

2.2.2 Stabiliser Compatibility

Stabiliser compatibility with the solid lipid and drug in SLN formulations is fundamental to form successful nanoparticles with optimal physical properties such as the colloidal stability and the Z average (D_z) and polydispersity (PdI) index, achieved from dynamic light scattering (DLS) techniques. In order to determine a suitable stabiliser for COMP-SLN development, a screen of several stabilisers were tested for their success in a solvent injection process to formulate SLNs. The stabilisers shown in Figure 2.5 were chosen from the Food and Drug Administration Centre for Drug Evaluation and Research (FDA CDER) list of inactive ingredients for preliminary testing.[12] The named polymers were chosen in particular due to the successful screening processes that lead to the encapsulation of lopinavir, efavirenz and maraviroc hydrophobic entities.[13–15]

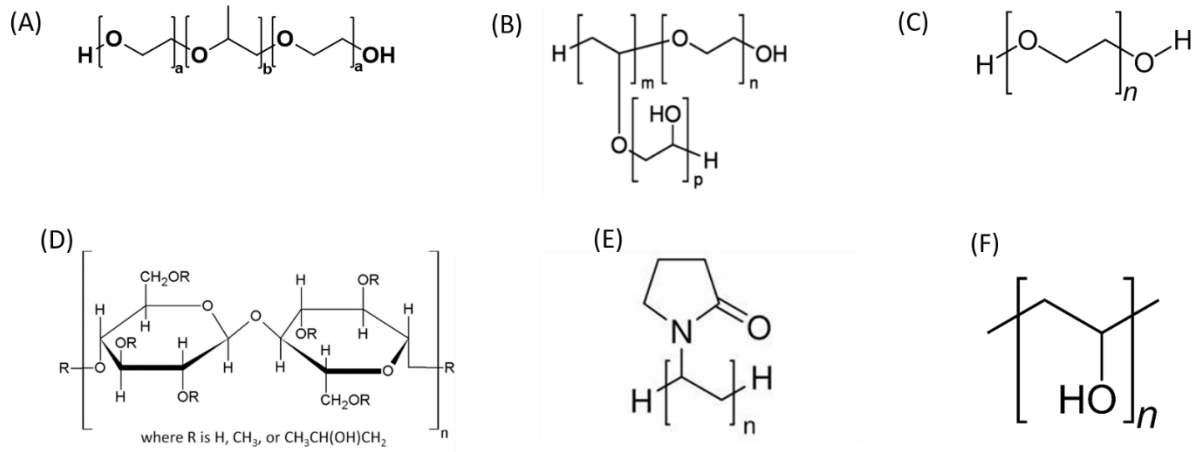

Figure 2.5: Chemical structure of stabilising polymers. The brand names, if applicable, are shown after each section in brackets. (A) Generic structure of poloxamer polyethylene oxide$_{(a)}$-polypropylene oxide$_{(b)}$-polyethylene oxide$_{(a)}$ block copolymers (Pluronics®), (B) Polyvinyl alcohol-*co*-polyethylene glycol (Kollicoat® Protect), (C) Polyethylene glycol 1K, (D) Hydroxypropyl methylcellulose, E) Polyvinyl pyrollidone K30 and (F) Polyvinyl alcohol.

There were two different subtypes of Pluronic® stabilisers (Figure 2.5A) that were used in the initial polymer screens. These stabilisers, denoted as Pluronic® F68 or Pluronic® F127, differ in their molecular weights (MW) and composition due to the different number of repeating units of both A and B blocks. Their individual compositions are shown below in Table 2.3.

Table 2.3:The composition and average MW of Pluronic® F68 and F127.

Pluronic®	**Formula (ABA block)**	**Average MW (g/mol)**
F68	PEO_{76}-PPO_{29}-PEO_{76}	8,400
F127	PEO_{100}-PPO_{65}- PEO_{100}	12,600

The preliminary success of the several stabilisers tested was determined by their ability to form nanoparticles with a narrow size distribution and ability to remain visually stable up to one hour after injection. The D_z of the dispersions and their visual appearance one hour after precipitation of the solid lipid are shown below in Figure 2.6. Polyvinyl pyrollidone K30, polyethylene glycol 1K, hydroxypropyl methylcellulose and polyvinyl alcohol are denoted as PVP-K30, PEG 1K, HPMC and PVA respectively.

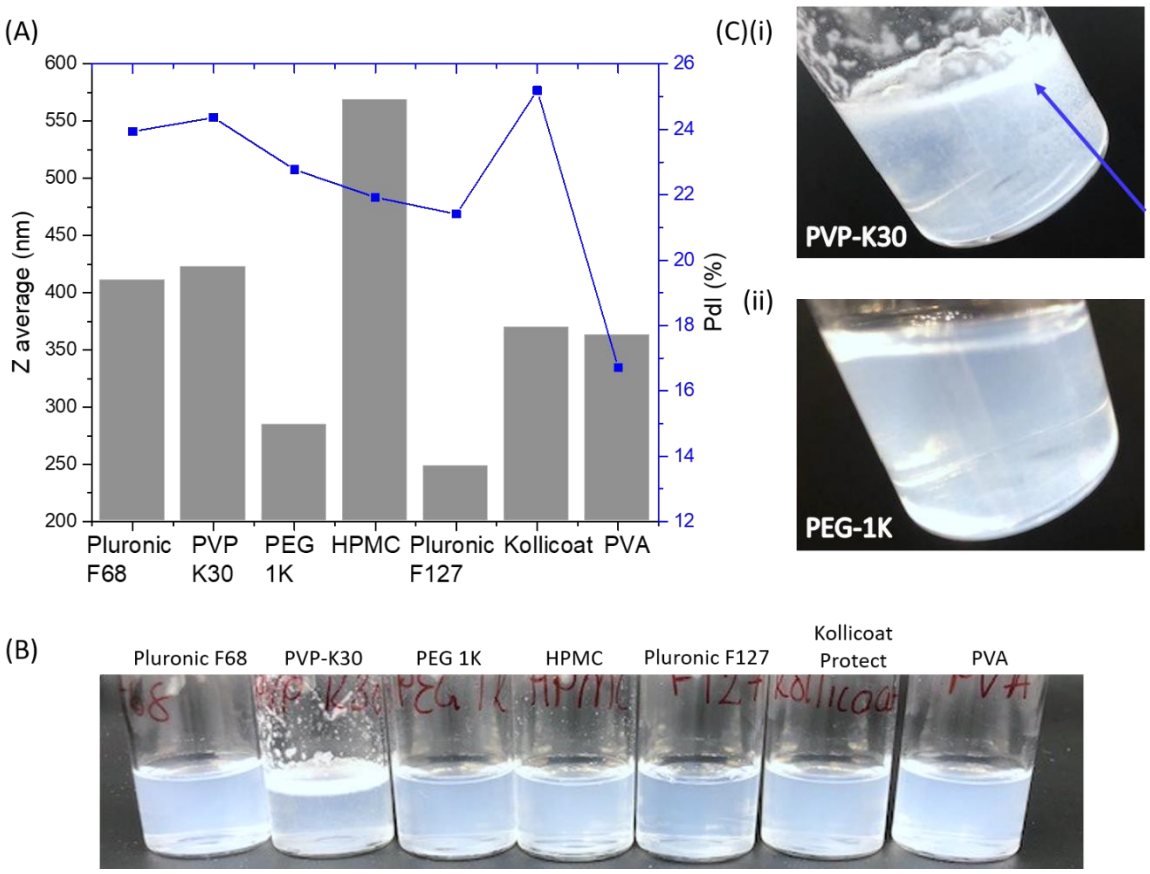

Figure 2.6: (A) A representation of the D_z of particles formed in using various polymeric stabilisers immediately after synthesis. (B) The visual appearance of the dispersions 1 hour after injection. (C) Creaming (blue arrow) of the solid lipid using (i) PVP-K30 and crystallisation using (ii) PEG 1K as polymeric stabilisers.

The characterisation of the SLNs formed using the different stabilisers are shown in Figure 2.6. From Figure 2.6A, it can be seen that there are a range of D_z values were obtained immediately after synthesis and were dependent on the stabiliser used. Most stabilisers were able to form COMP-SLN dispersions below 450 nm, with the exception of a larger D_z when using HPMC (568 nm). The PdI of all the dispersions immediately after synthesis showed narrow particle distributions with all dispersions, possessing a respectable PdI below 26%. Prior research within the literature also demonstrates that the D_z of SLNs has a dependency on the aqueous volume to lipid ratio and stabiliser concentration which is discussed later throughout this chapter.[16,17] The exact reason for the larger D_z associated with HPMC (568 nm) as a stabiliser is unknown. However, it may be resultant of its high MW (~10,000 g/mol) and bulkier ring structure, in comparison to other polymers with linear chains. Additionally, the high viscosity of HPMC may also result in slower diffusion and thus enable further nuclei growth prior to sufficient stabilisation. This may result in a larger particle size prior to adsorption of the polymer on the

surface of the lipid. As shown in Figure 2.6 B, one hour after precipitation the majority of samples remain slightly turbid with no precipitates or aggregates. However, the two samples shown more closely in Figure 2.6C using (i) PVP-K30 and (ii) PEG 1K destabilised through creaming or crystallisation, rendering these formulations unsuitable for further development. The inability of PVP-K30 and PEG 1K to colloidally stabilise the COMP-SLNs was attributed to their hydrophilic, polar nature and lack of amphiphilic character; likely meaning that these polymers were unable to successfully adsorb onto the solid lipid core to provide colloidal stability. In order to narrow down the polymer selection further, the samples were left overnight to see which samples displayed prolonged colloidal stability. This also helped draw a conclusion of which systems were able to withstand the presence of the 1-propanol remaining from the SIM. Destabilisation occurred for samples containing PVA and Kollicoat® Protect stabilisers. The remaining stabilisers were Pluronic® F68, Pluronic® F127 and HPMC and were therefore subject to further development. Their ability to stabilise COMP-SLNs was predicted to be as a result of their increased amphiphilic character which likely allowed for the more hydrophobic units within the stabilisers to adsorb onto the lipid core, whilst the hydrophilic moieties penetrate into the aqueous environment to provide steric stabilisation. The ability for these systems to withstand IND incorporation is discussed in the following section.

2.2.2.1 IND drug loading in to optimised COMP-SLNs

As the fundamental aim of these formulations was to encapsulate IND, the drug was incorporated at 1 wt%. As can be seen in Figure 2.7Aii, the sample incorporating HPMC underwent immediate precipitation with precipitates of drug clearly seen on the side of the vial and within the dispersion. Conversely, Pluronic® F127 and F68 formed stable particle dispersions. Both of these Pluronic® subtypes have both been extensively used in lipid nanoparticle systems.[18] Particles containing COMP and no IND drug content were denoted as blank-SLNs.

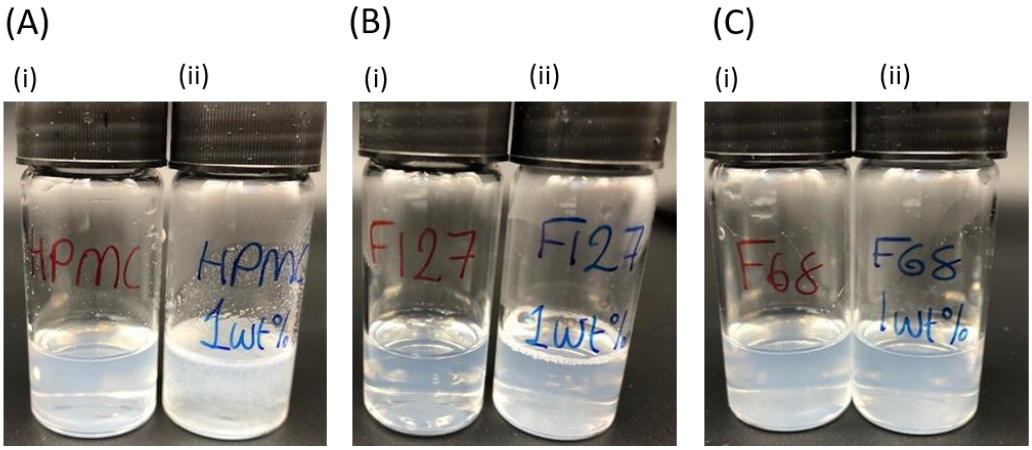

Figure 2.7: (A) HPMC dispersions containing (i) blank-SLNs and (ii) IND SLNs (B) Pluronic® F127 dispersions containing blank SLNs and (ii) IND SLNs and (C) Pluronic® F68 dispersions containing (i) blank SLNs and (ii) IND SLNs. All SLNs were drug loaded at 1 wt%. Samples stabilised using Pluronic® F68 and F127 remained colloidally stable upon the incorporation of IND.

Due to the inability of HPMC to stabilise drug loaded particles, this polymer was discarded from further testing. Further analysis of the size distribution traces of Pluronic®- COMP SLNs shown in Table 2.4.

Table 2.4: D_z and PdI of dispersions with and without IND drug loading.

	Pluronic® F68-blank SLNs	**Pluronic® F68-IND SLNs**	**Pluronic® F127-blank SLNs**	**Pluronic® F127-IND SLNs**
D_z (nm)	410	412	248	258
PdI (%)	24	22	21	14

For Pluronic® F68 and F127 the D_z was comparable at 0 wt% and 1 wt% at 410 to 412 nm (F68) and 248 to 258 nm (F127). All samples showed low dispersity with a PdI ≤24%. Therefore, both Pluronic® stabilisers were taken forward for formulation optimisation. The initial optimisation of the experimental parameters are discussed in the following section.

2.2 3 Incorporation of IND into SLN

Following on from optimisation of COMP-SLNs, the consequent aim was to introduce IND to the system to form IND-SLNs. Optimised experimental parameters for blank-SLNs were used. The experimental conditions were as follows: 0.8 mg/mL Pluronic® F68, 18 mg total hydrophobic mass (COMP + IND), 1:5 ratio of solvent: antisolvent with a total aqueous volume of 20 mL were implemented. The preliminary experiment explored the incorporation of 1.5, 2 and 3 wt% of IND with respect to the total solid mass. Unfortunately, there was significant disruption and immediate

precipitation of drug even with such low masses of IND being incorporated within the system shown in Figure 2.8. Figure 2.8A also highlights that there is significant increase in the mass of precipitate, in correlation with the increased mass of IND added into the system.

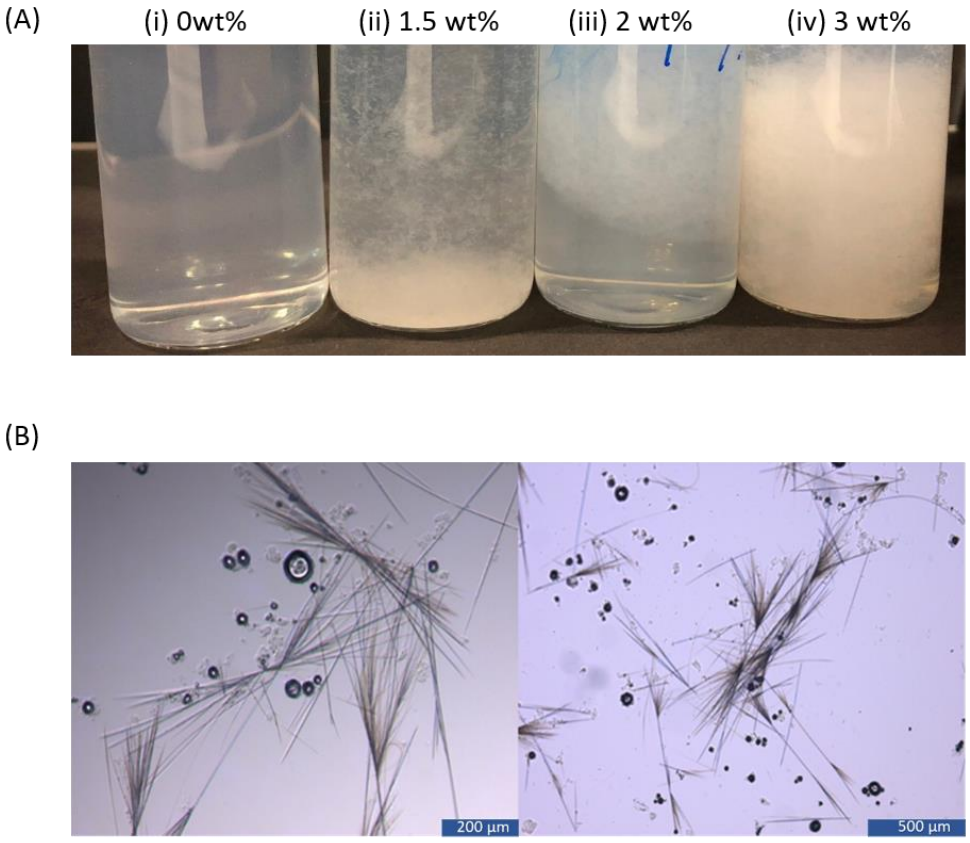

Figure 2.8: (A) Immediate precipitation of IND upon injection at concentrations (i) 0wt%, (ii) 1.5 wt%, (iii) 2 wt%, (iv) 3 wt% using Pluronic® F68 as the stabiliser. (B) Optical microscopy images of 3wt% IND sample showing the natural spindle-like crystals formed from insoluble IND crystals at different magnifications, scale bars are 200 µm (left) and 500 µm (right). The samples analysed on the optical microscope were taken from 3wt% IND SLNs.

Investigating the 3wt% IND sample (Figure 2.8Aiv) by optical microscopy (Figure 2.8B) revealed the needle-like crystals of IND, as similarly described by Sakdiset *et al*.[19] It has been previously suggested that when IND crystals have a needle-shaped morphology the drug is adopting the form II polymorph, whereas the common alternative form I lattice is significantly more 'plate-like'.[11] This finding is also supported by the change in the IND polymorph from form I to II after heating, as found from the DSC data for drug-lipid melts previously discussed in section 2.2.1. Moreover, a significant point is that the form II polymorph of IND has a reported increased aqueous solubility by 1.5 fold, in comparison to form I.[20] Given this potential for higher solubility it was important to investigate how the solvent/anti-

solvent composition controlled the amount of drug precipitation. Therefore, a 5 mg/mL solution of IND (1 mL) in 1-propanol was heated to 82 °C for 5 minutes to mimic the SIM process and injected into volumes of 3, 5, 7, 10 and 12 mL of water, in the absence of any stabilising polymers. Visual inspection of the resulting samples highlighted that IND in a 1:3 ratio of solvent: antisolvent remained completely solubilised in the solvent system, suggesting that at this ratio IND would be unable to nucleate. This finding is represented in Figure 2.9i. At a 1:5 solvent: anti-solvent ratio (the ratio used in the previous SIM procedures) and higher anti-solvent ratios IND precipitated when rapidly injected (Figure 2.9ii). The precipitation of IND in this environment, coupled with the quantified low solubility of IND (~0.2 mg/mL), reinforced that IND was able to nucleate in the existing SIM environment. This low solubility ~0.2 mg/mL suggested that 4 mg and therefore ≥80% of IND precipitated within this solvent environment. Therefore, in order to combat the problem of poor IND inclusion in the SLNs, two key approaches were considered. Firstly, whether an increase in stabiliser concentration was required in order to stabilise IND-SLNs and secondly, whether the addition of a secondary stabiliser would enhance IND-SLN formation and stability.

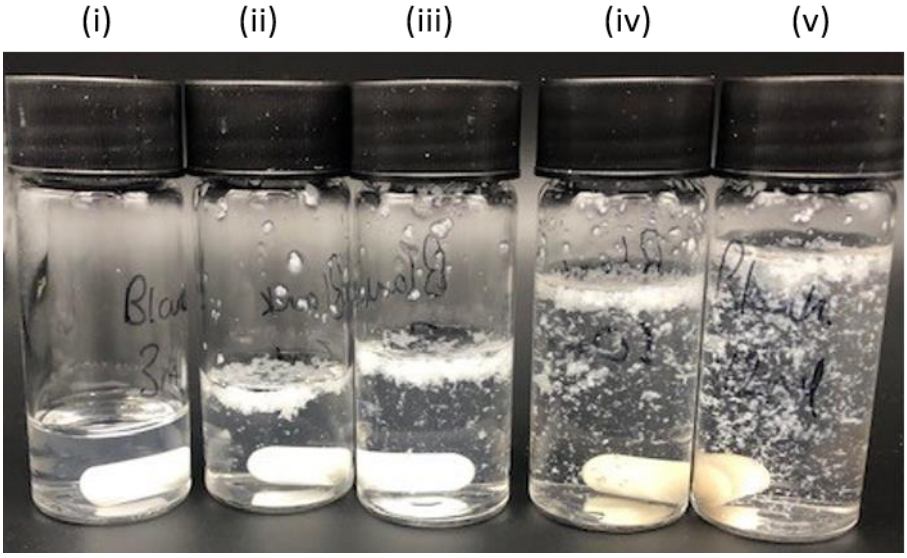

Figure 2.9: Precipitation of IND (1 mL of 5 mg/mL stock) into varying volumes of (i) 3 mL, (ii) 5 mL, (iii) 7 mL, (iv) 10 mL and (v) 12 mL of aqueous phase immediately after precipitation.

2.2.4 Investigating increased stabiliser concentrations

The concentrations of Pluronic® F68 were increased from 0.8 mg/mL used in the earlier experiments to 5, 10 and 20 mg/mL to assess viability of particle formation. The IND incorporation was maintained at 0.51 mg (1.5 wt%) and samples were prepared in triplicate. As shown in Figure 2.10, there was destabilisation of IND-SLNs within one hour of storage with clear evidence of creaming, for the with 5 mg/mL concentration proving non-viable. However, 10 and 20 mg/mL showed slightly turbid dispersions with no precipitate and monomodal size distributions as shown in Figure 2.10B.

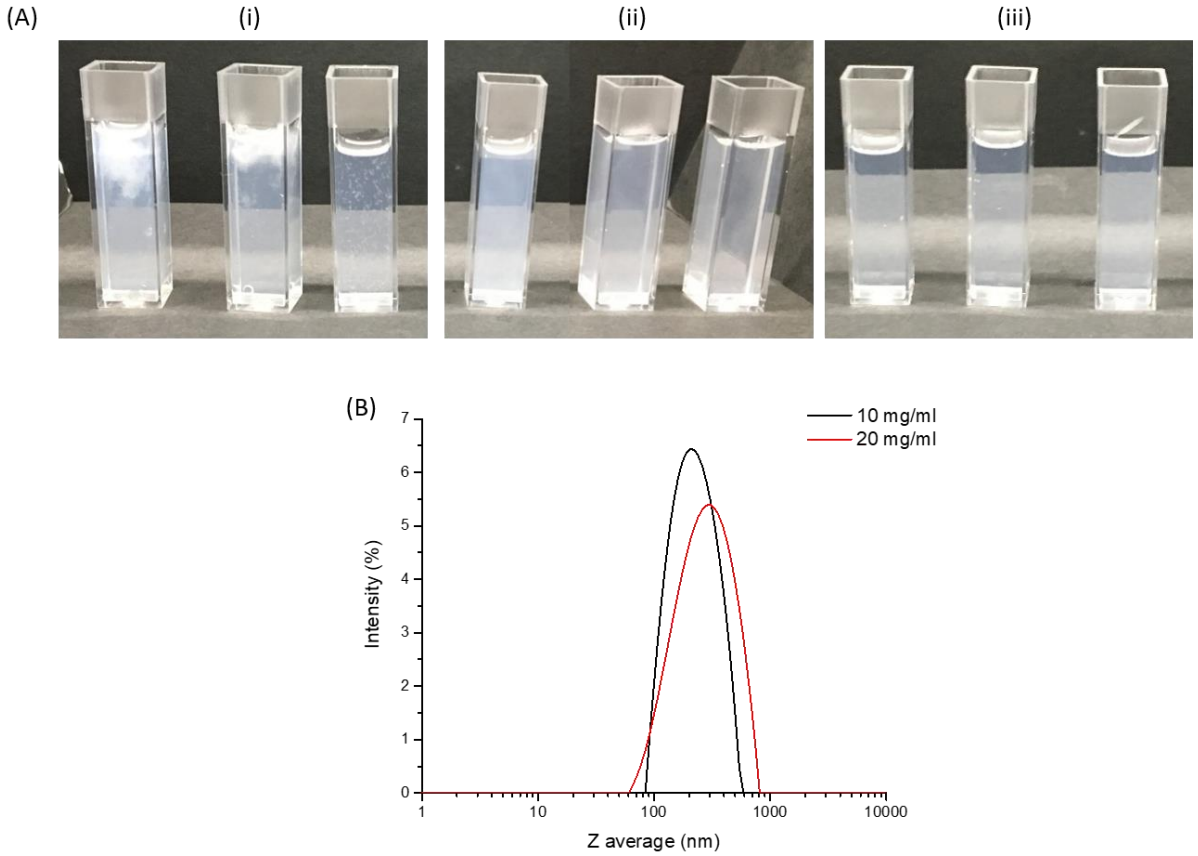

Figure 2.10: (A) Increased concentration of Pluronic® F68 to (i) 5 mg/mL, (ii) 10 mg/mL and (iii) 20 mg/mL. (B) Overlay of DLS chromatograms for formulations with Pluronic F68 at 10 mg/mL (black line) and 20 mg/mL (red line)

Although the increase in stabiliser concentration looked promising in terms of the particle properties, the increase to concentrations of 10 mg/mL or 20 mg/mL lowered the IND content to 0.23 wt% and 0.12 wt% of the total solid mass. As previously stated, the mass of IND in these systems was at 0.51 mg which was contained in 20 mL aqueous volume after the removal of the organic solvent. This

information coupled with the IV dosage requirements of IND (25 mg), means that a total volume of 980 mL would have to be administered in order to theoretically gain a therapeutic response, if 25 mg of active was still the required clinical dosage. This theoretical hypothesis is based upon the assumption that 100% of IND is released from all of the SLNs within a short enough time frame to reach an efficacious response. Although this volume seems of a significant value, when compared to alternative therapeutics it is a reasonable volume for a clinically translatable formulation. For example, commonly used chemotherapeutics e.g ifosphamide and mesna for the treatment of testicular cancer, require a 1000 mL IV infusion for five consecutive days every three to four weeks.[21,22] Nevertheless, in order to try and reduce this volume by increasing the drug loading within the system, the following section discusses how a blend of Pluronic® stabilisers may improve the formulation.

2.2.5 Investigating blends of Pluronic® F68 and F127

As previously seen in section 2.2.2, Pluronic® F68 and F127 were both viable polymers to stabilise COMP-SLN systems. In support of this, Pluronic® F127 and F68 have been widely used in previous COMP-SLN systems.[23,24] The key difference between these two Pluronics® chosen to be investigated in this section was their molecular weight of the polyethylene oxide (PEO) and polypropylene oxide (PPO) repeating units, as previously summarised in Table 2.3. Briefly F127 is significantly larger with average numbers of 200 PEO units and 65 PPO units *vs* F68 with 152 PEO units and 29 PPO units. Although previous literature has suggested Pluronic® stabilisers cause no biological toxicity up until dosage levels of 500 mg/mL when IV administered in rats, the concentration was standardised at 10 mg/mL to focus on the enhancing the drug loading.[25] Four different IND concentrations were explored at 1, 1.5, 2 and 3 wt% with respect to the total solid mass, equating to masses of 2.18, 3.27, 4.36 and 6.54 mg of IND. To relate this back to the dosage requirements of IND discussed in the previous section, if 3 wt% IND-SLNs were successful this equates to a total of 6.54 mg IND within a 20 mL dispersion. In order to gain a therapeutic effect at a 25 mg mass, this increase in drug loading would cause a simultaneous decrease in the administration volume to 76.4 mL, therefore providing ~13-fold reduction in IV fluids required. Importantly, an increase in drug content reduces the mass of the solid lipid used

in each system to maintain a total hydrophobic mass of 18 mg. The solvent: anti-solvent ratio was fixed at 1:5. The stabiliser concentrations were blended in 25 wt% increments as shown below in Table 2.8.

Table 2.8: Mass of Pluronic® F68 and Pluronic® F127 used in the stabiliser blends tested for IND-SLNs and the respective wt% ratios used for each blended system.

Pluronic® F68 (mg)	Pluronic® F127 (mg)	Ratio (wt%:wt%)
200	0	100:0
150	50	75:25
100	100	50:50
50	150	25:75
0	200	0:100

In order to test IND-SLN feasibility with Pluronic® blends, 1 wt% IND (2.18 mg) with respect to total solids was tested initially. Figure 2.11A shows the stability of the samples (i) immediately after synthesis followed by (ii) after 24 hours and (iii) after 48 hours. Figure 2.11B shows the DLS size distribution traces immediately after synthesis that shows a main population of IND-SLNs in the range 231 to 384 nm. Three of the formulations showed a smaller population likely represents Pluronic® micelles between 10-50 nm.

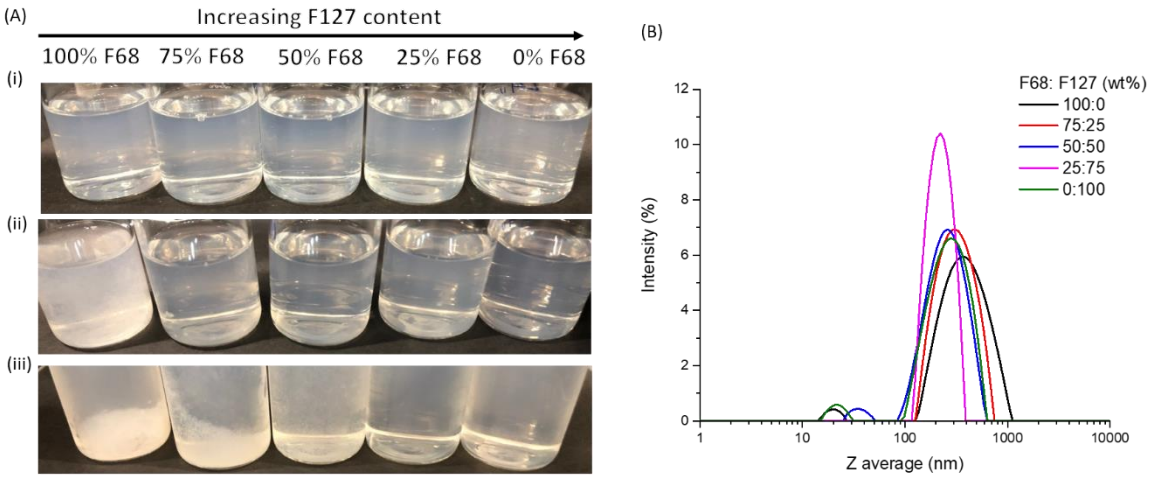

Figure 2.11: Sample stability of 1 wt% IND-SLNs (i) Immediately after synthesis (ii) After 24 hours and (iii) After 48 hours (B) Overlaid DLS size distribution traces for all F68:F127 stabiliser blends immediately after synthesis.

Interestingly, Figure 2.11 (ii) and (iii) highlights that samples with higher Pluronic® F68 content (left) destabilised more rapidly than those containing higher Pluronic® F127 content (right). This was demonstrated by an increase in precipitate of white crystallised material in the dispersions over time.

As 1 wt% IND-SLNs were successfully formed at higher Pluronic® F127 content and displayed a longer sample stability than 100 wt% Pluronic® F68 samples, higher IND contents (3 wt%, 6.54 mg) in F127 dominant systems were explored. From this stage 100 wt% Pluronic® F68 was excluded from future investigations. Subsequent samples with 75: 25 w/w%, 50:50 w/w%, 25:75 w/w% of Pluronic® F68: Pluronic® F127 and 100wt% Pluronic® F127, were prepared at 3 wt% IND and analysed by DLS Interestingly, when the data is compared between 1 wt% and 3 wt% IND-SLNs the D_z value for the higher IND content was significantly smaller in all cases, regardless of the Pluronic® blends used (Table 2.8). Although the mass of the hydrophobic material was maintained constant at 18 mg in each formulation, it was unexpected that an increase in drug content (and subsequent decrease in solid lipid content) would cause such a shift in the D_z to a noticeably lower value. The D_z decrease in the particle dispersions may be attributed to the difference in precipitation behaviour of COMP and IND compounds. Nevertheless, further work would need to be carried out to confirm the differences in their nucleation behaviour. Moreover, a secondary possibility to the smaller D_z identified may be due to the concentration of Pluronic® stabilisers (10 mg/mL) exceeding the CMC values (F68=4.8 $x10^{-4}$ M, F127= 2.8 x 10^{-6} M at 25°C).[18] This implies that there was a potential of IND to be micellised within the Pluronic® micelles within the dispersion. This hypothesis was explored in the followed section.

Table 2.8. Comparison of the D_z and PDI of IND-SLNs with either 1 or 3wt% IND content.

Pluronic® F68: Pluronic® F127 blend (wt)	**1 wt% IND-SLNs (D_z, nm)**	**PDI (%)**	**3 wt% IND-SLNs (D_z, nm)**	**PdI (%)**
75:25	384	25	198	26
50:50	244	21	202	21
25:75	231	22	184	21
0:100	241	24	164	24

2.2.6 Investigating IND micellisation

To determine the possibility of IND micellisation, IND (10 mg) was added to five vials containing a 10 mg/mL solution of Pluronic® F68 and F127 blends and were left to stir overnight. The vials shown in Figure 2.12 all displayed turbid, white suspensions with a small amount of remaining solid, independent

of the Pluronic® F68: Pluronic® F127 blends. On the contrary, when IND is saturated in a solution of water and left to stir, the solution remained transparent with insoluble solid drug (not shown).

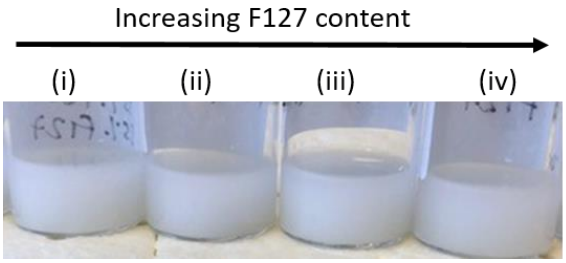

Figure 2.12: The micellisation of IND in Pluronic® F68: Pluronic® F127 blends. Pluronic® F68: F127 blends are as follows: (i) 75:25 wt/wt %, (ii) 50:50 wt/wt%, (iii) 25:75 wt/wt% and (iv) 100 wt% F127.

In order to quantitatively compare the different micellar systems and their ability to solubilise IND, the micellar dispersions were filtered to remove undissolved material and analysed by HPLC. Figure 2.13 shows the concentrations detected in the respective dispersions. This data showed that as the percentage of F127 in the composition in the micellar dispersions was increased then the greater the ability to solubilise IND within the Pluronic® micelles.

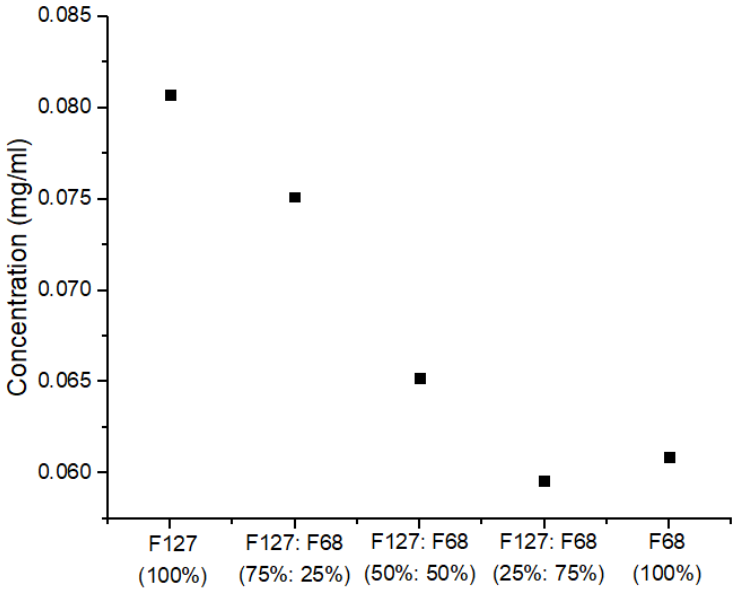

Figure 2.13: The concentration of IND solubilised in different Pluronic® F127: F68 micellar dispersions.

This finding can be attributed to the larger hydrophobic PPO core associated with F127 (PPO= 65 units), in comparison to F68 (PPO= 30 units) as shown in Figure 2.14.

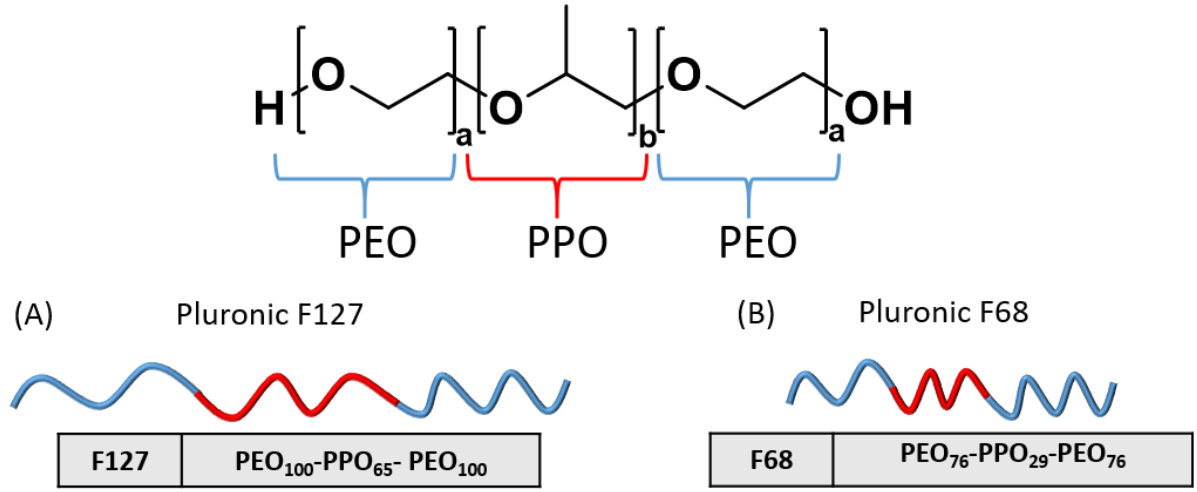

Figure 2.14: Illustration of the different PPO block lengths when using (A) F127 and (B) F68 Pluronic® stabilisers.

The ability for F127 to solubilise a greater amount of IND, suggests that the larger the PPO surface area, the increased ability to micellise hydrophobic IND monomers through increased Van Der Waals and hydrophobic interactions. With this formulation, the mass of stabilisers was at 200 mg. There is no evidence that we are aware of within the literature to suggest that this mass can cause significant biological toxicity, however the following section looks at the incorporation of Tween co-surfactants alongside Pluronic® stabilisers to reduce the mass of non-therapeutic excipients required.

2.2.7 Incorporation of Tween derivatives as potential co-surfactants

Polysorbate surfactants commonly branded as Tweens, are a group of six non-ionic amphiphilic surfactants that are most commonly often incorporated in clinically translatable formulations due to the ability of the oligo (ethylene glycol) chains to prevent non-specific protein absorption.[26] Tweens, predominantly Tween 20 and Tween 80 (Figure 2.15), have been thoroughly cited throughout the literature supporting their uses as co-surfactants in combination with Pluronic® stabilisers.[27] For example, COMP-SLN systems have been reported using Tween 80 blended with Pluronic® F68 for the formation of diazepam loaded SLNs.[27]

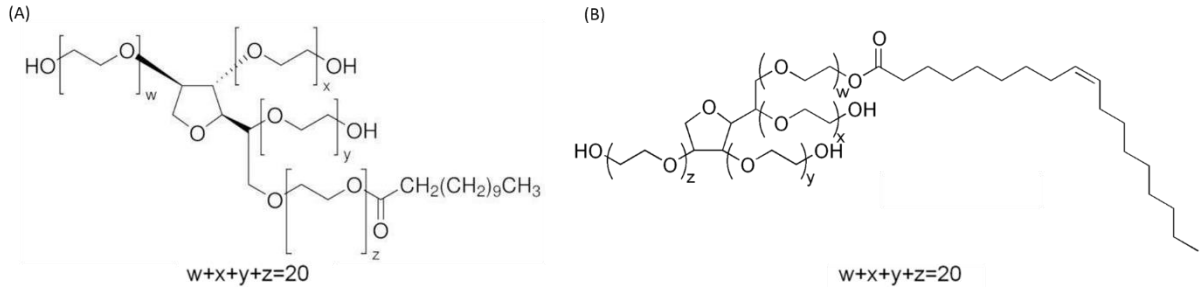

Figure 2.15: Chemical structure of commonly used (A) Tween 20 and (B) Tween 80

Most importantly for this research, it was key to identify whether there was any particular benefit of including Tween 20 or Tween 80 in the formulations. The overall stabiliser concentration was halved to 5 mg/mL. The total hydrophobic mass was kept constant at 18 mg and the solvent: anti-solvent ratio was set to 1:5. The initial set of experiments compared the particle properties of blank-SLNs containing Tween with those using only Pluronic® F68 or Pluronic® F127 as a sole surfactant. Firstly, SLNs were synthesised without the incorporation of drug by blending Pluronic® F68 and F127 with Tween 20 and Tween 80 in a 2:1 ratio (Pluronic®:Tween). The data for blank-SLNs in the absence of IND are shown below in Table 2.9.

Table 2.9: D_z size data and PDI (%) for Pluronic F68 and F127 stabilised samples without the presence of IND.

Polymer	**Co-surfactant**	**Dz (nm)**	**PdI (%)**
Pluronic® F68	Tween 20	390	23
Pluronic® F68	Tween 80	358	26
Pluronic® F127	Tween 20	307	20
Pluronic® F127	Tween 80	315	26

All particles formed SLN dispersions less than 400 nm and with PdI values below 30%. DLS traces for Tween 80 samples were monomodal, independent of Pluronic® stabiliser used. Tween 20 samples displayed evidence of a smaller micellar population within the dispersions. The DLS traces are shown in Appendix Figure A2. IND was then implemented at 1 wt% (1.18 mg) of the system to assess the ability to maintain a stable dispersion without any evidence of precipitation as previously seen. Fortunately, the dispersions formed remained turbid with no immediate evidence of precipitation or destabilisation within the formulations. Particles synthesised using Pluronic® F68 formed dispersions (Figure 2.16A) with a D_z of 342 nm and 242 nm when blended with Tween 20 and Tween 80

respectively. Particles synthesised using Pluronic® F127 formed dispersions with a D_z of 310 nm (Tween 20) and 250 nm (Tween 80) (Figure 2.16B).

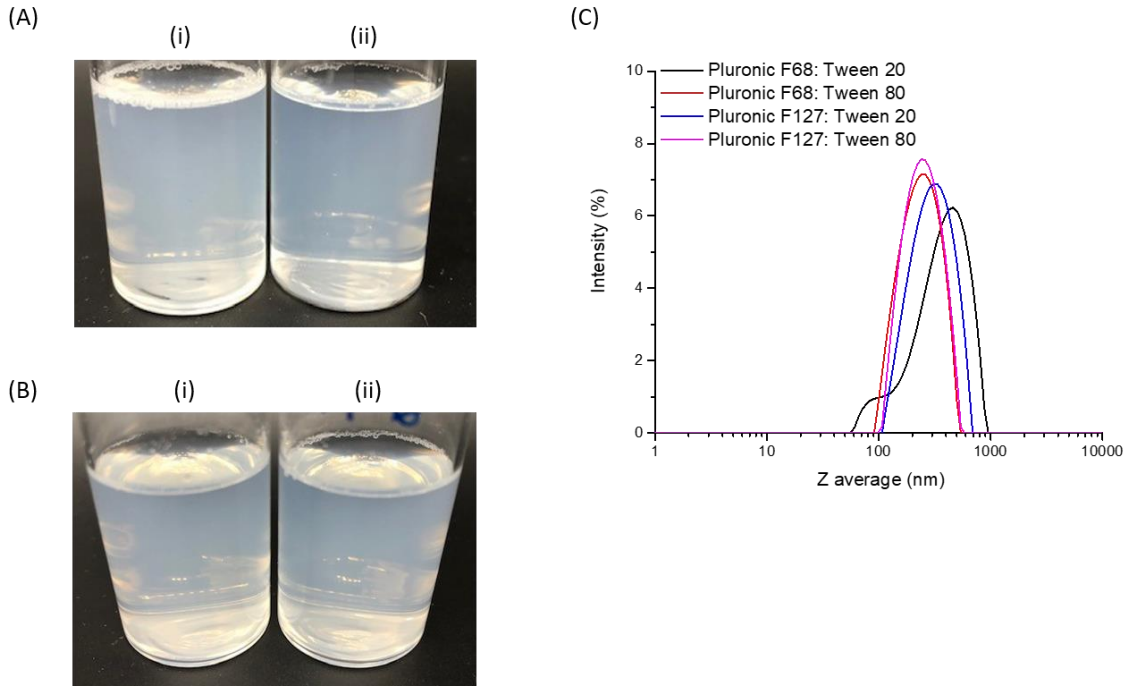

Figure 2.16: Analysis of the SLN dispersions formed with blends with Tween surfactant. (A) Pluronic® F68 with (i) Tween 20 and (ii) Tween 80 immediately after synthesis. (B) F127 blends with (i) Tween 20 and (ii) Tween 80. (C) DLS size distributions for each Pluronic®-Tween combinations.

The significant decrease in the D_z using Tween 80 in both cases may be attributed to the increased length of the alkyl chain on Tween 80 (C_{17} *vs* C_{11} for Tween 20). This creates a stronger association of the stabiliser to the drug-lipid nuclei upon precipitation.[28] The stronger adsorption of Tween 80 with the lipid core would therefore hinder particle growth, thus a smaller particle D_z. As a result of the successful inclusion of IND at 1 wt% the drug loading was increased to 3wt% (3.54 mg) with respect to the total solid mass. There was successful formation of particles using Pluronic® F68 at 467 and 281 nm when blended with Tween 20 and Tween 80 respectively and 360 nm and 349 nm for Pluronic® F127 samples blended respectively with Tween 20 and Tween 80 (Figure 2.17). There was no visible change to sample stability overnight.

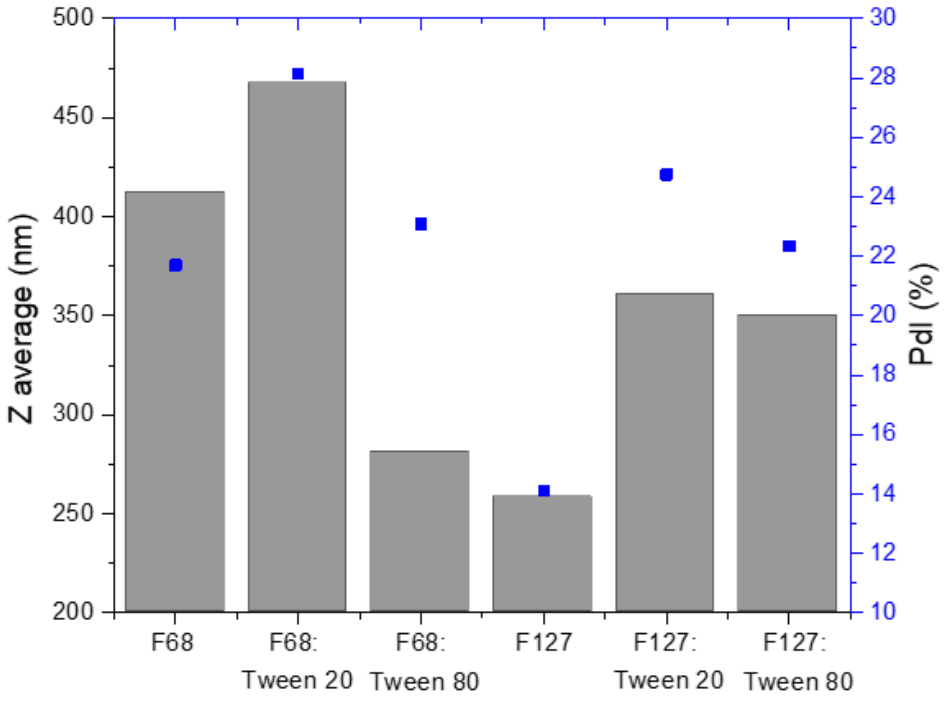

Figure 2.17: A graphical representation of the Dz and PdI of the 3wt% IND-SLN dispersions when incorporating Tween 20 or Tween 80 as a cosurfactants in either Pluronic® F68 or Pluronic® F127 stabilised systems.

From Figure 2.17, it is evident that there was no particular trend in the changes of the D_z or PdI of the dispersions dependent on the stabilisers used. With respect to the IV clinical dosage requirements for IND, there was a total of 3.54 mg within the dispersion which therefore required a total volume of 141.2 mL IV fluid to reach a therapeutic dosage of 25 mg. In comparison to the formulations containing solely Pluronic® stabilisers at 10 mg/mL, they required an administration volume of 76.4 mL. Therefore although the Pluronic®/Tween systems require a larger administration volume, they show a reduction by almost half in the masses of carrier materials required. For Pluronic®-only systems they contained a concentration of 10 mg/mL stabiliser (200 mg), 11.5 mg COMP and 6.5 mg IND totalling 211.5 mg of carrier materials. Conversely, Pluronic®/Tween systems contained 5 mg/mL stabiliser (100 mg), 14.5 mg COMP and 3.5 mg IND totalling 114.5 mg carrier materials. This is of significant importance with respect to the feasibility of the formulation as a lower mass of non-therapeutic excipients has potential to reduce the occurrence of biological toxicity, unwanted side effects and accumulation of carrier materials. For this reason, all samples containing Pluronic®/Tween combinations were taken forward to the next stage which involved the removal of 1-propanol from the dispersions.

2.2.7.1 Removal of 1-Propanol

During the solvent injection method, as the organic phase containing lipid, drug and the organic solvent is injected, the water-miscible organic solvent diffuses into the aqueous phase causing lipid precipitation.[28] However, the removal of 1-propanol from the dispersion was necessary as according to the FDA CDER list, 1-propanol is a class 3 solvent.[29] This signifies that there is no known human health hazard of 1-propanol, however concentrations of must be below 50 mg/day in administered formulations.[29] For the developed 3 wt% IND-SLNs, there was 4 mL of 1-propanol in addition to 20 mL of aqueous phase, equating to 3.2 g of 1-propanol. As it was important to stay conscious of the potential for clinical translation, the removal of 1-propanol was necessary for further testing. There are multiple methods available for the removal of non-volatile organic solvents, including dialysis, freeze drying, spiral evaporation or centrifugation of particles into a pellet followed by redispersion in aqueous media. The former two methods were trialled in detail and are discussed below.

2.2.7.2 Dialysis

Dialysis is a technique that works *via* the diffusion phenomenon, whereby molecules diffuse from an area of high concentration to an area of low concentration, through pores in a dialysis bag membrane with a carefully chosen molecular weight cut off (MWCO) in order to retain the desired components. Prior to undergoing dialysis, the stability of each of the SLN dispersions was required over a 1-week period. All samples remained stable for 1 week with no evidence of destabilisation, as shown in Table 2.10.

Table 2.10: Particle properties of Pluronic®: Tween combinations over a 7-day period containing 3 wt% IND.

Polymer	**Co-surfactant**	**D_z (nm)**	**PdI (%)**	**7 days D_z (nm)**	**7 days PdI (%)**
Pluronic® F68	Tween 20	342	26	308	19
Pluronic® F68	Tween 80	242	26	239	12
Pluronic® F127	Tween 20	360	25	310	19
Pluronic® F127	Tween 80	349	22	292	14

With no significant difference observed in the visual appearance of the dispersions or the reported size or PdI, the four SLN dispersion were placed in a dialysis bag (MWCO= 1 kDa) in aqueous sink conditions to allow the diffusion of individual 1-propanol molecules out of the bag to purify the lipid

nanoparticles. After 48 hours, the visual stability of the particles dispersions after dialysis appeared to contain precipitates plate-like drug crystals shown in Figure 2.18.

Figure 2.18: Sample stability after 48 hours of dialysis illustrated using the Pluronic® F68: Tween 80 sample.

This could suggest two key scenarios. Firstly, the occurrence of polymorphic transitions occurring of the drug from the metastable form II polymorph to a more stable form I or lesser stable form III or IV that have all been described as plate-like structures. Secondly, as the 1-propanol molecules are displaced and diffuse into the aqueous conditions, this initiates the lipid nuclei to precipitate out. This suggests that the 1-propanol may still be providing a slight solubility for hydrophobic excipients and as the 1-propanol molecules are displaced during dialysis, the stabiliser concentration is insufficient to stabilise the increasing concentration of precipitated material. In order to combat this further optimisation would be required for reducing the solvent volume and/or increasing the stabiliser concentration in future studies. However, as the volume of the solvent:anti-solvent was optimised within the initial stages of this project, other potential options for solvent removal were explored.

2.2.7.3 Freeze drying

Freeze drying, or lyophilisation, is one of the most efficient and easily scalable techniques to be used and is therefore favoured by pharmaceutical companies. However, drawbacks include destabilisation during the freezing or drying process causing polymorphic changes of the crystalline excipients and aggregation of the particles, thereby making the sample difficult to redisperse for administration. In order to combat this, a class of additives called cryoprotectants are added to the dispersions prior to freeze drying. The key role of cryoprotectants is to prevent particles from freezing stresses that cause aggregation and increase the chances of polymorphic transitions. The addition of cryoprotectants

initiates a glassy state within the water phase in the samples.[30] This is caused by an extensive increase in hydrogen bonding between water and cryoprotectants molecules, which reduces the rapid crystallisation of water. As a result the nanoparticles are situated within an amorphous continuous phase and reduce the occurrence of aggregation from freezing stresses.[30]

Samples containing Pluronic® F68: Tween 80 and Pluronic® F127: Tween 80 with IND at 3 wt%, were freeze dried in the absence and presence of cryoprotectants to assess the success of the dispersions. The cryoprotectants chosen were PEG 400, PEG 2K, PEG 5K, PEG 10K, trehalose, sucrose, dextrose and mannitol. Each cryoprotectant was trialled at 5, 10 and 20 mg/mL by adding 5 mL of each stock solution to 5 mL of SLN dispersion before freeze drying. These cryoprotectants where chosen as previous reports have praised their uses for successful monolith reconstitution.[31,32] The resultant samples of this were frozen in liquid nitrogen and lyophilised for 48 hours prior to reconstitution in 5 mL of phosphate buffer saline (PBS) solution. Unfortunately, all samples failed to redisperse showing a large presence of crystalline material, indicated by the pronounced shimmer-like effect shown in Figure 2.19. This shimmer-like effect occurs due to the presence of non-spherical particles scattering light at different angles through the dispersion. All samples shown below in Figure 2.19 were samples lyophilised with the highest 20 mg/mL cryoprotectants. Although reports have higher concentrations of cryoprotectants increase the susceptibility of agglomeration, all lower concentrations also showed similar results.[31]

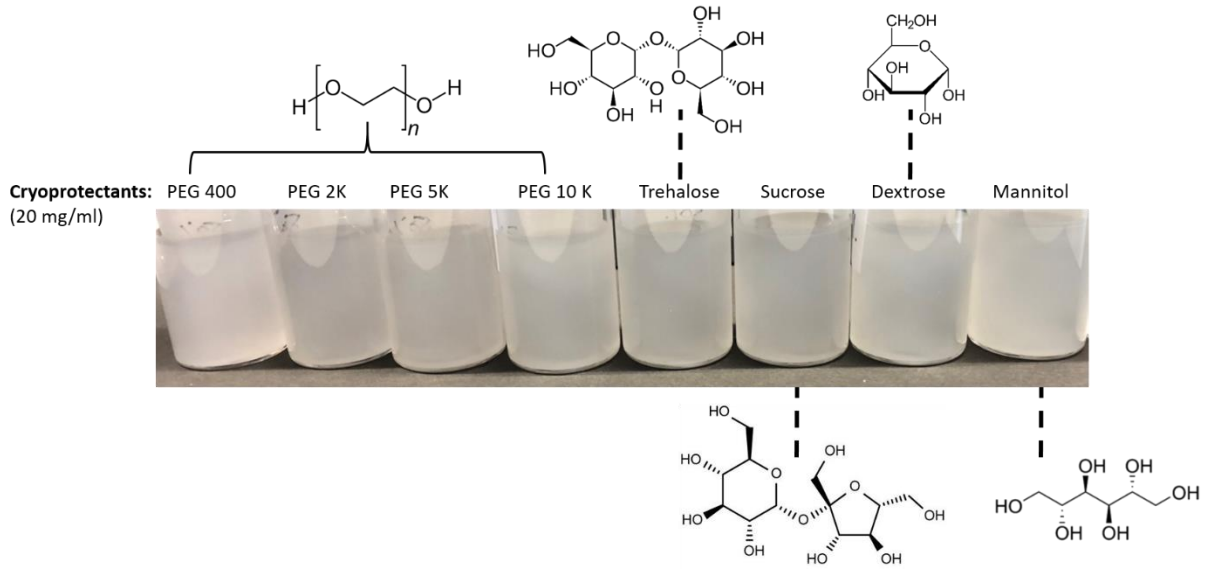

Figure 2.19: Samples after reconstitution in PBS when lyophilised with different cryoprotectants at a concentration of 20 mg/mL.

In situations where cryoprotectants work and allow successful reconstitution of particles, the cryoprotectants is often removed through dialysis or centrifugation. However, all cryoprotectants at a high concentrations (20 mg/mL) where proven to be unsuccessful as all samples represented visible particulates rendering the samples inadequate for accurate DLS measurement's. The cryoprotectant study was terminated before further optimisation of the SLNs.

2.2.7.4 Alternative methods

The spiral evaporator is a process that uses a high-powered vacuum to remove non-volatile high boiling point organic solvents or water from various dispersions or solid samples. The aim of this was to reduce the time required for the particles to be in larger volumes of water to rule out the potential increased solubility of the hydrophobic excipients in larger aqueous volumes causing destabilisation as potentially experienced during dialysis. As 1-propanol is a high boiling point, non-volatile organic solvent, the use of the spiral evaporator also required the sample to be heated to 40 °C to reduce evaporation time. Unfortunately, this also induced destabilisation of the particles and further optimisation to form organic-solvent free IND-SLNs *via* this method needs to be optimised.

An alternative method is centrifugation. This process involves centrifugation of the SLN dispersion to form a solid pellet of material in order to decant the continuous phase containing the organic solvent. This step is then followed by redispersion of the pellet in a concentrated aqueous physiological solution suitable for testing. An example of this was demonstrated by Singh *et al.* for the redispersion of resveratrol containing SLNs.[33] Briefly Singh *et al.* encapsulated resveratrol in SLNs using the solid lipid Gelucire 50/13. The authors used ethanol as the organic solvent *via* the same SIM and centrifuged at 50,000 rpm for 1 hour before washing and redispersing the pellet in deionized water followed by freeze drying to enhance storage stability.[33] It was not possible to achieve centrifugation at 50,000 rpm within our labs, therefore the 3 wt% IND-SLNs were centrifuged at 15,000 rpm for 4 hours. Unfortunately, the dispersions remained colloidally stable with no evidence of sedimentation. For this reason, this technique was not sufficient for translation to larger scale and therefore was discarded for further optimisation.

Unfortunately, the removal of the organic solvent from the developed SLN dispersions has proven difficult, with removal techniques requiring high levels of dilution and subsequent destabilisation, or other techniques requiring high temperatures which was not desirable. An alternative method for future development could potentially use a spray drying technique for organic solvent removal, however the type of solid lipid may have to be reconsidered to a lower melting point excipient than COMP (T_m = 72 °C), due to the technical high temperature restrictions on the machinery.[27]

2.3 Conclusions

Throughout this chapter we have demonstrated the extensive optimisation of COMP-SLNs and IND-SLNs through the choice of solid lipid, stabiliser, organic solvent choice, solvent: anti-solvent ratios and the optimisation of the masses of all excipients involved. The formation of SLNs is often developed through a time-consuming trial and error-based method, however this chapter aimed to show experimental optimisation that enables a more concise and detailed experimental progression to enhance SLN development. The use of drug-lipid compatibility testing through DSC and PXRD methods have become increasingly more common throughout the literature. This chapter has shown that these methods can reinforce the effectiveness of the qualitative interpretation of PXRD and the quantitative interpretation of DSC as joint indicators of potential good and bad drug-lipid compatibility. The strength of these two analytical techniques combined to determine drug-lipid compatibility was further reinforced through proof of concept precipitations using solid lipids (Gelot 64, Geleol), that were determined to be non-optimal from the data gained. Additional experiments highlighted the importance of the choice of organic solvent used in nanoprecipitation methods, the importance of optimising the hydrophobic lipids and the importance of screening stabilising excipients. The drawbacks of including IND was apparent when incorporated into systems containing 0.8 mg/mL of stabiliser and therefore alternative experimental routes were explored. Firstly, increasing the stabiliser concentration to 10 and 20 mg/mL was successful, however reduced the drug loading to 0.23 wt% and 0.12 wt% respectively. In order to reach the required therapeutic dosage, 980 mL of the dispersions would have to be administered. Further research showed that implementing various blends of different Pluronic® F68 and F127 which enabled an increase of drug content to 3 wt% and a consequent reduction in administration

volume to 76.4 mL. However, the masses of non-therapeutic excipients within these systems were then reduced by implementing Tween 20 and Tween 80 as a cosurfactant, alongside Pluronic® F68 and Pluronic® F127. In turn this increased the administration volume requirement to 141.2 mL. Nevertheless, this significantly decreased the masses of carrier excipients from 211.5 mg to 114.5 mg in comparison to the Pluronic®-only systems. This was a significant improvement in the IND-SLN formulation. Further studies required the removal of 1-propanol from the aqueous dispersions as the mass of the organic solvent exceeded the pharmaceutical requirement for translational therapeutics. Methods such as dialysis, freeze drying, spiral evaporation and centrifugation were trialled. Unfortunately all of these methods were unsuccessful and further work to aid 1-propanol removal from these samples should be considered.

2.4 References

1 P. Ghasemiyeh and S. Mohammadi-Samani, *Res. Pharm. Sci.*, 2018, 13.

2 A. Gordillo-Galeano and C. E. Mora-Huertas, *Eur. J. Pharm. Biopharm.*, 2018, **133**, 285–308.

3 Q. Zhong and L. Zhang, *Adv. Colloid Interface Sci.*, 2019, **273**, 102033.

4 A. Akbarzadeh, R. Rezaei-sadabady, S. Davaran, S. W. Joo and N. Zarghami, *Nanoscale Res. Lett.*, 2013, **8**, 1–9.

5 L. G. Souza, E. J. Silva, A. L. L. Martins, M. F. Mota, R. C. Braga, E. M. Lima, M. C. Valadares, S. F. Taveira and R. N. Marreto, *Eur. J. Pharm. Biopharm.*, 2011, **79**, 189–196.

6 F. Shi, J. H. Zhao, Y. Liu, Z. Wang, Y. T. Zhang and N. P. Feng, *Int. J. Nanomedicine*, 2012, **7**, 2033–2043.

7 A. Khosa, S. Reddi and R. N. Saha, *Biomed. Pharmacother.*, 2018, **103**, 598–613.

8 M. Yoshioka, B. C. Hancock and G. Zografi, *J. Pharm. Sci.*, 1994, **83**, 1700–1705.

9 B. Legendre and Y. Feutelais, *J. Therm. Anal. Calorim.*, 2004, **76**, 255–264.

10 E. Atef, H. Chauhan, D. Prasad, D. Kumari and C. Pidgeon, *ISRN Chromatogr.*, 2012, **2012**, 1–6.

11 S. Wada, S. Kudo and H. Takiyama, *J. Cryst. Growth*, 2016, **435**, 37–41.

12 U.S. Food and Drug Administration Center for Drug Evaluation and Research Inactive Ingredient Database, http://www.accessdata.fda.gov/scripts/cder/iig/index.cfm., (accessed March 2021).

13 M. Giardiello, N. J. Liptrott, T. O. Mcdonald, D. Moss, M. Siccardi, P. Martin, D. Smith, R. Gurjar, S. P. Rannard and A. Owen, *Nat. Commun.*, 2016, **7**, 1–10.

14 T. O. Mcdonald, M. Giardiello, P. Martin, M. Siccardi, N. J. Liptrott, D. Smith, P. Roberts, P. Curley, A. Schipani, S. H. Khoo, J. Long, A. J. Foster, S. P. Rannard and A. Owen, *Adv. Healthc.*

Mater., 2014, **3**, 400–411.

15 A. C. Savage, L. M. Tatham, M. Siccardi, T. Scott, M. Vourvahis, A. Clark, S. P. Rannard and A. Owen, *Eur. J. Pharm. Biopharm.*, 2019, **138**, 30–36.

16 W. Mehnert and K. Mader, *Adv. Drug Deliv. Rev.*, 2001, **47**, 165–196.

17 C. Vitorinoa, F. A. Carvalho, A. J. Almeida, J. J. Sousaa and A. A. C. C. Pais, *Colloids Surfaces B Biointerfaces*, 2011, **84**, 117–130.

18 A. M. Bodratti and P. Alexandridis, *J. Funct. Biomater.*, 2018, **9**, 1–24.

19 P. Sakdiset, T. Amnuaikit, W. Pichayakorn and S. Pinsuwan, *J. Drug Deliv. Sci. Technol.*, 2019, **52**, 760–768.

20 J. M. Aceves-Hernandez, I. N. Vázquez, F. J. Aceves, J. Hinojosa-Torres, M. Paz and V. M. V.M.Castaño, *J. Pharm. Sci.*, 2009, **98**, 2448–2463.

21 I. Güllü, Ş. Yalçin, Gül. Tekuzman, I. Barişlta, N. Alkiş, I. Çelik, N. Zengin, N. Güler, A. Kars, Eşm. Baltali, E. Kansu and D. Firat, *Cancer Invest.*, 1996, **14**, 239–242.

22 S. E. Schoenike and W. J. Dana, *Clin. Pharm.*, 1990, **9**, 179–191.

23 S.-H. Hsu, C.-J. Wen, S. A. Al-Suwayeh, H.-W. Chang, T.-C. Yen and J.-Y. Fang, *Nanotechnology*, 2010, **21**,.

24 M. Elmowafy, A. Samy, M. A. Raslan, A. Salama, R. A. Said, A. E. Abdelaziz, W. El-Eraky, S. El Awdan and T. Viitala, *AAPS PharmSciTech*, 2016, **17**, 663–672.

25 G. Ab and B. Ioioi, *Toxicol. Lett.*, 1986, **30**, 203–207.

26 L. Shen, A. Guo and X. Zhu, *Surf. Sci.*, 2011, **605**, 494–499.

27 Y. Duan, A. Dhar, C. Patel, M. Khimani, S. Neogi, P. Sharma, N. Siva Kumar and R. L. Vekariya, *RSC Adv.*, 2020, **10**, 26777–26791.

28 V. A. Duong, T. T. L. Nguyen and H. J. Maeng, *Molecules*, 2020, **25**, 1–36.

29 Guidance for Industry - U.S. Department of Health and Human Services Food and Drug Administration Center for Drug Evaluation and Research (CDER), https://www.fda.gov/media/133650/download, (accessed April 2021).

30 S. Shrestha, B. Wang and P. Dutta, *Adv. Colloid Interface Sci.*, 2020, **279**, 102162.

31 A. Almalik, I. Alradwan, M. A. Kalam and A. Alshamsan, *Saudi Pharm. J.*, 2017, **25**, 861–867.

32 T. M. Amis, J. Renukuntla, P. K. Bolla and B. A. Clark, *Pharmaceutics*, 2020, **12**, 1–15.

33 A. Singh, I. Ahmad, S. Ahmad, Z. Iqbal and F. J. Ahmad, *Drug Dev. Ind. Pharm.*, 2016, **42**, 1524–1536.

2.5 Appendix

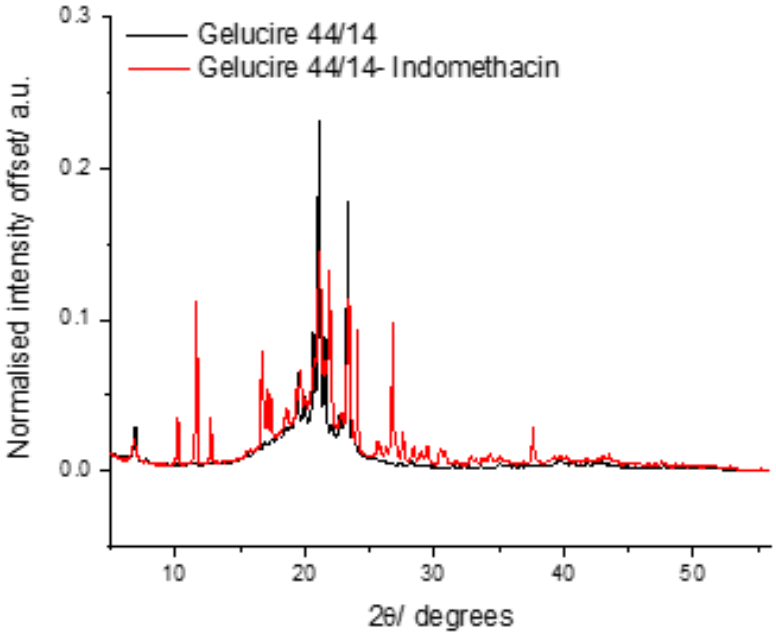

Appendix Figure A 1: PXRD of Gelucire 44/14 and IND. highly crystalline and not for further development.

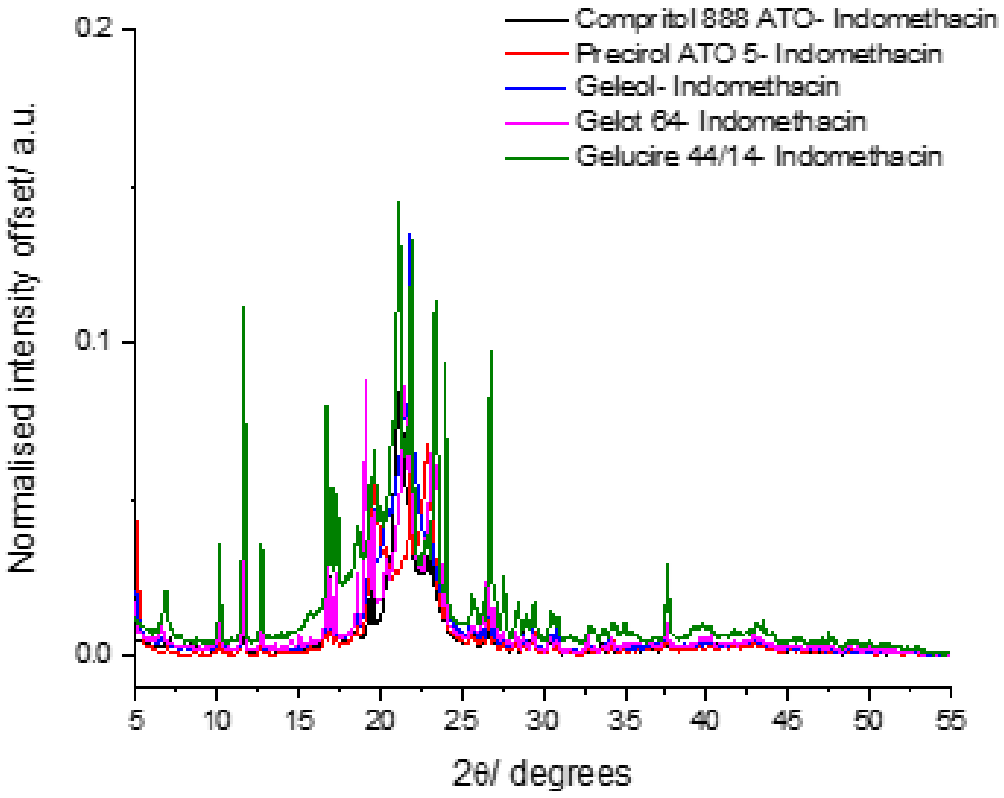

Appendix Figure A 2: PXRD of drug-lipid melts did not show a significant shift in the peaks identified to enable confident correlation to different indomethacin polymorphs.

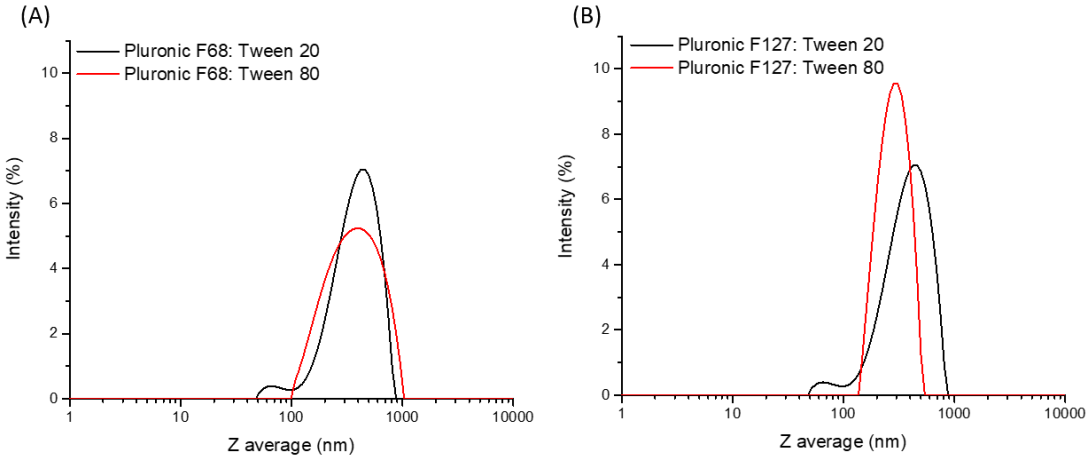

Appendix Figure A 3: DLS traces of blank SLNs when blending Tween 20 or Tween 80 with Pluronic F68 or F127

CHAPTER 3

Using Pyrene to Probe the Effects of Pluronic® Stabilisers on the Internal Core Lipid Environment in SLNs

Publication from this chapter in Nanoscale Advances (2020): Using pyrene to probe the effects of poloxamer stabilisers on internal lipid microenvironments in solid lipid nanoparticle.

Jessica M. Taylor [a], Kyle Scale [a], Sarah Arrowsmith [b], Andy Sharp [c], Sean Flynn [a], Steve Rannard [a] and Tom O. McDonald [a]

Chapter 3

3.1 Introduction

3.1.1Fluorescence spectroscopy

Fluorescence spectroscopy is one of several methods that can be used to monitor spatial, structural or environmental changes of molecules in an excited state.[1] Fluorophores, i.e. fluorescent compounds, exhibit photoluminescence properties and therefore emit light without any thermal input.[2] The fundamental physical chemistry of fluorescence is not required for the purpose of this thesis, however an introduction of how the fluorescent properties of pyrene can be used to identify environmental changes is required is given in the subsequent subsections.

3.1.2 Pyrene as a fluorescent probe

Pyrene ($C_{10}H_{16}$) is a polycyclic aromatic hydrocarbon, made from 4 fused planar ring structures (Figure 3.1).[3] Pyrene possesses unique electronic properties due to its inherent aromaticity, regardless of disobeying Huckels 4n+ 2π electron rule. [4,5]

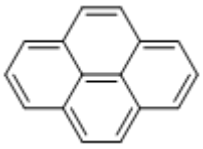

Figure 3.1: The chemical structure of pyrene.

The unique sensitivity of pyrene molecules to an external stimuli allows intricate structure-property relationships to be exploited. This may be achieved through varying experimental parameters to identify structure-property relationships and use that understanding to inform material and/or process optimisation. For example, recent research has demonstrated that pyrene is sensitive to its immediate microenvironment and spatial proximity to other fluorophore molecules, and has therefore been employed as a guest molecule to monitor protein folding phenomenons.[6–9] Alternative research has also explored the effects of temperature, pH, concentration, presence of ionic species and/or organic solvents and their effects on pyrene fluorescence.[10–13] Pyrene also responds to structural or electronic changes in

complex systems, that can be tracked not only through fluorescence, but also through nuclear magnetic resonance (NMR), isothermal titration calorimetry (ITC) and UV/Vis.[14] As a result, this has led to pyrene being extensively studied in several fields including biochemistry, supramolecular chemistry, catalysis, electronics, optical applications and nanotechnology.[15]

3.1.3 Pyrene Fluorescence

One disadvantage of many fluorophores is that they cannot accurately track polarity changes within heterogeneous systems. This difficulty occurs as many fluorophore molecules contain hydrophilic and hydrophobic functionalities. The amphiphilic nature of these fluorophores allows them to interact with the external environment *via* hydrogen and/or hydrophobic bonding. Consequently, the fluorophore localises at the hydrophilic/hydrophobic interfaces within the systems; thus not accurately tracking polarity changes.[18–21] However, due to the inherent hydrophobicity of pyrene, it can be determined that the small molecule would favourably partition into hydrophobic environments more so than other fluorophores. Glushko *et al*. explained that the ability to probe polarity changes through pyrene fluorescence is resultant of the unique interactions of pyrene dipoles in the single excited state, with the dipoles of surrounding molecules.[16] This finding is of significant benefit as it allows for changes within hydrophobic regions to be detected which have been caused by changes in external stimuli.[17] To the best of our knowledge, the use of pyrene to investigate complex polarity changes was first reported by Vanderkooi *et al.* in 1974.[18] In their work, pyrene was used to aid the understanding of the relationship between components in biological membranes, as well as the relationship of hydrophobic solutes passing through a biological membrane *via* lateral diffusion.[18]

3.1.4 Pyrene Emission Spectra

Pyrene has an emission spectrum characterised by 5 intense vibrational bands, denoted as I_1-I_5 and span from 375 to 405 nm, shown in Figure 3.2.

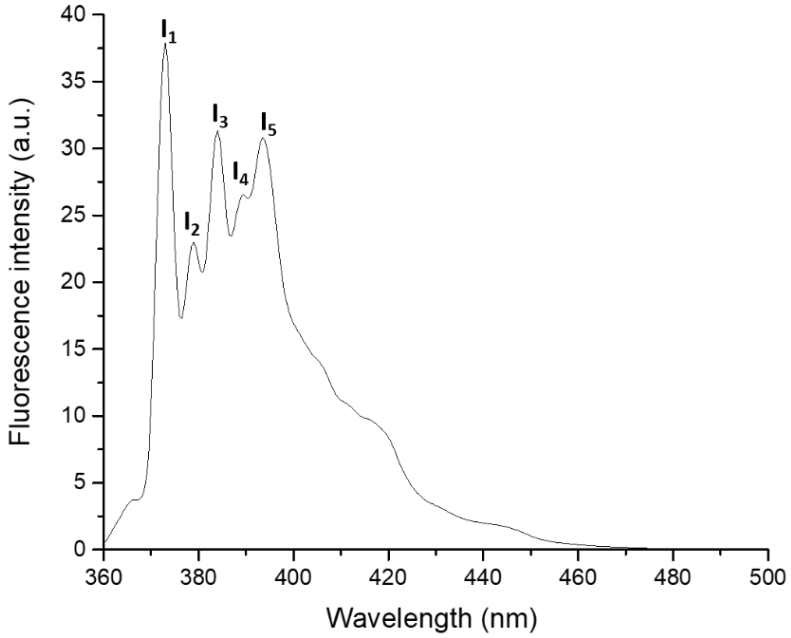

Figure 3.2: Emission spectra of pyrene dissolved in a solution of 1-propanol.

Pyrene is able to track polarity changes within a system due to the difference in the intensity of the first and third vibrionic band, commonly known as the I_1/I_3 ratio or the Py value. The I_1 band dominates the pyrene emission spectra in polar environments, and the I_3 band dominates in non-polar environments.[16] The higher the I_1/I_3 ratio, the more polar the microenvironment and vice versa for a lower I_1/I_3 detection.

A secondary feature of the pyrene emission spectrum is the excimer emission that appears as a broader band at ~460 nm (Figure 3.3), and is not present in all pyrene emission spectrums.

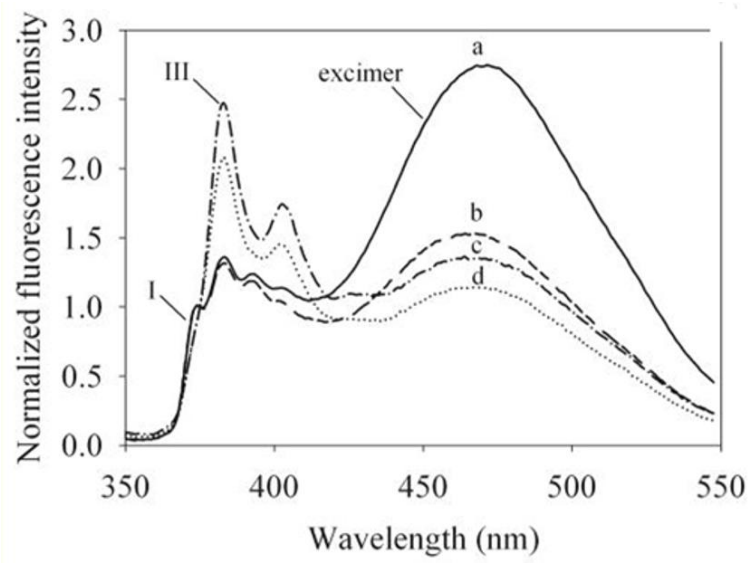

Figure 3.3: Pyrene emission spectra displaying intense, variable excimer emissions. Figure adapted from:Bains et al.[19]

For excimer emission to occur the pyrene molecules must be within a close enough proximity to transfer energy from one excited pyrene molecule to another, forming a pyrene-dimer.[18] Bains *et al.* reported that a change in the I_1/I_3 ratio coupled with excimer emission fluctuations can successfully detect intermolecular distances of pyrene labelled amino acids within 3.5 nm of each other in biological membranes.[20] Excimer emissions can be dependent on pyrene concentration, and additionally do not often occur in systems such as organic dispersions where the pyrene monomers are not confined to an area; thus not spatially proximal.[21] As a result of the attractive and informative properties of pyrene, it has been implemented in several nanoparticle systems. Examples are discussed in the following section.

3.1.5 Pyrene Uses in Nanoparticle Systems

Nanoparticles for therapeutics are often employed to overcome inherent aqueous solubility issues of hydrophobic drugs. As pyrene is a highly hydrophobic molecule with microenvironment sensitivity and poor aqueous dissolution, it can act as a 'model hydrophobic drug' to understand behaviours within these systems for material optimisation.[2] For example, pyrene has been used to track targeted delivery and to characterise its stimuli responsiveness within nanoparticles to factors such as pH, light and temperature.[22–26] The ability of pyrene to monitor polarity changes within a nanoparticle microenvironment has been exploited to probe

critical micelle concentrations (CMCs), to track the self-assembly behaviours of both commercial and bespoke polymers and also to monitor release kinetics from nanosystems though nanoparticle dissociation.[27,28,37,29–36]

Most importantly for our research, pyrene incorporation in SLNs has predominantly been used for the exploration of critical aggregation concentrations (CACs) and the triggered release of pyrene through external stimuli.[31] In a more recent study published in 2017, Tang *et al.* demonstrated how the core polarity of SLNs can be intuitive for SLN formation. It was clearly demonstrated that an increase in the chosen solid lipid mass (Geleol Mono and Diglycerides Nf) from 5 to 10wt% causes a significant increase in internal hydrophobicity, thus a decrease in the I_1/I_3. [38] This resulted in the amphiphilic block stabiliser used (mPEG-b-PCL), having better stabilisation in the presence of the lipid and was also able to successfully increase the oral bioavailability of anticancer agent, larotaxel, from 6.3 % to 13.1 % than in the corresponding polymeric nanoparticles.[38] This shows that core polarity is a fundamental parameter that can influence drug loading, with the ability to improve pharmacological bioavailability. This is key for SLN formulation, where their inability to encapsulate a high percentage of hydrophobic drug is a major drawback for their use. Therefore, this highlights that incorporating pyrene in the lipid core of SLN systems allows a relationship between chosen stabilisers and lipid core polarity to be detected, which in turn can be tailored for the specific encapsulation of a chosen therapeutic entity. This finding is of significant importance for the formulation development of SLNs and therefore probed the research into how the lipid core polarity can be tuned using different stabilisers throughout this chapter. The stabilisers implemented in this chapter are discussed in the following section.

3.1.6 Pluronic® stabilisers

Pluronics® are ABA triblock copolymers with the generic structure shown below in Figure 3.4. They are amphiphilic molecules consisting of hydrophilic polyethylene oxide (PEO) and hydrophobic polypropylene oxide (PPO) in a PEO-PPO-PEO arrangement.

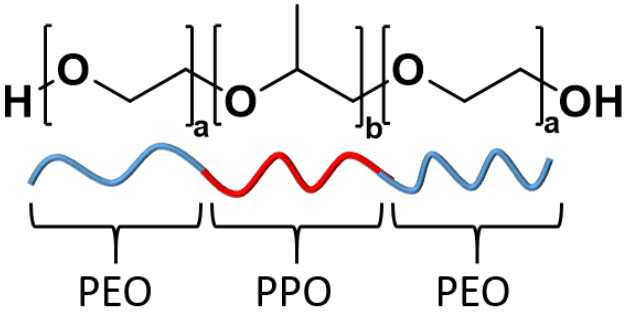

Figure 3.4: Generic structure of Pluronic® ABA block copolymers.

Amongst the family of Pluronic® stabilisers there is a wide range of variables including their hydrophilic lipophilic balance (HLB), PPO/PEO ratio, CMC and molecular weight (MW), all of which are parameters compared throughout this chapter. Table 3.1 below shows the polymers that were chosen due to their common use in nanoparticle systems and their physical properties.[39] Although each of the polymers are referred to as the branded Pluronic® denotation throughout this Chapter, Table 3.1 shows the generic poloxamer denotation for comparison.

Table 3.1: Pluronic® stabilisers chosen to assess the influence on core polarity.

Pluronic®	**Poloxamer**	**Formula**	**HLB value**	**PPO/ PEO ratio**	**Average MW (g/mol)**	**CMC at 25°C (M)**
P105	P335	PEO_{37}-PPO_{56}-PEO_{37}	15	0.76	6500	6.2×10^{-6}
F127	P407	PEO_{100}-PPO_{65}-PEO_{100}	22	0.33	12600	2.8×10^{-6}
F68	P188	PEO_{76}-PPO_{29}-PEO_{76}	29	0.20	8400	4.8×10^{-4}
L64	P184	PEO_{13}-PPO_{30}-PEO_{13}	15	1.2	2900	4.8×10^{-4}

3.1.7 Chapter Aims

From Chapter 2, it was shown that Compritol 888 ATO-SLNs (blank-SLNs) formed with different Pluronics®, namely Pluronic® F68 and Pluronic® F127, exhibited a significant difference in their ability to encapsulate and stabilise IND; with F127 demonstrating a better affinity for Indomethacin loaded SLNs (IND-SLNs). Interestingly this was dissimilar to the blank-SLNs, whereby both F68 and F127 provided satisfactory stabilisation with negligible difference in Z average (D_z), dispersity (PdI) and visual appearance in the absence of the drug molecule. Throughout this chapter, the effect that different Pluronic® stabilisers have on the internal lipid core environment of SLNs is explored. As IND is a non-polar compound, and thus prefers to be within a non-polar environment, we propose that the implementation of pyrene within the lipid core will gain insight on polarity changes occurring when incorporating different Pluronic® stabilisers. Consequently, if a relationship can be identified between the Pluronic® properties and their ability to influence the core lipid microenvironment, this enables a concept of lipid-polarity tuning to tailor the encapsulation of non-polar molecules. Throughout this chapter, pyrene is incorporated within the lipid core at 0.1 wt%. The Pluronic® stabilisers chosen were F127, F68, P105 and L64, based on their range of comparable properties and their abundant usage in nanoparticle systems.[39,40]

3.2 Results and Discussion

3.2.1 Synthesis of blank-SLNs

All SLNs discussed throughout this chapter were formulated *via* the solvent injection method (SIM). The SIM is a type of nanoprecipitation process where hydrophobic materials are precipitated in an aqueous environment, as thoroughly discussed and optimised for COMP-SLNs in Chapter 1, section 1.8.2.5. Briefly for blank (lipid only) nanoparticles, the hydrophobic phase consisted of COMP (18 mg) in 1-propanol (4 mL). The aqueous phase consisted of a Pluronic® stabiliser (0.8 mg/mL) in DI water (20 mL) whilst mechanically agitated at 350 rpm and at 26 °C. The hydrophobic phase was heated to 82 °C, 10 °C above the melting point of COMP (MP= 72 °C), followed by injection into the aqueous phase to form COMP-SLNs. The visual appearance of the blank-SLNs were significantly more turbid in comparison to the Pluronic® micellar dispersions which possessed clear transparent solutions as below in Figure 3.5Ai-iv for Pluronic® P105, F127, F68 and L64 respectively. Conversely, the blank-SLNs shown in Figure 3.5B i-iv with the same respective Pluronic® order.

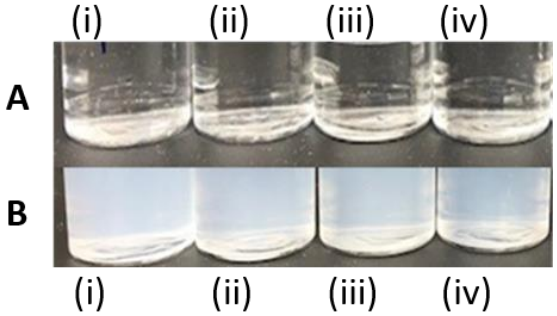

Figure 3.5: The difference in turbidity between (A) poloxamer micelle solutions and (B) poloxamer stabilised SLN stabilised by (i) P105, (ii) F127, (iii) F68 and (iv) L64.

All COMP-SLN dispersions displayed stable dispersions and the physical properties including D_z, PdI and a sustained derived count rate as shown below in Table 3.2.

Table 3.2: D_z, PdI and derived count rate measurements for blank loaded SLNs.

Pluronic®	**Formula**	**D_z (nm)**	**PdI (%)**	**Derived count rate (kcps)**
P105	PEO_{37}-PPO_{56}-PEO_{37}	236 ± 29	22 ± 3	454969 ± 10472
F127	PEO_{100}-PPO_{65}- PEO_{100}	246 ± 20	21 ± 4	474137 ± 44504
F68	PEO_{76}-PPO_{29}-PEO_{76}	227 ± 33	22 ± 2	472794 ± 31970
L64	PEO_{13}-PPO_{30}-PEO_{13}	212 ± 27	23 ± 3	447865 ± 35172

Figure 3.6 illustrates that nearly all dispersions formed a monomodal, intensity weighted D_z distribution for all SLNs containing COMP, denoted as blank-SLNs. This was with the exception of L64 with a presence of a shoulder at 22-37 nm, attributed to an additional smaller population which are most likely micellar aggregates. All Pluronic® stabilised SLNs were of similar D_z ranging between 212-246 nm and a respective PdI (%) range of 20-23 %. Although all samples were of negligible difference, the marginally smaller D_z for Pluronic® L64 (212 nm) may be attributed to the smaller PEG corona (PEO units = 13).

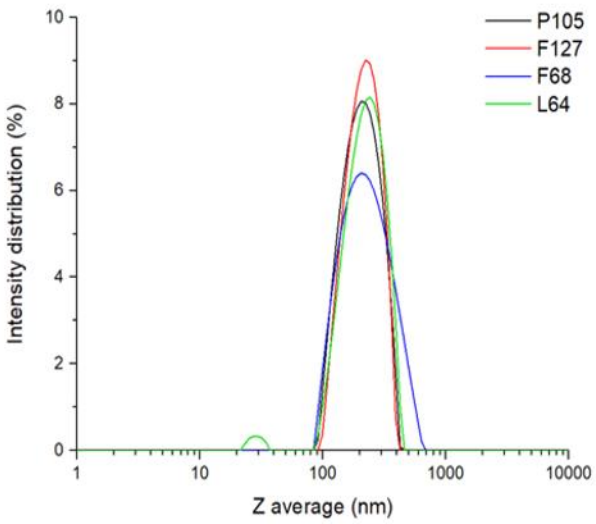

Figure 3.6: Size intensity monomodal trace of Pluronic® stabilised lipid particles.

3.2.2 Synthesis of Pyrene-COMP-SLNs

Pyrene containing SLNs, denoted as Py-COMP-SLNs, were synthesised as described previously in section 3.4.1. Similarly to COMP-SLNs, there was negligible difference in the D_z, PdI or derived count rate shown in Table 3.3

Table 3.3: D_z, PdI and derived count rate measurements for pyrene loaded SLNs

Pluronic®	**Formula**	**D_z (nm)**	**PdI (%)**	**Derived count rate (kcps)**
P105	PEO_{37}-PPO_{56}-PEO_{37}	254 ± 78	26 ± 2	437690 ± 17327
F127	PEO_{100}-PPO_{65}- PEO_{100}	237 ± 6	24 ± 2	457036 ± 30082
F68	PEO_{76}-PPO_{29}-PEO_{76}	235 ± 63	24 ± 1	484775 ± 15618
L64	PEO_{13}-PPO_{30}-PEO_{13}	243 ± 44	25 ± 2	527962 ± 96285

Figure 3.7 shows that all other Pluronic® stabilised SLNs were of similar size and PdI, with D_z values recorded between 235 to 254 nm, with a respective PdI range of 24-26 %. There are similarities in the D_z and PdI across all Py-COMP-SLN samples, with comparable data to the COMP-SLNs also, shown in Table 3.4.

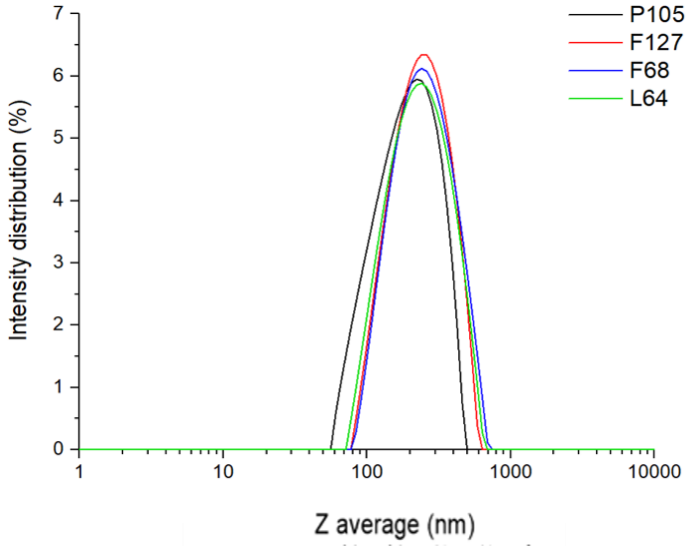

Figure 3.7: Overlay of Particle size distribution traces for Py-COMP-SLNs stabilised with P105 (black line), F127 (red line), F68 (blue line) and L65 (green line)

Table 3.4: Data comparison for COMP-SLNs vs Py-COMP-SLNs.

	Pluronic®	**D_z (nm)**	**PdI (%)**	**Derived count rate (kcps)**
Blank-SLN	P105	254 ± 78	26 ± 2	437690 ± 17327
Py-COMP SLN	**P105**	**236 ± 29**	**22 ± 3**	**454969 ± 10472**
Blank- SLN	F127	237 ± 6	24 ± 2	457036 ± 30082
Py-COMP SLN	**F127**	**246 ± 20**	**21 ± 4**	**474137 ± 44504**
Blank-SLN	F68	235 ± 63	24 ± 1	484775 ± 15618
Py-COMP SLN	**F68**	**227 ± 33**	**22 ± 2**	**472794 ± 31970**
Blank-SLN	L64	243 ± 44	25 ± 2	527962 ± 96285
Py-COMP SLN	**L64**	**212 ± 27**	**23 ± 3**	**447865 ± 35172**

Overall, COMP-SLNs and Py-COMP-SLNs were very similar in terms of particle properties. Therefore, it can be assumed that any differences in pyrene fluorescence measurements are as a result of Pluronic® interactions with the lipid core influencing the lipid microenvironment.

3.2.3 Fluorescence Control Measurements

3.2.3.1 Solvent Controls

For all experiments conducted within this chapter, all nanoparticles were synthesised in a 5:1 ratio of water:1-propanol, as well as two control samples of water and 1-propanol as individual solvent systems. For each solvent system, the I_1/I_3 maxima and the emission spectra were compared as shown in Figure 3.8.

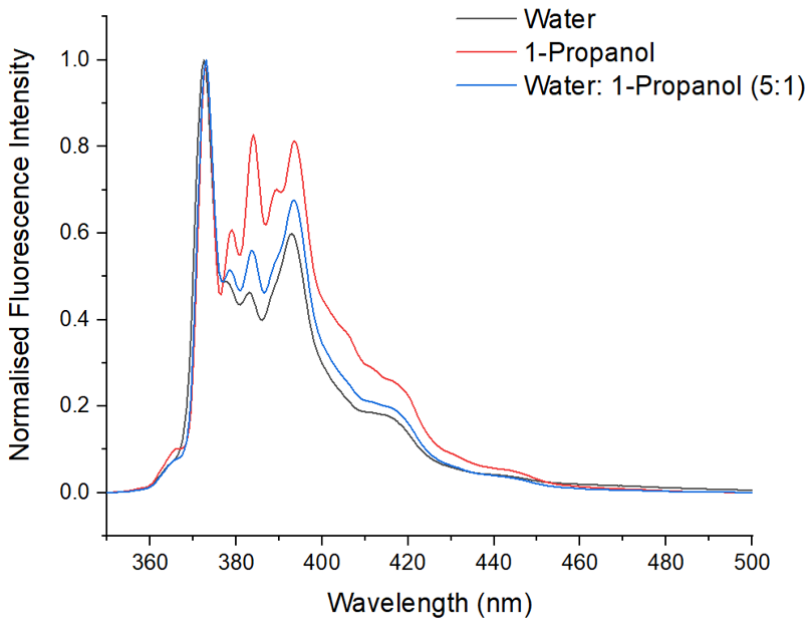

Figure 3.8: Solvent control samples of free pyrene in each respective solvent system: water, 1-propanol and the water:1-propanol mix. The emission spectra have been normalised with respect to the emission at 373 nm (I_1), the polarity independent peak.

As can be identified in Figure 3.8, there was a significant difference in the I_1/I_3 value for free pyrene in water and in 1-propanol with I_1/I_3 values of 2.18 ± 0.09 and 1.21 ± 0.002, respectively. This was to be expected as the sensitivity of pyrene to solvent polarity has been outlined previously. For the mixed solvent system, the addition of 1-propanol as a more hydrophobic solvent to water in a water:1-propanol 5:1 ratio gives an I_1/I_3 value of 1.79 ±

0.003. All fluorescent measurements are carried out after nanoparticle synthesis in this mixed solvent system, hence 1.79 ± 0.003 will be considered the maxima and represent 100% free pyrene.

3.2.3.2 Pyrene in Pluronic® Micellar Dispersions

All Pluronics® are used at a 0.8 mg/mL concentration for the consequent experiments. The ability of pyrene to preferentially diffuse into the more hydrophobic region of the polymeric micelles has been exploited throughout previous research; for example to determine CMC values of commercial and bespoke polymers.[41] With relevance to this research, the capability of pyrene to diffuse into the central Pluronic® micellar PPO core was highlighted. The purpose of the following experiments was to identify differences in the microenvironment of the generic 5:1 water:1-propanol solvent system in the presence or absence of Pluronic® stabilisers. The I_1/I_3 maxima for pyrene in the 5:1 water:1-propanol system has previously been established at 1.79 ± 0.003. In the presence of Pluronic micelles, the I_1/I_3 maxima were reduced dependent on the Pluronic® stabiliser used as highlighted below in Figure 3.9.

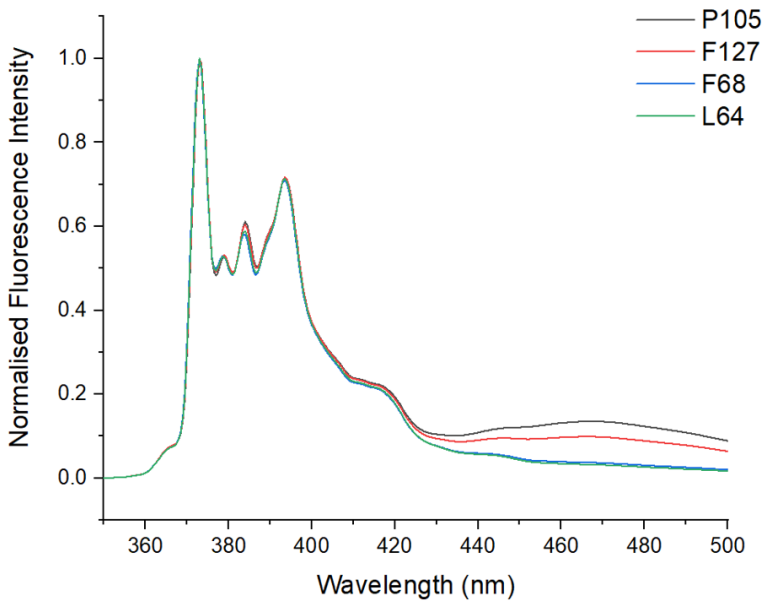

Figure 3.9: Pyrene emission in aqueous polymer dispersions in water and in water: 1-propanol mixed solvent system.

The I_1/I_3 values, D_z and PdI are shown in Table 3.5. The fluorescence intensity has been normalised with respect to the polarity independent emission at 373 nm, peak I_1. The I_1/I_3 values obtained for P105, F127, F68 and L64 where 1.63 ± 0.006, 1.66 ± 0.010, 1.72 ± 0.021 and 1.70 ± 0.001 respectively. Although the I_1/I_3 values were of small difference amongst the Pluronic®-micellar dispersions, Figure 3.9 emphasises the fact that Pluronic® F68 and L64 has no excimer emission and the fluorescence intensity returns to the baseline. Conversely, for Pluronic® P105 and F127 there are significant excimer emissions at ~440 nm. The excimer emissions demonstrate spatial proximity of pyrene molecules, suggesting a higher concentration of pyrene molecules packed more closely together in P105/F127 dispersions *vs* F68/L64 dispersions. This observation can be accredited to the difference in the PPO block length in the different Pluronic® stabilisers. From Table 3.5 it can be determined that the PPO block length of F127 and P105 have a significantly higher number of repeating units and therefore the micelles present have an increased density of non-polar PPO units within the cores. For this reason, the pyrene molecules experience a less polar environment in F127 and P105 micelles.

Table 3.5: The fluorescence and DLS data provided for Pluronic® micellar dispersions in a water:1-propanol mixed solvent system.

Pluronic®	**D_z (nm)**	**PdI (%)**	**I_1/I_3**	**PPO block length**
P105	86	21	1.66 ± 0.010	56
F127	82	23	1.63 ± 0.066	65
F68	107	17	1.72 ± 0.021	29
L64	84	15	1.70 ± 0.001	30

Therefore, after establishing the key differences between the individual I_1/I_3 maxima's in Pluronic® micellar dispersions, the corresponding fluorescence data can be directly compared to Py-COMP-SLNs discussed in further detail in the sections below.

3.2.3.3 Pluronic® micelle fluorescence

Prior to Py-COMP-SLN analysis it was deemed necessary to rule out any potential fluorescence input from any pyrene containing Pluronic® micelles. If the micelles and Py-

COMP-SLNs were to mutually coexist within the dispersion, this fluorescence measurement would be an 'average', therefore inaccurately indicating the influence that Pluronic® stabilisers have directly on the internal core lipid environment. Therefore, to prove that the fluorescence measurements obtained for Py-COMP-SLN dispersions was due to a dominant population of SLNs, each dispersion was centrifuged through a 10 kDa filter to remove pyrene containing Pluronic® micelles prior to further fluorescence analysis. The resultant measurements are displayed below in Figure 3.10.

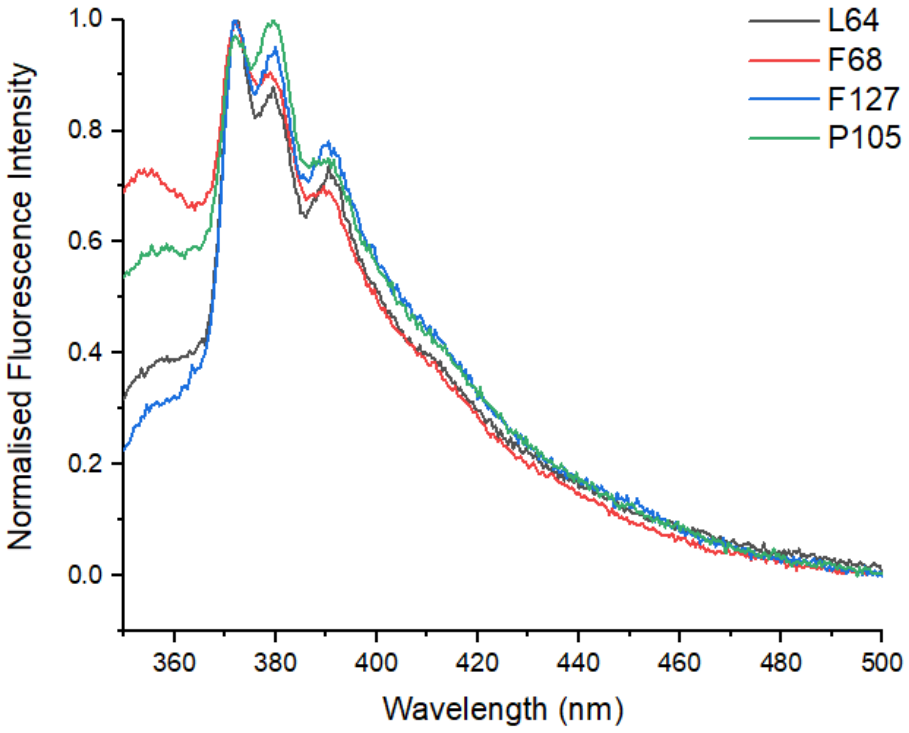

Figure 3.10: Fluorescence analysis of the supernatant of Py-COMP-SLN dispersions after centrifugation through a 10 kDa MW filter.

The fluorescence measurements from the supernatant obtained (Figure 3.10), highlights that there was very limited fluorescence, coupled with ill-defined emission spectra. This finding therefore supports that the pyrene was predominantly within the lipid cores of the Py-COMP-SLNs, independent of the stabiliser used. Herein, it was therefore assumed that all fundamental differences within the fluorescence emission spectra is resultant of the Pluronic® stabiliser interaction with the pyrene containing solid lipid core.

3.2.3.4 Pyrene entrapment in SLNs

It was hypothesised that the inclusion of a highly hydrophobic COMP solid lipid would decrease the I_1/I_3 value, as the pyrene monomers are expected to partition into the non-polar core of SLNs upon nucleation. As COMP consists of mono-, di- and tri- esters of behenic acid, illustrated in Figure 3.11, the pyrene molecules are able to be favourably trapped between the long C_{22} alkyl chains, providing a more hydrophobic environment than the Pluronic®-micellar PPO cores.

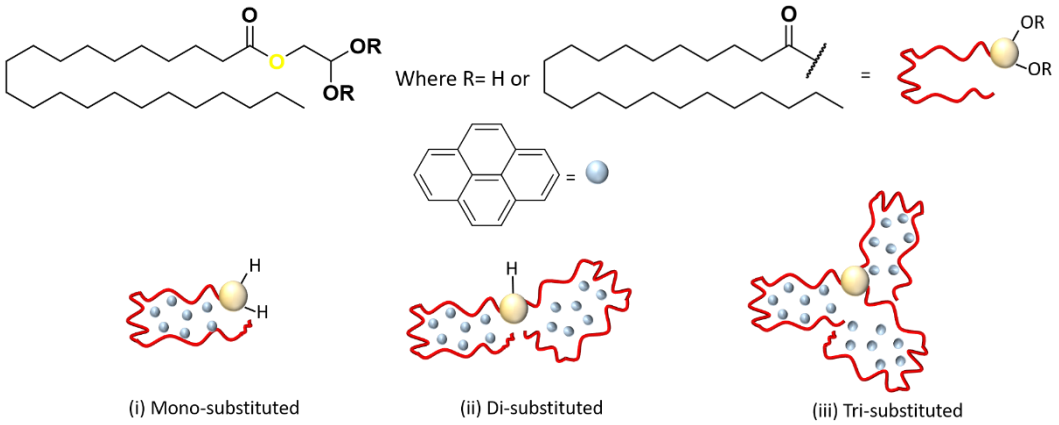

Figure 3.11: The entrapment of pyrene within the solid lipid upon injection and nucleation of the COMP lipid which consists of a mixture of (i) mono, (ii) di and (iii) tri-substituted glycerol with behenic acid.

The individual Py-COMP-SLN dispersions were analysed. Figure 3.12 below highlights a significant decrease in the I_1/I_3, regardless of the stabiliser used, in comparison to the Pluronic® micellar dispersions and therefore supports the hypothesis that pyrene entrapment is favoured within the lipid alkyl chains.

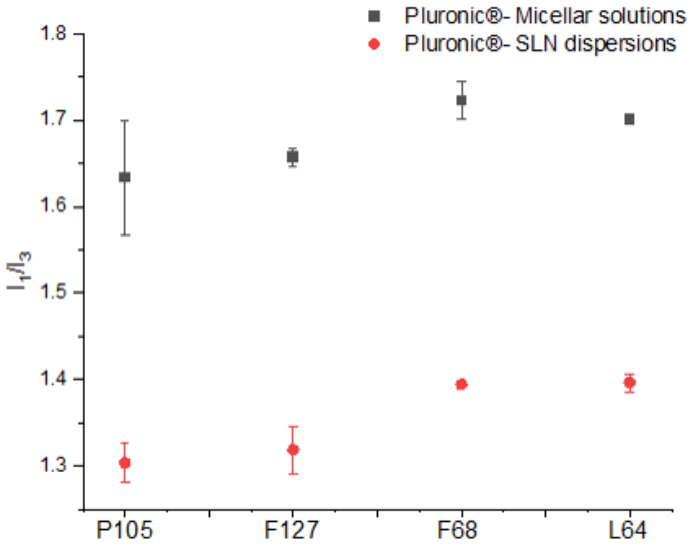

Figure 3.12: The I_1/I_3 values of Pluronic® micelle solutions vs SLN dispersions.

The fluorescence data shown in Figure 3.12 highlights the similarities between the I_1/I_3 of P105 and F127 stabilised SLNs with values of 1.30 ± 0.02 and 1.32 ± 0.03, in comparison to the more polar cores achieved when using F68 and L64 with respective values of 1.39 ± 0.01 and 1.40 ± 0.01. The fluorescence emission spectra for each Py-COMP-SLN dispersion is shown below in Figure 3.13.

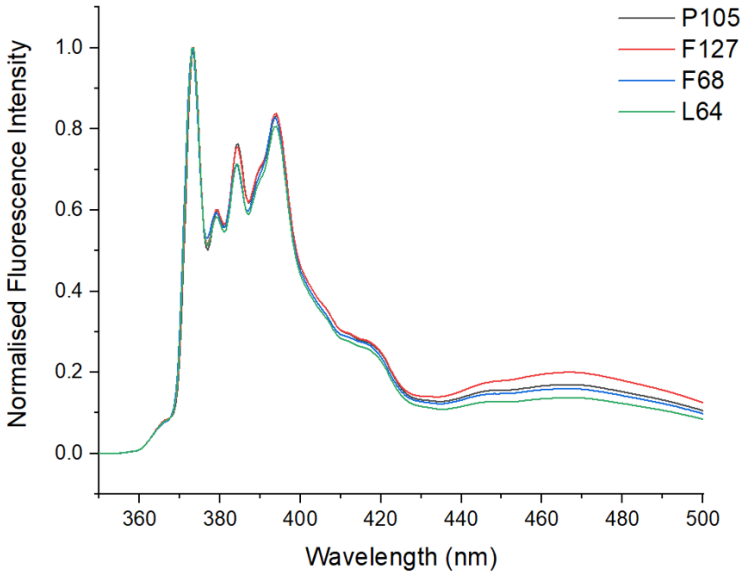

Figure 3.13: Pyrene emission in Py-COMP-SLN systems.

Table 3.6: Fluorescence and DLS data provided for Py-COMP-SLN systems.

Pluronic®	**Formula**	**D_z (nm)**	**PdI (%)**	**I_1/I_3**	***e/m* ratio**
P105	PEO_{37}-PPO_{56}-PEO_{37}	254 ± 78	26 ± 2	1.30 ± 0.02	0.18
F127	PEO_{100}-PPO_{65}- PEO_{100}	237 ± 7	24 ± 2	1.32 ± 0.03	0.21
F68	PEO_{76}-PPO_{29}-PEO_{76}	235 ± 63	24 ± 1	1.39 ± 0.02	0.17
L64	PEO_{13}-PPO_{30}-PEO_{13}	243 ± 44	25 ± 2	1.40 ± 0.01	0.15

Figure 3.13 highlights that Py-COMP-SLNs all contain an excimer emission, which was contrary to the earlier Figure 3.9 of Pluronic® micellar dispersions, whereby only Pluronic® F127 and P105 displayed significant excimer emissions. The increase in the excimer emissions for all stabilisers suggests that the Pluronics® provide a greater influence on the spatial packing of the pyrene molecules within the lipid core, thus forcing the pyrene molecules within a closer proximity. An additional significant parameter that can be calculated from Figure 3.13 is the excimer/monomer (*e/m* ratio). The *e/m* ratio is a function calculated *via* height of the excimer emission (~465-470 nm) divided by the first vibronic band I_1 and have previously been utilised to correlate the extent of spatial proximity and flexibility of pyrene molecules.[42]. The results of the *e/m* ratio for the SLN dispersions are shown in Table 3.6. A larger *e/m* ratio and intense excimer emission is due to increased intermolecular coupling of excited pyrene molecules that are more spatially proximal, which is predominantly shown for F127 and P105 stabilised systems.[42] On the contrary, Pluronic® F68 and L64 SLNs both exhibit lower intensity excimer emissions and *e/m* ratios, indicating that F68 and L64 stabilisers pack less densely on the lipid core surface therefore allowing pyrene to have a greater degree of flexibility and space within the lipid core. The fluorescence similarities (I_1/I_3, the excimer emission and the *e/m* ratio) between P105 and F127 *vs* F68 and L64 was hypothesised to be a result of the Pluronic® physical properties. These physical properties of each Pluronic® subtype, consisting of differences in the HLB, PPO/PEO ratio, CMC and MW shown below in Table 3.7.

Table 3.7: Properties of Pluronic® stabilisers explored

Pluronic®	**Formula**	**HLB value**	**PPO/PEO ratio**	**Average MW (g/mol)**	**CMC at 25 °C (M)**
P105	PEO_{37}-PPO_{56}-PEO_{37}	15	0.76	6,500	6.2×10^{-6}
F127	PEO_{100}-PPO_{65}-PEO_{100}	22	0.33	12,600	2.8×10^{-6}
F68	PEO_{76}-PPO_{29}-PEO_{76}	29	0.20	8,400	4.8×10^{-4}
L64	PEO_{13}-PPO_{30}-PEO_{13}	15	1.2	2,900	4.8×10^{-4}

The aim was therefore to understand a link between the physical properties of the stabiliser and its fluorescent properties, as modelled by the incorporation of pyrene. Moreover, this understanding will provide the foundation to tune the lipid core microenvironment to a more optimal polarity environment, based upon the polarity of the chosen chemical entity to be encapsulated within SLN systems. The physical properties are outlined and discussed below.

3.2.4 Comparing the Pluronic® properties

3.2.4.1 Critical Micelle Concentration

This section explores the relationship between the CMC values of Pluronics® and the impact on the I_1/I_3 value. It is important to note that the CMC values stated are for the Pluronic® stabilisers in water, not the water: 1-propanol mixture and will therefore differ. In order to rule out any difference in CMC effecting the internal polarity of the SLNs, all experiments were standardised to be used at 5 molar wt% with respect to the lipid mass. The physical properties are highlighted below in Table 3.8. The dispersions shown no significant impact on the dispersions for D_z, PdI and no significant drop in the derived count rate in comparison to previous SLN dispersions.

Table 3.8: Physical parameters of SLN dispersions formed with Pluronic® stabilisers standardised to 5 molar wt%.

Pluronic®	**CMC (mmol)**	**I_1/I_3 (0.8 mg/mL)**	**I_1/I_3 (5 molar wt%)**	**D_z (nm)**	**PdI (%)**	**Derived count rate (kcps)**
P105	$6.2x10^{-6}$	1.30	1.33	228	24	428267
F127	$2.8x10^{-6}$	1.32	1.34	193	19	440897
F68	$4.8x10^{-4}$	1.39	1.45	209	16	380936
L64	$4.8x10^{-4}$	1.40	1.44	176	23	420957

The I_1/I_3 values for all Pluronic® stabilisers increased slightly from 1.30 and 1.32 in the SLN dispersions at 0.8 mg/mL to 1.33 and 1.34 for 5 molar wt% dispersions when using P105 and F127 respectively. Similarly for F68 and L64, I_1/I_3 values increased from 1.39 and 1.40 to 1.45 and 1.44, respectively. This may be attributed to the decreased number of moles present for the stabilisers at 5 molar wt% in comparison to 0.8 mg/mL shown in Table 3.9.

Table 3.9: Molar comparison of Pluronic® stabilisers.

Pluronic®	**Moles at 0.8 mg/mL (mol)**	**Moles at 5 molar wt% (mol)**
P105	2.5×10^{-6}	8.5×10^{-7}
F127	1.3×10^{-6}	8.5×10^{-7}
F68	1.9×10^{-6}	8.5×10^{-7}
L64	5.5×10^{-6}	8.5×10^{-7}

However, in all cases the SLN dispersions at 5 molar wt% remained significantly lower than the Pluronic® micellar dispersions where the I_1/I_3 values ranged from 1.63-1.72. Herein, it is determined that differences in the internal polarity is independent of CMC values and instead as a result of a different Pluronic® physical property. The following sections discuss individual properties of Pluronic® stabilisers that may contribute to their effects on SLN formation and internal core polarity.

3.2.4.2 Hydrophobic-Lipophilic Balance and PPO/PEO ratio

In this section, two parameters denoted as the HLB and the PPO/PEO ratio are explored to investigate their impact on the microenvironment polarity. Firstly, the introduction of HLB as a indicative parameter for the behaviour of non-ionic surfactants was firstly introduced as an

arbitrary scale (1-20) by Griffin.[43] Importantly, although the Griffin scale is the most common HLB scale, it does not apply to Pluronic® stabilisers but they do follow the same trend. The trend states that the lower HLB values indicate water in oil (w/o) stabilisers and higher values indicate oil in water (o/w) stabilisers.[43] The method of HLB calculation of Pluronics® is not clear and is often just stated as a numerical value given by the appropriate manufacturers for the branded materials. Therefore, the HLB values for the Pluronics® used have been cited from the same source in the literature by Figueiras *et al.* and are discussed throughout this section.[44,45] Secondly, a parameter denoted as the PPO/PEO ratio was also explored. This parameter arises due to the ABA triblock nature of Pluronic® stabilisers and is calculated by dividing the molecular weight of each respective block. This parameter arguably has a more accurate prediction of Pluronic® behaviour over the HLB value, in particular due to HLB discrepancies seen amongst different brands and throughout the literature. Moreover, therapeutic relationships between the PPO/PEO ratio and the behaviour of Pluronic® stabilisers have been demonstrated. For example, Bahadur *et al*. shows that the larger the ratio, the larger capacity to solubilise clinically relevant hydrophobic entities within micelles.[39,46] Studies that explore further applications of Pluronics® have identified that the PPO/PEO ratio asserts a level of control on a range formulation properties including, mixed micelle behaviours, hydrogel properties and binding affinities to functionalities in lipid membranes.[47–50] As a result, it was apparent that due to the relationships identified for solubilisation of hydrophobic excipients and binding affinities to lipid membranes in particular; the PPO/PEO ratio was explored for its effect on the lipid core polarity. The fluorescence measurements and corresponding HLB values and PPO/PEO ratios are compared below in Table 3.10.

Table 3.10: Comparing the HLB and PPO/PEO properties of Pluronics® and their corresponding I_1/I_3 measurements.

Pluronic®	**Formula**	**HLB**	**PPO/PEO ratio**	**I_1/I_3**
P105	PEO_{37}-PPO_{56}-PEO_{37}	15	0.76	1.30 ± 0.02
F127	PEO_{100}-PPO_{65}- PEO_{100}	22	0.33	1.32 ± 0.03
F68	PEO_{76}-PPO_{29}-PEO_{76}	29	0.20	1.39 ± 0.02
L64	PEO_{13}-PPO_{30}-PEO_{13}	15	1.2	1.40 ± 0.01

Hypothetically the expected relationship between the HLB and the core polarity, is that the higher the HLB value, the more polar the internal core of the lipid microenvironment and therefore a higher I_1/I_3 value would be expected.[51] However, as demonstrated above in Table 3.10, both Pluronic® P105 and L64 have the same cited HLB value of 15, nevertheless with significantly different core polarities of 1.30 ± 0.02 and 1.40 ± 0.01 respectively. As a result, it can be determined that although the HLB parameter is useful for predicting the polymer application, it is not a viable parameter to predict the effects on the lipid core microenvironment.

Secondly, in accordance with Raval *et al*., the expected relationship between the PPO/PEO ratio and Py-COMP-SLNs is inversely proportional whereby the higher the PPO/PEO ratio, the lower the expected I_1/I_3 value, thus the least polar core.[46] This relationship was concluded as Raval *et al*. showed that the higher the PPO/PEO ratio, the more effective the systems were for solubilising hydrophobic material; therefore a higher PPO/PEO ratio would be required to solubilise the highly hydrophobic COMP solid lipid.[46] From the data provided in Table 3.10, the increase in PPO/PEO ratio with a corresponding decrease in I_1/I_3 was apparent for Pluronic® P105, F127 and F68, supporting the prediction of a higher PPO/PEO ratio leading to a less polar lipid core. The least polar core was exhibited by P105 with an I_1/I_3 value of 1.30 ± 0.02 and a respective PPO/PEO ratio of 0.76, in line with the identified trend. However, L64 was the stabiliser with the highest PPO/PEO ratio of 1.2, however possesses the most polar internal core microenvironment with an I_1/I_3 value of 1.40 ± 0.01, contrary to the desired trend. As a result, the PPO/PEO ratio would have to be explored further in order to identify if L64 was an anomalous result, or whether the ratios within a large library of Pluronics® are reliable predictions for core environment polarity and hence SLN formulation development.

3.2.4.3 Molecular Weight

The MW of Pluronic® stabilisers as a physical property controlling internal core lipid environments was explored.

Table 3.11: MW of Pluronics® and their corresponding relationship with lipid core polarity.

Pluronic®	**Formula**	**Average MW (g/mol)**	**Average MW PPO block (g/mol)**	**I_1/I_3**
P105	PEO_{37}-PPO_{56}-PEO_{37}	6,500	3248	1.30 ± 0.02
F127	PEO_{100}-PPO_{65}-PEO_{100}	12,600	3770	1.32 ± 0.03
F68	PEO_{76}-PPO_{29}-PEO_{76}	8,400	1682	1.39 ± 0.02
L64	PEO_{13}-PPO_{30}-PEO_{13}	2,900	1740	1.40 ± 0.01

From the data shown in Table 3.11, it is apparent that there was no direct relationship with the average MW (g/mol) of the Pluronics® and their influence on the core polarity. However, when the MW of the hydrophobic PPO block was calculated there was a clear relationship between the PPO block MW and the core polarity similarities seen with P105 and F127 *vs* F68 and L64. The higher the MW of the PPO block for P105 and F127 (3248 and 3770 g/mol) correlates to a lower I_1/I_3 of 1.30 ± 0.02 and 1.32 ± 0.03 respectively. The lower I_1/I_3 values correspond to a less polar lipid environment provided by the larger MW of the PPO block, contrary to lower MW PPO blocks of F68 (1682 g/mol) and L64 (1740 g/mol) that are coupled with higher I_1/I_3 values of 1.39 ± 0.02 and 1.40 ± 0.01 (Figure 3.14).

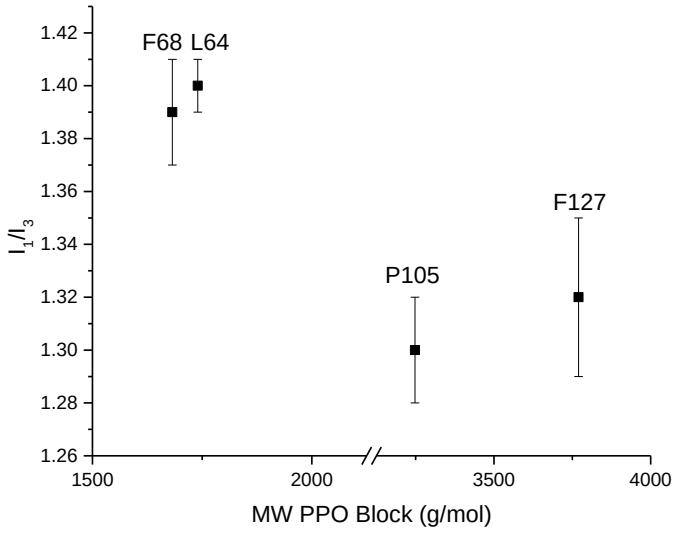

Figure 3.14: graphical representation of the influence of the PPO block MW and the polarity of the internal core microenvironment.

In order to understand how the MW of the PPO block influences the internal core lipid polarity, the mechanism of interaction between the lipid core and PPO unit must be understood. It is already known that Pluronics®, as o/w stabilisers, associate with the lipid core nuclei to lower the interfacial tension between the lipid core and continuous aqueous phase. In order to do so, the PPO block on the Pluronic® must adsorb, or be entrapped, within the core lipid whilst the PEO hydrophilic units protrude into the aqueous phase. The effectiveness of different Pluronic® to associate with the lipid materials in terms of controlling the physical properties of nanoparticles including stability, and release or rationalising the interaction between Pluronics® and lipids has been studied as other concepts in several other studies.[39,52–54] For example, previous research has hypothesised that a lower molecular weight Pluronics® may provide a more rapid stabilisation of hydrophobic material rather than larger MW Pluronics® that would have longer diffusion rates, thus leading to a more rapid adsorption onto hydrophobic nuceli. An example from Peltonen *et al.* has suggested that Pluronic® F68 (MW= 8,400 g/mol) could potentially diffuse and adsorb faster to a hydrophobic surface *versus* longer stabilisers like Pluronic® F127 (MW= 12,600 g/mol).[55] However, as the polarity trend in this study has a clear link with the MW of the PPO block rather than the overall MW of the Pluronic®, with negligible change in D_z or PdI of the SLN dispersions, it was clear that the rate of diffusion onto the lipid core is comparable in all four Pluronic® studies. Therefore, the dominant factor controlling the polarity of the lipid core was the extent of adsorption of the PPO blocks on the surface or entrapment within the lipid core microenvironment. The exact mechanism of stabilisation is unknown, whether the PPO cores solely adsorb onto the surface (Figure 3.15A) or whether the stabilisers, are entrapped within the lipid core with protruding PEO chains on the surface shown in Figure 3.15B.

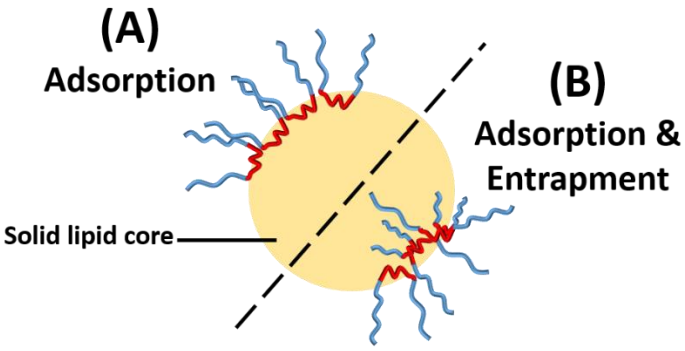

Figure 3.15: Mechanisms of stabilisation of SLNs by amphiphilic ABA block copolymers.

However, analysis of the data provided shows that the PEO block length has negligible impact on the internal core lipid microenvironment, as Pluronic® F127 consists of the longest PEO block (PEO = 100 units), whilst still possessing one of the lower polarity internal cores. This then leads to the assumption that the association of the PPO blocks is predominantly on the surface of the lipid core, with little association of the hydrophilic PEO units. Overall, F127 has the longest PPO block and therefore based on the PPO MW relationship, it would be assumed that this would provide the least polar internal microenvironment. However, the F127 I_1/I_3 value of 1.32 ± 0.02 was comparable to P105 with a value of 1.30 ± 0.03, despite the significantly different PPO block length of 100 units (F127) and 65 units (P105). This similarity may be attributed to the ability of each of the Pluronic® unimers to densely pack at the surface of the lipid core nuclei. As illustrated in Figure 3.16A, the different Pluronics® investigated have different PPO block lengths that associate with the lipid core to different degrees. In addition, Figure 3.16B highlights that the longer the PEO chains the larger the degree of steric hindrance between the neighbouring Pluronic® unimers. In turn, this prevents the F127 unimers densely packing together at the o/w interface and therefore synthesising SLNs with a less densely packed lipid core.

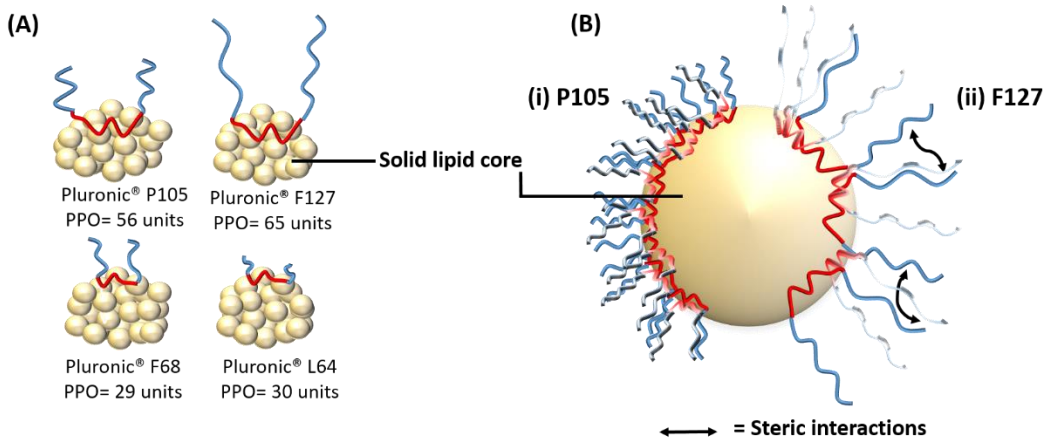

Figure 3.16: The ability of the unimers to pack at the surface of the lipid core based upon the chain length of the PEO blocks.

On the other hand, as also illustrated in Figure 3.16B, the ability of (i) P105 to pack more closely together on the lipid provides a comparable coverage of the longer PPO block provided by the (ii) F127 stabilisers and as a result provides a comparable lipid core microenvironment. An additional feature brought about by the ability of P105 to pack more closely on the surface is the increased density of the PEO corona into the aqueous environment. The PEO corona has been shown to aid avoidance of the immune system and also provide further nanoparticle stability. The stability of the dispersions is demonstrated in the section below.[56,57]

3.2.4.4 Stability of SLN dispersions

Interestingly, the stability of the SLN dispersions was increased in formulations with the lower polarity lipid cores. For L64, the most polar lipid core, it was evident that there was a larger degree of instability over 48 hours as shown below in Figure 3.17.

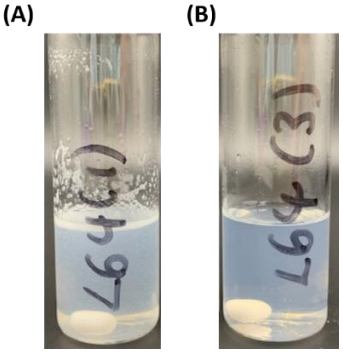

Figure 3.17: The instability of SLN dispersions stabilised by Pluronic® L64. (A) Represents the sample 48 hours and (B) Represents the sample immediately after synthesis.

The sample over 48 hours shows significant creaming of the lipid material (Figure 3.17A), in comparison to the dispersion after immediate synthesis shown in Figure 3.17B. This was followed by SLN dispersions stabilised by F68 that remained stable until 7 days before small particulates were vividly seen within the dispersion rendering the data collected by DLS inaccurate. Contrary to this, dispersions stabilised by Pluronics® with larger MW PPO blocks, i.e F127 and P105, remained stable over a 7-day period and were monitored in triplicate. The D_z values for F127 COMP- SLNs ranged from 205- 244 nm and P105 COMP-SLNs had a similar D_z range of 201- 220 nm.

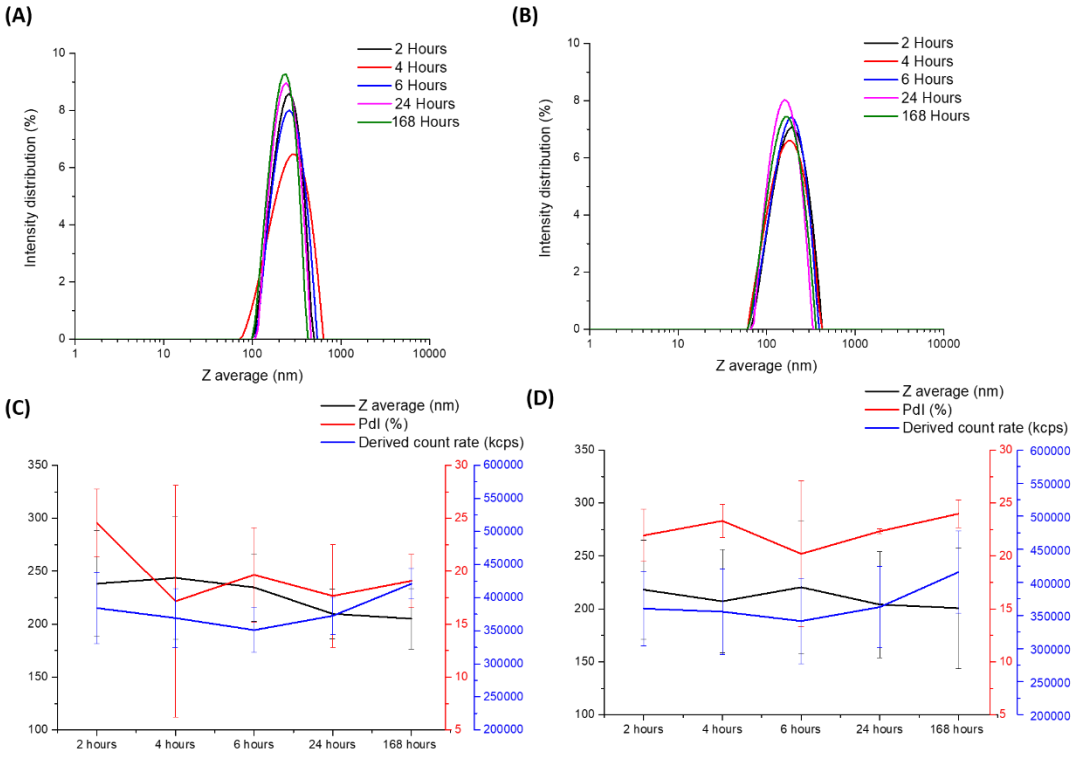

Figure 3.18: COMP-SLNs stabilised by (A) F127 and (B) P105 both show monomodal DLS traces with no evidence of destabilisation occurring over a 7-day period. (C) and (D) show the physical properties of F127 and P105 dispersions respectively, showing no significant impact on Dz (nm), PdI (%) and derived count rate.

Figure 3.18A and B highlights that size analysis on the dispersions over a one-week period remained monomodal, for both F127 and P105 respectively. Figure 3.18C and D further emphasises that the PdI across all dispersions remained low (<30 %), and negligible fluctuation in the derived count rate. The improved stability with F127 and P105 stabilised SLNs can be attributed to the longer PPO blocks enabling a higher adsorption affinity to the

hydrophobic lipid core. This finding further supports the hypothesis that the PPO MW dominates the lipid core polarity, with longer blocks increasing adsorption affinity thus increasing the non-polar character of the core and simultaneously increasing the colloidal stability of the dispersions. As neither set of F127 and P105 stabilised COMP-SLNs showed visual destabilisation of the particles and therefore were taken forward to assess their ability to tune the core polarity microenvironment when blended with Pluronic® F68, a stabiliser shown to possess a notably more polar lipid core environment.

3.2.4.5 Blending Pluronic® stabilisers to tune the lipid core microenvironment

The relationship between the PPO block length and lipid core polarity allows for the possibility of blending different Pluronic® stabilisers to intrinsically tune the lipid core microenvironment. Furthermore, the ability to tune this core environment may provide a preferred lipid core for the encapsulation of a desired chemical entity, without changing the D_z or dispersity of samples. In turn, helping to combat one of the key SLN drawbacks of poor drug encapsulation. This hypothesis is of significant importance as previous studies have successfully shown that pyrene molecules experience lower I_1/I_3 values in lower polarity organic solvents, effecting their partitioning behaviour in mixed solvent systems. Flynn *et al.*, previously identified that the I_1/I_3 value in EtOH is 1.36, in comparison to a more polar THF solvent with an I_1/I_3= 1.46, similarly to the change in I_1/I_3 seen in SLN dispersions when using Pluronic® P105 (I_1/I_3= 1.30) vs F68 ($I_1/I3$= 1.40).[58] As a result, it is predicted that the difference in polarity within these systems may drastically influence the partioning of organic solutes within the mixed solvent systems; thus changing the behaviour of chemical entity encapsulation within SLNs.[58] In addition, this may provide an explanation of the commonly used blends of Pluronic® stabilisers throughout the literature to provide colloidal stability. For example, Chen *et al.* shown that binary Pluronic® F127/P105 mixed micelles significantly enhanced the antitumor activity of chemotherapeutic methotrexate, whilst also demonstrating that a high degree of P105 (89 wt%) was required to increase methotrexate drug loading.[59]

Firstly, the total concentration of stabilisers were maintained at 0.8 mg/mL and different ratios of Pluronic® subtypes were blended to identify if there was any change in the physical properties of the SLN dispersions. The Pluronics® were blended in ratios of 25:75 w/w% , 50:50 w/w% and 75:25 w/w% (Figure 3.19). Pluronic® P105 and F127, F127:F68 and P105: F68 blends in presence of pyrene (Py-COMP-SLNs) and the absence of pyrene (blank-SLNs) were carried out. From analysis of the D_z values and the PdI of the dispersions there was no significant difference between the varying parameters, regardless of pyrene inclusion ranging between 200-300 nm shown in Appendix Figure A1.

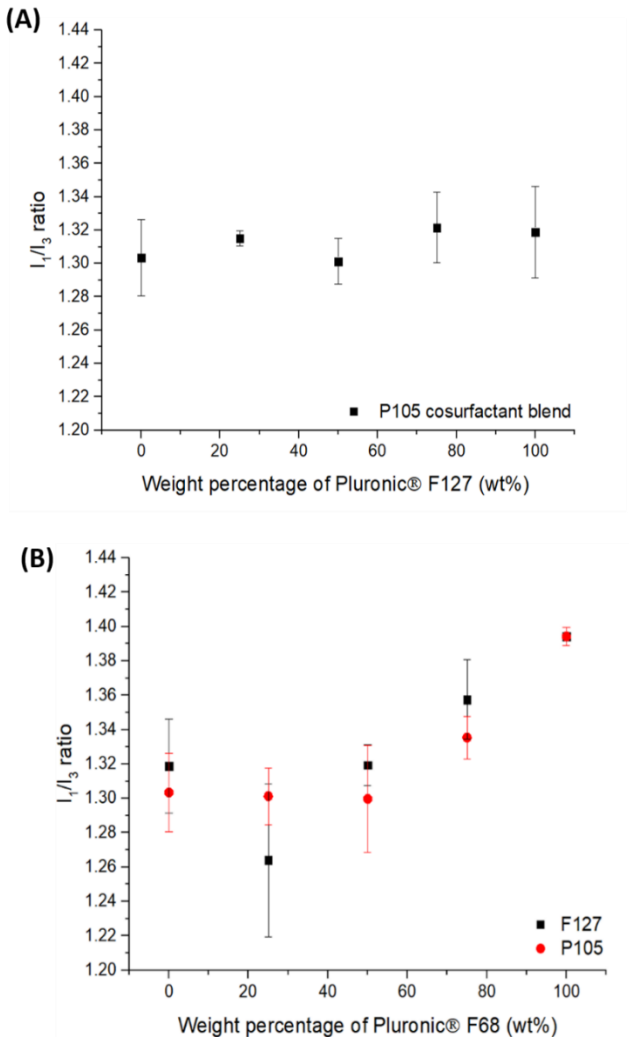

Figure 3.19: identification of polarity changes in the lipid core microenvironment through blending Pluronic® stabilisers

Figure 3.19A illustrates that blending F127 and P105 has negligible impact on the internal core polarity, which can be accredited to the similar number of PPO units (P105= 56, F127=

65) able to adsorb and penetrate onto the SLN lipid core. However, when F68, the Pluronic® with the shortest PPO unit (PPO= 29), was blended with Pluronic® P105 or F127 with longer PPO units, there were substantial changes in the lipid core found. Figure 3.19B highlights that blending F127 with F68 yields a range of I_1/I_3 values from 1.26 at 75 wt% F127 to 1.39 at 0 wt% F127. With reference to Flynn *et al.,* the difference in the experimental values now correlate to I_1/I_3 difference between organic solvent values for IPA (1.21) and THF (1.46) emphasising a controlled variation in the core polarity of SLNs.[58] This demonstrates the tuneability of COMP solid lipid cores and potentially allows for a controlled change in capacity or changeability in the type of guest molecules within the system.

3.3 Conclusions and future work

Throughout this chapter we have explored the use of commonly used Pluronic® ABA block stabilisers to successfully synthesise SLNs and monitor their effects upon the lipid core microenvironment. The polarity of the lipid core microenvironment has proven to be an experimental parameter worth considering during formulation optimisation for a chosen compound, as tuning the environment may enable the better accommodation of compounds of different polarities. In turn, the Pluronic® stabilisers investigated showed no significant difference in the immediate physical properties (D_z, PdI) of the SLNs. Interestingly we found that the MW of the hydrophobic PPO unit on the Pluronic® was the fundamental property controlling the internal core polarity, with an increased PPO unit simultaneously decreasing the I_1/I_3 value. Furthermore, this differs to previous studies that have shown that decrease in I_1/I_3 is predominantly coupled with a decrease in D_z. Conversely, this study shows that whilst maintaining a comparable D_z amongst samples, the I_1/I_3 can be significantly changed and tuned.

To build on this research, encapsulation of a range of non-polar compounds to develop a trend between the polarity of the molecules and the preferred polarity of the lipid environment is required. In turn, this will allow formulation development for SLN synthesis to be more accurately designed to enhance lipid core encapsulation of the chosen entities.

3.4 References

1 J. R. Lakowicz, *Principles of Fluorescence Spectrscopy*, 1999.

2 A. Jain, C. Blum and V. Subramaniam, *Fluorescence Lifetime Spectroscopy and Imaging of Visible Fluorescent Proteins*, Elsevier, First Edit., 2009.

3 S. J. Yao, Jehng-Jyun, Huang, Zhi-Heng, Masten, *Water Res.*, 1998, **32**, 3001–3012.

4 N. P. E. Barry and B. Therrien, *Pyrene : The Guest of Honor*, Elsevier Inc., 2016.

5 M. Randic, *Chem. Rev.*, 2003, **103**, 3449–3605.

6 C. J. Y. Cuichen Wu, Chunming Wang, Ling Yan, *J. Biomed. Nanotechnol.*, 2009, **5**, 495–504.

7 S. Kim, O. Kweon, R. C. Jones, J. P. Freeman, R. D. Edmondson and C. E. Cerniglia, *J. Bacteriol.*, 2007, **189**, 464–472.

8 F. Moggia, C. Videlot-ackermann, P. Raynal and H. Brisset, *J. Mater. Chem.*, 2006, **16**, 2380–2386.

9 T. M. Figueira-duarte and M. Klaus, *Chem. Rev.*, 2011, **111**, 7260–7314.

10 J. C. Seidel, *J. Biol. Chem.*, 1975, **250**, 5681–5687.

11 J. Dai and M. Fidalgo de Cortalezzi, *Heliyon*, 2019, **5**, e01922.

12 K. Z. Yuming Zhao, Wen Zhu, Ying Wu, Lin Qu, Zhengping Liu, *Polym. Chem.*, 2016, **7**, 6513–6520.

13 L. X. Chang-Bo Huang, Li-Jun Chen, Junhai Huang, *RSC Adv.*, 2014, **4**, 19538–19549.

14 N. P. E. Barry and B. Therrien, *Pyrene : The Guest of Honor*, Elsevier Inc., 2016.

15 C. Stoffelen and J. Huskens, *Small*, 2016, **12**, 96–119.

16 V. Glushko, M. S. R. Thaler and C. D. Karp, *Arch. Biochem. Biophys.*, 1981, **210**, 33–42.

17 B. Hochreiter, A. P. Garcia and J. A. Schmid, *Sensors*, 2015, **15**, 26281–26314.

18 J. M. Vanderkooi and J. B. Callisj, *Biochemistry*, 1974, **13**, 4000–4006.

19 G. K. Bains, S. H. Kim, E. J. Sorin and V. Narayanaswami, *Biochemistry*, 2012, **51**, 6207–6719.

20 R. D. Pensack, R. J. Ashmore, A. L. Paoletta and G. D. Scholes, *J. Phys. Chem. C*, 2018, **122**, 21004–21017.

21 J. Merz, J. Fink, A. Friedrich, I. Krummenacher, H. Al Mamari, S. Lorenzen, M. Haehnel, A. Eichhorn, M. Moos, M. Holzapfel, H. Braunschweig, C. Lambert, A. Steffen, L. Ji and T. B. Marder, *Chem. A Eur. J.*, 2017, **23**, 13164–13180.

22 Q. Zhou, J. Lin, J. Wang, F. Li, F. Tang and X. Zhao, *Prog. Nat. Sci.*, 2009, **19**, 1529–1536.

23 H. Wang and G. L. Rempel, *J. Polym. Sci. Part A Polym. Chem.*, 2013, **51**, 4440–4450.

24 G. S. Kwon, M. Naito, K. Kataoka, M. Yokoyama, Y. Sakurai and T. Okano, *Colloids Surfaces B Biointerfaces*, 1994, **2**, 429–434.

25 Z. Duan, Y. J. Gao, Z. Y. Qiao, G. Fan, Y. Liu, D. Zhang and H. Wang, *J. Mater. Chem. B*, 2014, **2**, 6271–6282.

26 S. Z. F. Phua, C. Xue, W. Q. Lim, G. Yang, H. Chen, Y. Zhang, C. F. Wijaya, Z. Luo and Y. Zhao, *Chem. Mater.*, 2019, **31**, 3349–3358.

27 C. C. Perry, T. S. Sabir, W. J. Livingston, J. R. Milligan, Q. Chen, V. Maskiewicz and D. S. Boskovic, *J. Colloid Interface Sci.*, 2011, **354**, 662–669.

28 G. Basu Ray, I. Chakraborty and S. P. Moulik, *J. Colloid Interface Sci.*, 2006, **294**, 248–254.

29 T. Wu, J. Oake, Z. Liu, C. Bohne and N. R. Branda, *Am. Chem. Soc. Omega*, 2018, **3**, 7673–7680.

30 J. Varshosaz, F. Hassanzadeh, H. Sadeghi-aliabadi, Z. Larian and M. Rostami, *Chem. Eng. J.*, 2014, **240**, 133–146.

31 B. Kim, K. Na and H. Choi, *Pharm. Sci.*, 2005, **24**, 199–205.

32 L. D. C. Baldi, E. T. Iamazaki and T. D. Z. Atvars, *Dye. Pigment.*, 2008, **76**, 669–676.

33 D. Kim, R. Amos, M. Gauthier and J. Duhamel, *Langmuir*, 2018, **34**, 8611–8621.

34 H.-C. L. Srinivasa Rao Nelli, Rajan Deepan Chakravarthy, Yue-Ming Xing, Jen-Po Wenga, *Soft Matter*, 2017, **13**, 8402–8407.

35 F. Nador, K. Wnuk, C. Roscini, R. Solorzano, J. Faraudo and D. Ruiz-molina, *Chem. A Eur. J.*, 2018, **24**, 14724–14732.

36 J. Nanobiotechnol, X. Li, X. Wang, C. Zhao, L. Shao, J. Lu, Y. Tong and L. Chen, *J. Nanobiotechnology*, 2019, 1–12.

37 A. Alwattar, A. Haddad, Q. Zhou, T. Nascimento, R. Greenhalgh, E. Medeiros, J. Blaker, A. Parry, P. Quayle and S. Yeates, *Polym. Int.*, 2018, **68**, 360–368.

38 J. Gou, S. Feng, Y. Liang, G. Fang, H. Zhang, T. Yin, Y. Zhang, H. He, Y. Wang and X. Tang, 2017, 3750–3761.

39 A. M. Bodratti and P. Alexandridis, *J. Funct. Biomater.*, 2018, **9**, 1–24.

40 S. Gupta, R. Kesarla, N. Chotai, A. Misra and A. Omri, *Biomed Res. Int.*, 2017, **2017**, DOI: 10.1155/2017/5984014.

41 A. Mohr, P. Talbiersky, H. Korth, R. Sustmann, R. Boese and D. Bla, *J. Phys. Chem. B*, 2007, **111**, 12985–12992.

42 G. K. Bains, S. H. Kim, E. J. Sorin and V. Narayanaswami, *Biochemistry*, 2012, **51**, 6207–6219.

43 R. C. Pasquali, N. Sacco and C. Bregni, *Lat. Am. J. Pharm.*, 2009, **28**, 313–317.

44 M. Almeida, M. Magalhães, F. Veiga and A. Figueiras, *J. Polym. Res.*, 2018, **25**, 1–14.

45 M. Y. Kozlov, N. S. Melik-Nubarov, E. V. Batrakova and A. V. Kabanov, *Macromolecules*, 2000, **33**, 3305–3313.

46 A. Raval, S. A. Pillai, A. Bahadur and P. Bahadur, *J. Mol. Liq.*, 2017, **230**, 473–481.

47 V. Singh, P. Khullar, P. N. Dave and N. Kaur, *Int. J. Ind. Chem.*, 2013, **4**, 1–18.

48 E. Russo and C. Villa, *Pharmaceutics*, 2019, **11**, 1–17.

49 W. Zhang, K. J. Haman, J. M. Metzger, B. J. Hackel, S. Frank, T. P. Lodge, U. States, U. States and U. States, *Langmuir*, 2018, **33**, 12624–12634.

50 M. Redhead, G. Mantovani, S. Nawaz, P. Carbone, D. C. Gorecki, C. Alexander and C. Bosquillon, *Pharm. Res.*, 2012, **29**, 1908–1918.

51 L. Li and S. Thayumanavan, *Langmuir*, 2014, **30**, 12384–12390.

52 G. Wu, J. Majewski, C. Ege, K. Kjaer, J. Weygand and K. Y. C. Lee, 2005, **89**, DOI: 10.1529/biophysj.104.052290.

53 V. Jannin, E. Pochard and O. Chambin, 2006, **309**, 6–15.

54 A. Hädicke and A. Blume, *Colloid Polym. Sci.*, 2014, **293**, 267–276.

55 A. Tuomela, J. Hirvonen and L. Peltonen, *Pharmaceutics*, 2016, **8**, 1–18.

56 L. Guerrini, R. A. Alvarez-puebla and N. Pazos-perez, *Materials (Basel).*, 2018, **11**, 1–28.

57 J. S. Suk, Q. Xu, N. Kim, J. Hanes, L. M. Ensign, H. Sciences and M. Sciences, *Adv. Drug Deliv. Rev.*, 2017, **99**, 28–51.

58 S. Flynn, A. B. Dwyer, P. Chambon and S. Rannard, *Polym. Chem.*, 2019, **10**, 5103–5115.

59 Y. Chen, X. Sha, W. Zhang, W. Zhong, Z. Fan, Q. Ren, L. Chen and X. Fang, *Int. J. Nanomedicine*, 2013, **8**, 1463–1476.

3.5 Appendix

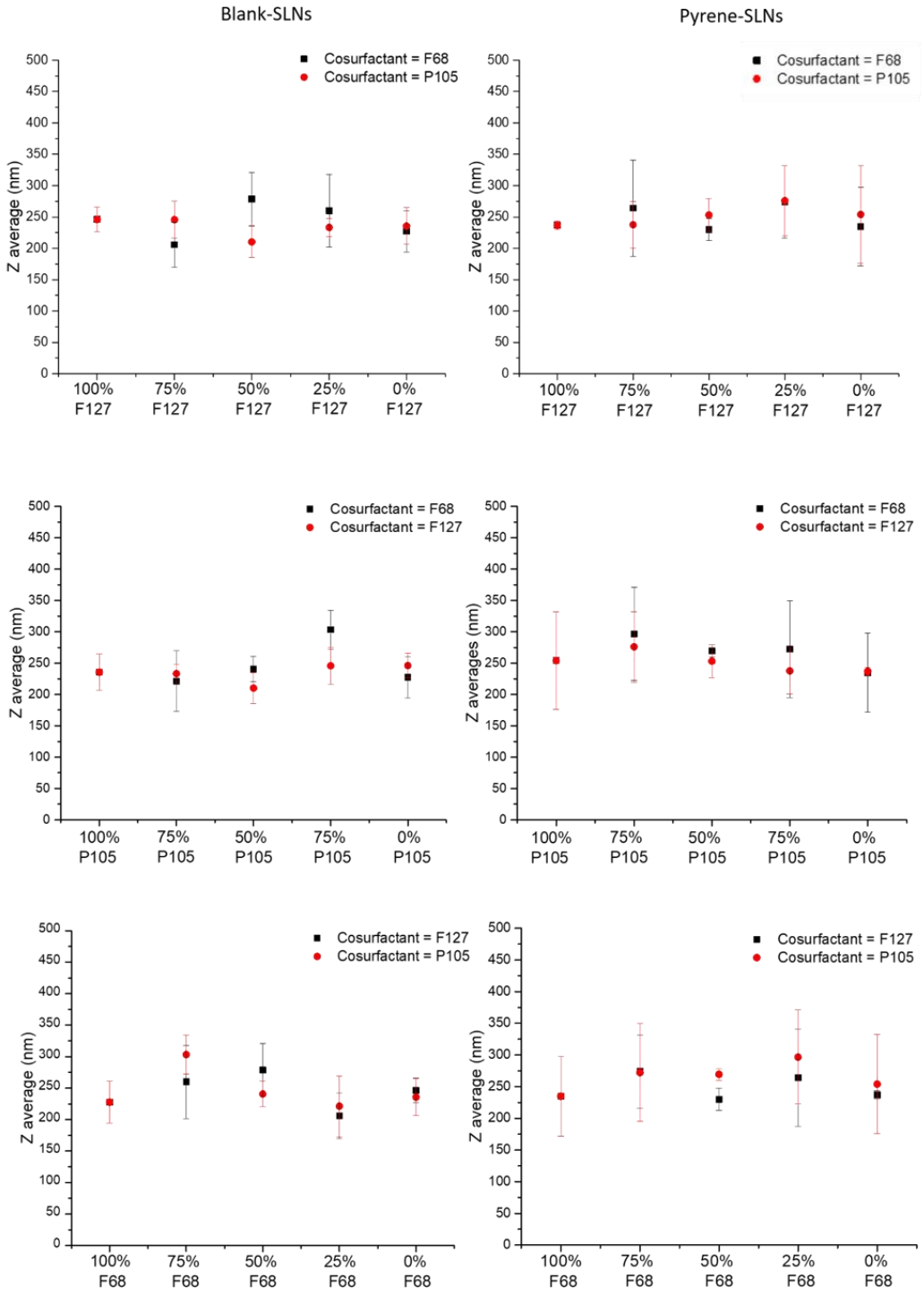

Appendix Figure A1: The Dz similarities shown between each of the Pluronic® blends

Chapter 4
The Development of Indomethacin loaded Nanostructured Lipid Carriers and Nanoemulsions

Chapter 4

4.1 Introduction

4.1.1 Nanostructured Lipid Carriers

Nanostructured Lipid Carriers (NLCs) are a subtype of lipid derived nanoparticles, often referred to as 'second-generation' lipid carriers that are able to transport hydrophobic guest molecules.[1] They consist of a solid lipid, liquid lipid and a guest molecule of choice (Figure 4.1).[1]

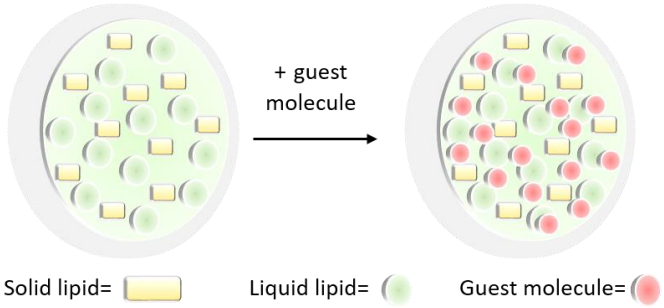

Figure 4.1: Chemical composition of NLCs.

NLCs were initially developed in order to overcome the drawbacks of solid lipid nanoparticles (SLNs). The fundamental advantages of NLCs include overcoming low drug loading and drug expulsion upon storage.[2] NLCs and SLNs as lipid nanoparticle systems are similar in terms of their composition and biological advantages.[3] However, the fundamental difference between SLNs and NLCs is the inclusion of a liquid lipid/oil within the core environment. Consequently, the liquid lipid increases the solubility of the guest molecule, and in turn the rate of drug expulsion upon storage is reduced and sample stability is simultaneously increased.[4,5] Throughout this chapter we aim to incorporate indomethacin (IND) as a tocolytic drug to formulate indomethacin-NLCs (IND-NLCs), suitable for the prevention of sudden preterm birth.

4.1.2 Liquid lipids

The liquid lipids used throughout this chapter are mineral oil, safflower oil, sunflower oil, soybean oil and castor oil. This subset of five lipids were chosen due to their biocompatibility,

in addition to their low cost and abundance.[6,7] Mineral oil contains hydrocarbons at varying chain length and saturation with many paraffins, naphthalenes and aromatic compounds within the liquid lipid (Figure 4.2A).[8] Conversely, the other four liquid lipids explored consist of saturated and unsaturated fatty acids and their glyceride counterparts. The generic structure of mono, di and triglycerides are shown in Figure 4.2B. Safflower, sunflower and soybean oil (Figure 4.2 C, D, E) consists of palmitic and stearic acid analogues, however safflower and sunflower oil also contain additional oleic and linoleic acids. A key difference between safflower and sunflower oil is that the latter contains a higher composition of oleic and linoleic glyceride derivatives.[9–11] Conversely, castor oil has a dominant composition of a more polar compound, named ricinoleic acid (Figure 4.2 F).[12,13]

It is important to note that the effects of these liquid lipids on uterine tissue in particular is not an area that is well studied. Previous literature has suggested the use of castor oil has the potential to initiate labour in full term pregnancies.[14] However, the research is somewhat controversial with alternative studies suggesting castor oil has no significant increase in labour incidence or uterine contractility.[15] Furthermore, additional studies emphasise the uncertainty about the direct link between castor oil and the increase of uterine activity. For example, Sicuranza *et al.* states that castor oil dosages largely range from 5 to 120 mL prior to initiating a uterine response.[16] Conversely, studies on emulsions containing safflower and soybean oil have been tested in pregnancy patients which showed no effect on the onset of labour or maternal health.[17] Interestingly the use of safflower oil in low birth weight preterm infants, has been used as an excipient in emulsions to administer nutrients for weight gain.[18] This further supports the use of safflower oil for IND-NLC optimisation. In addition, the use of sunflower oil has been used as a placebo in pregnancy related clinical trials and therefore poses no threat to maternal or fetal health.[14,19] There is negligible information to insinuate that mineral oil can cause significant harm to maternal or fetal health when used in drug delivery systems or on its ability to effect uterine contractility. Figure 4.2 shows the chemical structures of the components of all liquid lipids explored.

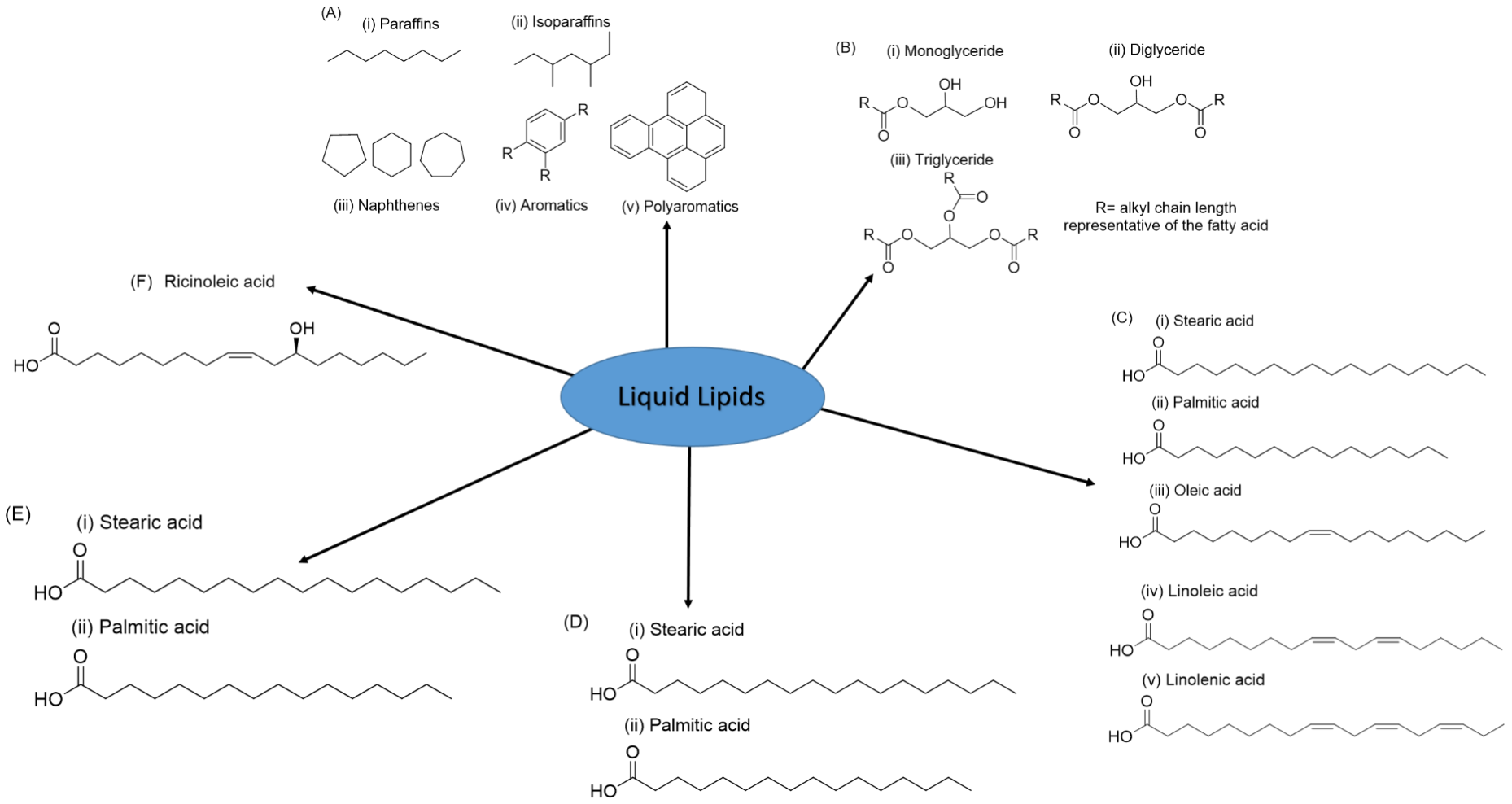

Figure 4.2: Chemical structure of liquid lipids chosen for NLC development. (A) Mineral oil, (B) Generic structure of glyceride derived materials, (C) Safflower oil, (D) Sunflower oil, (E) Soybean oil and (F) Castor oil.

4.2 Results and Discussion

4.2.1 Synthesis method of IND-NLCs

The preliminary investigations in this chapter utilise the optimised experimental parameters founded in Chapter 2 and are discussed briefly throughout the following sections. All NLCs were synthesised *via* the solvent injection method (SIM). The SIM is a particularly useful synthetic method due to the low cost, easy scalability and low mechanical strength required to synthesise IND-NLCs.[20,21]

Briefly, hydrophobic excipients: solid lipid (COMP), liquid lipid and IND had a combined total mass of 18 mg which were dissolved in 4 ml of 1-propanol to make up the hydrophobic phase. The hydrophobic phase was heated to 82 °C, 10 °C higher than COMP melting temperature (COMP T_m= 72 °C), and rapidly injected into the continuous aqueous phase (20 mL) containing Pluronic® stabilisers (0.8 mg/mL). All liquid lipids trialled where miscible with 1-propanol. The chemical structures of solid lipid COMP and the generic structure of Pluronic® stabilisers are shown below in Figure 4.3.

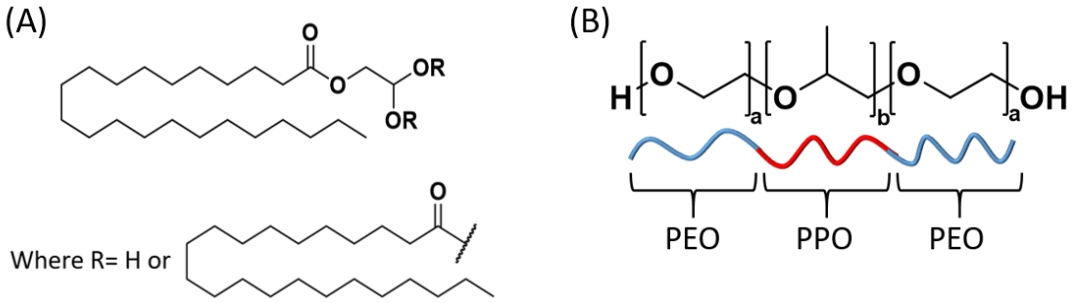

Figure 4.3: Chemical structure of (A) COMP and (B) The generic structure of ABA block Pluronic® stabilisers.

4.2.2 Liquid Lipid compatibility studies

IND and COMP were tested individually for the compatibility with the five liquid lipids. The terms ‘liquid lipids’ and ‘oils’ are used interchangeably. Firstly all samples were tested for visual solubility or miscibility. Secondly, differential scanning calorimetry (DSC) was implemented to quantify crystallinity changes within the systems. This was of significant

importance as NLC formulations benefit from a reduced crystallinity within the lipid core in order to increase their drug loading capacities.[22]

4.2.2.1 Differential Scanning Calorimetry

DSC enables the detection of a shift or change in the melting temperature (T_m) of the physical mixtures. The extent of the crystallinity disruption the liquid lipid imposes on the crystalline drug or solid lipid, can be quantified by the extent of a shift or depression on the bulk material T_m.[23,24] The change in T_m occurs as the addition of liquid lipids enable distortion within the bulk crystal lattice, reducing the intermolecular interactions and preventing the formation of a perfect crystalline structure.[24–26] This is a product of the plasticising effect which ultimately modifies the thermal and mechanical properties of the solid: oil and drug: oil mixtures *via* increasing the flexibility of the components in the core.[27] A secondary property that can be noted from DSC thermograms is an increase in the melting range, characterised by broadening of the T_m peaks. This suggests an increase in the dispersity of the crystals or an increased amount of imperfect crystals within the sample. In turn this disrupts the rigidity of the core and benefits the NLC drug loading capacity.[22] In summary, DSC was used to identify liquid lipid:solid lipid and liquid lipid:drug combinations that demonstrate a reduction in crystallinity and increased dissolution of the bulk COMP or IND material to provide the basis for NLC development.

4.2.2.2 Liquid lipid and drug compatibility

Liquid lipid and drug compatibility was initially assessed qualitatively through the visual ability of the oils to solubilise the drug molecule. For this experiment, the drug (100 mg) was saturated in liquid lipids (500 mg) at both 25 °C and 82 °C. The samples at room temperature showed no evidence of immediate solubility. However, once heated formed yellow transparent solutions with no visible solid. The presence of a yellow coloration indicates that the IND was soluble within the heated liquid lipid phase as similarly reported by Hippalgaonkar *et al.*[28] Mineral oil possessed negligible colour change at both 25 °C and at 82 °C suggesting the lowest solubility. This was coupled with significant material rapidly precipitating once

removed from the heat source and can be attributed to poorer solubility at lower temperatures. All liquid lipids showed varying degrees of precipitation when removed from the heat source as show in Figure 4.4.

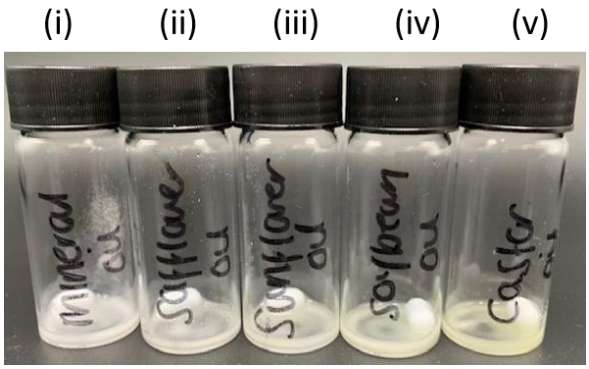

Figure 4.4: IND compatibility with liquid lipids (i) mineral oil, (ii) safflower oil, (iii) sunflower oil, (iv) soybean oil and (v) castor oil. All photographs were imaged 30 minutes after all samples had cooled to room temperature.

Figure 4.4v shows that IND-castor oil retains the most intense yellow colour after removing the sample from the heat source, therefore suggesting that castor oil possesses the highest IND solubility. All images were acquired 30 minutes after the samples were heated. Nevertheless, all liquid lipids presented adequate IND solubility at elevated temperatures that were relevant to the NLC synthesis conditions.

All liquid-lipid and IND physical mixtures were then further analysed by DSC (Figure 4.5). DSC analysis of the liquid lipid and IND physical mixtures not only identifies the dissolution of IND crystals, however also predicts the polymorphic form of the drug that is present. It is already known that IND exists as several polymorphic forms, where each polymorph is associated with varying degrees of thermodynamic stability.[29] Identifying the presence of thermodynamically unstable polymorphs within the physical mixtures, whilst simultaneously quantifying the degree of dissolution of IND crystals, provides a prediction on the most appropriate excipients for NLC development. All samples for DSC measurements were mixtures of IND and liquid lipid in a 50:50 w/w% ratio. All samples were heated at 5 °C/min from 21 °C to 200 °C to solubilise the IND in the lipid before being cooled. The DSC data

presented was for the 2nd heating cycle which would reveal any IND that had not dissolved as determined by the presence of crystalline IND.

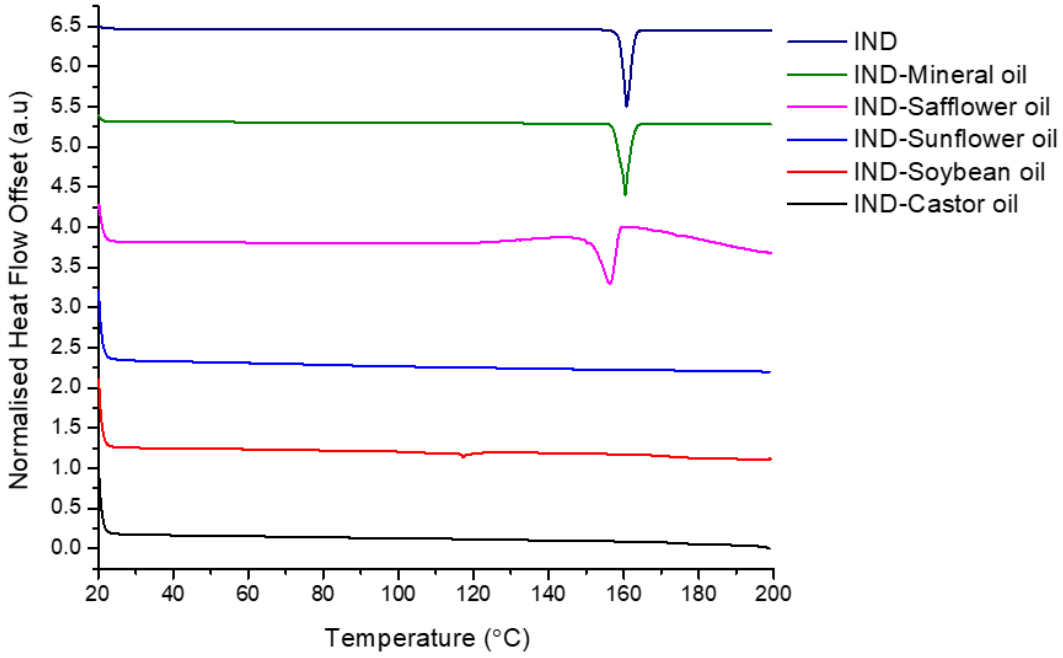

Figure 4.5: DSC thermograms comparing the melting temperature (T_m) for IND in comparison to liquid lipid physical mixtures using mineral oil, safflower oil, sunflower oil soybean oil and castor oil. Physical mixtures of IND and liquid lipid were mixed in a 50:50 w/w% ratio. All DSC experiments conducted were heat-cool-heat cycles from 21°C-100°C. All DSC thermograms shown are from the second heat cycle.

The T_m and quantification of crystalline IND in the individual physical mixtures are shown below in Table 4.1.

Table 4.1: T_m of IND in liquid lipid:IND physical mixtures.

Liquid lipid	**T_m (°C)**	**IND Crystallinity (%)**	**Predicted IND Polymorph**
None	160.7	100	I
Mineral oil	160.4	68.1	I
Safflower oil	156.1	33.5	II
Sunflower oil	N/A	0	-
Soybean oil	N/A	0	-
Castor oil	N/A	0	-

Figure 4.5 and Table 4.1 highlight that there was a significant presence of IND crystals within the IND-mineral oil mixture, which can be attributable to the poor solubility of the IND in physical mixtures with these oils. The T_m for bulk IND and IND-mineral oil was similar at

160.7 and 160.4°C, suggesting the presence of the most thermodynamically stable IND polymorph denoted form I or the γ polymorph.[29,30] As the crystallinity of IND within the mineral oil remained high at 68.1%, it was predicted that this liquid lipid would be disadvantageous for NLC development. Safflower oil-IND physical mixture displays an IND T_m at 156.1°C signifying the potential presence of the metastable polymorph, denoted α or form II.[29,30] Nonetheless, the presence of IND crystals within the safflower oil mixture was greatly reduced to 33.5 %, implying that 76.5% of the IND has dissolved in the lipid. The absence of a T_m for IND in sunflower, soybean oil and castor oil suggested that there is complete solubility of the drug in the liquid lipids. In theory, the increased solubility of IND in sunflower and soybean oil would be favourable to increase drug capacity within NLC systems. In summary, this demonstrates that sunflower, soybean and castor oil are predicted to be optimal for IND encapsulation. Nevertheless, all liquid lipids also require a mutual compatibility with the solid lipid. All liquid lipids were assessed for compatibility with COMP and are discussed in the following section.

4.2.2.3 Compatibility of liquid lipids with Compritol 888 ATO

COMP is insoluble in many organic solvents and many oil-based systems. Therefore compatibility between COMP and other excipients was determined through miscibility studies.[31] To assess the miscibility of COMP in the liquid lipids, the two excipients were mixed together at 25 °C and at 72 °C in a 50:50 w/w% ratio. The miscibility of each of the samples were assessed visually. Solid COMP was insoluble in all liquid lipids at 25 °C. At elevated temperatures all liquid lipids possessed complete miscibility with molten COMP. The impact that the five chosen liquid lipids had on the presence of COMP crystals and the T_m of COMP were explored *via* DSC. All samples were heated at 5 °C/min from 20 °C to 100 °C to solubilise COMP in the liquid lipids before being cooled. The DSC data presented is for the 2nd heating cycle which would reveal any crystalline COMP present. Figure 4.6 shows the DSC thermograms of the COMP-liquid lipid physical mixtures.

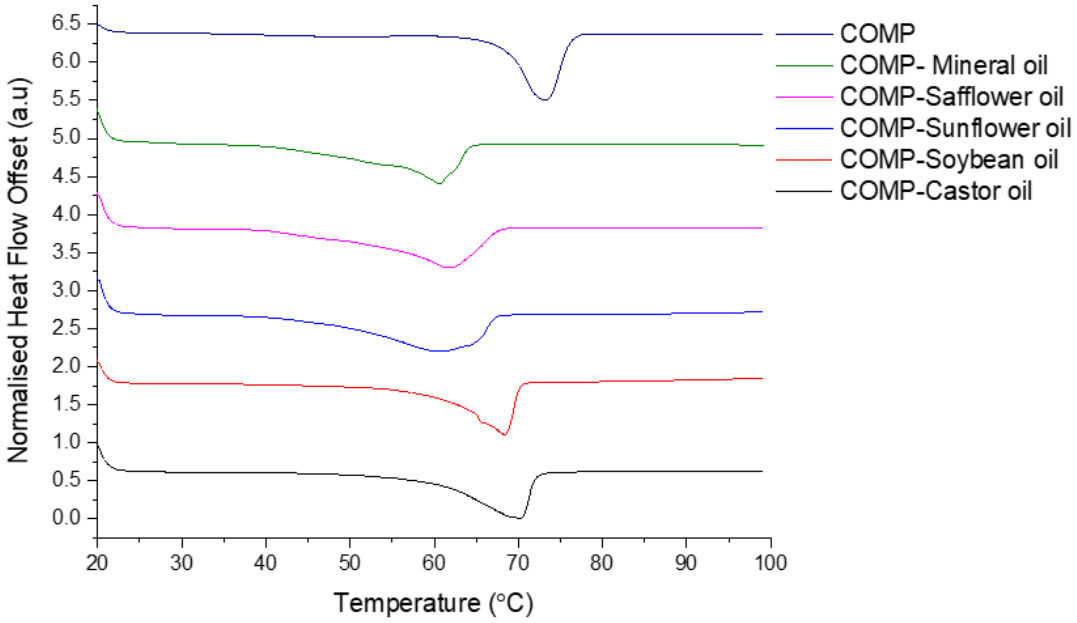

Figure 4.6: Identification of the T_m of COMP-liquid lipid physical mixtures through DSC thermograms. COMP bulk material was mixed with mineral oil, safflower oil, sunflower oil, soybean oil and castor oil in a 50:50 w/w% ratio. All DSC experiments conducted were heat –cool- heat cycles from 21 °C-100 °C. All DSC thermograms shown are from the second heat cycle.

Figure 4.6 showed that COMP as the bulk material obtained a T_m of 72 °C. Conversely, mixing COMP with any liquid lipid significantly decreased the overall crystallinity of the bulk material. In turn, this reduces the viscosity of the COMP lipid core and decreases the likelihood of solid lipid recrystallization occurring when formulated as NLCs.[32] The changes in T_m and quantification of the presence of COMP crystals are shown below in Table 4.2

Table 4.2: T_m of IND in liquid lipid: COMP physical mixtures.

Liquid lipid	**T_m (°C)**	**COMP Crystallinity (%)**
None	72.0	100
Mineral oil	60.6	47.8
Safflower oil	62.4	52.3
Sunflower oil	61.4	51.5
Soybean oil	64.7	64.6
Castor oil	64.9	58.1

Figure 4.6 and Table 4.2 showed that mixtures containing castor oil and soybean oil displayed decreased T_m values from 72°C (COMP) to 64.9°C and 64.7°C respectively, with a further decrease in COMP crystallinity to 58.1% and 64.6 % from 100% in the bulk lipid. However, there was a more prominent decrease in T_m for samples containing safflower and sunflower

oil to 62.4°C and 61.4°C respectively. The T_m depression and increase in broadness in the endotherm for safflower and sunflower oil samples suggests an increase in the degree of solubilisation of COMP at higher temperatures. The presence of COMP crystals was reduced to 52.3% (safflower oil) and 51.5% (sunflower oil). The ability for these oils to decrease the presence of COMP crystals to a greater extent than soybean and castor oil may be attributable to the similarity of their chemical composition; thus providing better physicochemical interactions and increasing dissolution. Both safflower and sunflower oil contain a range of mono, di and tri glycerides of steric, palmitic, oleic and linoleic acid structures. The wide range of components suggests that the greater reduction in COMP crystals may be resultant of an increase in the disorder within the lipid core, thus reducing the overall core crystallinity. In addition, safflower and sunflower oil have low and comparable viscosities. The viscosity of materials has a direct relationship with crystallinity; whereby as viscosity decreases, crystallinity decreases.[33] Diamante *et al.* determined that the viscosities of safflower and sunflower oil at 26 °C are 0.045 ± 0.0003 and 0.049 ± 0.0002 Pa.s respectively.[34] The greatest reduction in COMP crystallinity was identified with mineral oil (47.8%), however due to the significant crystallinity with IND (68.1%), this liquid lipid was predicted to be non-optimal for NLC formulations.

4.2.2.4 DSC data summary for the liquid lipid compatibility with COMP and IND

In summary, it was predicted that the use of soybean, castor and sunflower oils were presented as optimal liquid lipids for IND. This was concluded from the complete visual solubility of the bulk material at high temperatures and the absence of an IND T_m in the thermograms. Importantly, safflower oil also solubilised 76.5% of IND at 50: 50 w/w% and was therefore also considered a suitable candidate. The most disadvantageous lipid with respect to IND was mineral oil, as IND crystallinity was presented at 68.1%. Conversely for COMP, no liquid lipid provided complete solubility. However castor oil, safflower oil and sunflower oil produced a dominant shift in the T_m, coupled with broadening of the T_m peaks which supports a positive disruption to the crystallinity of the solid lipid. Although soybean oil was considered

compatible with IND, it displayed significant crystallinity (64.6%) with COMP and was therefore not predicted to be a mutually compatible liquid lipid. As a result, castor, safflower and sunflower oil were hypothetically the optimal liquid lipids for IND-NLC production. To test this hypothesis all liquid lipids were taken forward for preliminary investigation.

4.2.3 NLC formulation

Preliminary investigation of NLCs containing COMP and all five of the liquid lipids were investigated for potential NLC production. NLCs containing only liquid and solid lipid in the absence of drug are denoted as blank-NLCs. Liquid lipids and solid lipids were mixed in a 50:50 w/w% or 30:70 w/w% whilst maintaining a total mass of 18 mg total hydrophobic content. Pluronic® F68 was used as the stabiliser. Pluronic® F68 was chosen due to the common inclusion in lipid derived nanosystems.[35–38] All samples synthesised showed predominant monomodal distributions highlighted in Figure 4.7. Figure 4.7A represents the blank-NLCS containing 50:50 w/w% solid: liquid lipid and Figure 4.7B represents blank-NLCs comprised of 70:30 w/w% solid: liquid lipid, essentially all the dispersions were monomodal.

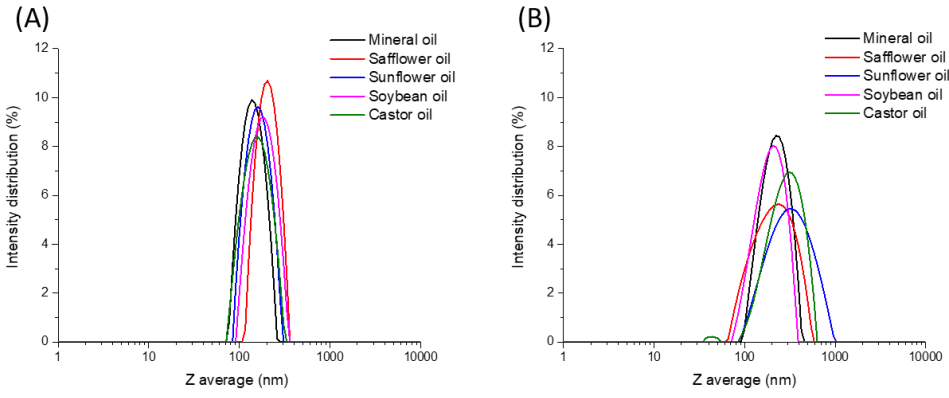

Figure 4.7: Size distribution traces of NLCs with (A) 50:50 w/w% solid lipid: liquid lipid and (B) 70:30 w/w% of solid lipid: liquid lipids.

There was notable difference in the observed Z average (D_z) dependent on the composition of the lipid excipients shown in Figure 4.7C and Figure 4.7D. It is important to note that all samples independent of the liquid oil or liquid:solid lipid ratio exhibited PdI values less than 26%. Samples containing 50:50 w/w% ratio ranged from 11-17 % immediately after synthesis

whilst 70:30 w/w% samples had slightly higher dispersities of 20-26% (see Appendix Figure A1). The data showed that significantly lower D_z values were found when using 50:50 w/w% solid: liquid lipid. For example, safflower oil NLCs and soybean NLCs using 50:50 w/w% solid: liquid lipid, had respective D_z values of 146 nm and 165 nm, in comparison to 70:30 w/w% systems for safflower oil (290 nm) and soybean oil (310 nm). The reduction in D_z with an increase in liquid lipid content has also been stated by Siahdasht *et al.* and Huang *et al.* and is a product of a reduced viscosity within the nanoparticle systems.[39,40] Therefore, higher content liquid lipid reduces the viscosity of the lipid core, thus obtains a smaller particle size. However Soleimanian *et al.* found that an increase in liquid lipid reduced the drug encapsulation efficiency within the lipid core. [41] This was attributed to the inability of the solid lipid to nucleate with the liquid lipid, causing the liquid lipid and solubilised drug to reside unencapsulated in the continuous phase.[41] Therefore, both properties must be taken into consideration for future development.

To further understand the effect that the addition of the liquid lipids had on the solid lipid core, the internal core microenvironment was studied. Pyrene was implemented as a fluorescent probe to monitor core polarity changes through fluorescence spectroscopy. These findings are discussed in the following section.

4.2.4 Assessing NLC core polarity using pyrene

Assessing the core polarity in NLCs can provide information on the effect that liquid lipids have on the internal core environment.[42] The polarity of the core environment is of particular importance as it can be tuned to accommodate the polarity of a specific guest molecule.[42] Using Pluronic® F68 as a stabiliser, NLCs were synthesised with the five chosen liquid lipids. All pyrene investigations used the 50:50 w/w% solid: liquid lipid NLC compositions. The 50:50 w/w% samples were chosen to investigate core polarity as the equal content of liquid and solid lipid gives a clearer insight into the effect of the liquid lipid on the polarity of the microenvironment. Pyrene was implemented into the NLC cores at 0.01 wt% to monitor internal polarity changes. These changes were noted as variations in the characteristic I_1/I_3 and

e/m ratio profiles of pyrene spectroscopy shown in Figure 4.8A. The I_1/I_3 value is a measure of internal core polarity and the *e/m* ratio is a measure of internal spatial proximity. The I_1/I_3 ratio was determined from the division of I_1 (the polarity independent band) and I_3 (the polarity dependent band). The *e/m* ratio was acquired through dividing the height of the excimer peak (~465-470 nm) by the first vibronic band, I_1. The larger the *e/m* ratio and excimer emission has been attributable to increased intermolecular coupling of excited pyrene molecules that are more spatially proximal.[43–45] The spectroscopic excimer emissions are highlighted in Figure 4.8B.

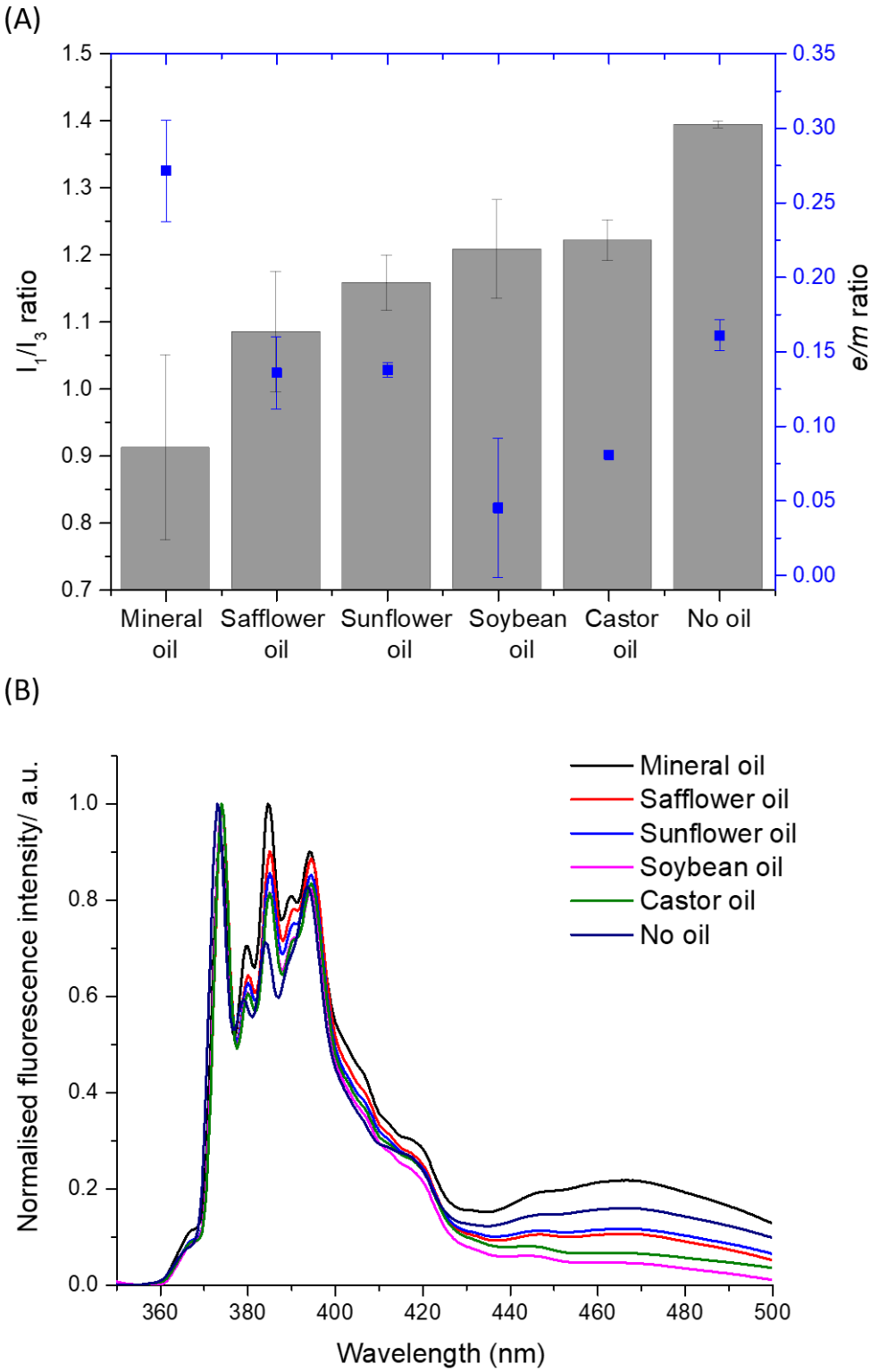

Figure 4.8: Shows the effect of liquid lipid inclusion on the internal core microenvironment of NLCs using Pluronic® F68 as a polymeric stabiliser. A) Shows the differences in internal core polarity using the I_1/I_3 parameter. B) Shows the variations in the excimer emissions for all NLC samples. All NLCs formed used the liquid lipid:solid lipid composition of 50:50 w/w%.

Importantly, Figure 4.8A highlights that the inclusion of a liquid lipid notably reduces the polarity of the internal core microenvironment *vs* samples containing no oils. The I_1/I_3 value

for F68 stabilised COMP cores with no associated liquid lipid was 1.39 ± 0.005. Conversely, liquid lipid -F68 stabilised cores ranged from 0.91 ± 0.1 (mineral oil-NLCs) to 1.22 ± 0.03 (castor oil-NLCs). This emphasises that the inclusion of a liquid lipid causes a decrease in the polarity of the lipid core, thus a decrease in the I_1/I_3 value. The significantly different environment that pyrene resides in can be compared by its fluorescence response in a range of different polarity organic solvents. For example, I_1/I_3 values achieved for pyrene in two different organic solvents, namely diethyl ether and 2-propanol are 1.09 and 1.26 respectively. [46] These similarities are mirrored for two different NLC systems using mineral oil (I_1/I_3=0.91) and castor oil (I_1/I_3=1.22). The significant reduction in the core polarity for mineral oil NLCs can be attributed to the chemical composition of the oil, which contains a mixture of non-polar hydrocarbon excipients. This is contrary to the other more polar glyceride and ester containing lipids. The similarities in the compositions of the alternative liquid lipids addresses their comparability of the I_1/I_3 values obtained.

A secondary informative parameter obtained is the *e/m* ratio. Figure 4.8A highlights that generally for NLCs, a decrease in the I_1/I_3 value causes a simultaneous increase in the *e/m* ratio. The increased *e/m* ratio indicates that the molecules are more spatially proximal within the cores. This finding demonstrates that increasing the non-polar nature of the internal core microenvironment, causes an increased spatial proximity of pyrene molecules within the core. This is because an increase in the non-polar nature of the core (decreased I_1/I_3), allows a simultaneous increase in the concentration of the non-polar pyrene molecules to pack within a given space. The closer proximity the pyrene molecules within the core, the higher the *e/m* ratio.[43,47] The emission spectra of the different samples (Figure 4.8B) highlights that mineral oil NLCs showed the most intense excimer emission coupled with the highest *e/m* ratio (0.27 ± 0.03) and the lowest and hence the least polar I_1/I_3 ratio (0.91 ± 0.1). Importantly, the sample containing only COMP (no oil) deviated from the trend identified. The sample containing COMP (no oil) possessed the most polar core (I_1/I_3= 1.39 ± 0.005), however with an *e/m* ratio (*e/m*= 0.16 ± 0.01) higher than all NLC formulations excluding mineral oil. The increase in

the *e/m* ratio for samples containing no oil may be attributed to differences in precipitation behaviours of the COMP (no oil) *vs* COMP-oil mixtures. More specifically for formulations with only COMP (no oil), the pyrene molecules are trapped immediately upon nucleation. The spatial proximity and therefore the *e/m* ratio is likely dependent on the kinetics of nucleation and entrapment within these samples. Conversely for samples containing liquid lipids the pyrene molecules were solubilised and dispersed throughout the core. This signifies that the *e/m* ratio may be dependent on the solubility of the pyrene molecules within the liquid lipid for this subset of samples. In order to confirm this hypothesis for solid lipid only samples, further work to carry out individual solubility tests would need to be carried out. Nevertheless, the identified trend amongst the NLC formulations was of significance for the work in this chapter.

From the previously discussed data, as mineral oil obtained the lowest polarity NLC core and highest excimer emission, it would be assumed that this system would be optimal for the encapsulation of IND. However, due to the previous DSC studies that showed mineral oil possessed the least IND solubility, it was predicted that this system would be the least successful for this research. Nevertheless, for alternative entities with a higher compatibility with mineral oil, this system would be considered optimal for further development. Due to the similarities in the I_1/I_3 values of the alternative oils, it was determined that there would be no significant difference in loading capacities for IND-NLCs dependent on the liquid lipid used. However from the DSC and fluorescence data combined, it was predicted that maximal drug loading would be achieved using safflower, castor or sunflower oil due to the mutual high compatibility for IND and COMP. All NLCs were taken forward for IND encapsulation to test this hypothesis.

4.2.5 Incorporation of Indomethacin

Pluronic® F68 was implemented to identify success of preliminary IND-NLCs. Sample subsets containing 50:50 w/w% and 70:30 w/w% solid: liquid lipid were investigated. IND loading was implemented at 1 wt% and 10 wt% with respect to the total solid mass within

each of the NLC systems. Figure 4.9 shows the D_z of the blank NLCs and IND NLCs containing 1 wt% and 10wt% of drug and their corresponding PdI values. Figure 4.9A represents all samples containing 50:50 w/w% solid:liquid lipid and Figure 4.9B represents all samples containing 70:30 w/w% solid:liquid lipid.

Figure 4.9Ai and Bi shows that an increase in drug wt% generally results in a larger particle size regardless of the liquid lipid used. Figure 4.9Ai shows that for 50:50 w/w% solid:liquid lipid NLCs using mineral oil has a significant increase in D_z from 146 nm (blank- NLCs) to 487 nm for 10wt% IND-NLCs. The larger increase in D_z for mineral oil NLCs in comparison to the other formulations was attributed to the poor compatibility of IND within the liquid lipid. This follows the intrinsic relationship between the solubility of a drug and drug particle size in solutions.[48] Figure 4.9Aii and Bii highlights that there was no trend in PdI amongst the samples as the drug loading increased. This demonstrates that although there was a general increase in D_z, uniformity of particle size was still maintained within the dispersions (all samples <30%). Nevertheless, there was a notable increase in PdI for 70:30 w/w% samples in comparison to 50:50 w/w% samples with average PdIs of 20 % ± 5.6 *vs* 13 % ± 4.6 for the respective NLC subsets. This is further discussed with comparable observations obtained in Figure 4.10B.

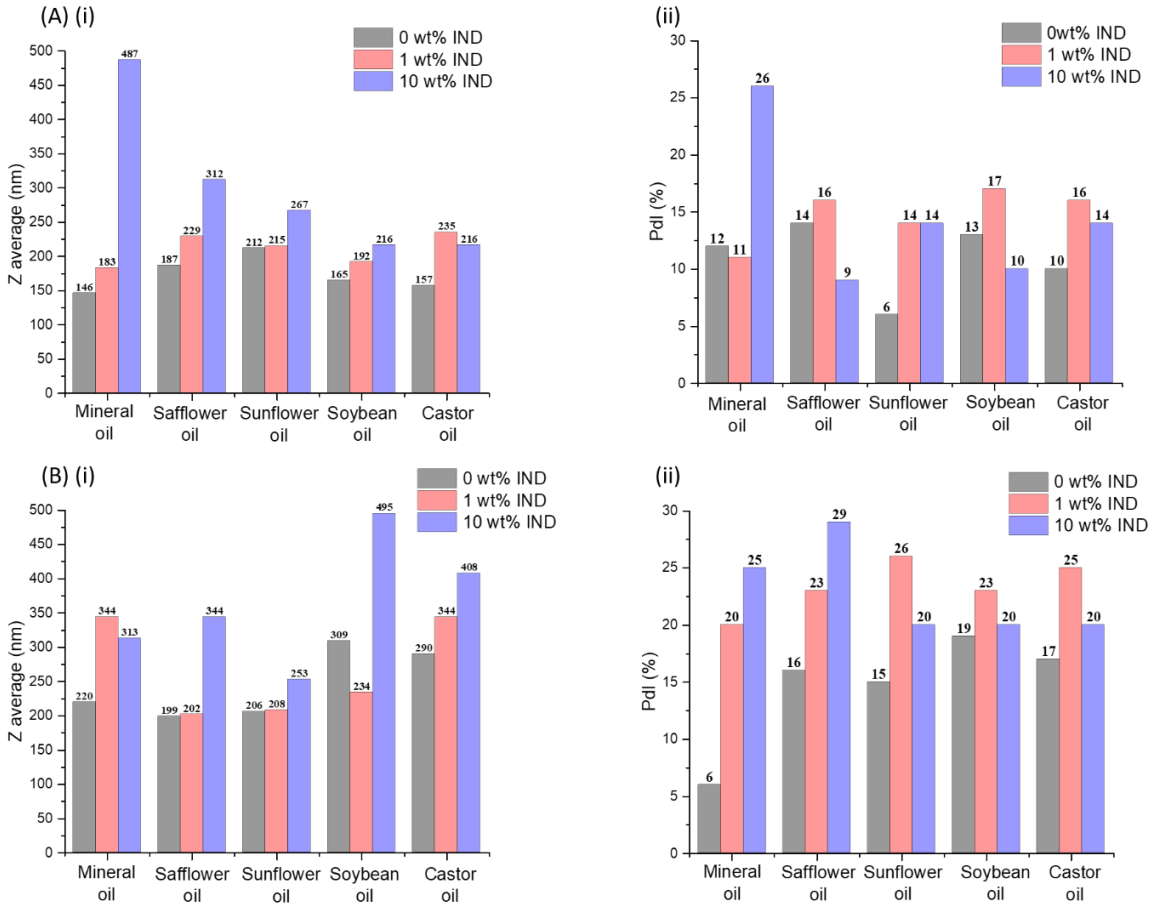

Figure 4.9: Shows the D_z and PdI of dispersions containing varying drug loadings of IND. A) The effect that an increasing IND content has on the (i) D_z and (ii) PdI on systems containing 50:50 w/w% solid:liquid lipids. B) The effect of increasing IND loading on (i) D_z and (ii) PdI in 70:30 w/w% solid: liquid lipid systems.

Figure 4.10A shows that the increased D_z of 50:50 w/w% samples containing mineral oil also contains a secondary population at the upper limit of reliable DLS detection (~1 μm). This population was assumed to be aggregates of IND crystals formed upon precipitation due to heterogeneity within the sample, resultant of poor mineral oil-IND solubility. The black arrow in Figure 4.10A represents the larger population of potential IND crystals formed. Figure 4.10B represents NLC dispersions synthesised from 70:30 w/w% solid: liquid lipid. Coupled with the increased PdI of 70:30 w/w% samples discussed previously, the size traces demonstrated less intense and more polydisperse samples compared to 50:50 w/w% samples. This was characterised by shorter, broader traces. The reduced intensity of 70:30 w/w% IND-NLCs can be attributed to the decreased overall solubility of IND in the lipid cores due to a decreased amount of liquid lipid present, thus increasing dispersity within the sample.[49] Although previous findings founded that higher wt% liquid lipids have previously shown a decrease in encapsulation efficiency as discussed in section 4.2.3, the 70:30 w/w% samples were taken forward to assess initial formulation development in the initial studies due to affording lower D_z and less polydisperse samples.[41]

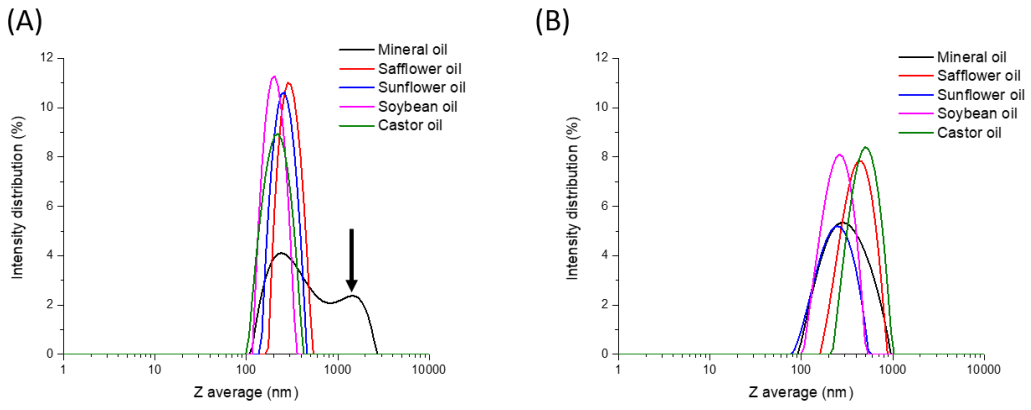

Figure 4.10: (A) Size distribution for 10wt% IND-NLC dispersions using 50:50 w/w% solid: liquid lipid samples. The black arrow highlights a population of IND crystals formed in the precipitation process. (B) Size distributions for 10wt% IND-NLC samples synthesised using 70:30 w/w% solid: liquid lipid. All samples using F68 as the stabiliser.

The following section demonstrates the effect of alternative Pluronic® stabilisers for IND-NLCs (50:50 w/w%) at 10wt% loading.

4.2.6 Exploring alternative Pluronic® stabilisers

All previous experiments within this chapter have employed Pluronic® F68 as the chosen stabiliser due to its profound usage with COMP as a solid lipid.[37,50] Nevertheless, this section explores alternative Pluronic® stabilisers for optimal NLC synthesis. This was to ensure optimal stability of the IND-NLCs. Pluronic® stabilisers chosen for this investigation have been successfully employed in multiple IND nanoparticle systems. [35,51] The properties of the Pluronic® stabilisers explored are shown below in Table 4.3.

Table 4.3: Pluronic® stabiliser properties used for IND-NLC development.

Pluronic®	**Formula**	**HLB value**	**PPO/PEO ratio**	**Average MW (g/mol)**	**CMC at 25 °C (M)**
P105	PEO_{37}-PPO_{56}-PEO_{37}	15	0.76	6500	6.2×10^{-6}
F127	PEO_{100}-PPO_{65}- PEO_{100}	22	0.33	12600	2.8×10^{-6}
F68	PEO_{76}-PPO_{29}-PEO_{76}	29	0.20	8400	4.8×10^{-4}
L64	PEO_{13}-PPO_{30}-PEO_{13}	15	1.2	2900	4.8×10^{-4}

All blank-NLCs in the absence of IND were successfully monomodal immediately after synthesis (Appendix Figure A2). Due to the successful formation of IND-NLCs at 10wt% IND using Pluronic® F68, the same excipient masses were used to trial alternative stabilisers. Pluronic® L64 was not able to maintain short term (1 hour) stability for 10 wt% IND-NLCs. The samples were characterised visually by the presence of solid particulates amongst the highly turbid dispersion shown in Figure 4.11.

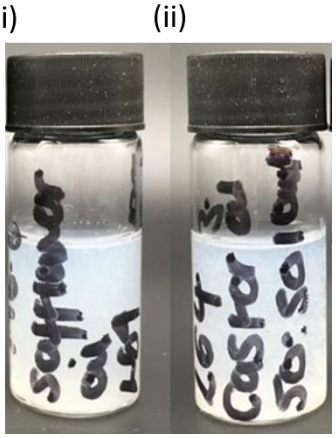

Figure 4.11: Sample destabilisation using Pluronic® L64 as the lone NLC stabiliser for 10 wt% IND dispersions. Representative samples shown were for (i) Safflower oil and (ii) Castor oil.

A potential reason for the rapid colloidal destabilisation when using L64 as a stabiliser may be attributed to the short PEO corona, which is responsible for the steric repulsion of co-existing colloids within the system. Pluronic® L64 consists only of 13 repeating PEO units in each hydrophilic block of the amphiphilic stabiliser, in comparison to 37 (P105), 76 (F127) and 100 (F68) shown in Figure 4.12A. Therefore, it is assumed that the smaller PEO units did not have the capacity to sterically stabilise 10 wt% IND-NLC lipid cores, thus increasing the likelihood of particle aggregation (Figure 4.12B).

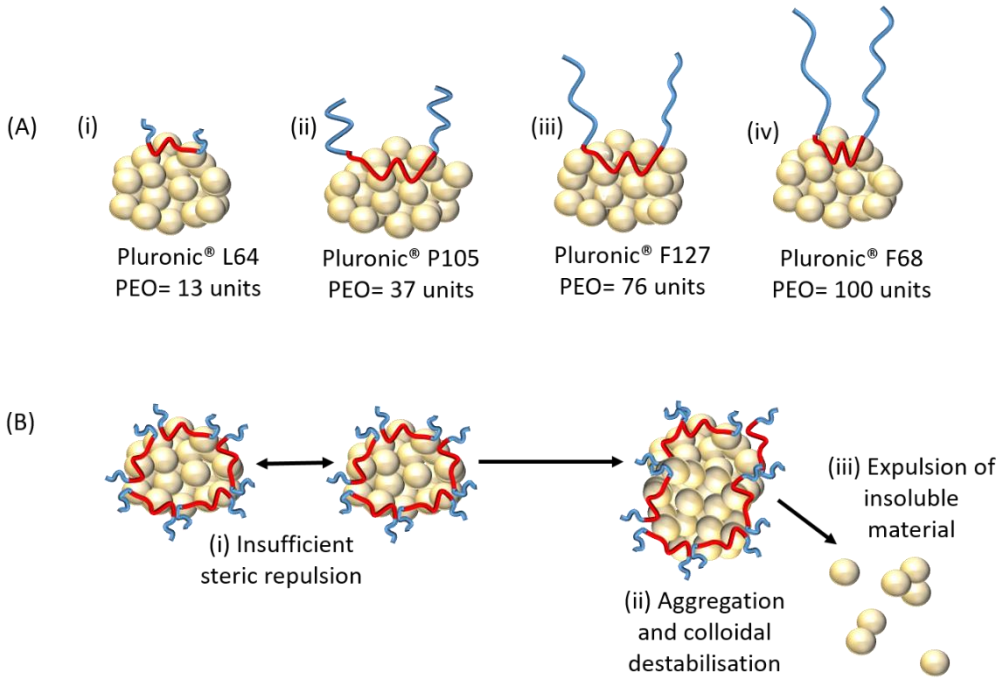

Figure 4.12: (A) The difference in PEO compositions for Pluronic® stabilisers (i) L64, (ii) P105, (iii) F127 and (iv) F68. (B) Illustration of the smaller PEO blocks on L64 provide (i) Insufficient steric stabilisation for the lipid core which results in (ii) Aggregation of particles stabilised by shorter PEO chains causing colloidal destabilisation of NLCs and (iii) subsequent expulsion of insoluble material.

This finding has been similarly observed in other studies investigating the effects of PEO length on colloidal stability.[52,53] In addition, a study by Sandez-Macho *et al*. explored the interactions of similar amphiphilic polymers (poloxamines) within lipid monolayers.[54] They showed that poloxamines with shorter PEO blocks are able to incorporate themselves within lipid monolayer and cause an increase in lipid surface area.[54] This infers that the Pluronic® L64 stabiliser, as a short PEO block polymer, is insufficient at providing steric stabilisation and may instead intercalate with the lipid cores. This process causes colloidal destabilisation

and expulsion of insoluble excipients. For this reason, Pluronic® L64 was not carried forward for optimisation of IND-NLCs.

Conversely, IND-NLC dispersions synthesised with Pluronic® F127 and P105 using castor oil and safflower oil obtained enhanced visible stability over seven days. From the previous DSC and fluorimetry data; safflower, sunflower and castor oils were predicted to be the most suitable for NLC development. These findings have shown that when incorporating IND at 10 wt%, sunflower oil displayed destabilisation prior to that of safflower and castor oil NLC dispersions. This may be attributed to the increased solubility of IND within the sunflower oil causing a decreased encapsulation of the active molecule, thus a slow precipitation of drug over time. All IND-NLC dispersions were compared to previous samples synthesised with Pluronic® F68. All IND-NLCs formed D_z dispersions with narrow polydispersity as shown in Table 4.4.

Table 4.4: Reproducibility data of 10wt% IND-NLCs using Safflower and Castor oil as liquid lipids. Pluronic® F68, P105 and F127 were implemented as three different stabilisers.

Stabiliser	Liquid lipid	Z average (nm)	PdI (%)
F68	Safflower oil	186 ± 27	17 ± 3
P105	Safflower oil	195 ± 20	15 ± 2
F127	Safflower oil	131 ± 23	19 ± 1
F68	Castor oil	218 ± 50	17 ± 3
P105	Castor oil	124 ± 22	21 ± 3
F127	Castor oil	124 ± 19	20 ± 2

Importantly Table 4.4 highlights that F68-castor oil samples are characterised by a slightly larger D_z at 218 ± 50 in comparison to P105- castor oil (124 ± 22 nm) and F127- castor oil (124 ± 19 nm) samples. The increase in D_z was also coupled with an increased turbidity shown in Figure 4.13.

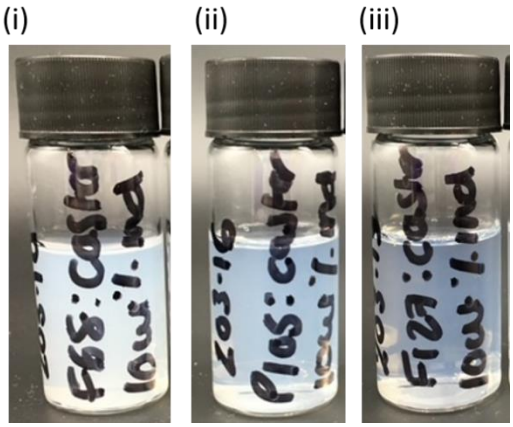

Figure 4.13: The turbidity of samples immediately after synthesis using Castor oil: COMP (50:50 w/w%) NLC lipid cores to stabiliser 10wt% IND dispersions using Pluronic® stabilisers (i) F68 (ii) P105 and (iii) F127.

The D_z increase in Pluronic® F68 stabilised systems may be resultant of a shorter PPO block associated with the stabiliser (PPO =29) in comparison to P105 (PPO = 56) and F127 (PPO =65), thus explaining the difference in the turbidity's of the samples. Pluronic® stabilisers use the PPO block to anchor into the internal lipid core environment to reduce interfacial tension between the core and the external aqueous phase (Figure 4.14).

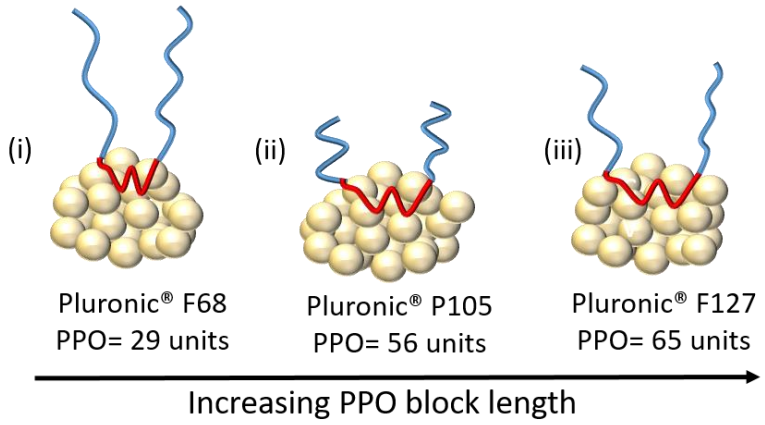

Figure 4.14: Illustration emphasising that the shorter the PPO block, the less able the stabiliser to anchor into the lipid core. (i) Pluronic® F68 is significantly smaller (PPO= 29) in comparison to (ii) P105 (PPO= 56) and (iii) F127 (PPO =65).

Therefore the shorter the PPO block, the smaller surface area available for the ability to anchor into the lipid core. This may cause a decrease in overall stability, causing swelling of the particles and thus the appearance of increased turbidity, or consequent leakage of the hydrophobic material causing complete destabilisation.[35,55]

Nevertheless, the ability to form 10 wt% IND-NLCs using Pluronic® F127 and P105 was of significant importance. This formulation consisting of 3.4 mg of IND, clinically translates tp an applicable therapeutic IV infusion of 147 mL to hypothetically reach the 25 mg IV dosage requirement. For this reason, samples stabilised by Pluronic® F127 or P105 were taken forward for to explore techniques to remove 1-propanol.

4.2.7 Removal of 1-propanol

The next step in formulation development was to remove the organic solvent, 1-propanol, from the IND-NLC dispersions. The removal of 1-propnaol was of significant important as it is a class 3 solvent in accordance with the FDA-CDER list. [56] Therefore a maximum of 50 mg/day is allowed in clinically relevant formulations.[56] Lyophilisation and spiral evaporation were trialled.

4.2.7.1 Lyophilisation

Unfortunately, lyophilisation without the presence of cryoprotectants formed samples that were unable to be efficiently reconstituted (data not shown). The dispersions were turbid with a dominant presence of large aggregates of material that were unable to be redispersed, with or without vortexing. A range of several cryoprotectants were explored, including different MW PEG molecules to freeze dry 10 wt% IND-NLCs. PEG was chosen as the cryoprotectants due to their previous reported success.[57,58] All PEG molecules explored had respective MWs of 400, 2000, 5000 and 10,000 g/mol. Concentrations of 5 or 10 mg/mL of each PEG dispersion (1 mL) was added to 1 mL of nanoparticle dispersions prior to freezing. Unfortunately, the addition of cryoprotectants in both castor and safflower oil samples, independent of the Pluronic® stabiliser used, consisted of large crystals within the dispersions. Alternative methods for solvent removal were explored.

4.2.7.2 Spiral Evaporation

Spiral evaporation is a method that utilises the removal of organic solvents or water under a continuous vacuum. Figure 4.15 shows the dispersions after spiral evaporation, where visible

solid material was seen on the inside of the vials and throughout the dispersion, suggesting disrupted destabilisation.

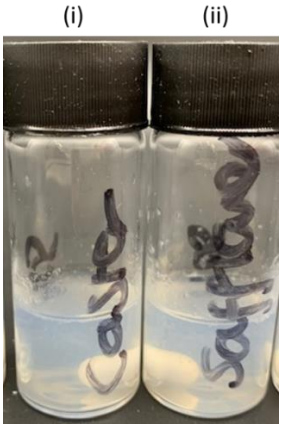

Figure 4.15: Spiral evaporation of (i) F127-Castor oil and (ii) F127 Safflower oil 10 wt% IND-NLCs.

It was unknown whether the destabilisation was as a result of heating the sample to 40 °C to remove the 1-propanol or due to the loss of the organic solvent. To understand this in more detail further experiments would need to be carried out. Due to the difficulties removing the organic solvent, alternative formulations were explored. For all of the NLC dispersions discussed throughout this chapter, 1-propanol is required to ensure the full addition of a molten COMP. However if the solid lipid were to be removed, the nanoparticle formulation type is classed as a nanoemulsion (NE). The development of indomethacin NE's (IND-NEs) is discussed in the section below.

4.3 Nanoemulsions

NEs consist of two immiscible phases that are dispersed within one another and stabilised by amphiphilic emulsifying molecules.[59] NEs consist of a hydrophobic guest molecule dissolved in an oil (liquid lipid) that is dispersed within an aqueous continuous phase (oil in water (o/w)). Alternatively, there may be a hydrophilic guest molecule dissolved in water dispersed in a hydrophobic organic continuous phase (water in oil (w/o)). For the purpose of this research the former o/w dispersions are relevant for the encapsulation of IND. Often with nanoemulsions, a volatile organic solvent is required to implement the drug and oil into the

continuous phase which is left to evaporate over time. IND-NE synthesis is discussed in the following sections.

4.3.1 Alternative organic solvents

A suitable solvent to replace 1-propanol for the addition of IND was explored. A range of organic solvents with IND solubility where trialled including tetrahydrofuran (THF) (IND solubility = 100 mg/mL), ethanol (EtOH) (IND solubility = 102 mg/mL) and acetone (IND solubility = 133 mg/mL). Secondly, organic solvent miscibility tests were carried out with five of the liquid lipids (mineral oil, safflower oil, sunflower oil, soybean oil and castor oil) to determine suitability. Both THF and acetone had full miscibility with all five liquid lipids, however EtOH showed immiscibility with the liquid lipids. EtOH formed a mixture of cloudy immiscible phases with all five liquid lipids. As proof of concept to show that the immiscibility between the oils and the organic solvent negatively impacts NE development, EtOH was analysed for its ability to form IND-NEs using Pluronic® F127 was implemented as the stabiliser for preliminary testing. All NE samples upon solvent removal showed highly turbid dispersions containing precipitated material in all samples independent of the liquid lipid. The visual observations are shown below in Figure 4.16.

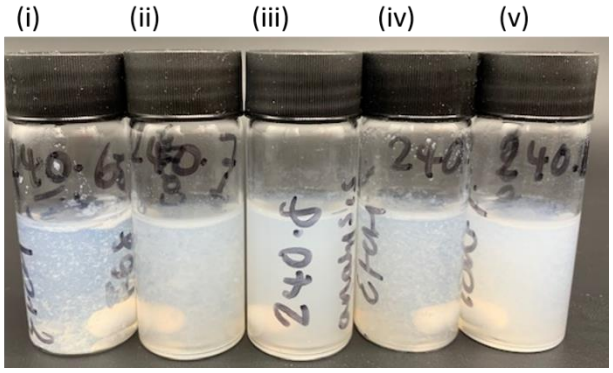

Figure 4.16: Stability of IND-NEs using EtOH as the organic solvent with 10 wt% IND. Pluronic® F127 was as the stabiliser for IND-NEs containing (i) mineral oil, (ii) safflower oil, (iii) sunflower oil, (iv) soybean oil and (v) castor oil.

EtOH was discarded from further testing. THF was also excluded from further studies due to the associated health and safety risks and suspected ability to cause cancer.[60] Acetone, as a less hazardous solvent was taken forward for IND-NE synthesis.

4.3.2 IND-NE synthesis

Pluronic® P105 and F127 were explored as potential IND-NE stabilisers as they were both the most successful for IND-NLC dispersions. The stabiliser concentration was maintained at 0.8 mg/mL in 5 mL DI water and the total hydrophobic mass (liquid lipid and drug) was kept constant at 4.5 mg in 4 mL analytical acetone. The removal of acetone was confirmed after overnight evaporation through ^{1}H NMR shown in Figure 4.17. The removal of acetone over a 12-hour period was supported by the absence (in the blue trace) of the peak at 2.23 ppm. The peak at 4.79 ppm is D_2O as a reference solvent as referenced by Babij et al.[61]

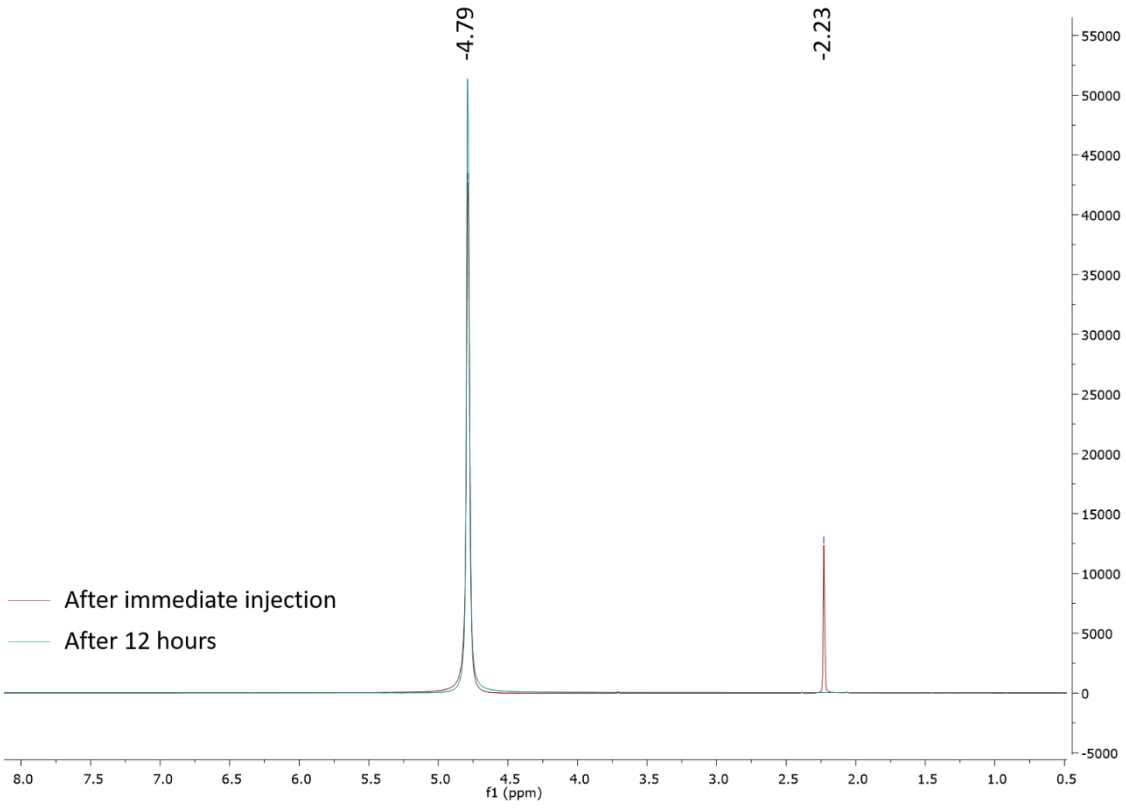

Figure 4.17: ^{1}H NMR spectra of IND-NE dispersions highlight that the complete removal of acetone after stirring for minimum of 12 hrs.

The development of IND-NEs at 10wt% drug of the total solid mass was explored in the following section.

4.3.2.1 Nanoemulsion stabilisers: Pluronic® P105

As the IND content was standardised at 10wt% of the total solid mass, this translates 0.85 mg IND. The size distributions for blank-NEs and 10 wt% IND-NEs using Pluronic® P105 as the stabiliser are shown in Figure 4.18A and B respectively.

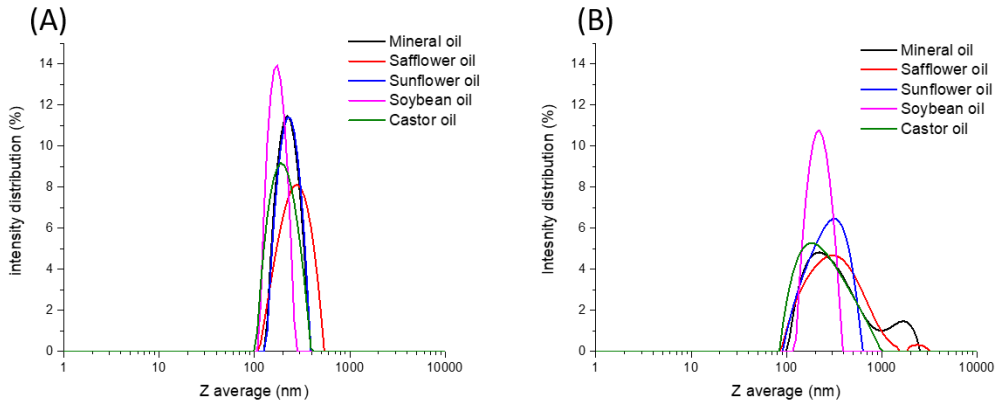

Figure 4.18: Size distributions for Pluronic® P105 stabilised nanoemulsions. (A) NEs formed using liquid lipids in the absence of IND, denoted as blank-NEs and (B) NEs formed used 10 wt% IND.

Figure 4.18 highlights that P105 was a successful stabiliser for forming blank NEs containing all five liquid lipids, however all but one of the formulations were polydisperse upon the inclusion of IND. Soybean oil appeared as the lone exception in Figure 4.18B, forming a narrow monomodal distribution for IND-NEs, however it was found to rapidly destabilise overnight by forming visible aggregates of material. Pluronic® P105 was therefore discarded from further development. The inability for P105 to maintain steric stability for IND-NEs may be resultant of the shorter PEO chains associated with the polymer. For example, P105 contains only 37 PEO repeat units in comparison to F127 with 100 PEO units (Figure 4.19). In turn this reduces the ability of the PEO chains to adequately cause steric repulsion between the co-existing emulsion droplets within the dispersion. The inability of P105 to stabilise IND-NEs in comparison to the successful ability for P105 to stabilise IND-NLCs, may be attributed to the removal of COMP from the lipid core. Therefore, there was a possibility of P105 to be partially solubilised in the emulsion droplet, rather than be adsorbed onto the surface of NLCs containing the COMP solid lipid. This hypothesis requires further work to confirm the ability

for the liquid lipids to solubilise P105, however it does remain a theoretical explanation for clear destabilisation seen in P105 IND-NE systems.

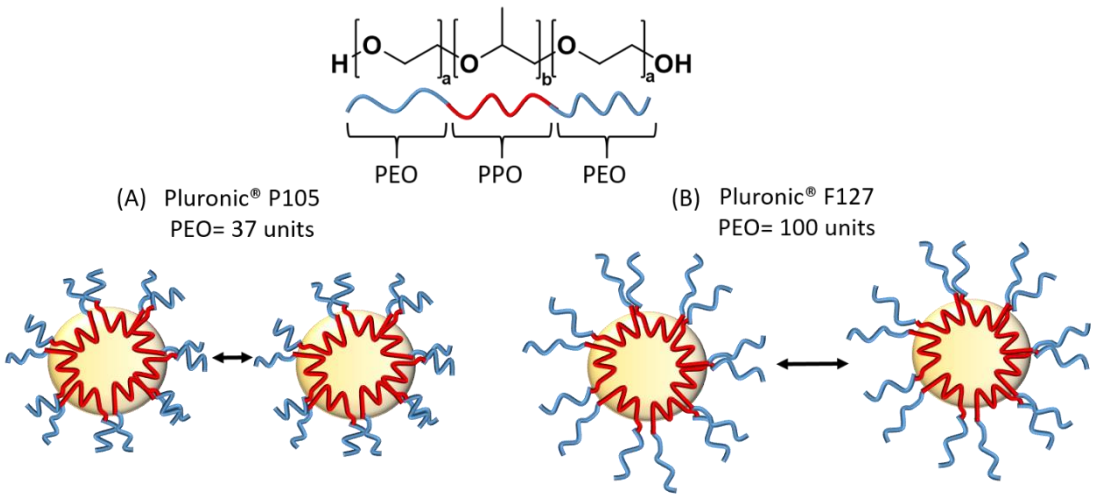

Figure 4.19: Illustration to show that the PEO units on (A) P105 and (B) F127 differ significantly in their chain length from 37 repeating units to 100 repeating units respectively. This may influence ability of the P105 IND-NEs the steric stabilise co-existing IND droplets within the dispersion.

Interestingly, previous research has also shown that polymers with shorter PEO units can be fully inserted into the lipid structure.[54] This hypothesis therefore assumes that P105 stabilised blank-NEs would also become unstable over time. This destabilisation mechanism may occur more rapidly in IND-NEs *vs* blank-NEs due to increased hydrophobicity within the core of system. Consequently, this may cause an accelerated interaction between the lipid core and PPO unit on the stabiliser. In turn, this reduces the effectiveness of the PEO block to sterically stabilise the IND-NEs, causing multimodal distributions and samples of high dispersity. Consequently, Pluronic® F127 was explored and is discussed in the following section.

4.3.2.2 Nanoemulsion stabilisers: Pluronic® F127

IND-NE samples stabilised by F127 displayed optimised behaviour. IND drug loadings of 5 wt% (0.425 mg) and 10 wt% (0.85 mg) were explored. IND-NEs at 10 wt% presented a small amount of precipitated material in the samples that were absent in 5 wt% IND-NEs. Figure 4.20 shows the comparative D_z and PdI data obtained for blank-NEs (0wt%) and 5 wt% IND-NEs. From Figure 4.20A it's clear that there was no significant difference in the D_z of the dispersions regardless of the drug loading. All samples maintained low dispersity (≤25%)

across all dispersions. Figure 4.20B identifies that although mineral oil dispersions appear to have a small D_z, reasonable reproducibility and low dispersity, a larger population of aggregates or crystals are detected. Although there was no initial visual evidence to suggest aggregates in the sample, the secondary peak detected *via* DLS demonstrates the presence of larger a population that may cause disruption within the system. This may be attributable to the poor mineral oil-IND compatibility, leading to the presence of larger insolubilised IND crystals. Therefore mineral oil was discarded from further testing.

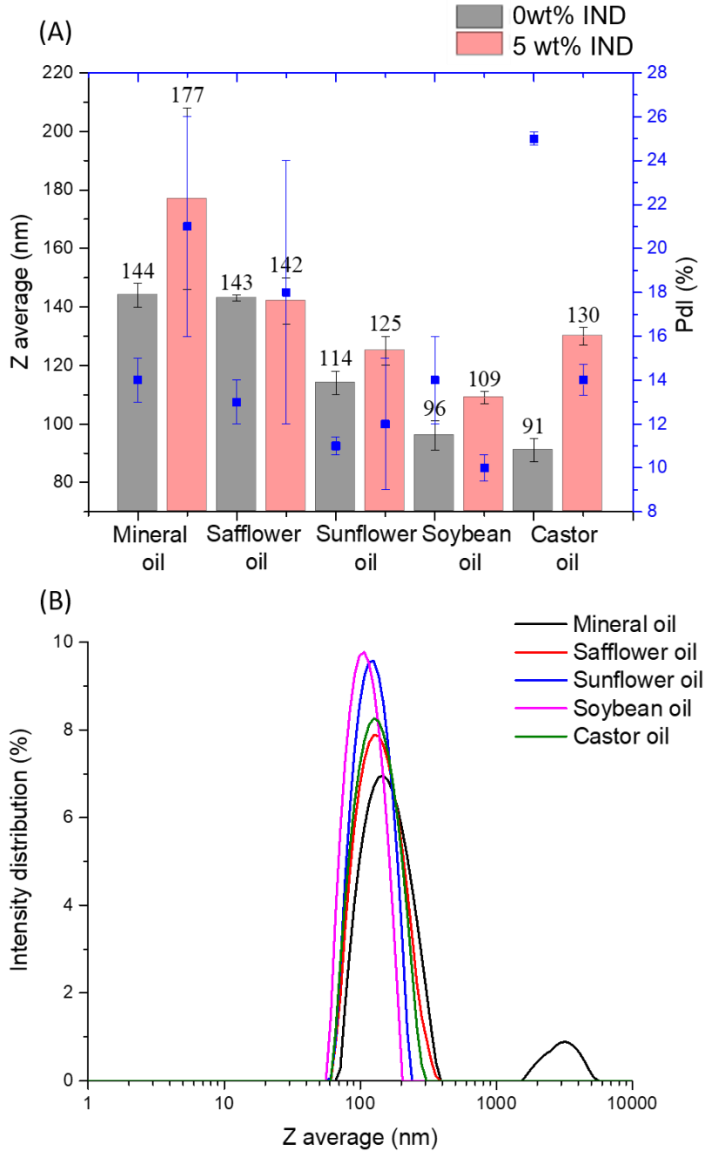

Figure 4.20: (A) Graphical representation of the D_z and PdI obtained for blank NEs and IND-NEs at 5 wt% drug loading. (B) The intensity size distribution curve for IND-NLCs at 5 wt%.

In addition to discarding of mineral oil NLCs, the development of castor NLCs was also terminated due the controversial effects of the upregulation of uterine contractility.[14] The release behaviours of safflower, sunflower and soybean oil containing 5 wt% IND are discussed in the following section.

4.3.2.3 Release behaviour of 5 wt% IND-NEs

From a clinically translatable approach, the IV dosage requirement of IND remains at 25 mg, however due to the reduction of active to 5 wt%, this equates to a theoretical IV infusion volume of 294.1 mL, assuming that 100% of the drug was released. Consequently, IND-NEs were observed for the cumulative release profiles of the dispersions at into DI water at 37.5 °C. After 48 hours IND was released in concentrations of 0.004 mg/mL, 0.003 mg/mL and 0.004 mg/mL for safflower oil, for sunflower, soybean NEs respectively. The percentage drug release profiles are shown in Figure 4.21

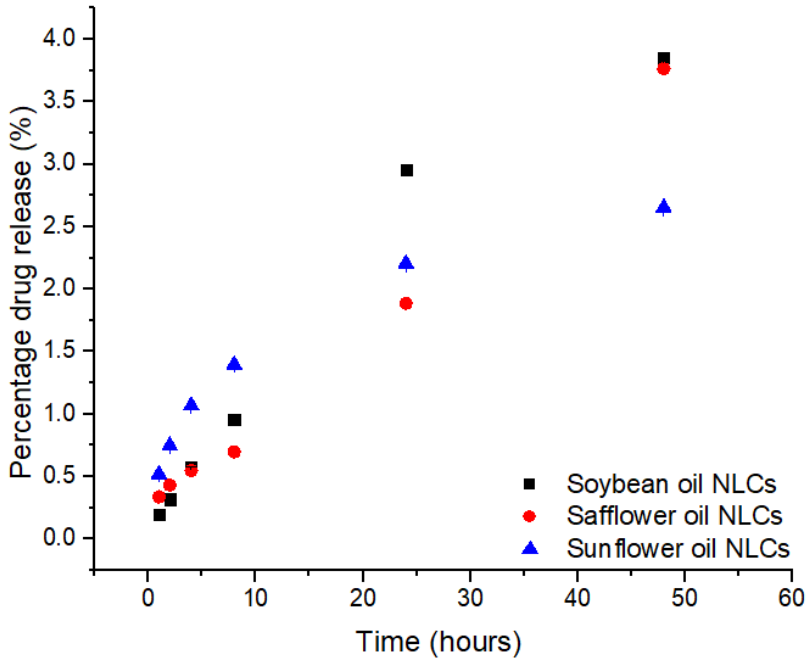

Figure 4.21: Cumulative release profiles of IND-NE dispersions using Pluronic® F127 as the stabiliser. HPLC methods determined the concentration of IND released in each of the IND-NLC samples.

The initial concentration of IND within all IND-NE dispersions was 0.085 mg. After 48 hours a total percentage of IND released from the individual NEs were 3.8 % for safflower oil, 2.7

% for sunflower oil and 3.9 % for soybean oil. As a result, the NEs are suitable for scale up to a clinically translatable content of IND, however the release of IND from these dispersions is slower than ideal for clinical translation. Furthermore, the continuous phase used as the release reservoir was DI water. Further investigation using a more clinically relatable buffer solution that contains physiological salts should be carried out. Other external parameters that should also be tested include pH triggered and enzymatic triggered release.

4.4 Conclusions and Future Work

Throughout this chapter a range of NLC formulations using several low cost, abundant liquid lipids were formed. Preliminary investigations optimised IND-NLC formulation development through the use of liquid lipid compatibility studies and fluorescence spectroscopy. Compatibility studies used visual miscibility and DSC measurements to optimise the excipients used for IND-NLC formulation development. DSC measurements emphasised that sunflower, soybean and castor oil provided complete dissolution of IND, whereas safflower oil showed a notable dissolution by solubilising ≥76 % of the drug. Mineral oil displayed the worst IND compatibility. With respect to COMP, DSC results showed that mineral oil displayed the most favourable dissolution; however, safflower, sunflower and castor oil also showed a positive reduction in COMP crystallinity. Consequently, mutual excipients for further testing were considered to be safflower, sunflower and castor oil as optimal, mutual liquid lipids for IND and COMP. Fluorescence spectroscopy emphasised that the incorporation of a liquid lipid in the lipid core significantly reduction the internal core polarity, supported by a reduction in the I_1/I_3 value in comparison to systems containing solely COMP solid lipid. Safflower and sunflower oil liquid lipids as mutual excipients for IND and COMP also displayed an excimer emission in the fluorescence spectra, supporting the close spatial proximity of pyrene molecules within the lipid core. Following on from this, the successful formation of 10wt% IND-NLCs was achieved using all liquid lipid excipients. However, safflower and sunflower oil stabilised by Pluronic® F127 displayed increased stability amongst all of the samples. This emphasised that DSC and fluorescence spectroscopy can be used to

enhance the choice of excipients used for NLC development. Although IND-NLCs containing 10wt% drug were successfully synthesised, the removal of organic solvent resulted in destabilisation of the system. Further work in this area would include the exploration of alternative stabilisers, commercial or bespoke, for the stability of the NLCs should be explored for their ability to withstand freezing and drying stresses. Further exploration on the dependence of the stabiliser concentration on their stability should also be optimised.

As the solid lipid, COMP, requires the addition of 1-propanol within the solvent injection method to form the optimised NLCs, COMP was removed from the formulation to allow exploration of alternative organic solvents. The consequent set of nanomaterials known as NEs were synthesised using EtOH, THF and Acetone. EtOH displayed poor miscibility with the liquid lipids and inadequately enabled the formation of IND-NEs. Both THF and Acetone possessed miscibility with all liquid lipids. Acetone was taken forward for IND-NE synthesis which successfully formed 5 wt% IND-NEs which would theoretically require an IV infusion of 294 mL. However, a fundamental drawback of this formulation was the release profiles obtained in DI water at 37.5C. The release profiles for safflower, sunflower and soybean oil IND-NEs showed only a ≤3.9% release of the active. Evidently these release profiles of IND were greatly slower than ideal and therefore further investigation, potentially for external triggering release factors, is required.

4.5 References

1 A. Khosa, S. Reddi and R. N. Saha, *Biomed. Pharmacother.*, 2018, **103**, 598–613.

2 P. Ghasemiyeh and S. Mohammadi-Samani, *Rsearch Pharm. Sci.*, 2018, **13**, 288–303.

3 C. Tapeinos, M. Battaglini and G. Ciofani, *J. Control. Release*, 2017, **264**, 306–332.

4 N. S.El-Salamouni, R. M.Farida, A. H.El-Kamel and S. S.El-Gamalb, *Int. J. Pharm.*, 2015, **496**, 976–983.

5 S. Das, W. K. Ng and R. B. H. Tan, *Eur. J. Pharm. Sci.*, 2012, **47**, 139–151.

6 A. V. Rawlings and K. J. Lombard, *Int. J. Cosmet. Sci.*, 2012, **34**, 511–518.

7 K. S. M. Rahman, T. J. Rahman, S. McClean, R. Marchant and I. M. Banat, *Biotechnol. Prog.*, 2002, **18**, 1277–1281.

8 W. B. Rowe, *Princ. Mod. Grind. Technol.*, 2009, 113–144.

9 A. M. Abdelghany, S. Zhang, M. Azam, A. S. Shaibu, Y. Feng, J. Qi, Y. Li, Y. Tian, H. Hong, B. Li and J. Sun, *J. Agron.*, 2020, **10**, 1–18.

10 Y. C. Lee, S. W. Oh, J. Chang and I. H. Kim, *Food Chem.*, 2004, **84**, 1–6.

11 B. Arslan, *J. Agron.*, 2007, **6**, 415–420.

12 M. R. Akkaya, *J. Food Sci. Technol.*, 2018, **55**, 2318–2325.

13 S. N. Naik, D. K. Saxena, B. R. Dole and S. K. Khare, *Potential and perspective of castor biorefinery*, Elsevier B.V., 2018.

14 R. Gilad, H. Hochner, B. Savitsky, S. Porat and D. Hochner-Celnikier, *Women and Birth*, 2018, **31**, 26–31.

15 M. E. Boel, S. J. Lee, M. J. Rijken, M. K. Paw, M. Pimanpanarak, S. O. Tan, P. Singhasivanon, F. Nosten and R. McGready, *Aust. New Zeal. J. Obstet. Gynaecol.*, 2009, **49**, 499–503.

16 G. B. Sicuranza and R. Figueroa, *J. Matern. Neonatal Med.*, 2003, **13**, 133–134.

17 P. Amato and R. A. Quercia, *Nutr. Clin. Pract.*, 1991, **6**, 189–192.

18 J. L. Bosarge, in *Enclyclopedia of Human Nutrition (Third addition)*, 2013, pp. 104–110.

19 C. Willmann, S. Budik, I. Walter and C. Aurich, *Therigenology*, 2011, **76**, 61–73.

20 R. Nair, A. C. Kumar, V. K. Priya, C. M. Yadav and P. Y. Raju, *Lipids Health Dis.*, 2012, **11**, 1.

21 A. Singh, I. Ahmad, S. Ahmad, Z. Iqbal and F. J. Ahmad, *Drug Dev. Ind. Pharm.*, 2016, **42**, 1524–1536.

22 B. Gaba, M. Fazil, S. Khan, A. Ali, S. Baboota and J. Ali, *Bull. Fac. Pharmacy, Cairo Univ.*, 2015, **53**, 147–159.

23 S. Anantachaisilp, S. M. Smith, A. Treetong, S. Pratontep, S. Puttipipatkhachorn and U. R. Ruktanonchai, *Nanotechnology*, 2010, **21**,.

24 C. Houacine, D. Adams and K. K. Singh, *J. Mol. Liq.*, 2020, **316**, 113734.

25 A. P. B. Ribeiro, M. H. Masuchi, E. K. Miyasaki, M. A. F. Domingues, V. L. Z. Stroppa, G. M. de Oliveira and T. G. Kieckbusch, *J. Food Sci. Technol.*, 2015, **52**, 3925–3946.

26 T. Delmas, A. Fraichard, P. Bayle, I. Texier, M. Bardet, J. Baudry, J. Bibette and A. Couffin, *J. Colloid Sci. Biotechnol.*, 2012, **1**, 16–25.

27 N. Suderman, M. I. N. Isa and N. M. Sarbon, *Food Biosci.*, 2018, **24**, 111–119.

28 K. Hippalgaonkar, G. R. Adelli, K. Hippalgaonkar, M. A. Repka and S. Majumdar, *J. Ocul. Pharmacol. Ther.*, 2013, **29**, 216–228.

29 B. Legendre and Y. Feutelais, *J. Therm. Anal. Calorim.*, 2004, **76**, 255–264.

30 M. Yoshioka, B. C. Hancock and G. Zografi, *J. Pharm. Sci.*, 1994, **83**, 1700–1705.

31 Gattefosse, Developing Sustained Release Tablets with Compritol ® 888 ATO Formulation Guidelines, https://www.pharmaexcipients.com/wp-content/uploads/2020/03/Compritol-888_ATO_Formulation_Guideline_pdf.pdf.

32 T. Delmas, A. Couffin, P. Alain, F. De Crécy, E. Neumann, F. Vinet, M. Bardet, J. Bibette and I. Texier, *J. Colloid Interface Sci.*, 2011, **360**, 471–481.

33 R. Pantani, A. De Meo, V. Speranza and G. Titomanlio, *AIP Conf. Proc.*, 2015, **1695**, DOI: 10.1063/1.4937343.

34 L. M. Diamante and T. Lan, *J. Food Process.*, 2014, **2014**, 1–6.

35 A. M. Bodratti and P. Alexandridis, *J. Funct. Biomater.*, 2018, **9**, 1–24.

36 J. M. R. Albano, L. N. de M. Ribeiro, V. M. Couto, M. Barbosa Messias, G. H. Rodrigues da Silva, M. C. Breitkreitz, E. de Paula and M. Pickholz, *Colloids Surfaces B Biointerfaces*, 2019, **175**, 56–64.

37 S. A. El-Gizawy, G. M. El-Maghraby and A. A. Hedaya, *Pharm. Dev. Technol.*, 2019, **24**, 1287–1298.

38 J. Sun, C. Bi, H. M. Chan, S. Sun, Q. Zhang and Y. Zheng, *Colloids Surfaces B Biointerfaces*, 2013, **111**, 367–375.

39 F. N. Siahdasht, N. Farhadian, M. Karimib and L. Hafizi, *RSC Adv.*, 2020, **10**, 9462–9475.

40 W. Huang, H. Dou, H. Wu, Z. Sun, H. Wang and L. Huang, *J. Nanomater.*, 2017, **2017**, 1–10.

41 Y. Soleimanian, S. Amir, H. Goli, J. Varshosaz and S. Mohammad, *Food Chem.*, 2018, **244**, 83–92.

42 J. M. Taylor, K. Scale, S. Arrowsmith, A. Sharp, S. Flynn, S. Rannard and T. O.

McDonald, *Nanoscale Adv.*, 2020, **2**, 5572–5577.

43 G. K. Bains, S. H. Kim, E. J. Sorin and V. Narayanaswami, *Biochemistry*, 2012, **51**, 6207–6719.

44 G. K. Bains, S. H. Kim, E. J. Sorin and V. Narayanaswami, *Biochemistry*, 2012, **51**, 6207–6219.

45 A. Mohr, P. Talbiersky, H. G. Korth, R. Sustmann, R. Boese, D. Bläser and H. Rehage, *J. Phys. Chem. B*, 2007, **111**, 12985–12992.

46 S. Flynn, A. B. Dwyer, P. Chambon and S. Rannard, *Polym. Chem.*, 2019, **10**, 5103–5115.

47 A. Manicardi, L. Guidi, A. Ghidini and R. Corradini, *Beilstain J. Org. Chem.*, 2014, **10**, 1495–1503.

48 K. T. Savjani, A. K. Gajjar and J. K. Savjani, *ISRN Pharm.*, 2012, **2012**, 1–10.

49 G. Zoubari, S. Staufenbiel, P. Volz, U. Alexiev and R. Bodmeier, *Eur. J. Pharm. Biopharm.*, 2017, **110**, 39–46.

50 A. K. Kushwaha, P. R. Vuddanda, P. Karunanidhi, S. K. Singh and S. Singh, *Biomed Res. Int.*, 2013, **2013**, 1–9.

51 S. Gupta, R. Kesarla, N. Chotai, A. Misra and A. Omri, *Biomed Res. Int.*, 2017, **2017**, DOI: 10.1155/2017/5984014.

52 S. F. Tehrani, F. Bernard-Patrzynski, I. Puscas, G. Leclair, P. Hildgen and V. G. Roullin, *Nanomedicine Nanotechnology, Biol. Med.*, 2019, **16**, 185–194.

53 H. Jo, M. Gajendiran and K. Kim, *J. Ind. Eng. Chem.*, 2020, **82**, 234–242.

54 I. Sandez-Macho, M. Casas, E. V. Lage, M. I. Rial-Hermida, A. Concheiro and C. Alvarez-Lorenzo, *Colloids Surfaces B Biointerfaces*, 2015, **133**, 270–277.

55 B. Erlandsson, *Polym. Degrad. Stab.*, 2002, **78**, 571–575.

56 U.S. Food and Drug Administration Center for Drug Evaluation and Research Inactive Ingredient Database, http://www.accessdata.fda.gov/scripts/cder/iig/index.cfm., (accessed March 2021).

57 G. Rhodes, *Protein Crystals*, 2006.

58 T. Hogg and R. Hilgenfeld, *Protein Crystallography in Drug Discovery*, 2007.

59 A. K. Singh, T. P. Yadav, B. Pandey, V. Gupta and S. P. Singh, in *Applications of Targeted Nano Drugs and Delivery Systems*, Elsevier Inc., 2019, pp. 411–449.

60 Tetrahydrofuran, https://www.sigmaaldrich.com/catalog/product/sial/401757?lang=en&region=GB.

61 N. R. Babij, E. O. Mccusker, G. T. Whiteker, B. Canturk, N. Choy, L. C. Creemer, C. V. De Amicis, N. M. Hewlett, P. L. Johnson, J. A. Knobelsdorf, F. Li, B. A. Lorsbach, B. M. Nugent, S. J. Ryan, M. R. Smith and Q. Yang, *Org. Process Res. Dev.*, 2016, **20**, 661–667.

4.6 Appendix

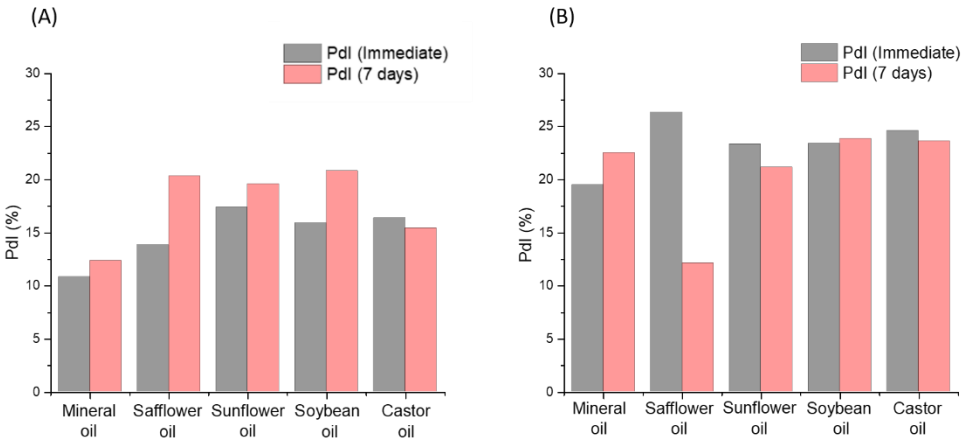

Appendix Figure A 1:Graphical representation of the PdI for (A) 50:50 w/w% solid: liquid lipid samples and (B) 70:30 w/w% solid: liquid lipid samples, immediately after synthesis and aftera 7 day period. A slight increase in dispersity was shown for 50:50 w/w% samples and no particular trend was identified for 70:30 w/w% samples. All PdI values remained narrow (≤26%) displaying uniformity over time.

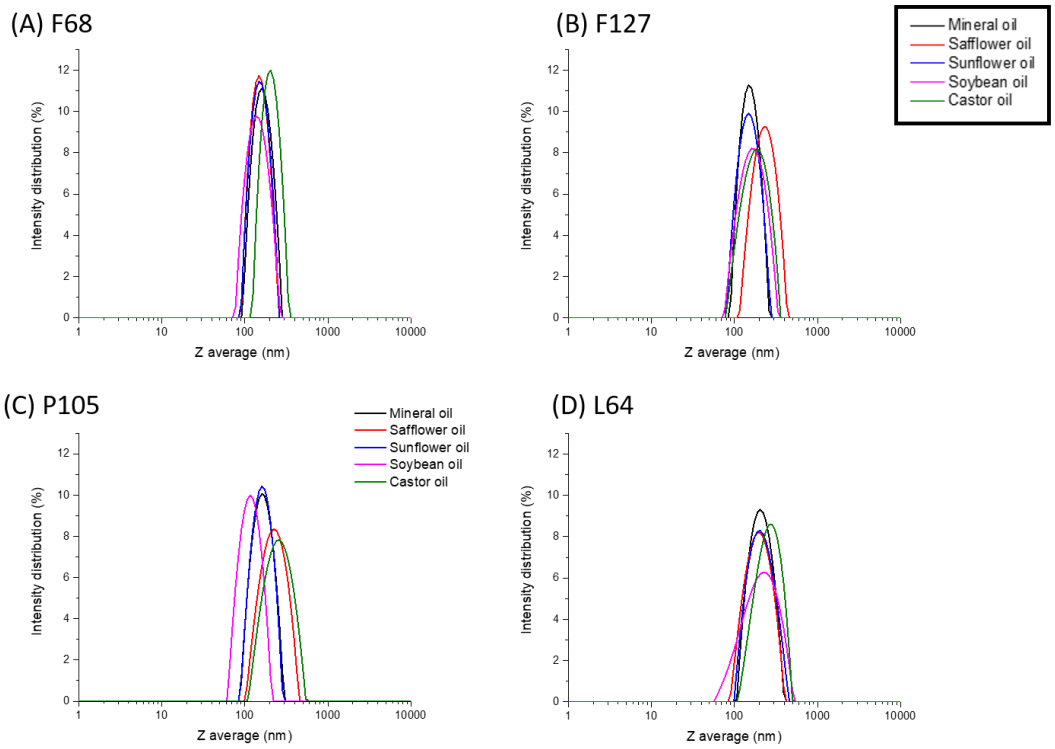

Appendix Figure A 2: Size distribution graphs for blank-NLCs stabilised by (A) F68, (B), F127, (C) P105 and (D) L64.

Chapter 5
The Synthesis of Indomethacin Analogues for the Formation of Solid Drug Nanoparticles by Emulsion Templated Freeze Drying

Chapter 5

5.1 Introduction

5.1 Solid Drug Nanoparticles

Solid Drug Nanoparticles (SDNs) are an alternative form of nanoparticle system that can be used for the delivery of therapeutic agents. SDNs do not include lipid excipients, unlike alternative formulations such as solid lipid nanoparticles (SLNs), nanostructured lipid carriers (NLCs) and nanoemulsions (NEs) discussed throughout this thesis. They consist solely of a drug/active molecule, a polymer and a surfactant shown below in Figure 5.1.

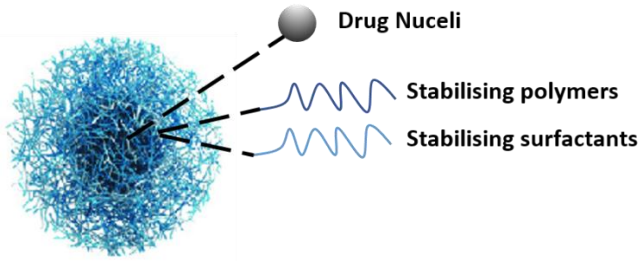

Figure 5.1: The excipients contained in a SDN particle.

SDNs have advantages overall several other nanoparticle subtypes, particularly due to the high drug loading (DL) values that are able to be achieved. This is result of the high ratio of drug to the excipients used within a single dose.[1] Consequently, a higher DL ratio translates to a reduced amount of non-therapeutic material having to be administered. The reduction in payload excipients carries significant advantages, particularly pharmacologically, as there is a reduction in the risk of toxic or adverse effects, whilst maintaining *in vivo* efficacy. The versatility of SDNs has been emphasised through the encapsulation and improved bioavailability of several clinically relevant hydrophobic drugs. For example, high weight percent loadings of antiretroviral agents maraviroc (DL= 80 wt%), lopinavir (DL= 70wt%) and efarvienz (DL= 70wt%) in SDN formulations have been achieved and translated for further immunological testing.[2–4]

SDNs are often synthesised through high pressure homogenisation techniques or by nanomilling.[5] Industrially, the nanomilling process has been efficacious for the production of

several therapeutics such as Rapamune and TriCor for the treatment of organ transplant rejection and high cholesterol as successful examples.[5,6] Nevertheless, nanomilling has also been associated with aggregation during production.[7] Consequently, emulsion templated freeze drying (ETFD), has also become an alternative and attractive option for SDN synthesis.[8] The ETFD process was discussed thoroughly in Chapter 1 section 1.8.1.2, however the process is outlined briefly below.

5.1.1 Emulsion Templated Freeze Drying (ETFD)

Firstly, the ETFD process combines the advantages of nanosizing bulk therapeutic materials, whilst maintaining the advantages of the bottom-up approach of nanoparticle synthesis.[9,10] The bottom-up approach of synthesising nanoparticles provides better control of the particle size and often obtains narrower particle size distributions in comparison to top-down approaches that commonly have to undergo repeated cycles.[9] The ETFD approach is a quick, low costly and easily scalable process, which has advantages over alternative synthetic techniques. For example, the polymer scaffold obtained in the porous monolith significantly reduces nanoparticle aggregation upon storage and simultaneously forms colloidally stable nanoparticle dispersions upon reconstitution.[9] This combats the drawbacks of the nanomilling approaches and has therefore become of significant interest in recent years.[7]

5.1.2 Chapter aims

The aim of this Chapter is to explore the implementation of the ETFD process for the formation of indomethacin (IND) loaded SDNs. Additionally, in order to investigate the effect of the drug's physiochemical properties, a series of several IND esters were synthesised through a Steglich esterification process and screened for their success in SDN formation. The esters synthesised ranged in their functionality and alkyl chain length which in turn altered their physical properties. Throughout this chapter the successes and drawbacks of IND-SDNs and the IND analogue SDNs are discussed. The successfully screened SDN formulations were tested for their reproducibility and stability for future studies.

5.2 Results and Discussion

5.2.1 Formation of IND-SDNs

The ETFD process briefly involves the screening of six different surfactants and seven different polymeric stabilisers, resulting in 42 different binary combinations. All excipients are taken from the U.S. Food and Drug Administration Centre for Drug Evaluation and Research (FDA-CDER) list.[8,11] The structures of the excipients used are summarised in Figure 5.2 (next page). Each of the binary combinations were assessed post-lyophilisation for their ability to be successfully reconstituted in deionised (DI) H_2O. The samples were analysed by the dynamic light scattering (DLS) and data quality of each sample was assessed based on their Z average (D_z) to represent mean sample size, polydispersity index (PdI) to assess sample uniformity and their redispersibility rating. The samples were rated for their visual redispersibility based on an arbitrary scale shown below in Table 5.1

Table 5.1: Redispersibility scale for assessment of sample quality in SDN screens.

Redispersibility rating	Visual appearance
I	Complete redispersion. No visual evidence of solid material, drug crystals or aggregates.
II	Formation of a turbid dispersion upon reconstitution. No evidence of solid material, drug crystals or aggregates.
III	Sample had mainly redispersed, however coupled with the presence of solid material, drug crystals or aggregates.
IV	Poor redispersion. Sample remains mainly solid.

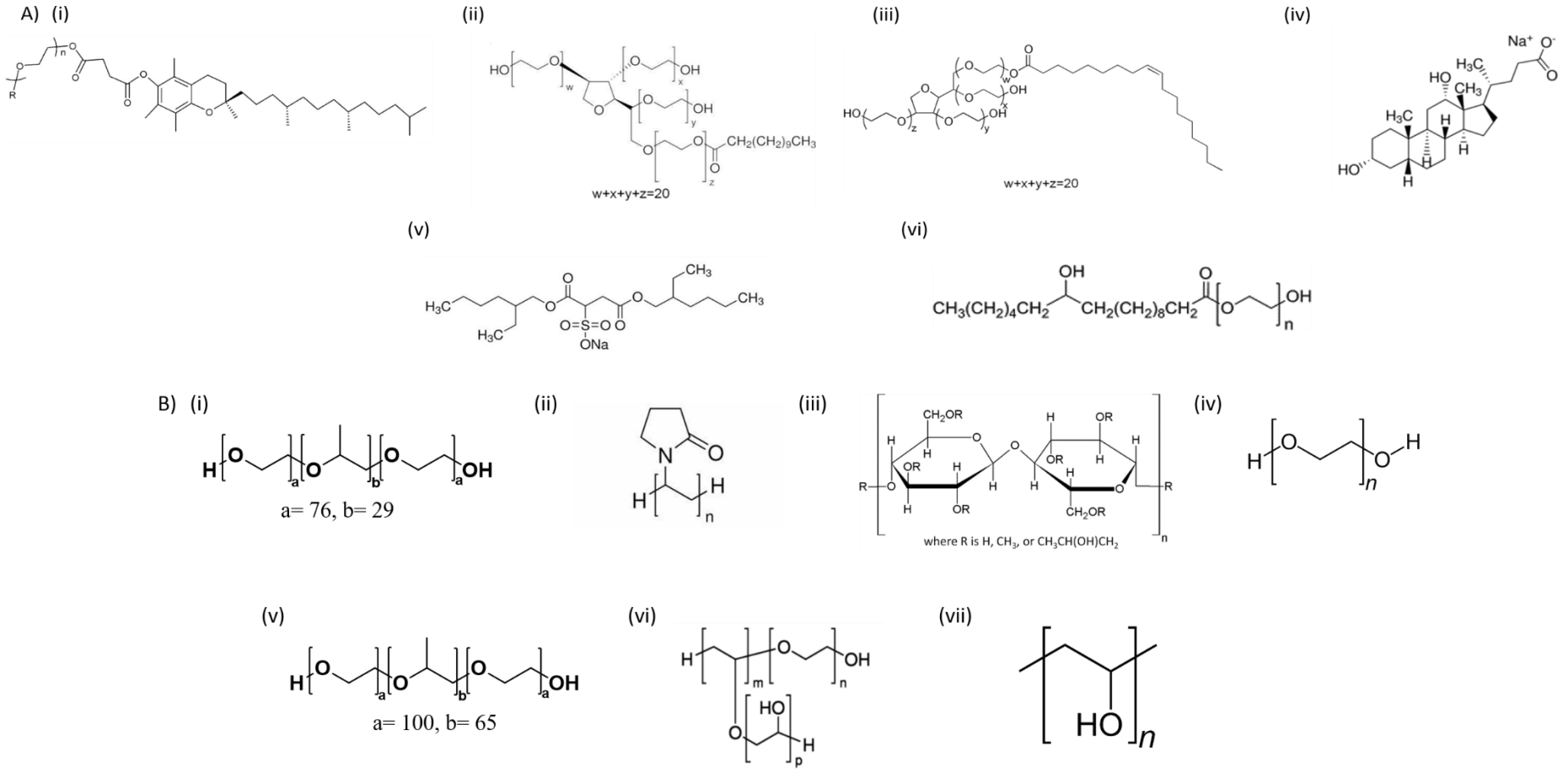

Figure 5.2: Summary of the six surfactants and seven polymeric stabilisers employed in the screening process of SDN formulations. A) Represents the surfactants used, all denotations for the individual excipients are shown in brackets after each surfactant: (i) d-α-tocopheryl polyethylene glycol 1000 succinate (TPGS) (ii) Tween 20, (iii) Tween 80, (iv) Sodium deoxycholate (NDC) (v) Dioxytl sulfosuccinate sodium salt (AOT) and (vi) Polyethylene glycol (15)- hydroxyl stearate (Solutol). B) Represents the polymeric stabilisers (i) Polyethylene $glycol_{76}$-polypropylene $glycol_{29}$-polyethylene $glycol_{76}$ (Pluronic® F68), (ii) Polyvinylpyrrolidone K30 (PVPK30) (iii) Hydroxypropyl methylcellulose (HPMC), (iv) Polyethylene glycol 1000 (PEG1K) (v) Polyethylene $glycol_{100}$-polypropylene $glycol_{65}$-polyethylene $glycol_{100}$ (Pluronic® F127),(vi) Polyvinyl alcohol-polyethylene glycol copolymer and polyvinyl alcohol (Kollicoat Protect) and (vii) Polyvinyl alcohol (PVA).

During the screening process the mass of polymer, surfactant and drug were kept constant at a total value of 10 mg. Polymers and surfactants are added in a 2:1 ratio. For further experimental details see Chapter 6, section 7.3.4.1. The initial screening process was carried out trialling 10 wt% IND loaded SDNs. The results are discussed in the following section.

5.2.2.1 Screening of 10 wt% IND-SDNs

The ETFD process was carried out screening IND at a 10 wt% total drug loading. The criteria for successful samples were those that obtained a D_z <500 nm and a standard deviation between triplicate measurements <10% to represent sample stability. The PdI of the reconstituted dispersions was <0.3 to indicate uniformity within the samples and the redispersibility was rated at a value of I or II. Samples that meet these criteria are denoted as 'HIT' samples. Figure 5.3 shows that there were 14 successful hits for 10 wt% IND-SDNs. All samples that are represented by a flat, red circle are those that obtained a D_z >1µm.

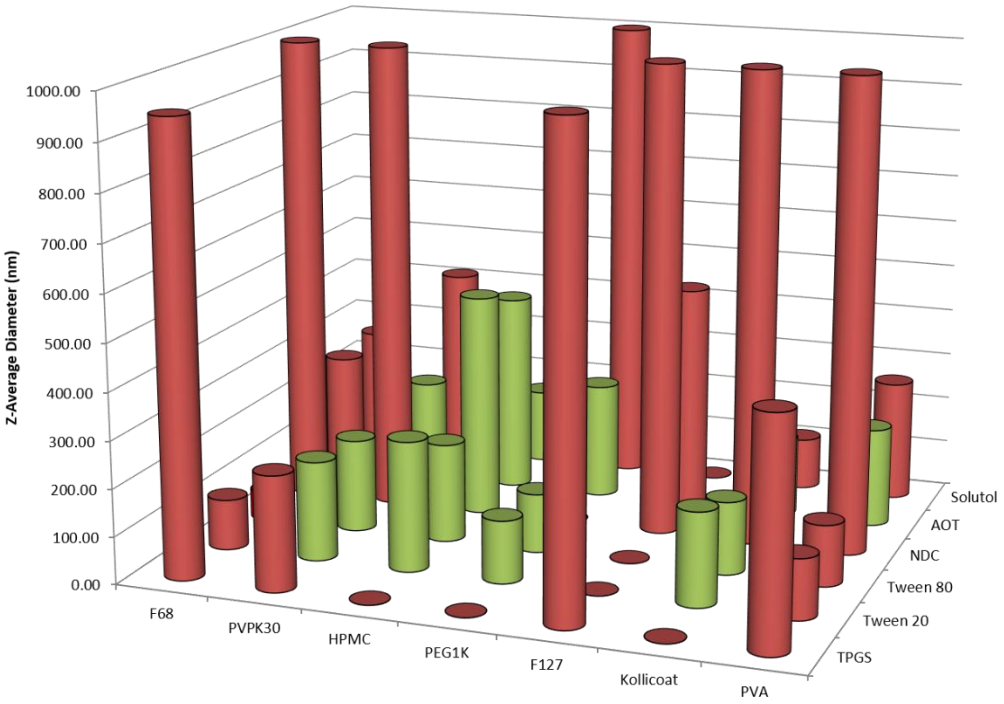

Figure 5.3: Graphical representation of sample hits (green) *vs* unsuccessful samples (red) for 10wt% IND-SDNs. Samples with a D_z >1µm are represented as red circles.

With the apparent success of 14 out of 42 HITs for 10 wt% IND-SDNs, the next experimental step was to increase the drug content. The DL was increased to 30 wt% from 10 wt% and the formulations are discussed in the following section.

5.2.2.2 Screening of 30 wt% IND-SDNs

In order to identify the samples that could withstand higher drug content, the sample subset was narrowed down by tripling the drug loading. The hit criteria was modified to D_z <600 nm, standard deviation <10%, redispersibility I or II and the PdI limit was increased to <0.5.This was altered in line with an arbitrary scale due to the shift in the data quality criteria in comparison to 10 wt% IND SDNs. Figure 5.4 highlights that with an increased drug loading, there was a significant decrease in the number of HITs identified for IND-SDNs, with only three binary combinations remaining successful.

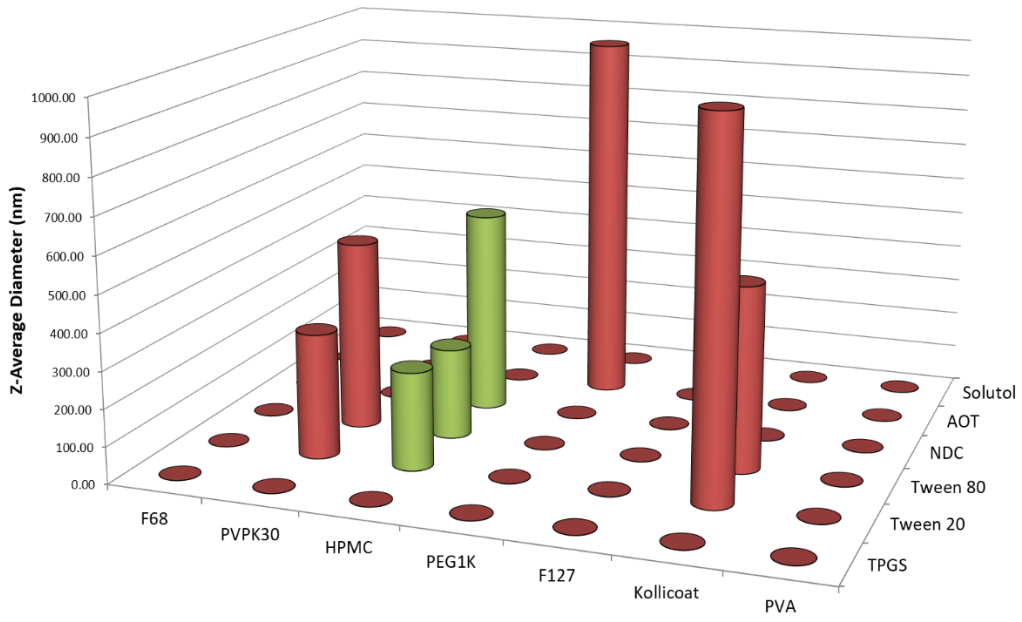

Figure 5.4: Graphical representation of hits identified for 30wt% IND-SDNs. Hit samples are represented by the green bars, unsuccessful samples are shown by the red bars. All binary combinations represented with a red circle equate to samples with a D_z above 1µm.

Interestingly, all three successful hits contained the same polymeric stabiliser, HPMC. The exact reason for HPMC as the main polymer providing enhanced stability for increased drug loaded SDNs is unknown. However, the use of HPMC as a polymer in IND-SDNs is also of

significant benefit as it is a popular excipient used for therapeutics to improve sustained release profiles.[12] Interestingly, previous research has suggested that HPMC has the ability to maintain its stabilising properties through the freeze drying process of nanoparticles.[13] This is contrary to previous research that has suggested the drying process causes dissociation of the stabilisers from the drug crystals.[13] A study by Kayaert *et al*. founded that increasing the concentration of HPMC increased the polymer layer thickness on naproxen drug crystals, even after drying.[13] This finding means that HPMC remains associated with hydrophobic drug crystals throughout the drying process, therefore explaining the increased probability of HPMC remaining a successful polymeric stabiliser upon nanoparticle reconstitution. This was confirmed through their successful redispersion of HPMC stabilised naproxen nanocrystals.[13]

In the IND screens, initial combinations of HPMC: Tween 20 and HPMC: Tween 80 formed particles with respective D_z and PdI values of 265 nm, PdI= 0.39 (Tween 20) and 247 nm, PdI= 0.42 (Tween 80). The size distribution traces for HPMC: Tween 20 and HPMC: Tween 80 are shown in Figure 5.5.

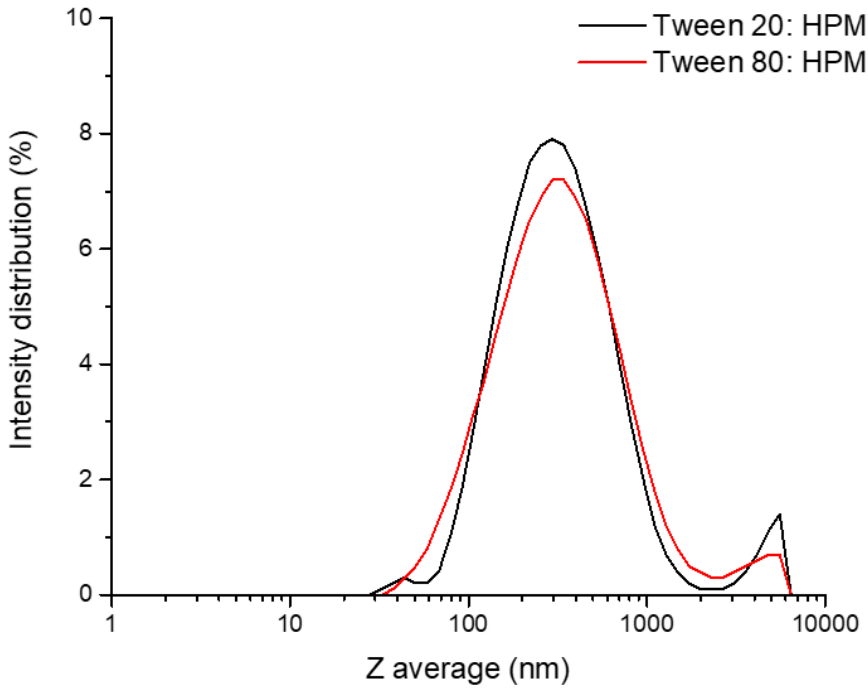

Figure 5.5: Size distribution traces of HPMC:Tween 20 and HPMC:Tween 80 30wt% IND-SDNs.

Although the size distribution traces show a secondary, larger population in both samples which may be attributed to unencapsulated IND crystals, or aggregated IND-SDNs, the predominant population is of IND-SDNs. The third binary polymer: surfactant combination of HPMC: NDC unfortunately produced a higher D_z of 550 nm, PdI of 0.43 and a significant appearance of a secondary population > 1 µm (Appendix Figure A1). For this reason, HPMC: NDC was removed from further testing. The binary combinations containing HPMC and Tween 20 or Tween 80 were tested for reproducibility across triplicate samples and are discussed below.

5.2.2.3 Reproducibility

Triplicate production of two binary combinations containing HPMC as the polymer stabiliser and Tween 20 and Tween 80 as the respective surfactants were carried out (Figure 5.6).

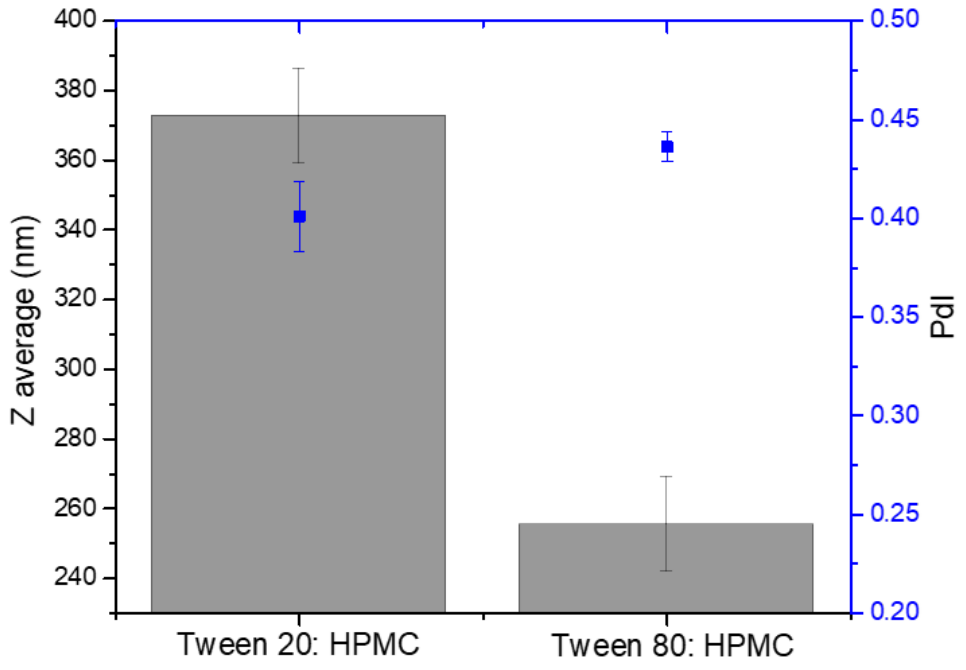

Figure 5.6: Reproducibility of 30wt% IND-SDNs using HPMC as the polymeric stabiliser and (i) Tween 20 and (ii) Tween 80

Interestingly, triplicate samples containing Tween 80 had a smaller average D_z (255 ± 13 nm PdI= 0.4 ± 0.02) than those containing Tween 20 (372 ± 14 nm, PdI= 0.4 ± 0.001). This may be attributable to the longer fatty acid chain associated with Tween 80 ($C_{18,}$ oleic acid) *vs* Tween 20 ($C_{12,}$ lauric acid). Therefore, it is possible that Tween 80 has an increased affinity

with the hydrophobic IND drug crystals within the polymer/surfactant scaffold created during the lyophilisation step of the ETFD process. However, although the D_z appeared smaller and reproducible the distribution traces suggested the significant presence of larger aggregates >1 μm, as previously similarly indicated in the initial screening process (Figure 5.5). Nevertheless, the consistent finding of a larger particle population was also coupled with destabilisation of the 30 wt% IND-SDNs within six hours of reconstitution as shown in Figure 5. 7.

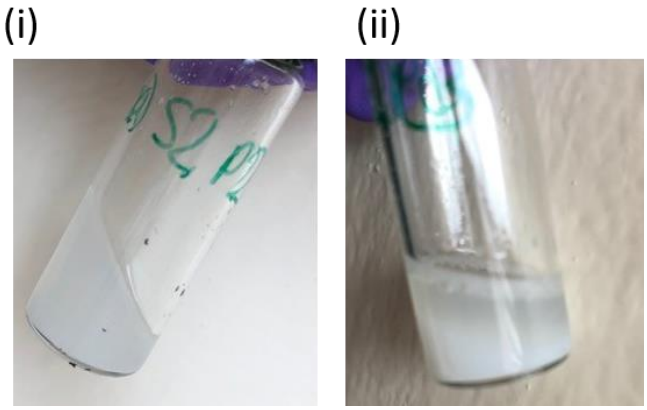

Figure 5.7: Stability of 30 wt% IND-SDNs using stabilisers HPMC: Tween 20 as an example. Sample (i) Demonstrates the sample after immediate reconstitution and (ii) Shows the sample after six hours with the significant presence of sedimented solid material.

From Figure 5.7ii, it was evident that there was significant sedimentation within the sample over a six-hour period. This may be attributed to the larger population of aggregates or drug crystals impacting the colloidal destabilisation. This is due to heterogeneity within a sample causing populations of material with varying density, spatial distribution and varying degrees of stabiliser thickness on the surface of the particles.[14] Consequent Ostwald ripening occurs whereby smaller particles within the dispersion deposit on to larger particulates and results in complete colloidal destabilisation.[15] In this case, as IND is denser than the aqueous continuous phase (1.3 g/cm^3 *vs* 1.0 g/cm^3 respectively), the solid material sediments. In order to try and combat the stability issues amongst 30 wt% IND-SDNs, the ratio between polymer and surfactant were adjusted to eradicate any potential effects of excess polymer and/or insufficient surfactant. Ratios of 1:1 and 1:2 were trialled, contrary to the previous 2:1 ratio in

the screening studies. Unfortunately this was unsuccessful and the samples formed particles of incomparable D_z values between 300-1000 nm. There was no evidence of reproducibility or uniformity between the triplicate samples. As a result, alternative methods were explored. The following section discusses how the esterification of IND to synthesise several different drug analogues can overcome the drawbacks of IND-SDN synthesis.

5.2.3 Esterification of IND

IND is a non-polar, hydrophobic molecule as indicated by the logP value of 3.69. The logP, i.e. the partition coefficient of a molecule is a measure of lipophilicity of a chemical entity, whereby a value > 0 indicates favourable partioning in the organic phase. The higher the logP value, the more hydrophobic the molecule, with Lipinski's rule denoting that a value ≥5 renders the drug inadequate for therapeutic translation as they often display poor pharmacokinetic properties due to poor aqueous solubility.[16] Additionally, the carboxylic acid group functionality on IND has an average pKa value of ~4.5, therefore has the ability to partially dissociate in water (Figure 5.8).[17] This suggests that the presence of any deprotonated drug may influence the drug crystal formation or interfere with negatively charged ionic surfactants such as NDC or AOT within the polymer/surfactant scaffold upon freeze drying.

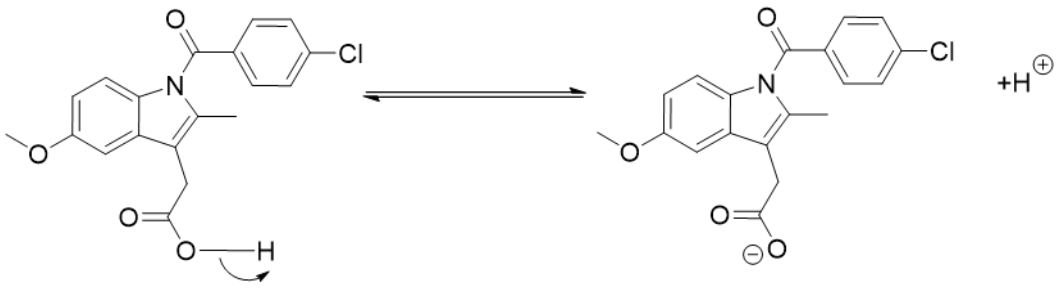

Figure 5.8: Summary of IND dissociation in neutral conditions.

For this reason, it was hypothesised that the esterification of the carboxylic acid functionality would successfully overcome the drawbacks of IND-SDNs. An additional advantageous point is that naturally occurring esterase enzymes would hypothetically activate the IND analogue upon the release of the IND esters from the SDN vehicle. With respect to the therapeutic uses of these IND-SDNs in preterm labour; there is an abundance of esterase enzymes present in

blood plasma and erythrocytes and therefore there is a high concentration of these enzymes amongst the maternal/fetal placental barrier.[18] As the presence of these enzymes would catalyse the hydrolysis of the ester, this theoretically allows the activated IND molecule to exert a therapeutic effect, allowing avoidance of pharmacological implications from the IND analogue molecules. Therefore, the following section explores the masking of the carboxylic acid group through a series of several hydrophobic analogues. The esterification process is discussed in the following section.

5.2.4 Synthesis of hydrophobic indomethacin analogues

Throughout this section the synthesis of IND esters are described. The use of different alkyl chain length alcohols were used, which increased the logP of the IND analogues within a range of 4.29-11.04.

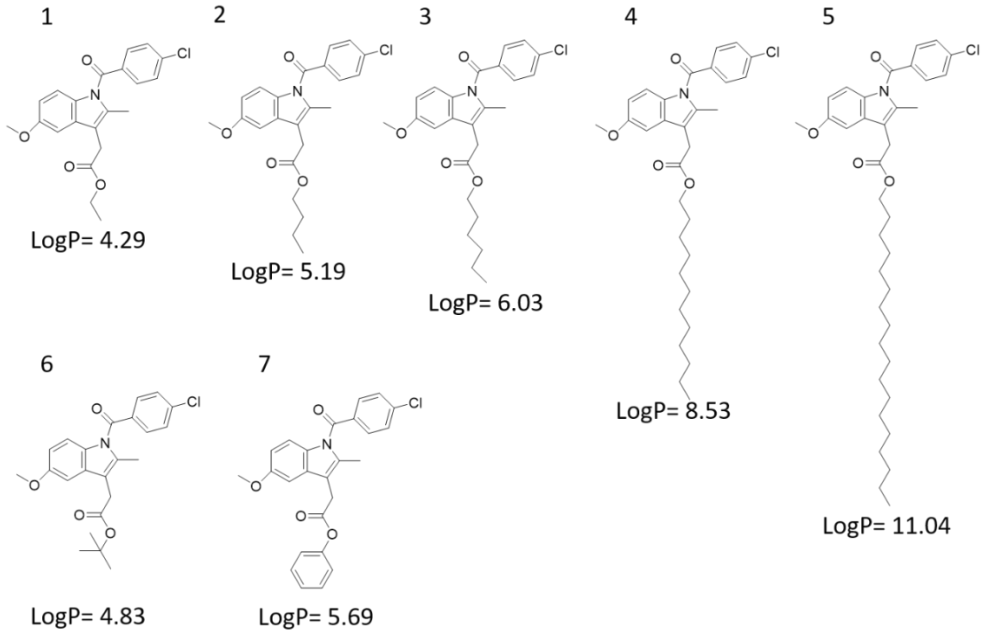

Figure 5.9: Hydrophobic esterified analogues of IND. Esters synthesised are denoted as 1-7 and represent: 1) Ethyl ester, 2) nButyl ester, 3) Hexyl ester, 4) Dodecyl ester, 5) Stearyl ester, 6) tButyl ester and 7) Benzyl ester.

All IND esters were synthesised through the Steglich esterification process which is described in the following section.

5.2.4.1 Steglich Esterification

The Steglich esterification process is a convenient method for the esterification of alcohols, thiols and carboxylic acids.[19,20] It utilises dicyclohexylcarbodiimide (DCC) as a coupling agent and 4-dimethylaminopyridine (DMAP) as a catalyst. The reaction takes place at room temperature and under anhydrous conditions for 48 hours. A summary of the reaction is shown in Figure 5.10.

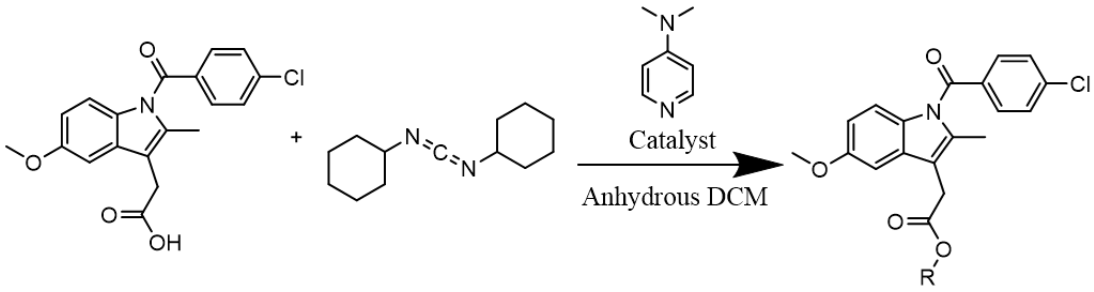

Figure 5.10: Summary of the Steglich esterification process. The R group represented on the product varies dependent on the alkyl chain lengths. R represents ethyl, propyl, nbutyl, hexyl, dodecyl, stearyl, tbutyl and benzyl ester analogues.

The reaction mechanism is displayed in Figure 5.11.

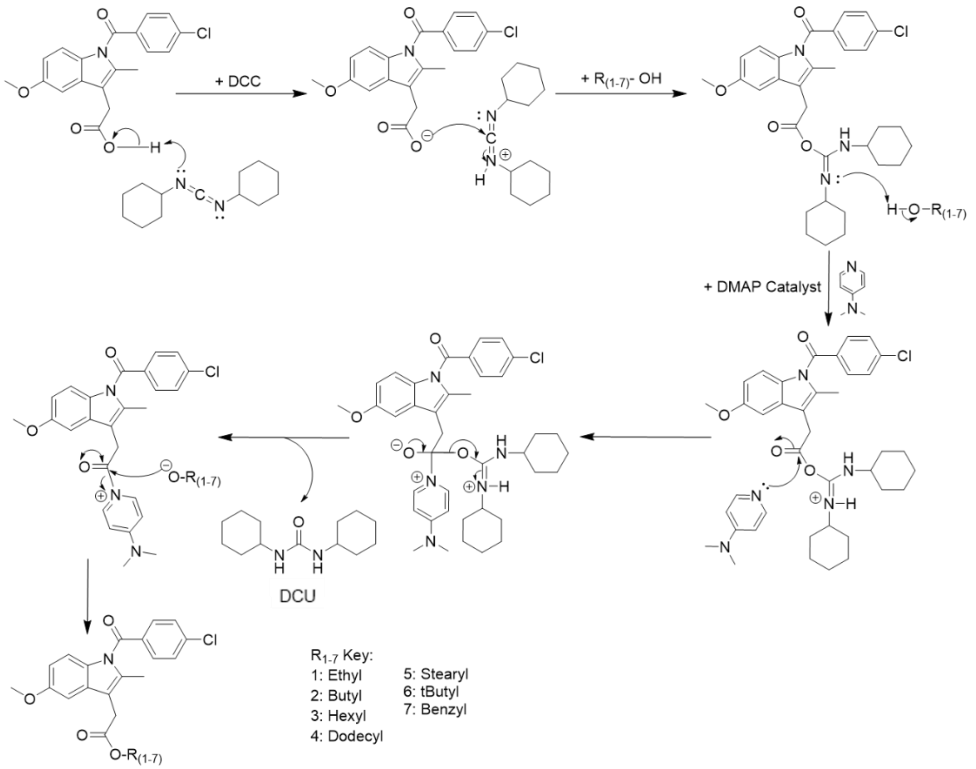

Figure 5.11: Steglich esterification reaction mechanism for the formation of IND analogues 1-7. The reaction occurs in anhydrous conditions over 48 hours.

The Steglich esterification mechanism is initiated through the addition of DCC to IND, which forms an *O*-acylisourea intermediate, which has a comparable reactivity to a corresponding deprotonated carboxylic acid ($R\text{-}COO^-$) functionality.[21] The consequent addition of the alcohol ($R_{1\text{-}7}$), allows protonation of the urea functionality which consequently is expelled as a DCU by-product upon the addition of the DMAP catalyst. [21] As the DMAP is a stronger nucleophile than the corresponding alcohol species ($R_{(1\text{-}7)}O^-$), the addition of the DMAP species renders an activated amide. The $R_{(1\text{-}7)}O^-$ nucleophile can then rapidly add to this activated amide species to successfully form the desired esterified product. The synthesis of all seven IND analogues *via* the Steglich esterification were successful without complications. Upon the completion of the reaction, the removal of DCU was required. The DCU mainly crashes out of solution as a white powder that can be filtered off. Nevertheless, as the DCU species is partially soluble in the DCM solvent the second step of purification requires the DCM to be removed *in vacuo* and the crude material is resuspended in cold EtOAc to remove any additional DCU. The crude mixtures where further purified through flash column chromatography and were characterised by ^1H and ^{13}C nuclear magnetic resonance (NMR), mass spectrometry, elemental analysis and infrared (IR) spectroscopy. For further experimental details see Chapter 7, section 7.3.4.2.

5.2.5 Characterisation of hydrophobic analogues

The characterisation of all analogues were in agreement with the desired products. The analysis of the ethyl IND ester is thoroughly discussed in this section. The elemental analysis of the ethyl IND analogue and the molecular ion peak identified is shown in Table 5.1. All additional elemental analysis and mass spectrometry spectrums are shown in the Appendix Table A1 and Appendix Figure A3 to A9 respectively.

Table 5.2: Elemental analysis and mass spectrometry data for the molecular ions of the indomethacin ethyl analogue.

Indomethacin analogue	C (%)	H (%)	N (%)	Molecular ion (m/z) ($M^+ + Na^+$)
Ethyl	65.37	5.22	3.53	408
Expected	65.38	5.25	3.63	408

The ^{1}H NMR spectra of the ethyl ester analogue is given as an example spectra below. All subsequent analogues are all shown in the Appendix at the end of this chapter.

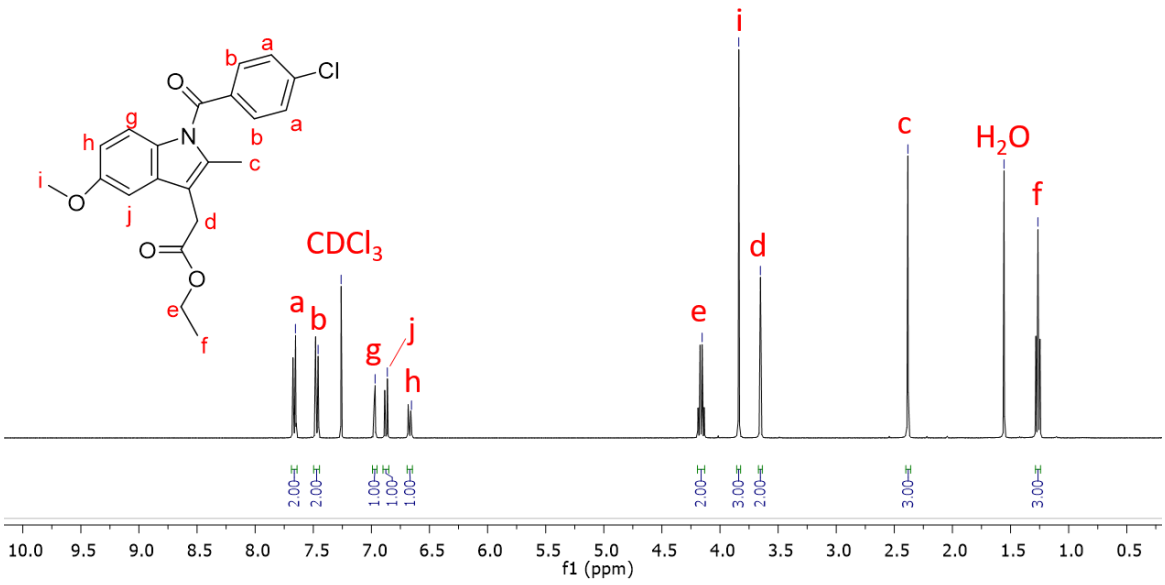

Figure 5.12: ^{1}H NMR ($CDCl_3$, 400 MHz) spectrum for the IND ethyl ester.

The ^{1}H NMR spectra shows that there was an increase in the number of hydrogen environments in comparison to IND (^{1}H NMR, Appendix Figure A10). This can be attributed to the successful addition of the ethyl group which gives rise to the quartet at 4.15 ppm and the triplet at 1.26 ppm. These additional peaks corresponds to environments e and f, respectively. There were 19 ^{13}C environments identified as expected shown below in Figure 5.13. The ^{13}C NMR for alternate analogues are shown in the appendix.

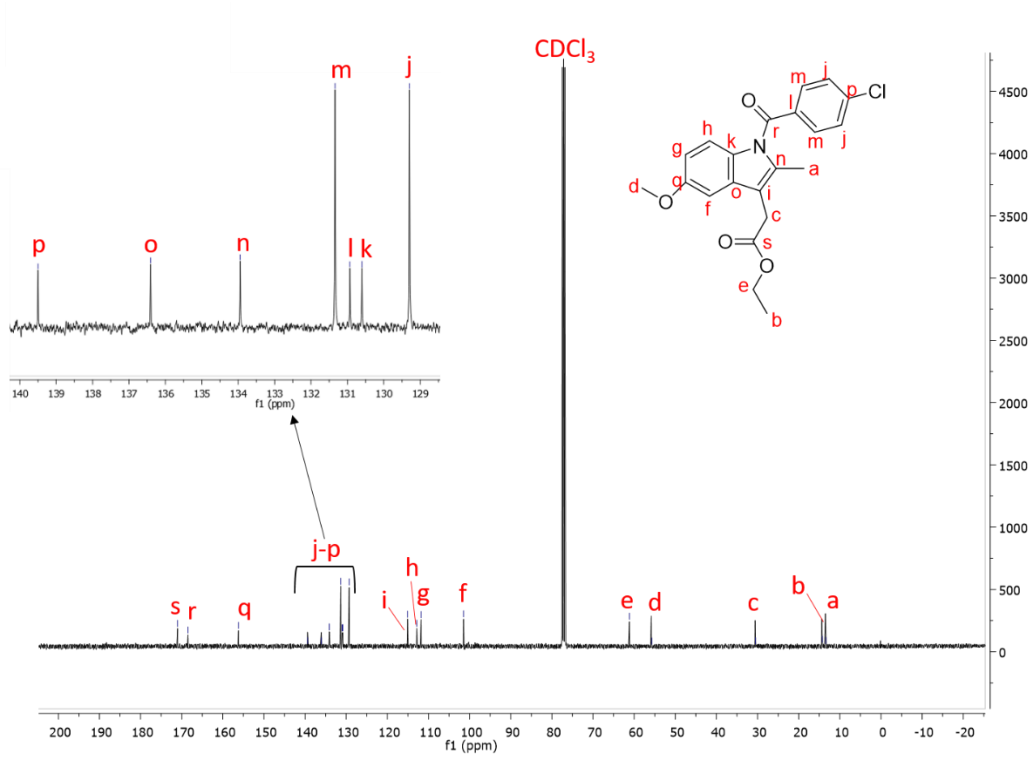

Figure 5.13: ^{13}C NMR ($CDCl_3$, 400 MHz) spectrum for the IND ethyl ester.

The IR spectra showed significant peaks at 1726 cm^{-1} (C=O stretch, ester), 1673 cm^{-1} (C=O stretch, amide), and several peaks between 2836-3107 cm^{-1} (aromatic and non-aromatic C-H stretches). The IR spectra is shown in Figure 5.14.

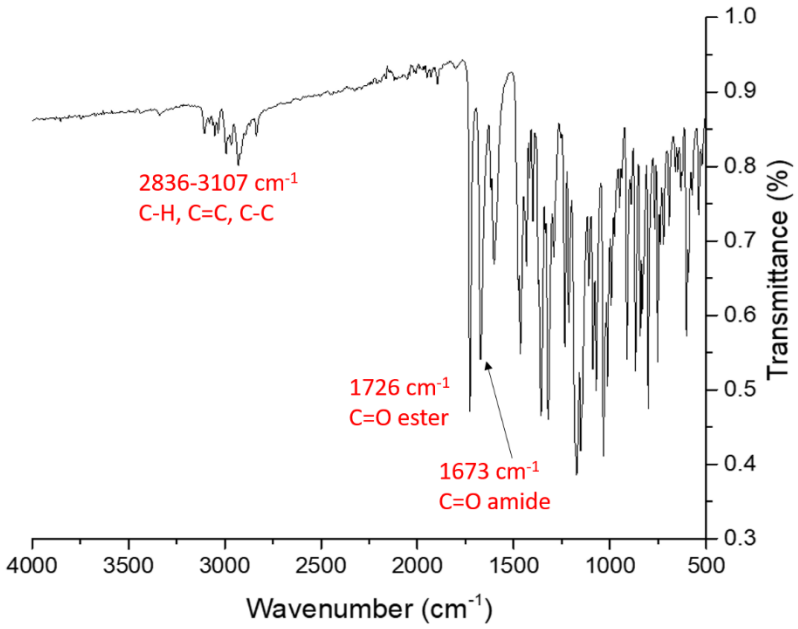

Figure 5.14: IR spectra of the IND ethyl ester showing significant carbonyl stretches at 1726 (ester) and 1673 cm^{-1} (amide).

All IR spectrums for subsequent analogues are shown in the appendix. All seven esterified analogues of IND were screened for HIT samples *via* the ETFD approach. The results are discussed in the following section.

5.2.6 Screening hydrophobic analogues

The initial screening process of the IND analogues was standardised at 30wt% loading. However, an important point to note was that the increasing chain length, decreased the molar wt% of the drug as shown in Figure 5.15. For example, 30 wt% of the stearyl ester as the highest molecular weight (MW) analogue equates to 58 mole% of active IND in the initial screen, translating to 17.5 wt% of active therapeutic IND.

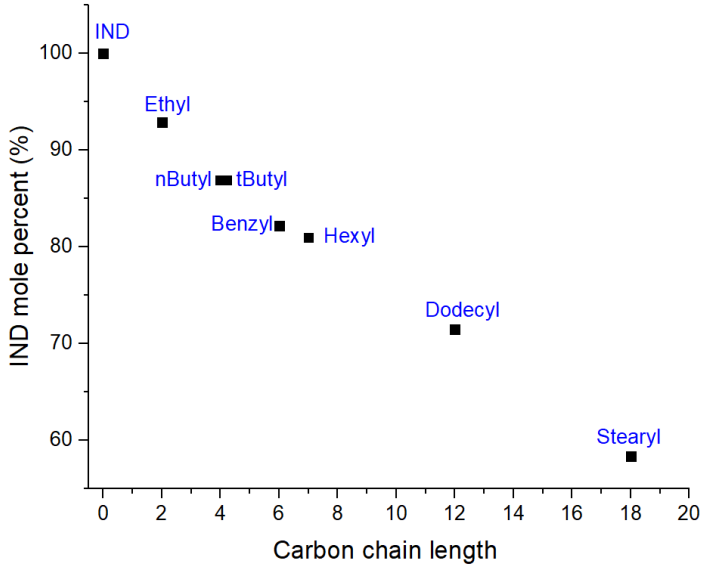

Figure 5.15: A graphical representation of the molar wt% of active IND within each IND analogue.

Although the reduction in the mole% of the active ingredient was a fundamental factor to be aware of, the range of the consequent drug loadings where higher than many pre-existing, polymer-based IND nanoformulations. For example, successful studies from Andonova *et al.* have showed a 1 w/v % IND in 10 w/v % PVA scaffolds, translating to a total drug loading of 10 wt% IND.[22]

To test the SDN formulations of the different IND analogues all samples where redispersed in phosphate buffer saline (PBS) solution at 1 mg/mL active, unless stated otherwise in any of the consequent sections. Unfortunately, the initial screening process of 30 wt% of the IND analogues revealed that the SDN formulations of the ethyl ester were unsuccessful. All ethyl ester dispersions where characterised with a large $D_{z,}$ high dispersity and notably broad intensity traces, with no evident HITs to provide grounds for continuation (Appendix Figure A 31). Interestingly, the relationship between the increasing LogP of the samples showed a positive relationship with the increasing number of HITs as shown in Figure 5.16, as the carbon chain length increased from C_4 (n-Butyl) through to C_{12} (dodecyl). This suggested that the increasing hydrophobicity of the esterified IND molecule increased the loading capacity of the molecules within the SDN formulation. However, the most hydrophobic analogue, the stearyl ester (LogP= 11.04) failed to successfully form any HITs from the ETFD process.

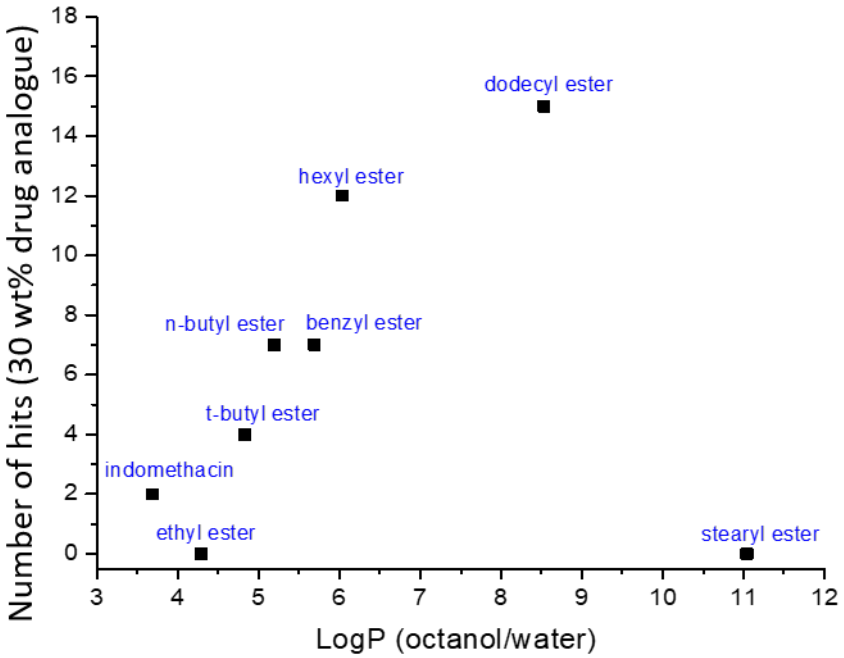

Figure 5.16: Graphical representation of the number of HITs achieved for each IND-ester at 30 wt% loading.

The relationship between the increasing LogP and the increased number of HITs of the remaining esterified IND samples was hypothesised to be as a result of increasing amphiphilic character. For example, the increase in alkyl chain length, thus an increase in overall

hydrophobicity also increases the polarity of the molecule. The consequent increase in amphiphilic character, enables stronger hydrophobic interactions between the ester's alkyl chains and the stabilising polymer or surfactant. This same trend was demonstrated by Tóth *et al.* whereby 4-hydroxy benzoate as a model drug was esterified with increasing chain lengths of methyl, ethyl, properly, butyl, heptyl and octyl chains. The increase in alkyl chain length, thus an increase in LogP was coupled with an increased encapsulation efficiency of their target molecules in PLGA nanoparticles.[23] This finding was similarly concluded to be as a result of an increased strength of intermolecular interactions allowing the active molecule to be successfully incorporated within the core matrix of the nanoparticles.[23] Further research presented by Saad *et al*. also highlighted that the higher LogP of the active molecules also increases the supersaturation conditions required for nanocrystal nucleation in the aqueous phase, thus further increasing the success of nanoparticle formation.[24] Conversely, the reason for the poor SDN results obtained for the stearyl ester was hypothesised to be as a result of the longer alkyl chain (C_{18}). It was hypothesised that the longer chain may induce aggregation of the particles through causing disruption of the polymer-surfactant scaffold obtained in the ETFD. During the freezing and sublimation of the solvent, the longer alkyl chains on the ester may sterically prevent the successful adsorption of the excipients on to the stearyl ester drug crystals, thus forming aggregated hydrophobic material that was unable to be reconstituted. The properties of the polymer-surfactant scaffold formed is of fundamental importance to the redispersion ability of the monolith and therefore the stearyl ester was discarded from further testing. The data obtained in the ETFD screens at 30 wt% is discussed the section below.

5.2.6.1 Analysis of the screening process for 30 wt% SDNs

As previously stated in the section above, the number of HITs obtained increased with increasing LogP. Upon analysis of the samples, all HIT samples chosen for further analysis all had average D_z <400 nm and PdI values <0.4 when redispersed at 1 mg/mL active. For all samples, the data obtained in the initial ETFD screening of the IND esters is highlighted in Figure 5.17. As shown in the key, the colour of the circles represent average D_z of the samples

after triplicate measurements within the same sample. Green circles represent the smaller populations <250 nm and the orange represent dispersions displaying a D_z between 250-500 nm. The actual D_z obtained is displayed next to each respective circle. The size of the circle represents the PdI value within the dispersions. All samples obtained PdI values less than 0.4.

From the HIT samples identified, there was no evident trend to suggest that a particular one polymer or one surfactant was significantly more successful for SDN formulation. Nevertheless, for hexyl and dodecyl analogues, as the number of HITs increase, similarities of HIT excipients amongst the individual analogues were highlighted. For example, NDC as a surfactant excipient was present in 42 % of HIT samples identified for the hexyl ester. NDC as a stabilising molecule is negatively charged, and therefore provides electronic stability between the coexisting colloids in solution.[25] As a small molecule stabiliser, it is associated with excellent dispersion properties allowing rapid diffusion to the particle surface, thus providing overall enhanced stability.[25] Comparably in similar research, Singla *et al.* incorporated NDC in to Pluronic® P84 to formulate mixed micellar dispersions to enhance the solubilisation of clozapine; a viable antipsychotic drug.[26] This supports the use of NDC in therapeutic drug systems in order to optimise their pharmacokinetic properties. Additionally, there was a 33% HIT rate using TPGS as an alternative surfactant for hexyl ester SDNs. Contrary to NDC, TPGS is a non-ionic amphiphilic surfactant and therefore provides steric stabilisation through the adsorption of the lipophilic tocopheryl group.

Conversely for the dodecyl ester, there seemed to be a dependence on the polymer used rather than the surfactant, with 10/15 HITs containing either HPMC or PVA as polymeric stabilisers. From the literature it is apparent that HPMC or PVA are commonly implemented as stabilising polymers for nanoparticles. For example, recent work by Ibrahim *et al*. has showed the use of HPMC is able to influence the cytotoxicity and release profiles of docetaxel as a chemotherapeutic agent.[25] It is unknown whether there was a trend in the dependency of the excipients used or whether there success of the SDN HITs was randomised. In order to confirm this further investigation would have to be carried out.

Figure 5.17: Illustration to show the data obtained from the initial ETFD screen of IND ester analogues: (i) Benzyl, (ii) tButyl, (iii) nButyl (iv) Hexyl and (v) Dodecyl. The HIT samples are shown in the boxes representing the successful binary combinations. The colour of the circle represents the average D_z obtained after triplicate measurements of the same sample and the PdI represents the dispersity within the sample, as demonstrated by the key.

Figure 5.17 highlighted that all HIT samples met the initial arbitrary data quality threshold, (D_z <400 nm and PdI values <0.4), and therefore considered appropriate for continuation the next step was to assess reproducibility. The reproducibility of the esters was assessed across individual triplicate samples and is discussed in the following section.

5.2.7 Reproducibility of SDN formulations

All HIT samples were tested in triplicate to identify reproducibility in formulation, reconstitution and characterisation. In order to narrow down the number of the samples identified as HITs, the HIT criteria was stricter so all samples had a D_z = <350 ± 50 nm, PdI= ≤0.3 ± 0.1. The reproducibility of the remaining samples is shown in Figure 5.18. Interestingly, although the hexyl and dodecyl esters originally had the highest numbers of successful HITs in the initial screen, only four of the samples for the hexyl ester and three of the samples for the dodecyl ester provided consecutively reproducible results with a small D_z and low polydispersity. For this reason, a select few binary combinations were considered for further development and are shown in Figure 5.18.

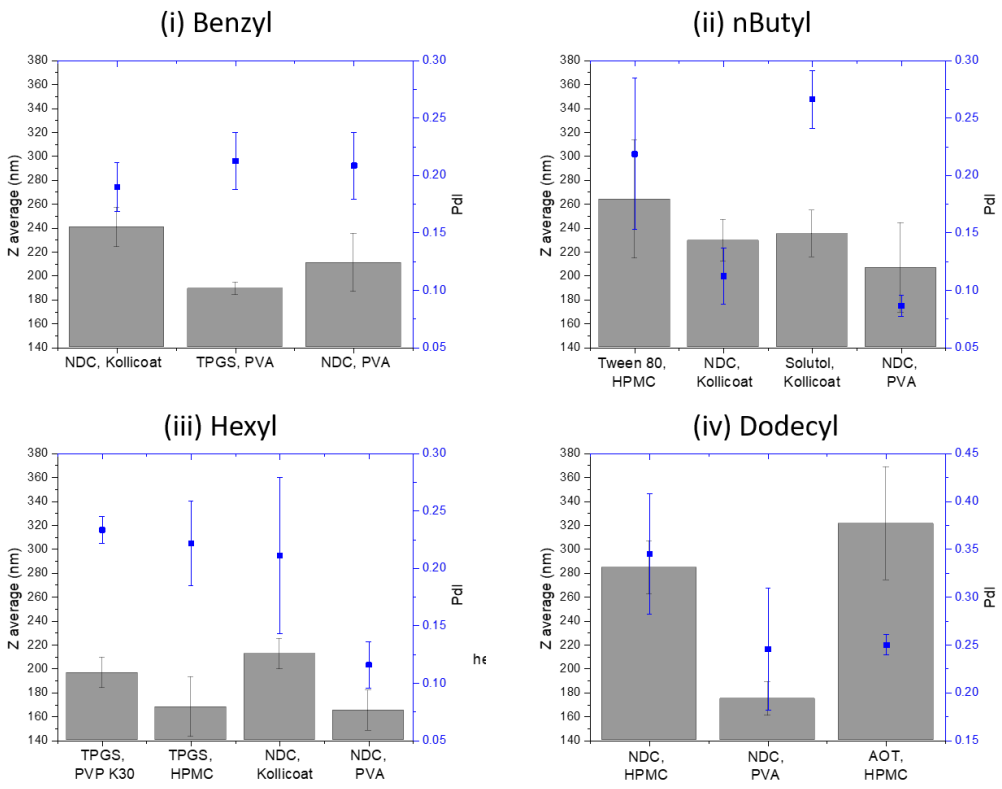

Figure 5.18: The reproducibility of successful HIT samples are graphically represented for the following IND analogues: (i) benzyl ester, (ii) nButyl ester, (iii) hexyl ester) and (iv) dodecyl ester.

A key point demonstrated in Figure 5.18 is that all four esters have a mutual binary combination of NDC and PVA that was successful for all individual analogues. Consequently, the four formulations each containing NDC and PVA out of the total 14 SDN samples were taken forward for comparison. The DLS traces for the individual triplicate samples were averaged and compared as shown in Figure 5.19. As graphically represented, there was evidence of some larger aggregates in the benzyl and dodecyl samples, suggested by the secondary peak at >1 μm. Nevertheless, there was no visual evidence of aggregates or solid material within the dispersions.

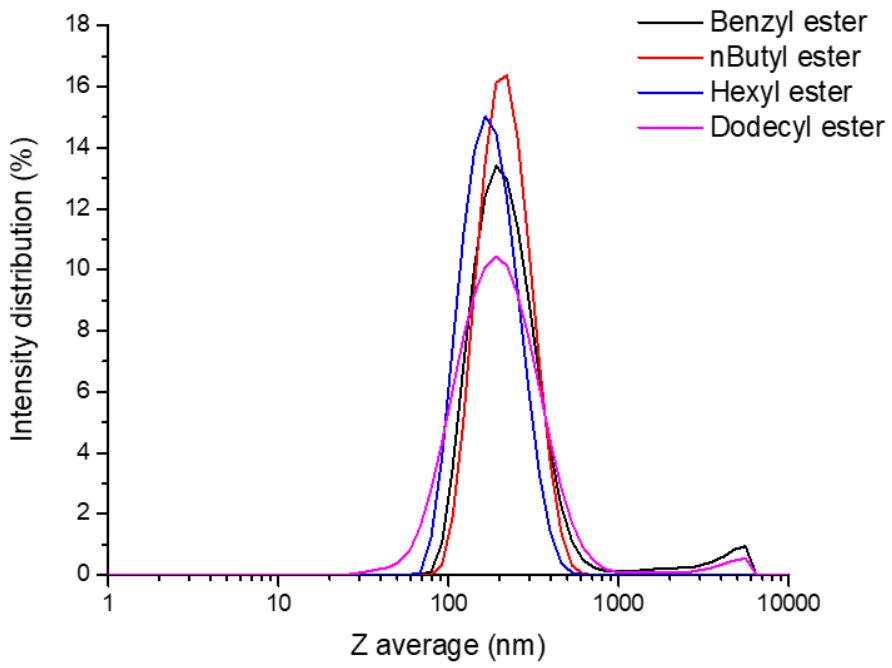

Figure 5.19: DLS traces for the benzyl, nButyl, hexyl and dodecyl IND esters containing NDC and PVA as the polymer and surfactant excipients for 30 wt% SDNs.

As a result, this binary combination for each IND ester analogue was taken forward for stability testing. This is discussed in the following section.

5.2.8 PVA: NDC stability

5.2.8.1 Dispersion stability

SDNs are often subject to short time-dependent stability, however it is necessary that the dispersions stay colloidally stable to allow reconstitution, administration and a substantial circulation time of the colloidal SDNs. The threshold requirements for stability are therefore dependent on the administration route and the therapeutic dosage requirements. With respect to IND guidelines for IV administration, IND is injected every 6 hours for a maximum of 48 hours.[27] For this reason, a time scale of 6 hours was set as the minimum time required for stability for this stability study in order to allow for administration time, systemic circulation and appropriate uterine accumulation. For this reason, the nButyl, hexyl, dodecyl and benzyl analogues were reconstituted and tested for the time dependent stability. Interestingly, after the samples where left for <6 hours, there was a clear sedimentation of nButyl analogue SDNs highlighted by the blue box shown in Figure 5.20 ii.

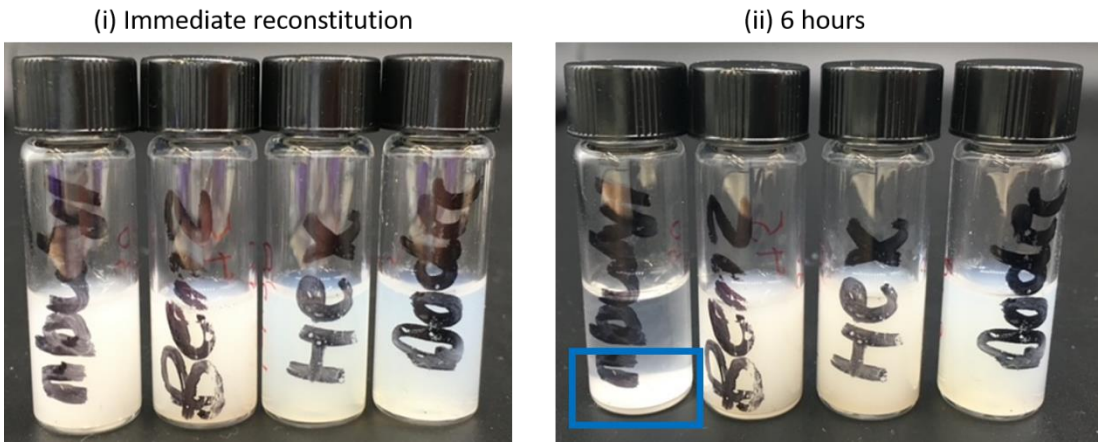

Figure 5.20: Pictorial representation of the 30wt% SDN samples after (i) immediate reconstitution when redispersed at 1 mg/mL active in PBS (0.01 M) and (ii) after 6 hours of reconstitution. The blue box highlights the sedimented solid seen with 30 wt% nButyl-IND SDNs.

The subsequent benzyl, hexyl, and dodecyl analogues were left overnight and the DLS analysis was compared after 24 hours. The benzyl analogue destabilised overnight, supported by the presence of complete sedimentation of solid material and transparent solution. The hexyl and dodecyl analogue samples remained visually stable, with negligible difference after 24 hours in D_z or PdI as shown in Figure 5.21.

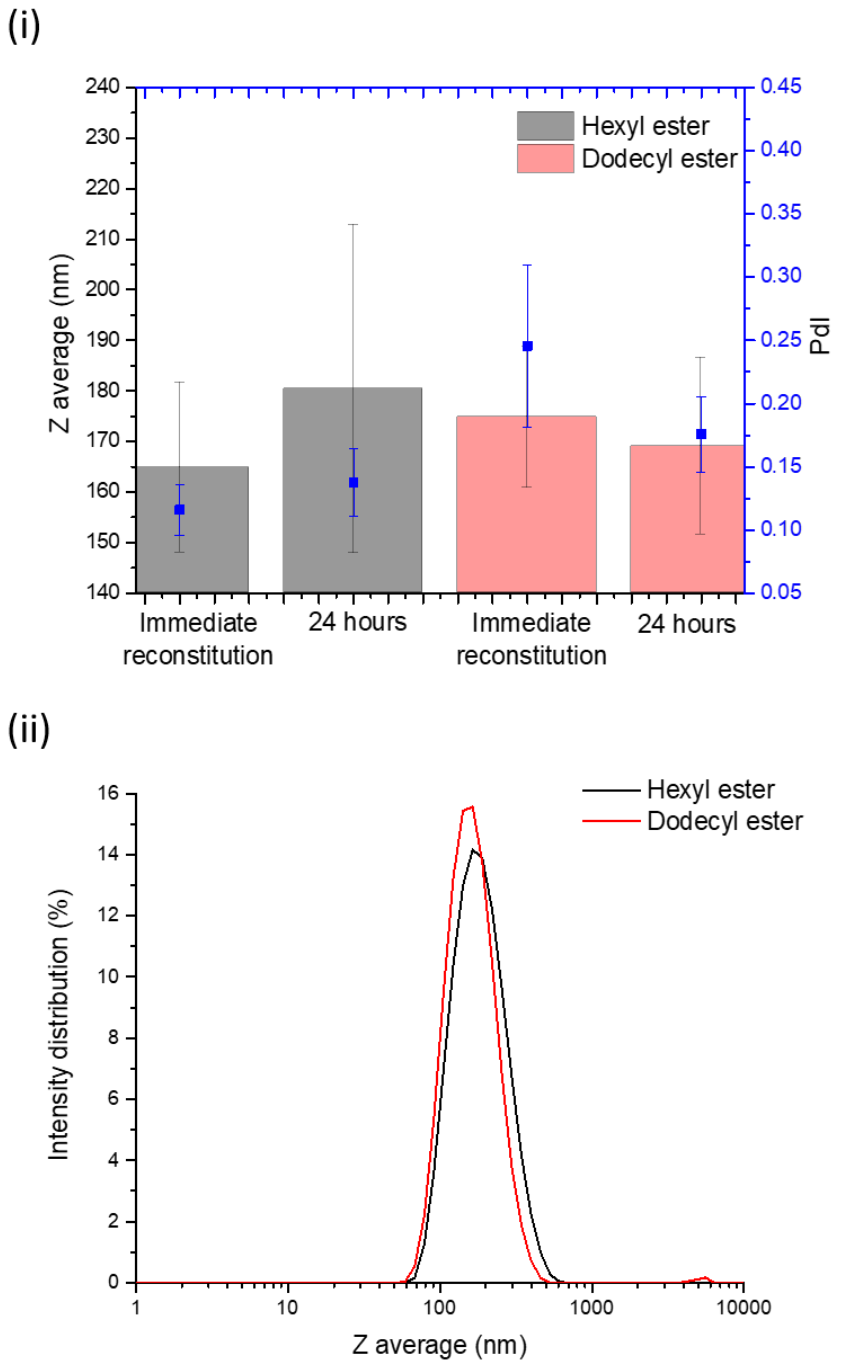

Figure 5.21: 24 hour stability of hexyl and dodecyl ester analogues of IND. (i) Graphical representation of the comparable D_z for the hexyl analogue (165 ± 17 nm , 24 hours= 180 ± 32 nm) and the dodecyl analogue (175 ± 14, 24 hours= 169 ± 17 nm). All samples maintained a PdI value ≤ 0.25. (ii) DLS size intensity distributions of the hexyl ester and the dodecyl ester analogues 24 hours after reconstitution.

Figure 5.21 i indicates that the hexyl analogue and dodecyl analogues have comparable D_z values with respect to the samples after immediate reconstitution. The hexyl analogue D_z averages were 0 hours= 165 ± 17 nm and 24 hours = 180 ± 32 nm, comparably to the dodecyl analogues at 0 hours= 175 ± 14 and 24 hours= 169 ± 17 nm. All samples maintained

uniformity within the dispersions as emphasised by narrow PdI values (≤ 0.25) and monomodal traces shown in Figure 5.21 ii. The storage stability of the monoliths is discussed in the following section.

5.2.8.2 Storage stability

The storage stability of each of the monoliths after freeze drying was assessed. The samples after freeze drying where kept in a desiccator prior to reconstitution in PBS solution (0.01 M). The hexyl and dodecyl IND ester SDN samples were analysed in triplicate after six weeks storage and immediately assessed by DLS. The hexyl- IND ester analogue at 30wt% maintained stability after six weeks displaying a D_z of 180 nm, PdI= 0.09. Conversely, DLS analysis of the dodecyl-IND analysis suggested the presence of larger sedimenting particles. This suggests that the dodecyl IND analogue was subject to destabilisation of the particle upon storage. This may be attributed to the increased logP of the dodecyl analogue enabling increased hydrophobic interactions between the particles in the monolith. This is also coupled with visual shrinking of the monolith over time from a homogeneous cake structure post lyophilisation, often due to the absorption of water. For this reason, the dodecyl analogue using the PVA: NDC binary combination was discarded from further analysis. Conversely, the successfully reconstituted hexyl analogue was assessed for dispersion stability after six weeks storage, with DLS measurements every 15 minutes for 7.5 hours and a final measurement after exactly 24 hours (Figure 5.22).

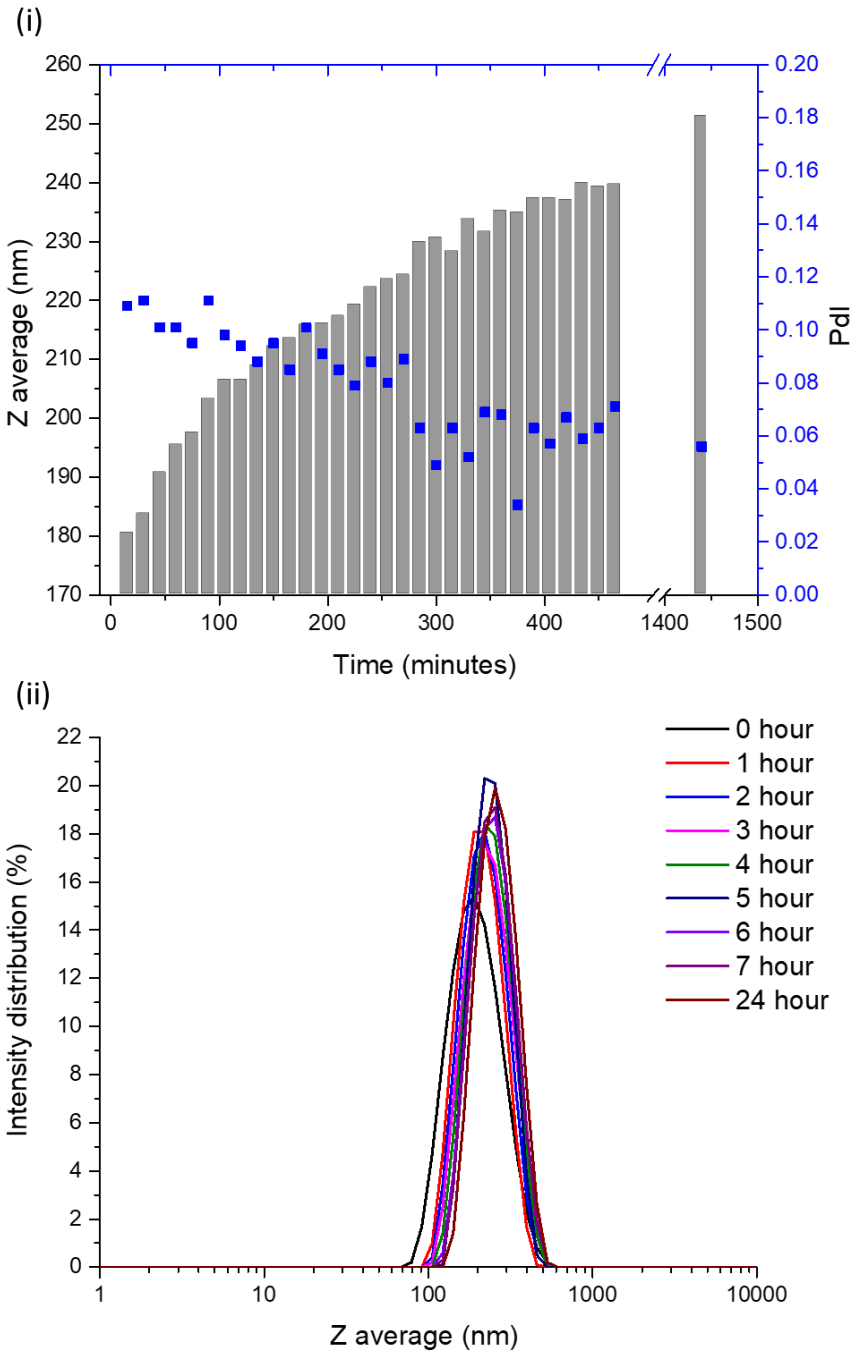

Figure 5.22: 24 hour dispersion stability of the hexyl ester analogue at 30wt% loading into PVA: NDC SDNs after six weeks storage. (i) Graphical representation of the change in D_z and PdI over a 24 hour period, assessed by DLS measurements every 15 minutes. (ii) The DLS intensity distribution traces shown hourly after reconstitution and at 24 hours post redispersion. The monolith was reconstituted in PBS (0.01 M)

From the data provided in Figure 5.22 i, it was evident that the D_z increased slightly from 180 nm to 250 nm with for the hexyl analogue SDN dispersions after reconstitution in PBS, with respective PdI values of 0.1 and 0.06. The PdI values across the samples at all-time points are

all narrow suggesting a maintained uniformity of particle distributions over time. The increase in D_z of approximately 70 nm (from 180 to 250 nm) in the hexyl PVA: NDC SDNs over time can be attributed to swelling of the SDNs within the dispersion. This is explained as PBS as a dispersant contains several salts including disodium hydrogen phosphate, sodium chloride, potassium chloride and potassium dihydrogen phosphate. The ionic species in the salts may potentially interfere with NDC as an ionic stabilising species for the SDNs and thus cause swelling and consequent aggregation due to electrostatic interactions. However, importantly there was no visual signs of destabilisation and the DLS traces shown in Figure 5.22 ii show no significant difference in the dispersions after 0 hour or 24 hour. It was therefore concluded that the hexyl analogue using PVA: NDC excipients in SDN formulations were able to maintain storage up to eight weeks with consequent dispersion stability ≥ 24 hours. This finding is of significant importance as the development of 30wt% SDNs containing an IND hexyl ester analogue and therefore 81 molar wt% of IND have been successfully synthesised. As the addition of the ester reduced the molar wt% of the active IND therapeutic from 100 molar wt% to 81 molar wt%, the consequent drug loading of the successful formulation was 24 wt%. This drug loading value is significantly higher per payload than alternative lipid derived formulations explored in Chapter 2 (3 wt% IND) and Chapter 4 (5 wt% IND). In order to compare to the theoretical dosage requirements for IND, 25 mg IV administration of active is necessary to terminate uterine contractility for preterm birth prevention. Therefore, a total IV infusion, assuming a concentration of 1 mg/mL active, would equate to a 25 mL IV requirement. This is also based on the assumption that 100% of the hexyl ester would be cleaved to form the active IND within the required time frame to exert a therapeutic effect. Consequently, from this stage of the investigation's esterase cleavage experiments, release profiles, toxicity and pharmacokinetic testing is required.

5.4 Conclusions and Future Work

Throughout this chapter we have demonstrated that firstly IND as a small molecule was unsuccessful at forming stable IND-SDNs at 30wt%. Nevertheless, this problem was

overcome by synthesising IND ester analogues through the Steglich esterification process to form a range of several analogues with different physical characteristics. It was apparent that an increase in the hydrophobicity of the analogues increased the number of HIT samples achieved. However, strict reproducibly of the samples rendered 14 samples across the benzyl, nButyl, hexyl and dodecyl esters that were suitable for continuation. Nevertheless, it was found that all four suitable esters all contained a HIT sample using PVA: NDC as the polymer: surfactant combination. Consequent stability studies highlighted that nButyl was unstable ≤6 hours, followed by benzyl destabilisation overnight. The hexyl and dodecyl samples remained stable, however the hexyl sample had enhanced storage stability and was successfully reconstituted after eight weeks of storage in a desiccator. For this reason, hexyl ester SDNs containing 24 wt% active IND were considered the most suitable for further continuation for future studies. The following experimental steps would require exploration of the esterase activation to mimic ester cleavage to release the therapeutic IND coupled with release studies and cellular toxicity testing.

5.4.1 Future work: Esterase activation

Preliminary work to assess the activation of the IND analogue back to the active tocolytic IND using porcine liver esterases (PLEs) was carried out for the hexyl ester analogue. PLEs were chosen as they are a class of abundant hydrolase enzymes present *in vivo* with high catalytic efficiency to reform carboxylic acids and amide functionalities.[28] Unfortunately there were difficulties within the experiments due to no identified solvent to maintain a mutual solubility between the PLEs and the hexyl analogues. Solvent systems of PBS: AcCN: H_2O were trialled in several ratios due to the predetermined solubility of IND analogues (> 30 mg/mL) in AcCN: H_2O in an 80:20 ratio. At this solvent ratio the IND analogues remained solubilised, however the PLEs precipitated. Conversely, the only solvent system that the PLEs had a partial solubility in was the 20:80 AcCN:H_2O solvent system which was inadequate for the IND analogues. Future work requires additional solubility tests to be performed to identify a complimentary solvent system for both excipients to carry out the ester cleavage.

5.6 References

1 R. P. Bakshi, L. M. Tatham, A. C. Savage, A. K. Tripathi, G. Mlambo, M. M. Ippolito, E. Nenortas, S. P. Rannard, A. Owen and T. A. Shapiro, *Nat. Commun.*, 2018, **9**, 1–8.

2 A. C. Savage, L. M. Tatham, M. Siccardi, T. Scott, M. Vourvahis, A. Clark, S. P. Rannard and A. Owen, *Eur. J. Pharm. Biopharm.*, 2019, **138**, 30–36.

3 M. Giardiello, N. J. Liptrott, T. O. Mcdonald, D. Moss, M. Siccardi, P. Martin, D. Smith, R. Gurjar, S. P. Rannard and A. Owen, *Nat. Commun.*, 2016, **7**, 1–10.

4 M. Siccardi, P. Martin, D. Smith, P. Curley, T. Mcdonald, M. Giardiello, N. Liptrott, S. Rannard and A. Owen, *J. Interdiscip. Nanomedicine*, 2016, **1**, 110–123.

5 T. O. Mcdonald, M. Giardiello, P. Martin, M. Siccardi, N. J. Liptrott, D. Smith, P. Roberts, P. Curley, A. Schipani, S. H. Khoo, J. Long, A. J. Foster, S. P. Rannard and A. Owen, *Adv. Healthc. Mater.*, 2014, **3**, 400–411.

6 C. Li, J. Wang, Y. Wang, H. Gao, G. Wei, Y. Huang, H. Yu and Y. Gan, *Acta Pharm. Sin. B*, 2019, **9**, 1145–1162.

7 E. Bilgili, M. Rahman, D. Palacios and F. Arevalo, *Adv. Powder Technol.*, 2018, **29**, 2941–2956.

8 J. J. Hobson, A. Al-khouja, P. Curley, D. Meyers, C. Flexner, M. Siccardi, A. Owen, C. F. Meyers and S. P. Rannard, *Nat. Commun.*, 10AD, **1**, DOI: 10.1038/s41467-019-09354-z.

9 U. Wais, A. W. Jackson, Y. Zuo, Y. Xiang, T. He and H. Zhang, *J. Control. Release*, 2016, **222**, 141–150.

10 S. M. Dizaj, Z. Vazifehasl, S. Salatin, K. Adibkia and Y. Javadzadeh, *Res. Pharm. Sci.*, 2015, **10**, 95–108.

11 U.S. Food and Drug Administration Center for Drug Evaluation and Research Inactive

Ingredient Database, http://www.accessdata.fda.gov/scripts/cder/iig/index.cfm., (accessed March 2021).

12 W. F. da Silva Júnior, J. G. de Oliveira Pinheiro, C. D. L. F. A. Moreira, F. J. J. de Souza and Á. A. N. de Lima, *Alternative Technologies to Improve Solubility and Stability of Poorly Water-Soluble Drugs*, Elsevier Inc., 2017.

13 P. KAYAERT and G. VAN DEN MOOTER, *J. Pharm. Sci.*, 2012, **101**, 3916–3923.

14 M. Horáček, D. J. Engels and P. Zijlstra, *Nanoscale*, 2020, **12**, 4128–4136.

15 B. Liu and X. Hu, *Hollow Micro- and Nanomaterials: Synthesis and Applications*, Elsevier Inc., 2019.

16 V. Mandlik, P. R. Bejugam and S. Singh, *Application of Artificial Neural Networks in Modern Drug Discovery*, Elsevier Inc., 2016.

17 B. B. Petković, M. Ognjanović, M. Krstić, V. Stanković, L. Babincev, M. Pergal and D. M. Stanković, *Diam. Relat. Mater.*, 2020, **105**, DOI: 10.1016/j.diamond.2020.107785.

18 J. M. Chan, in *Pharmacology and Physiology for Anesthesia (Second Edition)*, 2019, pp. 70–90.

19 V. Gilles, M. A. Vieira, J. Valdemar Lacerda, E. V. R. Castro, R. B. Santos, E. Orestes, J. W. M. Carneiro and S. J. Greco, *J. Braz. Chem. Soc.*, 2015, **26**, 1–18.

20 C. E. Müller and P. R. Schreiner, *Angew. Chemie - Int. Ed.*, 2011, **50**, 6012–6042.

21 O. C. Portal, Steglich Esterification, https://www.organic-chemistry.org/namedreactions/steglich-esterification.shtm#:~:text=Mechanism of the Steglich Esterification DCC %28dicyclohexylcarbodiimide%29 and,form the stable dicyclohexylurea %28DHU%29 and the ester%3A, (accessed May 2021).

22 V. Y. Andonova, G. S. Georgiev, V. T. Georgieva, N. L. Petrova and M. Kasarova,

Folia Med. (Plovdiv)., 2013, **55**, 76–82.

23 T. Tóth and É. Kiss, *J. Drug Deliv. Sci. Technol.*, 2019, **50**, 42–47.

24 W. S. Saad and R. K. Prud'Homme, *Nano Today*, 2016, **11**, 212–227.

25 M. A. Ibrahim, G. A. Shazly, F. S. Aleanizy, F. Y. Alqahtani and G. M. Elosaily, *Saudi Pharm. J.*, 2019, **27**, 49–55.

26 P. Singla, O. Singh, S. Chabba, V. K. Aswal and R. Kumar, *Spectrochim. Acta Part A Mol. Biomol. Spectrosc.*, 2018, **191**, 143–154.

27 D. M. Haas, T. Benjamin, R. Sawyer and S. K. Quinney, *Int. J. Womens. Health*, 2014, **6**, 343–349.

28 Q. Zhou, Q. Xiao, Y. Zhang, X. Wang, Y. Xiao and D. Shi, *Sci. Rep.*, 2019, **9**, 1–12.

5.7 Appendix

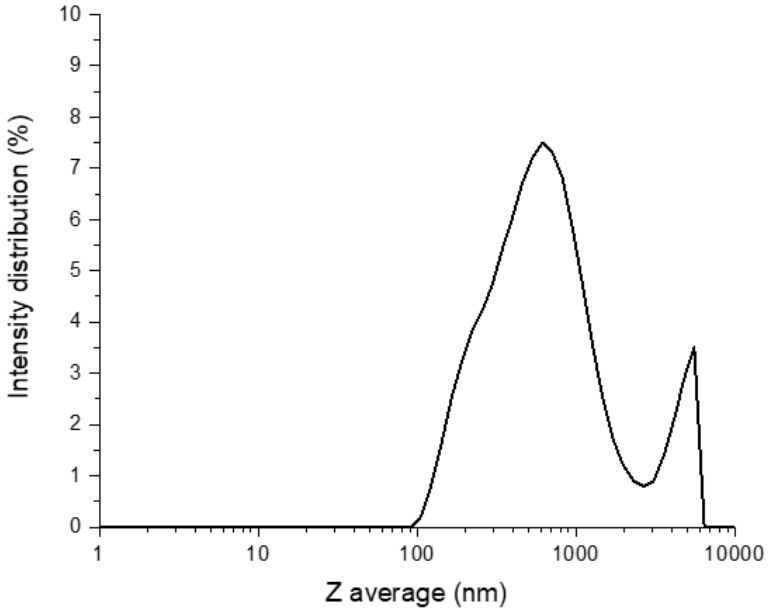

Appendix Figure A 1: Graphical illustration showing the size distribution of the binary combination HPMC: NDC used to form 30wt% IND-SDNs.

Appendix Table A 1:

Indomethacin analogue	C (%)	H (%)	N (%)	Molecular ion (m/z) ($M^+ + Na^+$)
1- Ethyl	65.37	5.22	3.53	408
2- nButyl	66.95	5.88	3.38	436
3- Hexyl	68.29	6.50	3.16	464
4- Dodecyl	71.25	7.68	2.69	548
5- Stearyl	72.69	8.66	2.32	632
6- tButyl	66.73	5.86	3.40	436
7- Benzyl	69.81	4.92	3.12	470

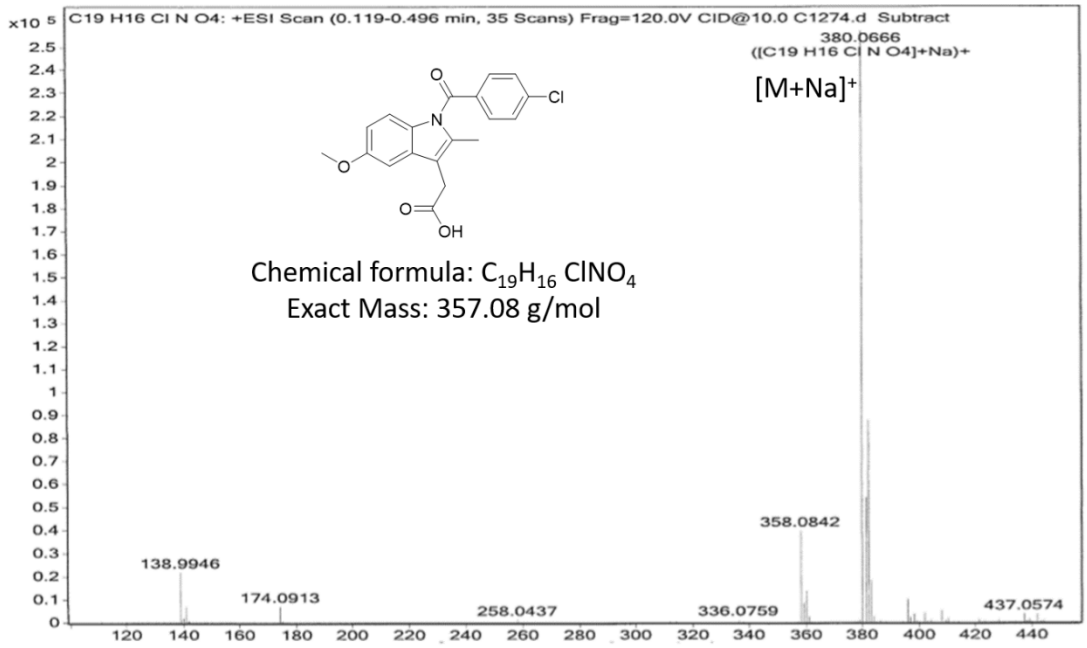

Appendix Figure A2: Mass Spectrometry analysis of IND showing the $[M+Na]^+$ molecular ion peak.

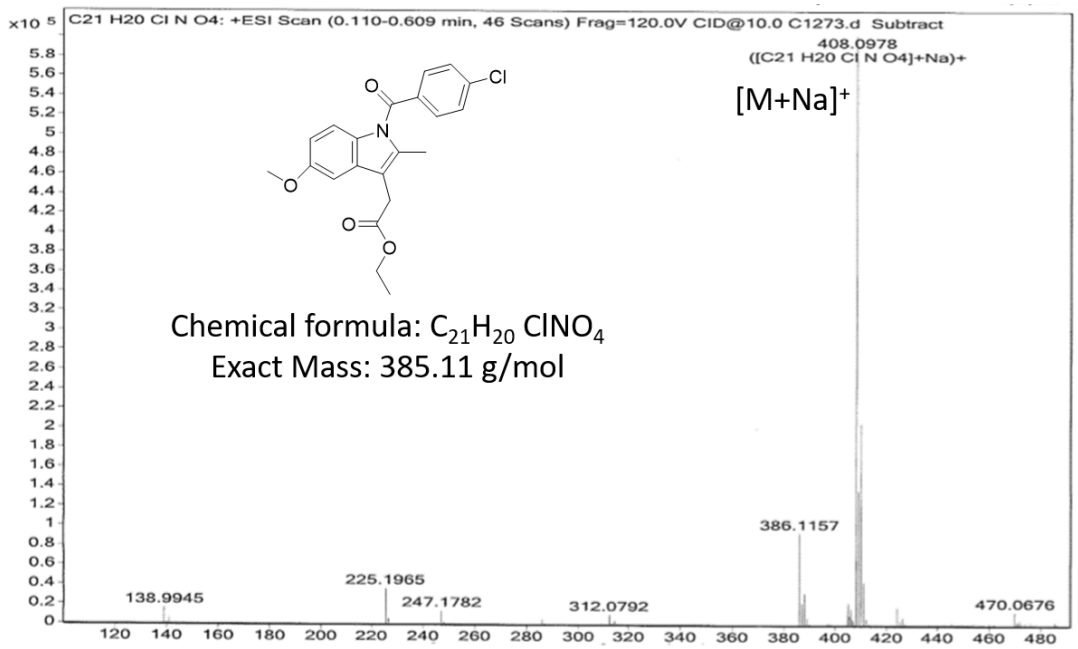

Appendix Figure A3: Mass Spectrometry analysis of IND-ethyl ester showing the $[M+Na]^+$ molecular ion peak.

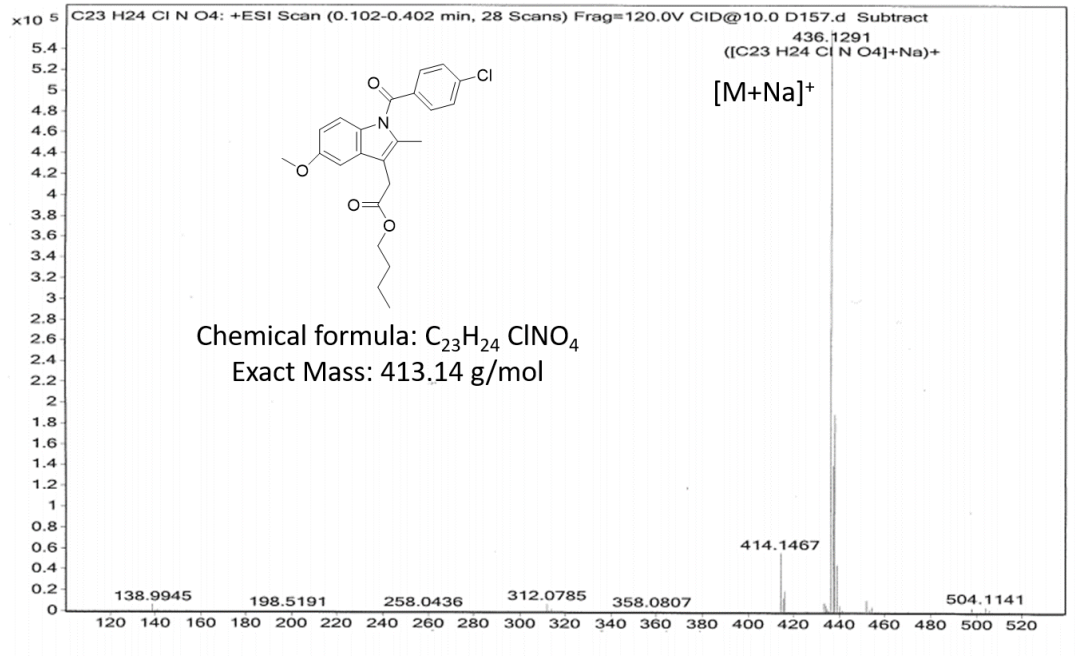

Appendix Figure A4: Mass Spectrometry analysis of IND-butyl ester showing the $[M+Na]^+$ molecular ion peak.

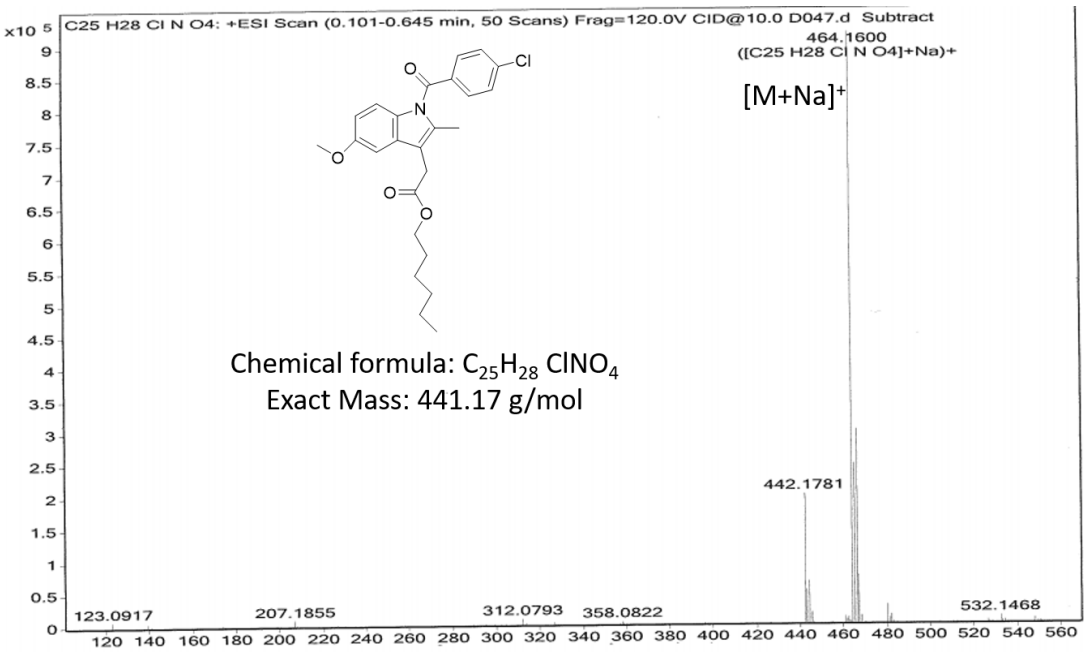

Appendix Figure A 5: Mass Spectrometry analysis of IND-hexyl ester showing the $[M+Na]^+$ molecular ion peak.

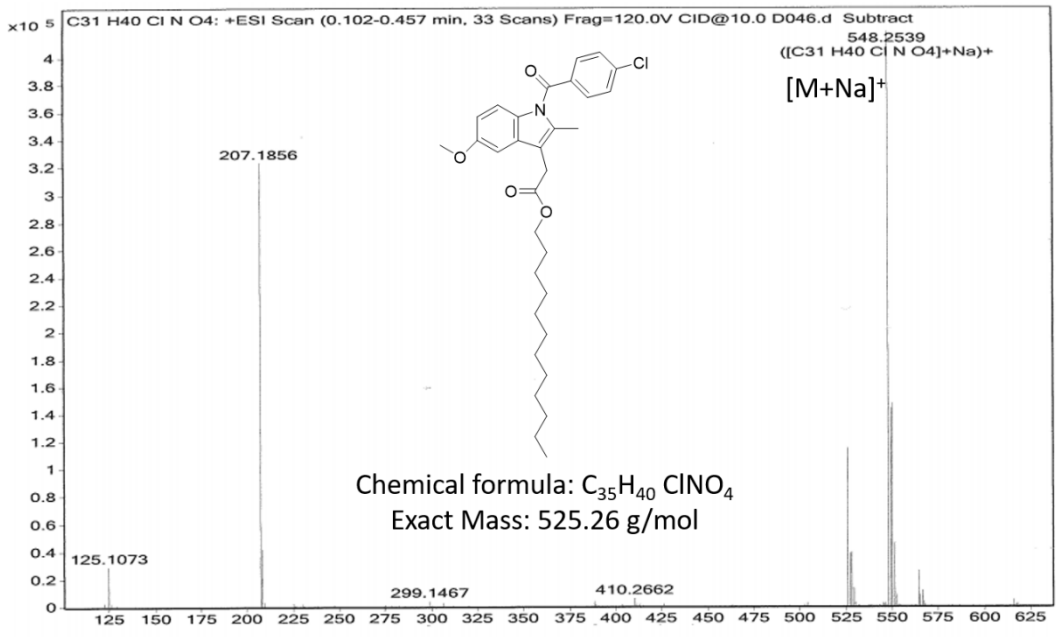

Appendix Figure A 6: Mass Spectrometry analysis of IND-dodecyl ester showing the $[M+Na]^+$ molecular ion peak.

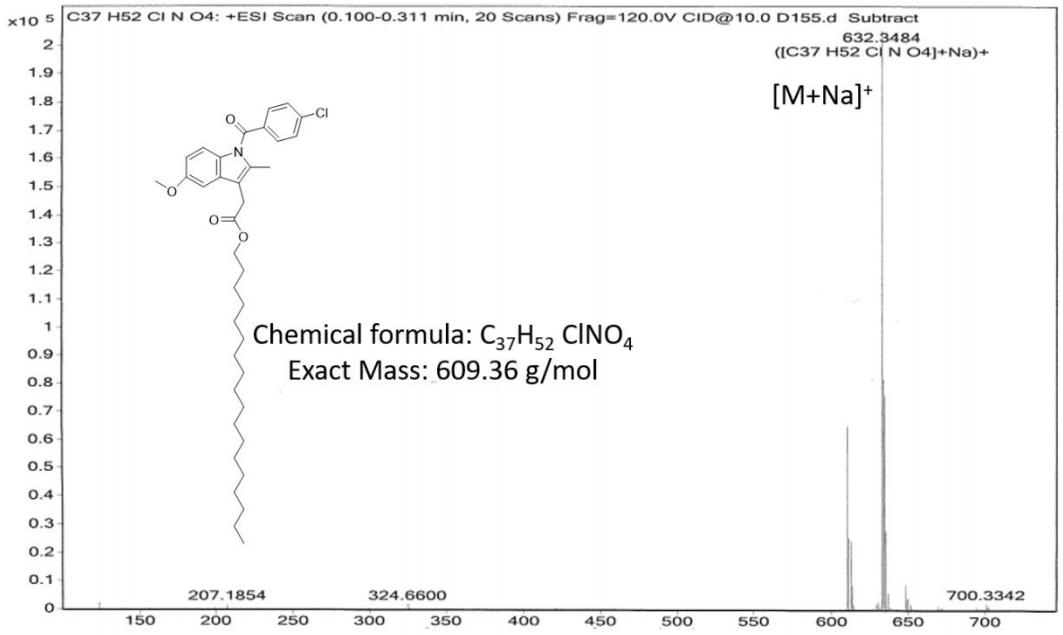

Appendix Figure A 7: Mass Spectrometry analysis of IND-stearyl ester showing the $[M+Na]^+$ molecular ion peak.

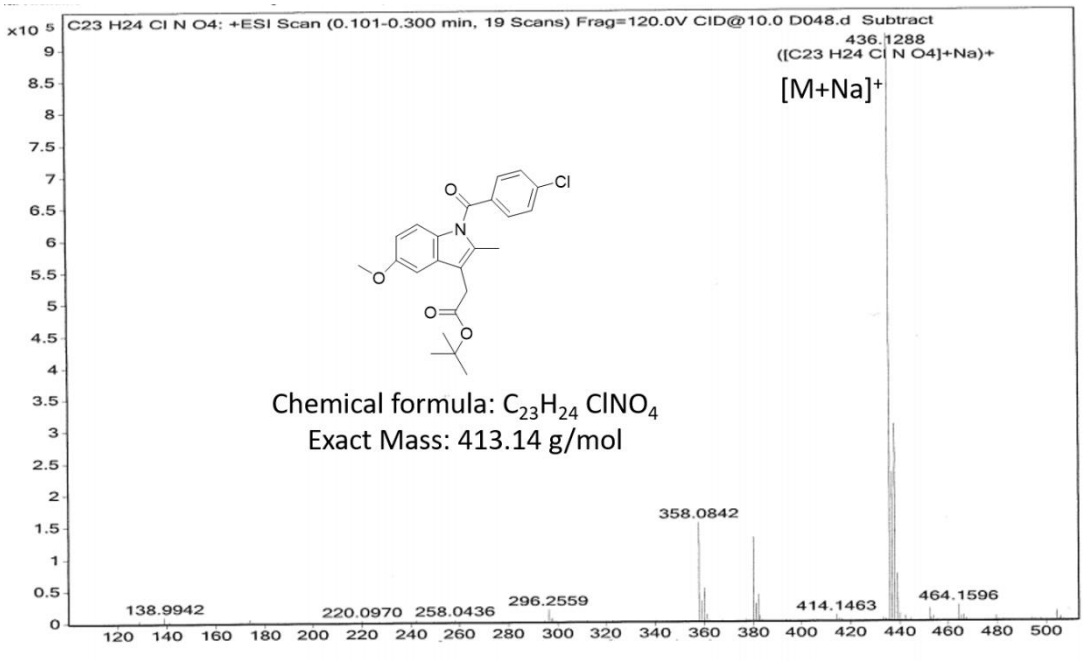

Appendix Figure A 8: Mass Spectrometry analysis of IND-tButyl ester showing the $[M+Na]^+$ molecular ion peak.

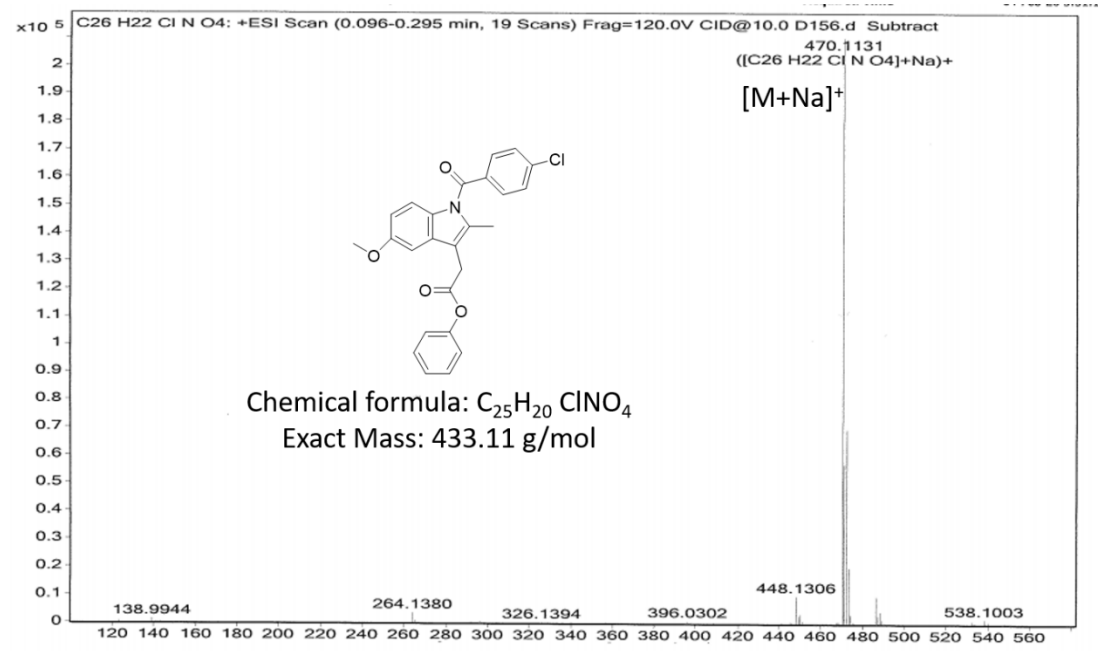

Appendix Figure A 9: Mass Spectrometry analysis of IND-benzyl ester showing the $[M+Na]^+$ molecular ion peak.

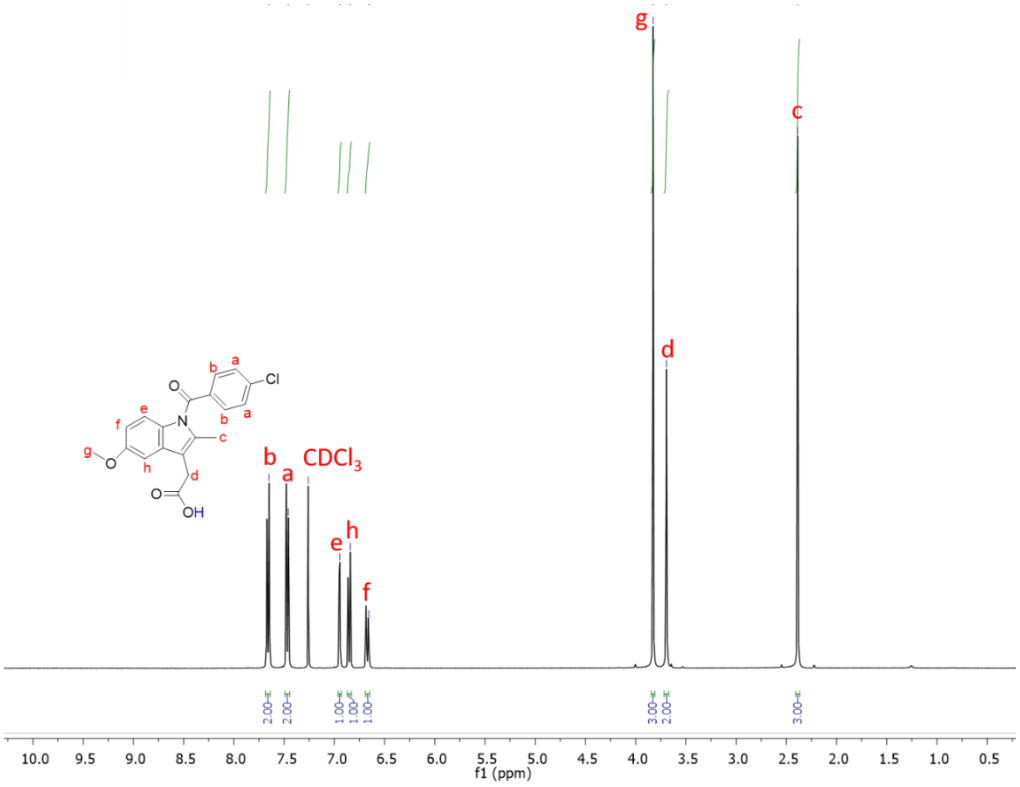

Appendix Figure A 10: ^{1}H NMR of IND. The carboxyl proton highlighted in blue is not present in the spectra due to deuterium exchange with the $CDCl_3$ solvent.

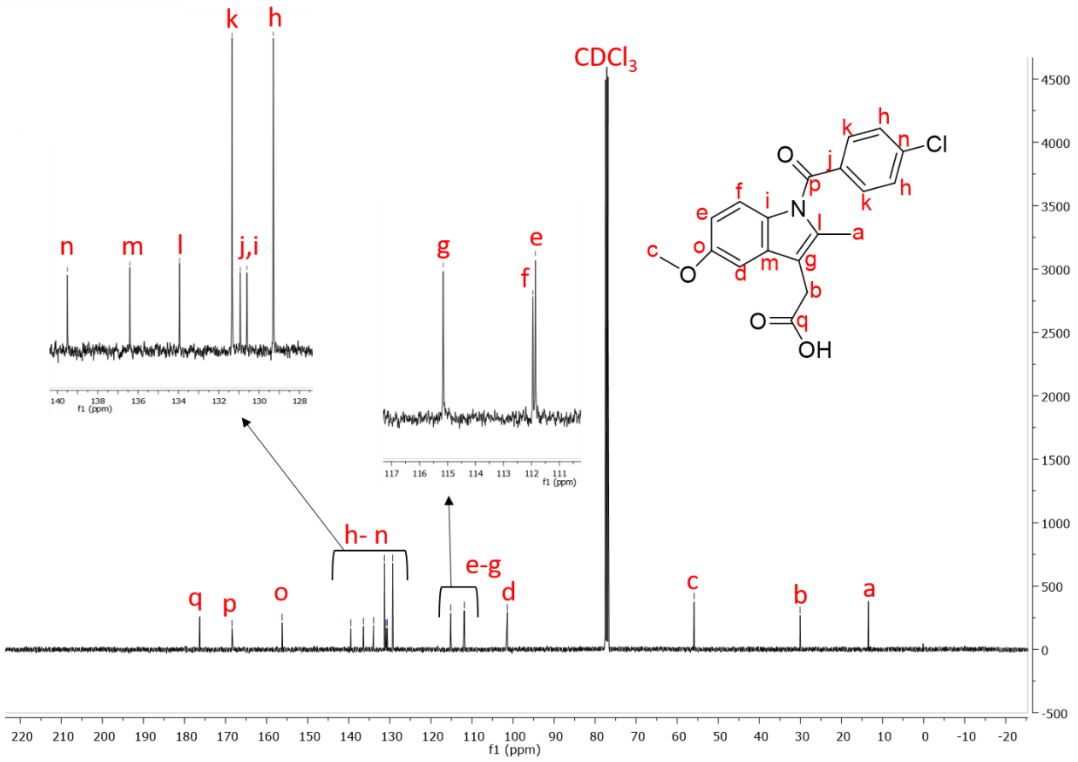

Appendix Figure A 11: ^{13}C NMR ($CDCl_3$, 400 MHz) of IND

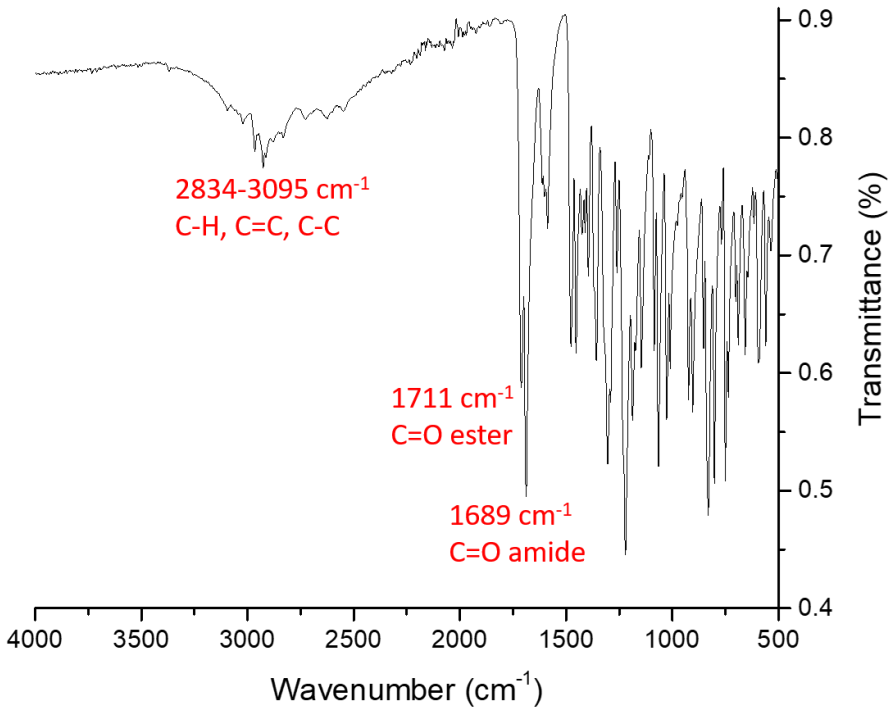

Appendix Figure A 12: IR spectra of IND.

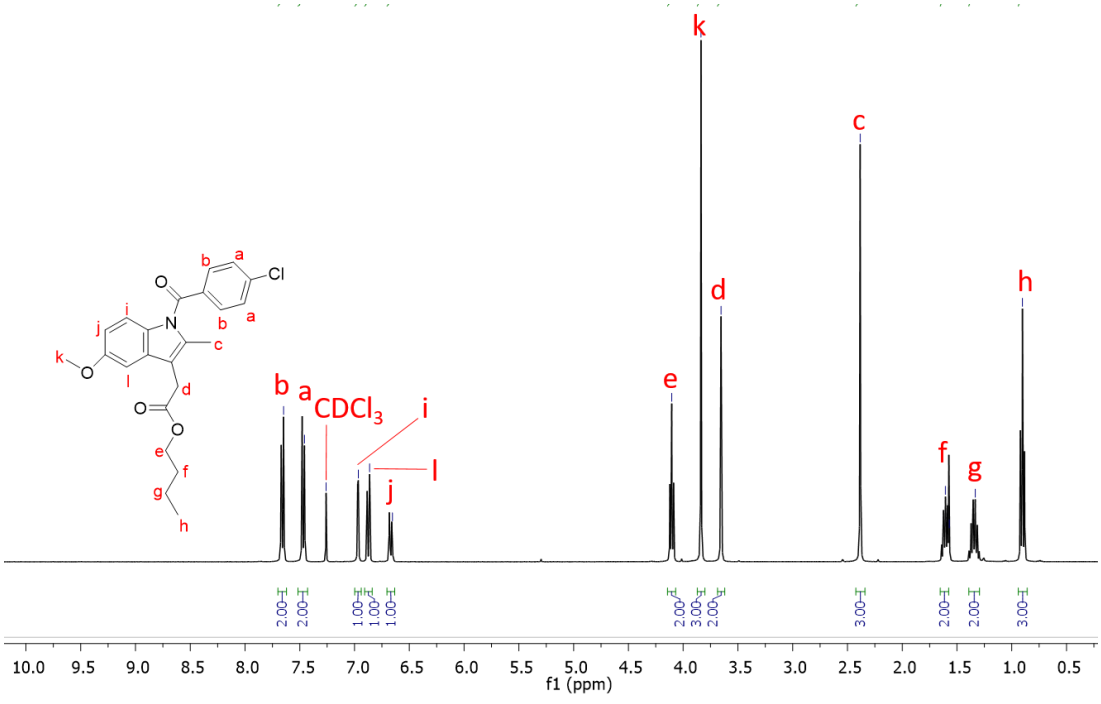

Appendix Figure A 13: ^{1}H NMR ($CDCl_3$, 400 MHz) of IND nButyl ester

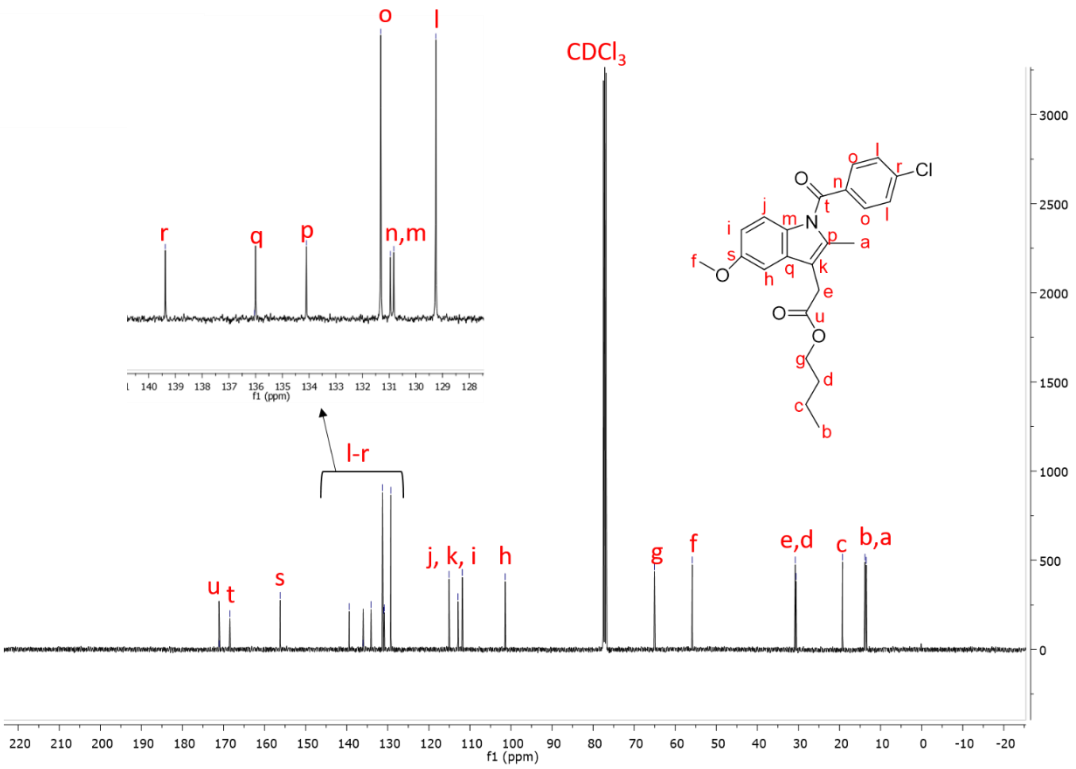

Appendix Figure A 14: ^{13}C NMR ($CDCl_3$, 400 MHz) of IND nButyl ester.

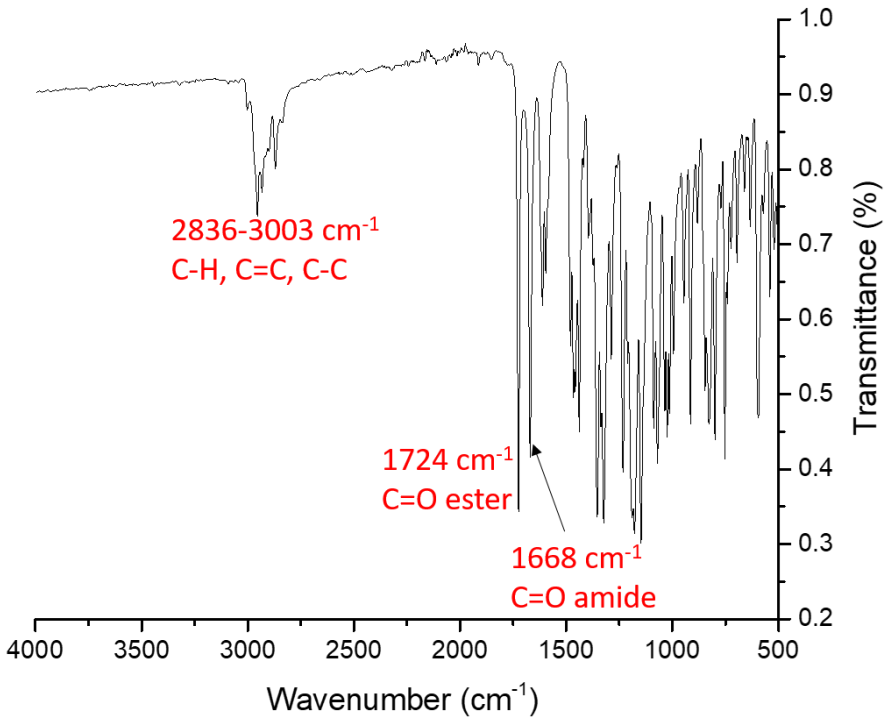

Appendix Figure A 15: IR spectra of IND nButyl ester.

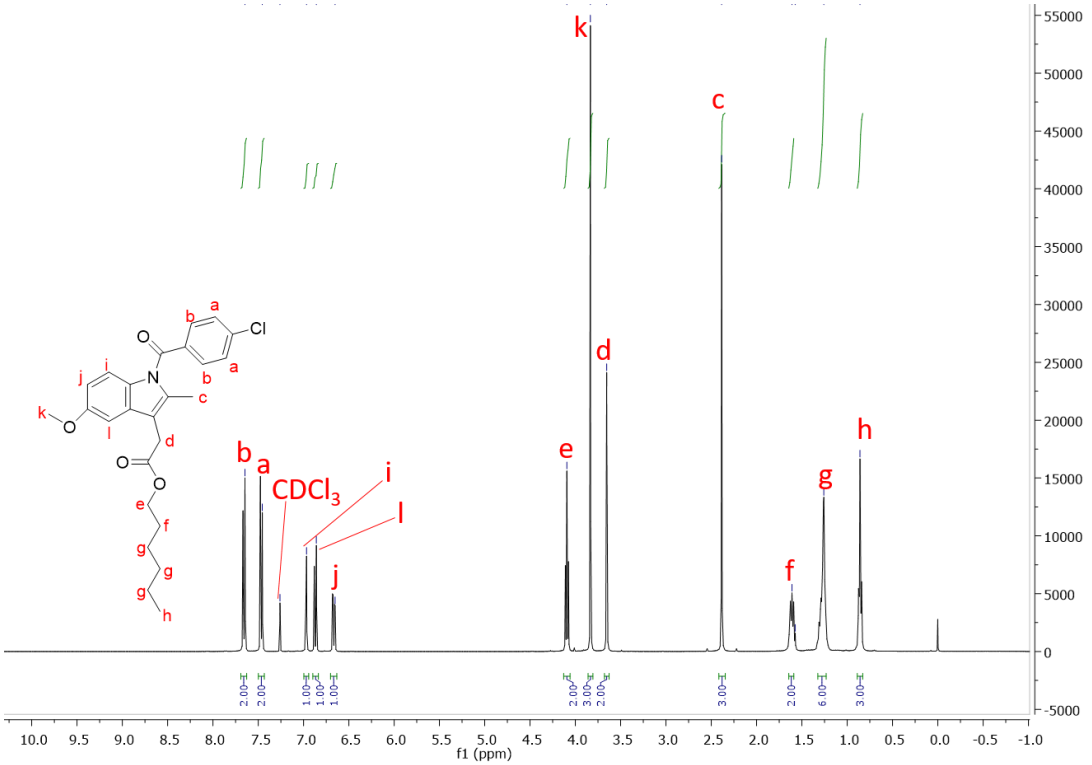

Appendix Figure A 16: ^{1}H NMR ($CDCl_3$, 400 MHz) of IND hexyl ester

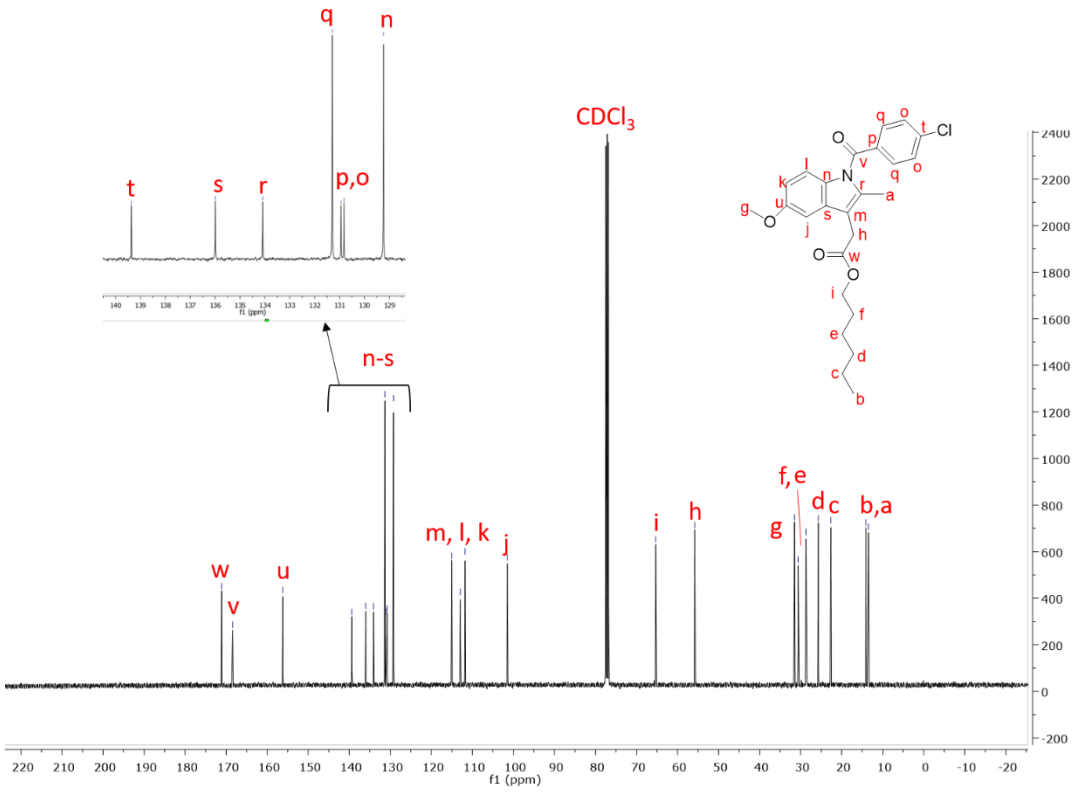

Appendix Figure A 17: ^{13}C NMR ($CDCl_3$, 400 MHz) of IND hexyl ester.

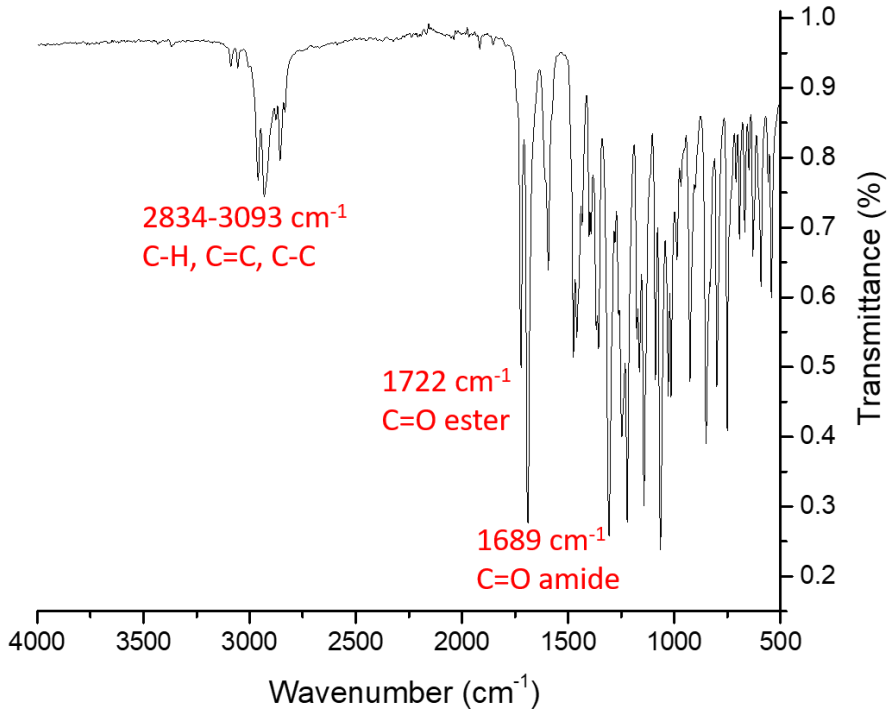

Appendix Figure A 18: IR spectra of IND hexyl ester.

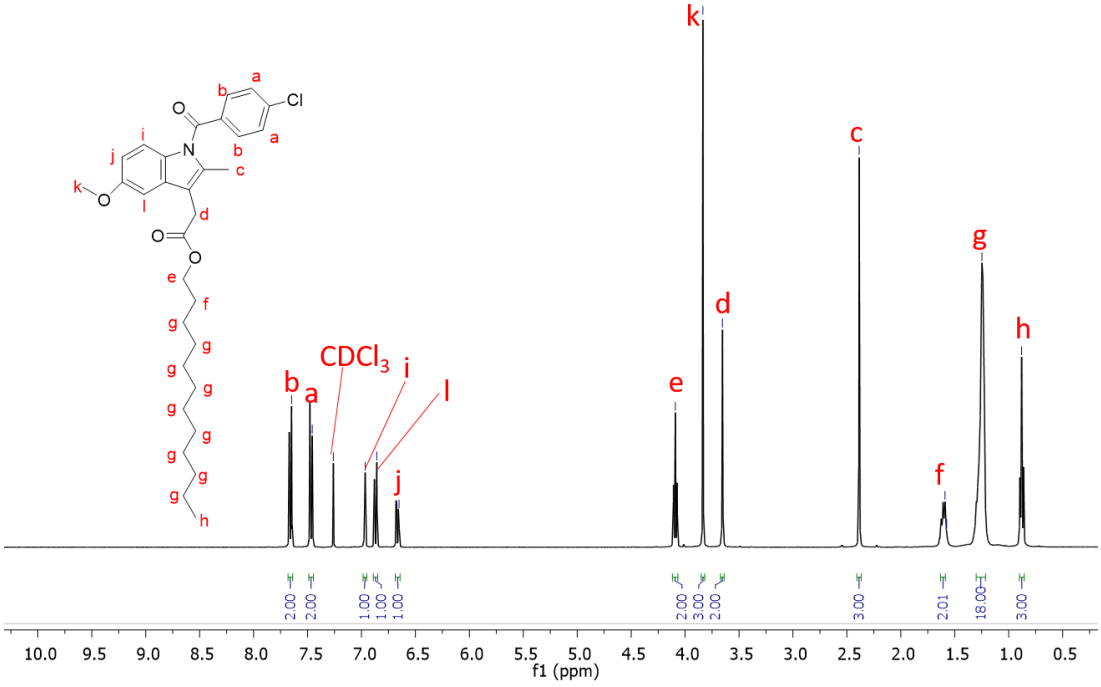

Appendix Figure A 19: ^{1}H NMR ($CDCl_3$, 400 MHz) of IND dodecyl ester

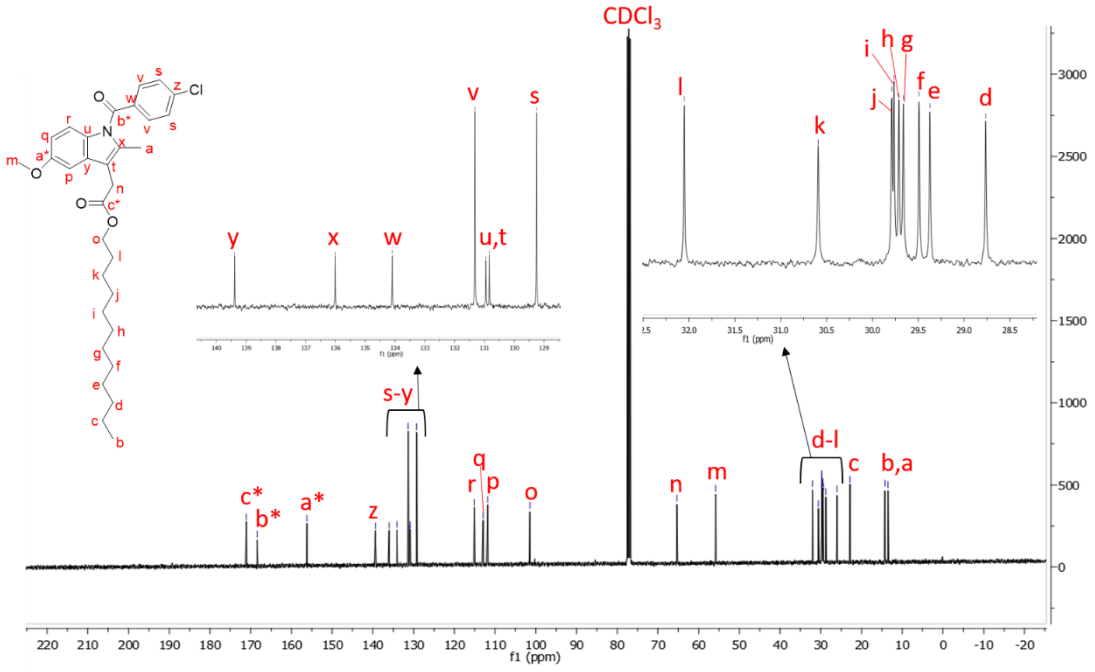

Appendix Figure A 20: ^{13}C NMR ($CDCl_3$, 400 MHz) of IND dodecyl ester.

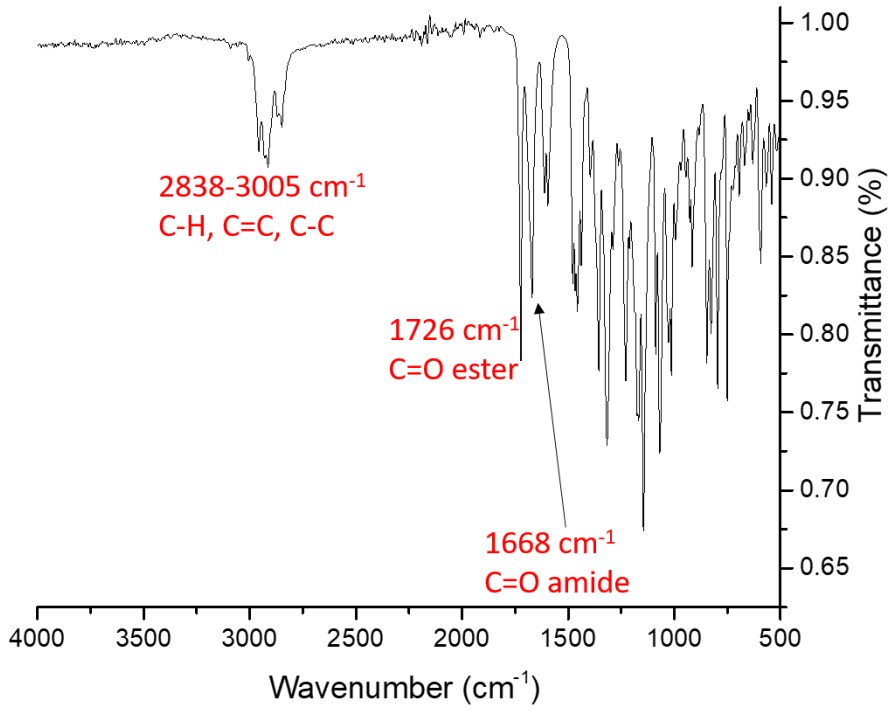

Appendix Figure A 21: IR spectra of IND dodecyl ester.

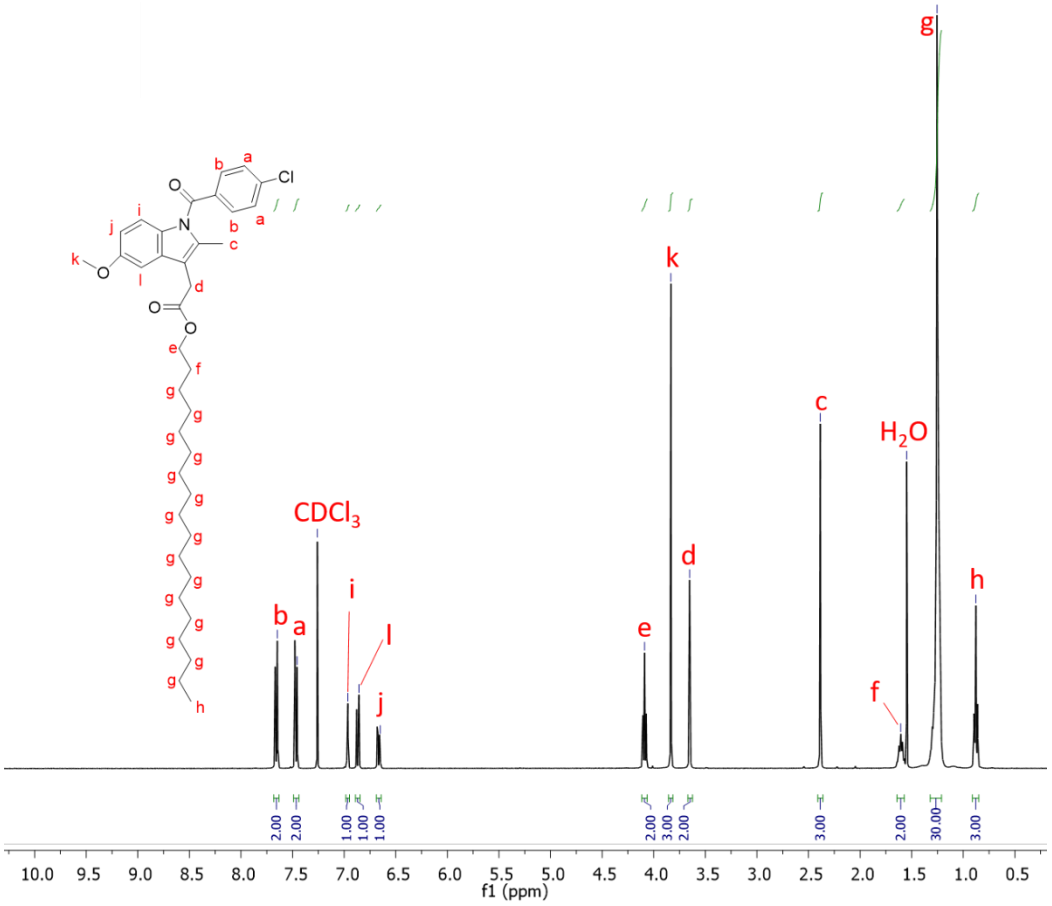

Appendix Figure A 22: ^{1}H NMR ($CDCl_3$, 400 MHz) of IND stearyl ester

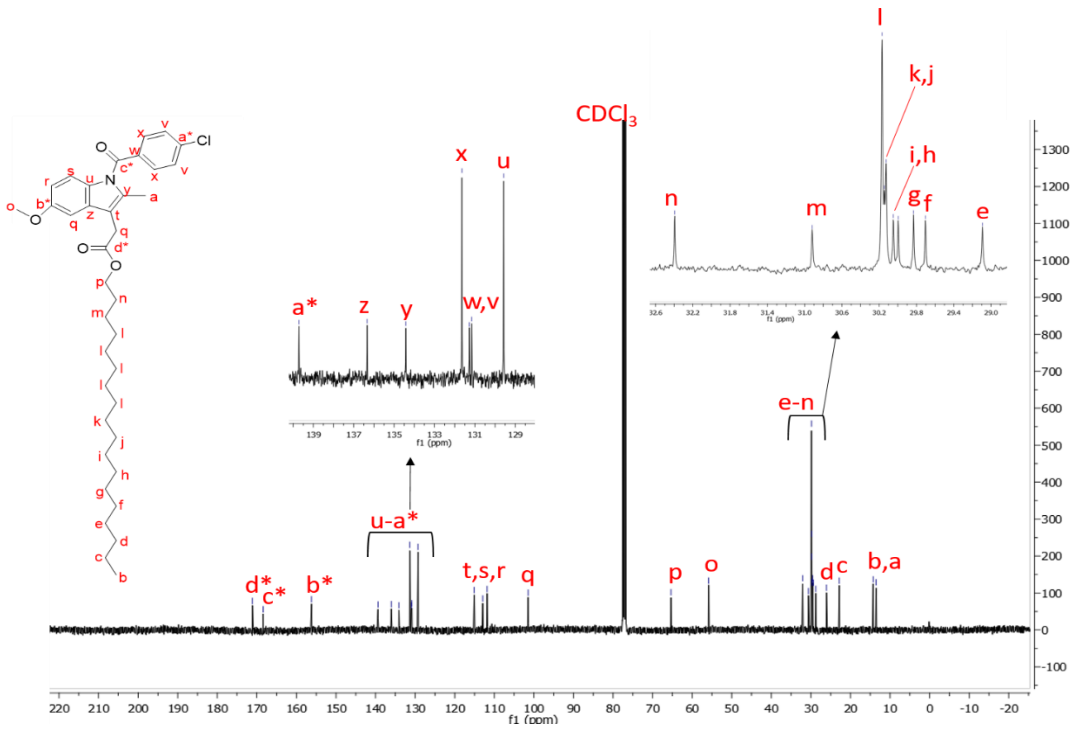

Appendix Figure A 23: ^{13}C NMR ($CDCl_3$, 400 MHz) of IND stearyl ester.

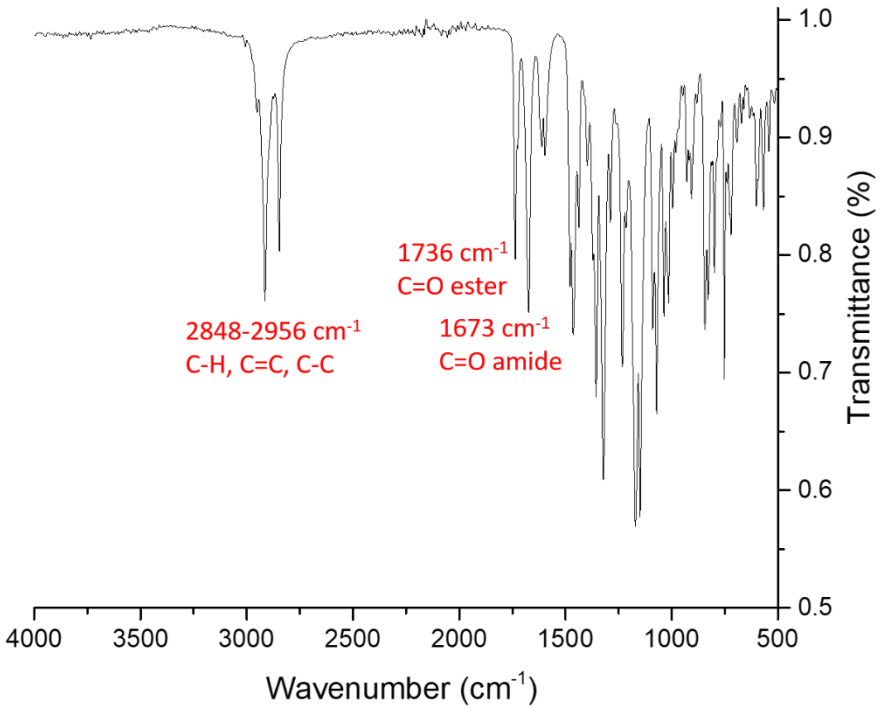

Appendix Figure A 24: IR spectra of IND stearyl ester.

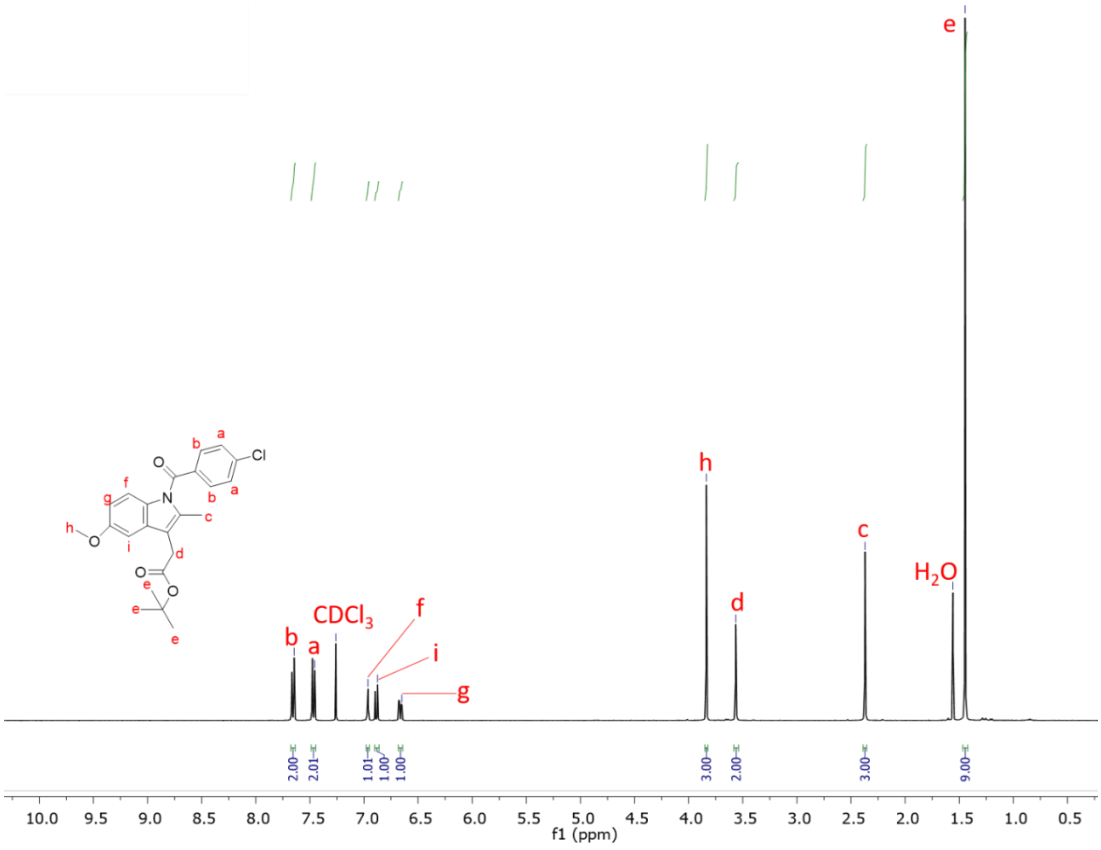

Appendix Figure A 25: 1H NMR ($CDCl_3$, 400 MHz) of IND tButyl ester

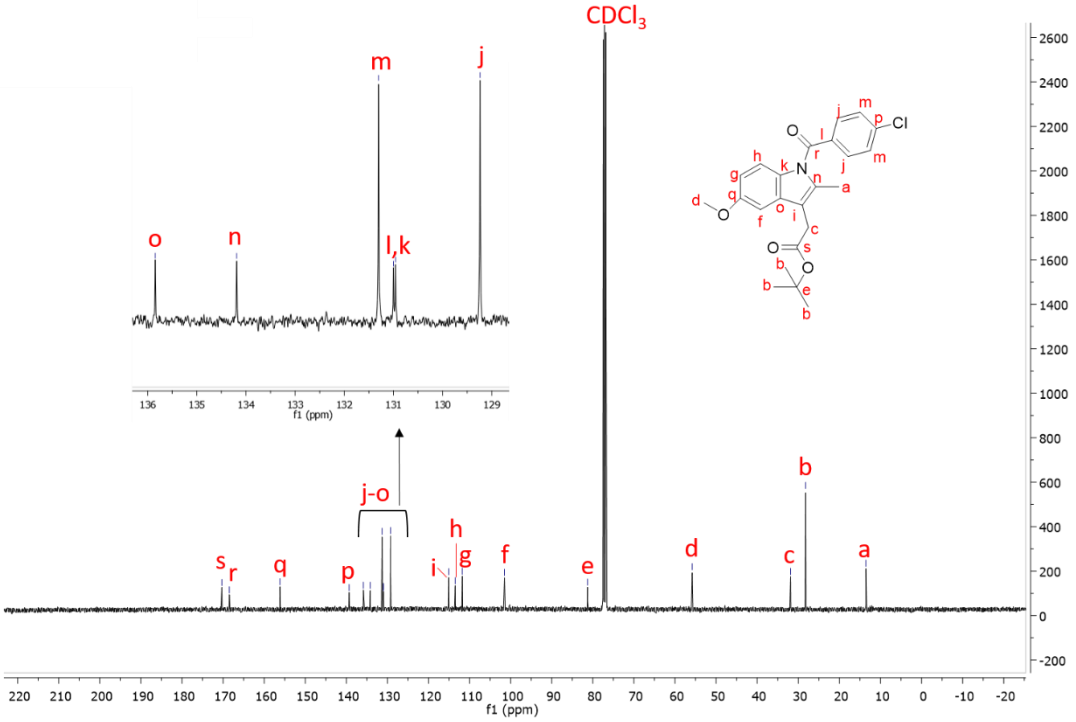

Appendix Figure A 26: 13C NMR ($CDCl_3$, 400 MHz) of IND tbutyl ester.

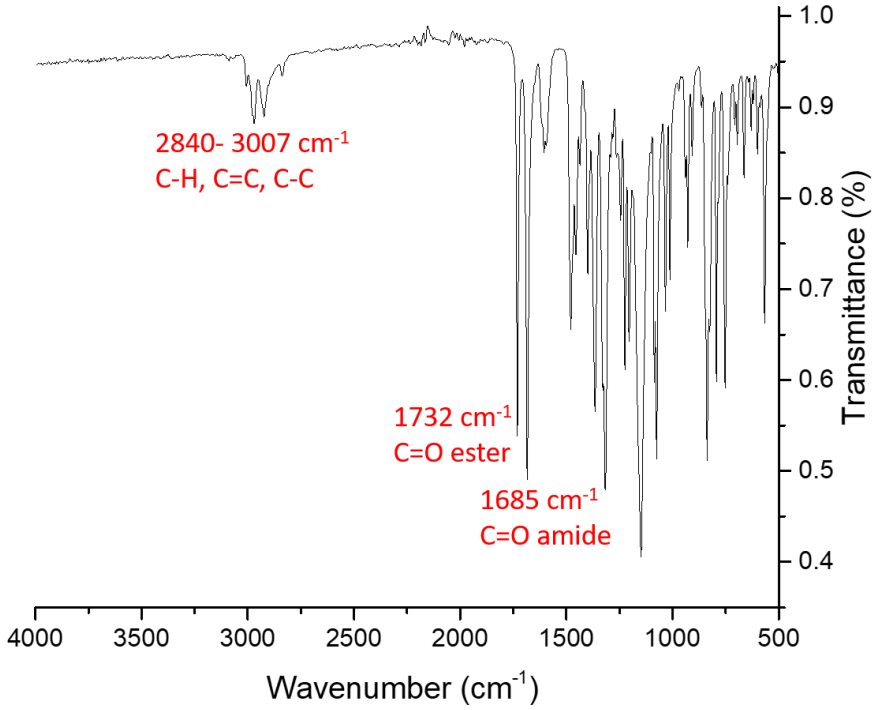

Appendix Figure A 27: IR spectra of IND tButyl ester.

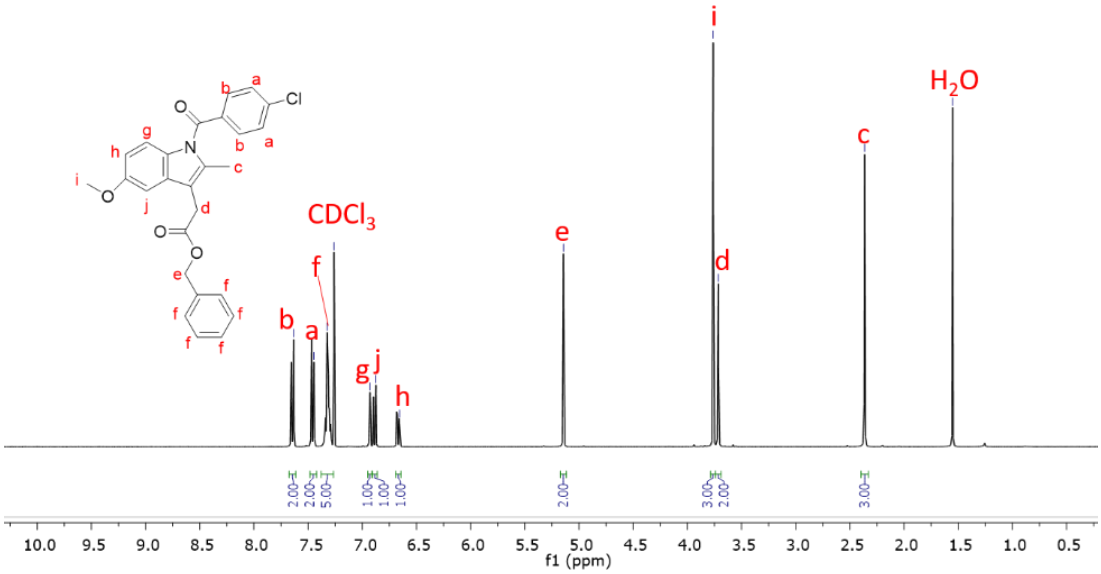

Appendix Figure A 28: ^{1}H NMR ($CDCl_3$, 400 MHz) of IND benzyl ester.

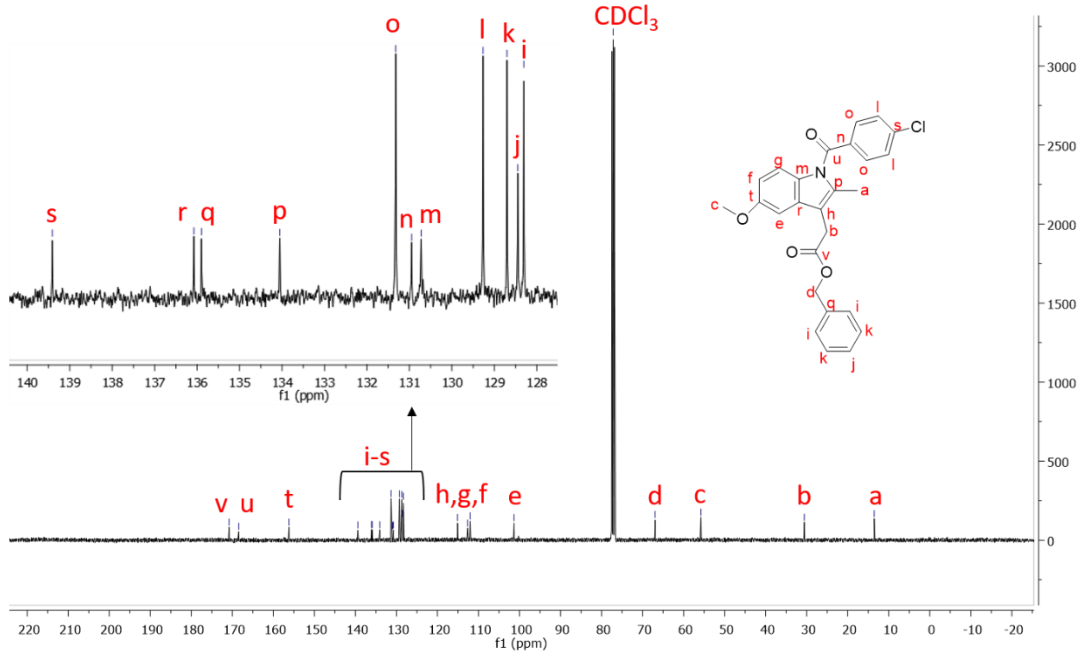

Appendix Figure A 29: ^{13}C NMR ($CDCl_3$, 400 MHz) of IND benzyl ester.

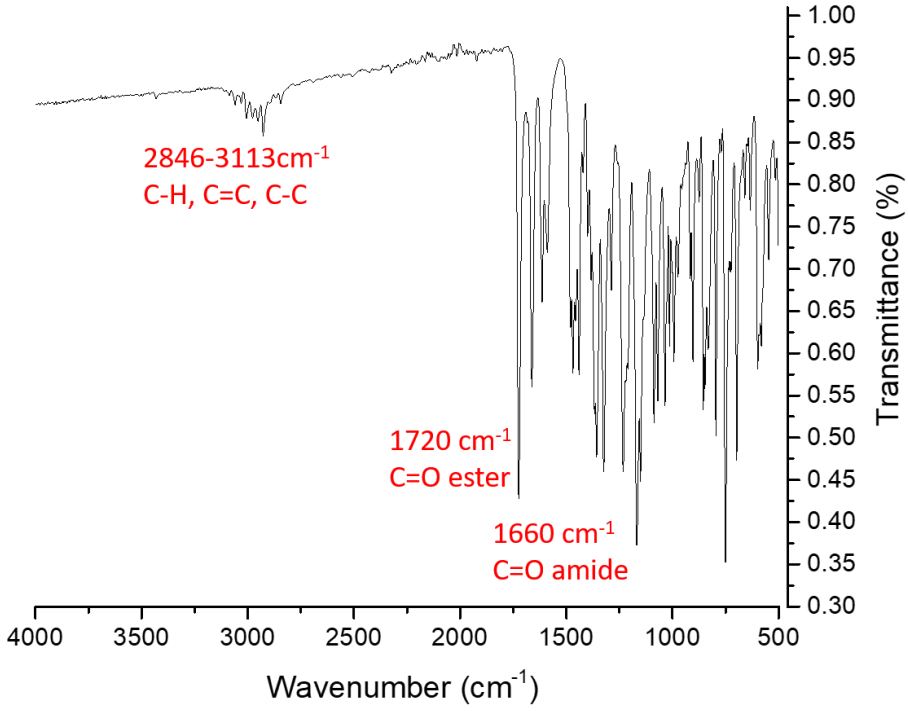

Appendix Figure A 30:IR spectra of IND benzyl ester.

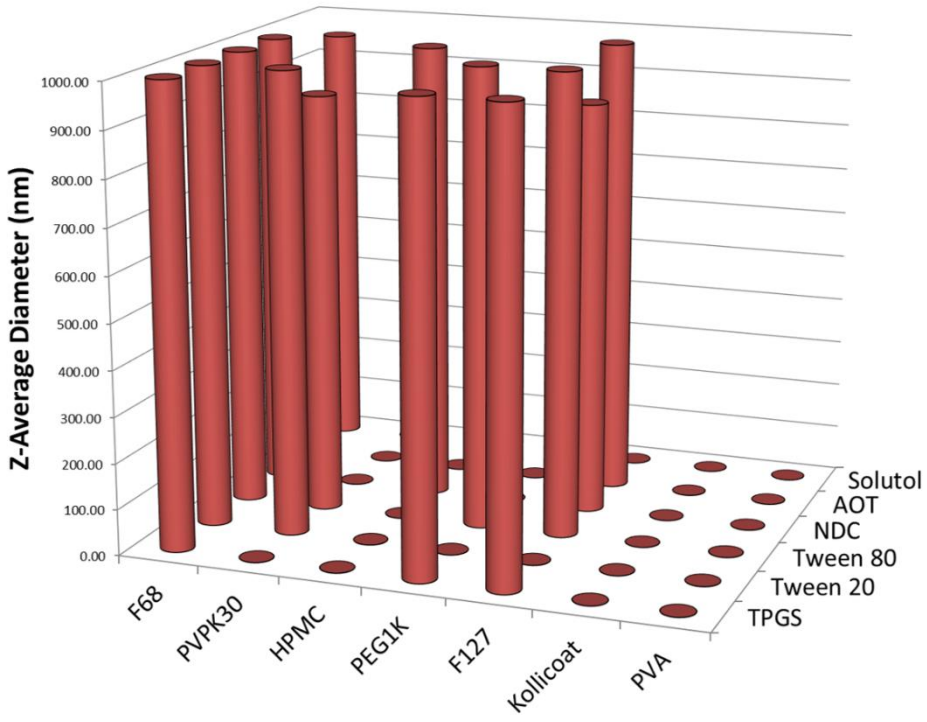

Appendix Figure A 31:IND-ethyl ester 30wt% SDN screen.

Chapter 6
Conclusions and Future Work

Chapter 6

6.1 Conclusions and Future Work

Nanomedicine has proved to be a rapidly evolving field of research, bridging expertise between chemistry, pharmacology and biomedical science to overcome clinical implications of pre-existing therapeutics. The clinical focus for this research has been focussed on improving clinically available treatments for the prevention of sudden preterm birth; occurring in 1 in 10 neonates in the UK alone. Currently existing tocolytic therapies used to inhibit myometrial contractions are coupled with high dosage requirements and moderate to severe maternal and/or fetal side effects. Our tocolytic of choice was indomethacin (IND) which acts a prostaglandin inhibitor to reduce, or temporarily terminate myometrial contractions. Nevertheless, the high (25 mg) and repetitive IV dosage requirements increase placental transfer and fetal accumulation which leads to a range of several severe side effects causing chronic or fatal implications. As a result, we hypothesised that formulating IND into a nanosystems could potentially reduce dosage requirements and thus reduce associated pharmacological and clinical risks. Throughout this thesis, several different types of nanosystems have been explored including solid lipid nanoparticles (SLNs), nanostructured lipid carriers (NLCs), nanoemulsions (NEs) and solid drug nanoparticles (SDNs). All approaches where associated with a mutual aim to formulate IND into a nanoparticle formulation *via* top down synthetic approaches. The following sections discuss each of different chapters; focussing on their aims, outcomes and future work.

6.2 Chapter 2

Chapter 2 explored the use of SLNs as suitable nanoparticle system for the encapsulation of IND *via* the solvent injection method (SIM). The development of SLNs in research are often carried out through time consuming trial and error derived methods, predominantly starting with excipients trialled throughout the literature. In order to develop a more detailed experimental progression for the active ingredient of interest, this chapter focussed on optimising the process of excipient choice for SLN formulation development. Extensive studies were carried out to test the applicability of several solid lipids through the synthesis of drug-lipid melts and analysis by DSC and PXRD. Optimal drug-lipid compatibility was identified through the increased dissolution of IND crystals and decreased IND

crystallinity within the melt structure to increase the amorphous character. Consequently, this allows a prediction for a compatible solid lipid core, whereby amorphous character is preferred to reduce the potential of spontaneous polymorphic transitions and drug expulsion. The use of DSC enabled the detection of polymorphic forms of IND present through changes in the presence of crystalline drug material through depression or shifts in the T_m. The simultaneous use of PXRD enabled the detection of depression of the crystallinity of IND within the drug lipid melts in comparison to the bulk materials. Jointly, this shown that these methods can reinforce the effectiveness of the qualitative interpretation of PXRD and the quantitative interpretation of DSC as joint indicators of potential good and bad drug-lipid compatibility. A secondary significant finding from Chapter 2 highlighted the importance of the stabiliser choice from a screening process of carefully chosen polymers that exist on the FDA-CDER list. The stabilisers with the best performance where Pluronic® F68 and Pluronic® F127, whereby consequent blends of these two polymers enabled the formation of SLNs up to a maximum IND loading of 3 wt%. This was of significant importance as experiments using F68 alone as a polymeric stabiliser, was only able to achieve a lower drug loading of 0.23 wt%. From a clinical perspective, an IND dosage of 25 mg must be administered IV in order to inhibit myometrial contractility. For the SLN formulations containing both F68 and F127 stabilisers at 3 wt% IND, this translates to an infusion volume of 76.4 mL, assuming all IND in released to maintain a pharmacological efficacious time window. Further advances throughout this chapter then showed that the inclusion of Tween 20 and Tween 80 as a cosurfactants alongside Pluronic® F68 or Pluronic® F127 enabled a significant reduction in the masses of stabilisers required to stabilise 3wt% IND-SLN systems. More specifically, systems using Pluronic® F68 and F127 blends required 211.5 mg of carrier excipients, whereas Pluronic®/ Tween systems required 114.5 mg of carrier excipients. This was a significant improvement in the IND-SLN formulation as a reduction in carrier materials reduces the pharmacological risks of accumulation and unwanted side effects.

Further studies required the removal of 1-propanol from the aqueous dispersions as the mass of the organic solvent exceeded the pharmaceutical requirement for translational therapeutics. Methods such as dialysis, freeze drying, spiral evaporation and centrifugation were trialled. Unfortunately all of these

methods were unsuccessful and further work to aid 1-propanol removal from these samples should be considered. This may entail additional investigations into other potential cryoprotectants to enable lyophilisation to be the primary form of solvent removal. In addition, alternative organic solvents may be trialled to carry out the solvent injection method. However, those considered must have a boiling point above 82 °C to enable the melting of COMP and be miscible with water.

6.3 Chapter 3

Throughout Chapter 3 the use of commonly used Pluronic® ABA block stabilisers to successfully synthesise SLNs and monitor their effects upon the lipid core microenvironment were investigated. All SLNs were synthesised by the SIM. The Pluronic® stabilisers investigated, denoted as F68, F127, P105 and L64, differed in their physical properties including the cited hydrophobic lipophilic balance (HLB), average molecular weight (MW), the ratio between the polypropylene oxide and polyethylene oxide units (PPO/PEO ratio) and the critical micelle concentration (CMC). Regardless of their different physical properties of the Pluronic® stabilisers, there was no significant difference in the immediate physical properties (D_z, PdI) of the blank or pyrene containing SLNs and showed no significant difference between the stabilisers used. In order to monitor the internal core microenvironment, pyrene as a small molecule fluorophore was used. Pyrene has a unique, polarity dependent emission spectra that is characterised by five intense vibrational bands, denoted I_1-I_5. A ratio between the first polarity dependent band, I_1 and the third polarity independent band, I_3, gives an I_1/I_3 ratio that reflects the polarity of the immediate microenvironment; whereby the higher the value, the higher the polarity. For SLNs designed to carry a hydrophobic active/drug, the lipid core should be less polar, thus possess a lower I_1/I_3 value to enhance the drug-lipid affinity. Interestingly, after exploring the different Pluronics® and their different physical properties, we found that the MW of the hydrophobic PPO unit on the Pluronic® was the fundamental property controlling the internal core polarity. The inversely proportional relationship identified shown an increase in the PPO unit simultaneously decreased the I_1/I_3 value. The Pluronics® containing higher MW PPO blocks (P105 (3248 g/mol) and F127 (3770 g/mol)), presented respective I_1/I_3 values of 1.30 ± 0.02 and 1.32 ± 0.03. This was significantly lower, thus less polar than Pluronic® F68 (I_1/I_3 = 1.39 ± 0.02) and L64 (I_1/I_3 = 1.40 ± 0.01) stabilised systems with shorter MW

PPO block lengths of 1682 g/mol and 1740 g/mol, respectively. This occurred independently of the D_z (all samples ranged between 212-254 nm) and PdI (all samples ranged between 21- 26 %) of the particle dispersions. This differs to previous studies that have shown that a decrease in I_1/I_3 is predominantly coupled with a decrease in D_z. Additionally, the excimer/monomer (*e/m*) ratio that has been implemented throughout the literature to monitor spatial proximity of pyrene molecules. This *e/m* parameter was recorded in this chapter and it was found that Pluronic® stabilisers that possessed lower I_1/I_3 values (therefore the least polar lipid core environments), simultaneously possessed the higher excimer emissions. This suggests that SLN systems containing Pluronic® stabilisers with the higher MW PPO blocks also increase the density of pyrene molecules within the lipid core. This chapter highlighted that the polarity of the lipid core microenvironment and the *e/m* ratio possessed has proven to be an experimental parameters worth considering during formulation optimisation for a chosen compound, as tuning the environment can better accommodate compounds of different polarities. To build on this research, encapsulation of a range of non-polar compounds to develop a trend between the polarity of the molecules and the preferred polarity of the lipid environment is required. In turn, this will allow formulation development for SLN synthesis to be more accurately designed to enhance lipid core encapsulation of the chosen entities.

6.4 Chapter 4

The primary focus of Chapter 4 was to develop IND loaded NLCs using the SIM. NLCs are classed as second generation SLNs, with advantages such as increased storage stability and increase drug loading capacity. Consequently, NLCs were explored to potentially increase the IND drug loading achieved with SLNs (3 wt%). A range of several NLC formulations were developed using a various low cost, abundant liquid lipids, namely mineral oil, safflower oil, sunflower oil and castor oil. Preliminary investigations optimised IND-NLC formulation development through the use of liquid lipid compatibility and fluorescence spectroscopy. The solid lipid excipient used was COMP, similarly to all previous SLN formulations. Stabilisers explored were Pluronic® F68, F127, P105 and L64. Compatibility studies between the liquid and solid lipid used visual miscibility and DSC measurements to optimise the excipients used for IND-NLC formulation development. DSC measurements

emphasised that safflower, castor and sunflower oils were mutually compatible excipients with both the drug and solid lipid. The initial successful formation of 10wt% IND-NLCs was achieved using Pluronic® F68 as a stabiliser, achieved a D_z range of 234- 495 nm with respective PdI range of 15- 29 % dependent on the liquid lipid used. However, safflower and sunflower oil stabilised by Pluronic® F127 displayed increased stability amongst all of the samples. Although IND-NLCs containing 10wt% drug were successfully synthesised, the removal of organic solvent resulted in destabilisation of the system. Further work in this area would include the exploration of alternative stabilisers, commercial or bespoke, for the stability of the NLCs should be explored for their ability to withstand freezing and drying stresses. Conversely, a range of cryoprotectants may be trialled in order to successfully remove the solvents through lyophilisation to enhance the stability of the particle dispersions. Further exploration of the dependence of the stabiliser concentration on their stability should also be optimised.

A consequent aim of Chapter 4 was to explore NEs as an alternative system to encapsulate IND, due to the ability to remove the implications of 1-propanol as the organic solvent and removing COMP as an excipient from the system. Acetone was used in a nanoprecipitation method whereby successful particles where synthesised containing 5wt% IND-NEs that were stabilised using Pluronic® F127. Clinically this particular formulation would require an IV infusion of 294 mL, assuming that all IND would be released within a time frame to maintain pharmacokinetic efficacy. However, further work assessing the release behaviour on the IND-NEs displayed that optimal NEs containing safflower, sunflower and soybean oil IND-NEs showed a maximum release of ≤3.9% IND in DI water at 37.5 °C. Evidently these release profiles of IND were greatly slower than ideal assuming that systemic administration runs the risk of only partial uterine accumulation. Therefore further investigation is required to assess *in vivo* accumulation of the nanoparticles. For future work this may involve assessing the release of IND in the presence of physiological relevant solutions such as phosphate buffer saline (PBS), in the presence of biological enzymes and/ or the effects at varying pH.

6.5 Chapter 5

In chapter 5 the ability to form solid drug nanoparticles (SDNs) loaded with IND was assessed. SDNs are a subtype of nanoparticle system, consisting of a polymer and/or surfactant and the drug/ active

molecule. SDNs have shown to be particularly successful for overcoming pharmacological implications of therapeutic molecules; predominantly due to their ability to significantly increase the aqueous solubility. In turn this reduces clinical dosage requirements, benefitting from a reduction in unwanted side effects and potential adverse reactions. SDNs have also proven to be particularly desirable as a nanosystems due to the high ratio of drug/active to carrier excipients able to be achieved. It was demonstrated that IND as a small molecule was unsuccessful at forming stable IND-SDNs at 30wt%. Consequently, a range of IND ester analogues where synthesised *via* the Steglich esterification process to form a range of several analogues with different physical characteristics. All IND ester analogues where then screening using the emulsion templated freeze drying (ETFD) technique using seven different polymers and six different surfactants to obtain 42 different potential binary combinations. It was apparent that an increase in the hydrophobicity of the analogues increased the number of HIT samples achieved. However, strict reproducibly of the samples rendered 14 samples across the benzyl, nButyl, hexyl and dodecyl esters that were suitable for continuation. Nevertheless, it was found that all four suitable esters all contained a HIT sample using PVA: NDC as the polymer: surfactant combination. Consequent stability studies highlighted that nButyl was unstable at ≤6 hours, and the benzyl ester showed destabilisation overnight. The hexyl and dodecyl samples remained stable over a 24 hour time period, however the hexyl sample had enhanced storage stability and was successfully reconstituted after eight weeks of storage in a desiccator. For this reason, hexyl ester SDNs containing 24 wt% active IND were considered the most suitable for further continuation for future studies. The following experimental steps would require exploration of the esterase activation to mimic ester cleavage to release the therapeutic IND coupled with release studies and cellular toxicity testing. From this data the rate of cleavage can be coupled with the ability for the analogues to exert a therapeutic effect *ex vivo*, with consequent potential translation to *in vivo* studies.

6.6 Overall summary

The work in this thesis has provided several optimal novel formulations containing IND or IND analogues, suitable for further studies. Lipid derived and non-lipid derived carrier systems have been thoroughly explored to benefit the nanoformulation of IND loaded systems, for the clinical prevention

of preterm birth. Chapter 2 afforded two IND-SLN dispersions containing 3 wt% IND stabilised by a binary combination of Pluronic® F68: Tween 80 or Pluronic® F127: Tween 80. Chapter 3 explored the relationship between Pluronic® stabilisers and the lipid core environment. It became apparent that the polarity of the lipid core could be controlled by the MW of the PPO block on the individual Pluronic® stabilisers. The relationship between a non-polar lipid core able to be tuned by stabilisers then lead to the idea that the lesser polar lipid cores would be able to increase drug loading capacities of low polarity chemical entities. This led to the development of IND-NLCs at 10 wt% drug loading. Implications arose upon the removal of the organic solvent leading to the successful formation of 5 wt% IND-NEs. Finally, an alternative approach investigating IND hydrophobic analogues as potential prodrugs were explored throughout Chapter 5. The prodrugs were synthesised through a Steglich esterification route, prior to formulating the IND analogues into SDNs. Optimal experiments afforded 30 wt% IND-hexyl ester analogues, that were able to successfully synthesised through the ETFD method and successfully be reconstituted after 8 weeks. In summary, there are several formulations suitable for further development from the basis of the work presented throughout this thesis.

Chapter 7
Materials and Methods

Chapter 7

7.1 Materials

Indomethacin (≥99%), poly(ethylene glycol) methyl ether (average M_n 400, 1,000, 2,000, 5,000, 10, 000), Pluronic® F68, Pluronic® F127, Pluronic® P105, Pluronic® L64, Sucrose, Trehalose, Mannitol, Dextrose, polyvinyl alcohol (PVA), Hydroxypropyl methylcellulose (HPMC), polyvinyl alcohol-co-polyethylene glycol (Kollicoat protect), polyvinyl pyrollidone K30 (PVP-K30), tween 20, tween 80, analytical grade ethanol, *n*-butanol, *n*-hexanol, *n*- dodecanol, *tert*-butanol, benzyl alcohol, pyrene (≥99%), safflower oil, sunflower oil, mineral oil, castor oil, soybean oil, d-α tocopheryl polyethylene glycol 100 succinate (TPGS), sodium deoxycholate (NDC), dioxtyl sulfosuccinate sodium salt (AOT), polyethylene glycol (15)-hydroxy stearate (Solutol), dicyclohexylcarbodiimide (DCC), anhydrous dichloromethane (DCM) and 4-dimethylamino pyridine (DMAP) were all purchased from Sigma Aldrich. 1-propanol (HPLC grade), 2-propanol (IPA, HPLC grade), acetonitrile (HPLC grade), ethyl acetate, *n*-hexane and analytical grade acetone were purchased from Fisher Scientific. Compritol 888 ATO, Precirol ATO5, Gelucire 44/14, Geleol, Gelot 64 were all kindly gifted from Gattefossé. All materials were used as received.

7.2 Characterisation

7.2.1 Dynamic Light Scattering

Dynamic light scattering (DLS) were carried out at 25 °C using an Anton Paar Litesizer™ 500 (Chapter 2-4) or a Malvern Zetasizer Nano ZS instrument (Chapter 5 only) at a nanoparticle concentration of 1 mg mL^{-1}. All measurements were taken using standard conditions at 25 °C, a laser wavelength of 630 nm, nanoparticle viscosity of 1.33 m.Pa.s. All measurements of individual samples were taken in triplicate.

7.2.2 Nuclear Magnetic Resonance

^{1}H and ^{13}C nuclear magnetic resonance (NMR) spectra were recorded in $CDCl_3$ using a Bruker Avance spectrometer operating at 400 and 100 MHz respectively. Chemical shifts (δ) are reported in parts per million (ppm) and TMS was used as an internal standard for both ^{1}H and ^{13}C NMR spectra.

7.2.3 Electrospray mass Spectrometry

Electrospray (ESI) mass spectrometry data were recorded in the Mass Spectrometry Laboratory at the University of Liverpool using a MicroMass LCT mass spectrometer using electron ionisation and direct infusion syringe pump sampling. All materials were diluted with methanol. Dilution concentration was dependent on the molecular weight of the entity.

7.2.4 Elemental Analysis

Elemental analyses were obtained from a Thermo FlashEA 1112 series CHNSO elemental analyser.

7.2.5 Powder X Ray Diffraction

Powder X-Ray Diffraction (PXRD) patterns were carried out on samples using a PAN analytical X'pert powder diffractometer using CuKα radiation. Spectra was produced using the Bragg Bretano Geometry transmission mode across 1-56 2θ, with a step size of 0.016 degrees.

7.2.6 Differential Scanning Calorimetry

Differential scanning calorimetry (DSC) was carried out using Q2000 DSC (TA instruments). The methods used for DSC measurements were a heat/cool/heat for two cycles. All thermograms shown throughout this thesis are from the second heat cycle unless stated otherwise. All samples used a heating rate of 5 °C/min with Tzero Hermetic pans.

7.2.7 Fourier Transform Infrared Spectroscopy

Fourier-transform infrared spectroscopy (FT-IR) was performed using a Thermo NICOLET IR200, between 400 cm^{-1} to 4000 cm^{-1}. Samples were loaded neat, using an attenuated total reflectance accessory.

7.2.8 High Performance Liquid Chromatography

For HPLC analysis the column used was an Agilent Poroshell 120 EC-C18 (4.5 x 50 mm, pore size = 2.7 μm).The solvent used was 80 % AcCN, 20% DI H_2O and 0.1 % formic acid. The flow rate was kept constant at 0.6 mL/min. The injection volume was 5 μL and DAD signals where captured at λ= 250 nm. The column was held at 30°C.

7.2.9 Fluorescence Spectroscopy

For fluorescence spectroscopy: all fluorescence data was obtained using a Hitachi Spectrophotometer 2700. Emission spectra for pyrene were recorded between 350 and 500 nm. An excitation wavelength of λ_{ex} = 335 nm was used for all studies as well as an excitation slit width of 2.5 nm and an emission slit width of 2.5 nm with a scan rate of 60 nm/min. All fluorescence measurements for SLN samples were in a mixed solvent system of water: 1-propanol (5:1) unless stated otherwise.

7.3 Methods

7.3.1 Chapter 2

7.3.1.1 General solvent injection method:

All solid lipid nanoparticles (SLNs) where synthesised by the solvent injection method (SIM). The hydrophobic phase consists of the organic, water miscible solvent (4 mL), indomethacin (IND) and Compritol 888 ATO (COMP). The aqueous phase consisted of deionised (DI) water (20 mL) and variable polymeric stabilisers that was warmed to 26 °C. The polymeric stabilisers used are dependent on the experiments conducted and are further stated in the respective sections throughout this chapter. The hydrophobic phase was heated to 82 °C, 10 °C above the melting point of COMP, for five minutes unless stated otherwise. Once the hydrophobic phase was a homogeneous molten mixture, it was aspirated through an 18 gauge needle (exit width = 1.25 mm), and injected directly into the vortex of the aqueous phase using a 21 gauge needle (exit width = 0.9 mm). The mixture was mechanically agitated at 350 rpm and left to stir for a further 5 minutes. Immediate DLS measurements were taken.

7.3.1.2 Differential Scanning Calorimetry (DSC) of lipid-drug melts

DSC of the drug lipid melts were carried out using 50: 50 w/w% COMP: IND with a total solid mass of 1 g. For the different solid lipids screened (Compritol 888 ATO, Precirol ATO 5, Gelot 64, Geleol, Gelucire 44/14) were heated 10 °C above their approximate respective melting points shown in Table 7.1.

Table 7.1: Solid lipids used in to screen drug-solid lipid melts

Solid Lipid	Melting Point (°C)
Compritol 888 ATO	72
Precirol ATO 5	65
Gelot 64	65
Geleol	40
Gelucire 44/14	65

The drug lipid melts were heated with mechanical agitation for 10 minutes, and where left to cool down to room temperature overnight. The resultant samples were analysed by DSC. The thermograms were obtained using a heat/cool/heat programme from 21 °C to 200 °C, followed by cooling to 21 °C before reheating. All samples where heated at a rate of 5 °C/ min.

7.3.1.3 Powder X Ray Diffraction (PXRD) crystallinity analysis

The samples were prepared in an identical manner as described above in section 7.3.1.1. The PXRD diffraction patterns were obtained scanning 2θ 1 to 56 over 30 minutes.

7.3.1.4 Lipid screening analysis using the solvent injection method

All SLNs were synthesised by the general SIM discussed in section 7.3.1.1. The solid lipids chosen for screening where COMP, Gelot 64 and Geleol. Solid lipids (4 mg) where heated in 2-propanol (4 mL) for two minutes to form a homogeneous melt. The hydrophobic phases where injected into DI water containing Pluronic® F68 as a polymeric stabiliser at 5 mg/mL.

7.3.1.4 Stabiliser compatibility screening

Several polymers including: Pluronic® F68, Pluronic® F127, hydroxypropyl methylcellulose (HPMC), polyvinyl pyrollidone K30 (PVP-K30), polyvinyl alcohol (PVA), polyvinyl alchol-co-polyethylene glycol (Kollicoat Protect) and polyethylene glycol -1K (PEG-1K) where implemented at 5 mg/mL in the aqueous phase. The SIM was carried out, as per section 7.3.1.1. The mass of COMP was maintained at 4 mg in 2-propanol (4 mL).

7.3.1.5 Incorporation of IND into optimised SLNs

The SIM as per section 7.3.1.1 was carried out. IND was incorporated at varying drug loadings shown in Table 7.2

Table 7.2: Experimental masses of excipients and IND for systems exploring preliminary IND loading.

Pluronic® F68 (mg/mL)	Solvent: Antisolvent ratio	Total stabiliser mass (mg)	Compritol 888 ATO (mg)	IND (mg)	IND wt% w.r.t. solid content
0.8	1: 5	16	18	0	0
0.8	1: 5	16	17.49	0.51	1.5
0.8	1: 5	16	17.32	0.68	2
0.8	1: 5	16	16.98	1.02	3

7.3.1.6 Investigating IND nucleation in alternative antisolvent ratios

IND (5 mg) was heated in 1-propanol (1 mL) and injected into DI water as an antisolvent, at varying volumes of 3, 5, 7, 10 and 12 mL. The aqueous phase was at 26 °C. The solutions of precipitated solid where then rolled overnight. The insoluble IND was filtered off, dried and weighed by difference to determine the mass of insoluble IND within the solvent: antisolvent system.

7.3.1.7 Investigating increased stabiliser concentrations

The SIM as per section 7.3.1.1 was carried out. The solvent: antisolvent ratio was maintained at 1:5. COMP (17.49 mg) and IND (0.51 mg) masses were standardised. However, the concentrations of the Pluronic® F68 stabiliser were increased in trial 5 mg/mL, 10 mg/mL and 20 mg/mL stabiliser concentrations.

7.3.1.8 Investigating Pluronic® F68 and F127 blends

The SIM was carried out as per section 7.3.1.1. Pluronic® F127 as a polymeric stabiliser was introduced in addition to Pluronic® F68.The concentration of the combined polymeric stabilisers were standardised at 10 mg/mL. Pluronic® F68 and F127 where blended in 25 wt% increments as shown in Table 7.3. IND-SLNs were trialled at 1 wt% of the total solid mass, using IND (2.18 mg) and COMP (15.32 mg).

Table 7.3: Masses of blended Pluronic® F68 and Pluronic® F127 to trial 1wt% loaded IND-SLNs.

Total stabiliser mass (mg)	Pluronic® F68 (mg)	Pluronic F127 (mg)	Ratio (w/w%)
200	200	0	100: 0
200	150	50	75: 25
200	100	100	50:50
200	50	150	25:75
200	0	200	0:100

Upon successful inclusion of IND at 1 wt% for all samples except 100 wt% Pluronic® F68, the IND content was increased to 3 wt% (6.54 mg IND, 11.46 mg COMP).

7.3.1.9 Investigation of IND micellisation

The micellisation behaviour of IND in 10 mg/mL blends of Pluronic® F68: F127 within all blended systems displayed in Table 7.3 was explored using high performance liquid chromatography. IND (10 mg) was added to vials containing 5 mL of the respective Pluronic® F68: F127 combinations at a 10 mg/mL concentration. The samples where mechanical agitated overnight at 250 rpm. The resultant dispersions where filtered through a 0.2 μm filter and analysed by HPLC.

7.3.1.10 Incorporation of Tween derivative as co-surfactants in IND-SLN dispersions

The SIM was conducted as per section 7.3.1.1. However, the stabiliser concentration was increased to 5 mg/mL. The stabilisers used where explored in this section, with the combinations shown below in Table 7.4. The Pluronic® and Tween stabiliser where used in a 2:1 w/w% ratio in all cases. The solvent: antisolvent ratio was maintained at 1:5 and the total hydrophobic solid mass was maintained at 18 mg.

Table 7.4: Combinations of Pluronic®: Tweens used for IND-SLN dispersions.

Stabiliser 1	Stabiliser 2
Pluronic® F68	Tween 20
Pluronic® F68	Tween 80
Pluronic® F127	Tween 20
Pluronic® F127	Tween 80

Initial experiments explored IND at a 1 wt% loading with respect to the total solid mass, thus IND at 1.18 mg and COMP at 16.82 mg. Consequent experiments explored IND-SLNs at 3 wt%, thus IND at 3.54 mg and COMP at 14.46 mg.

7.3.1.11 Removal of 1-propanol: dialysis

All 3 wt% IND-SLN dispersions synthesised previously (in section 7.3.1.10) where taken forward for dialysis to remove the 1-propanol organic solvent. The IND-SLN dispersion (1 mL) where placed dialysis tubing with a 1 kDa molecular weight cut off (MWCO) to retain any particles and allow the

removal of 1-propanol. The dispersion was placed in DI water (100 mL) to retain sink conditions. The DI water reservoir was changed daily.

7.3.1.12 Removal of 1-propanol: Freeze drying

Freeze drying was explored to remove 1-propanol from 3 wt% IND-SLNs synthesised in section 7.3.1.10. A range of cryoprotectants were trialled and at three different concentrations: 5 mg/mL, 10 mg/mL and 20 mg/mL. The cryoprotectants screened where as follows: polyethylene glycol (PEG) 400, PEG 2K, PEG 5K, PEG 10 K, trehalose, sucrose, dextrose and mannitol. Each of the 3 wt% IND-SLN dispersions (1 mL) was taken and added to a solution of cryoprotectant at each explored concentration (1 mL) prior to freeze drying. All samples were frozen in liquid nitrogen before being freeze dried in a VirTis BenchTop K freeze dryer (SP Scientific, Ipswich, UK) with a condenser temperature set to −100 °C and vacuum of <40 μbar. All samples remained in the freeze dryer for 48 hours prior to immediate reconstitution in phosphate buffer saline (PBS) solution.

7.3.2 Chapter 3

7.3.2.1 Blank-SLN and Py-COMP-SLN synthesis

All blank-SLN samples where synthesised in an analogous manner as section 7.3.1.1. In order to incorporate pyrene into the samples, a stock solution of pyrene in acetone (0.1 mg/mL) was made. This pyrene solution (340 μL, 0.17 mM) was added to a vial and the acetone was left to evaporate overnight. 1-Propanol (4 mL) and Compritol 888 ATO (18 mg) was added to the vial and rolled overnight to ensure total dissolution of the pyrene. The SIM was then carried out similarly to section 7.3.1.1. Pluronic® stabilisers explored were F68, F127, P105 and L64 and were all standardised at a total concentration of 0.8 mg/mL in the antisolvent phase.

7.3.2.2 Generic fluorescence measurements

7.3.2.3 Investigating the effect of solvent composition on fluorescence

340 μL of the pyrene stock solution (0.1 mg/mL in acetone) was added to 3 separate vials and the acetone was left to evaporate. The different solvent systems (water, 1-propanol and water:1-propanol (5:1)) was added to each of the vials (4 mL/ vial) and left to roll for 48 hours to ensure total

solubilisation. The samples were then analysed through fluorescence spectroscopy (fluorimetery experimental, refer to section 7.3.2.2).

7.3.2.3 Investigating pyrene fluorescence from Pluronic® micelles

Py-COMP-SLNs were synthesised as previously described. 1 mL of the dispersion was placed in a 10 kDa centrifuge tube and centrifuged at 9,000 rpm for 30 minutes. This was repeated in triplicate for each sample to have 3 aliquots of supernatant. The supernatant was then analysed by fluorescence spectroscopy.

7.3.2.4 Blending Pluronic stabilisers to tune the internal core polarity

The SIM was carried out as previously described, however with a range of Pluronic® stabiliser blends. The total stabiliser concentration was maintained at 0.8 mg/mL. The blends and their compositions are highlighted in Table 7.5.

Table 7.5: Pluronic® stabiliser blends and their respective compositions to assess their effect and tuneability on the internal core microenvironment of SLNs.

Pluronic® 1	**Pluronic® 2**	**Pluronic® 3**	**Ratio (w/w%)**
F68	F127	-	100: 0
F68	F127	-	75:25
F68	F127	-	50:50
F68	F127	-	25:75
F68	F127	-	0:100
F68	-	P105	100: 0
F68	-	P105	75:25
F68	-	P105	50:50
F68	-	P105	25:75
F68	-		0:100
-	F127	P105	100: 0
-	F127	P105	75:25
-	F127	P105	50:50
-	F127	P105	25:75
-	F127		0:100

All samples were analysed by DLS and fluorescence spectroscopy (fluorimetery experimental, refer to section 7.3.2.2).

7.3.3 Chapter 4

7.3.3.1 Generic synthesis of nanostructured lipid carriers (NLCs)

All nanostructured lipid carriers (NLCs) where synthesised by the solvent injection method (SIM). The hydrophobic phase consists of the organic, water miscible solvent (4 mL), IND and a mixture of COMP solid lipid and variable liquid lipids. The total solid mass of the hydrophobic excipients was standardised at 18 mg, 53 wt% with respect to the total solids (liquid lipid + solid lipid + drug + stabiliser). The hydrophobic phase was heated to 82 °C, 10 °C above the melting point of COMP, for five minutes unless stated otherwise. Once the hydrophobic phase was a homogeneous molten mixture, it was aspirated through an 18 gauge needle (exit width = 1.25 mm), and injected into the aqueous phase using a 21 gauge needle (exit width = 0.9 mm). The mixture was injected into directly into the vortex of the DI water (20 mL) as the antisolvent containing variable Pluronic® stabilisers at 0.8 mg/mL (47 wt% wrt total solids). The aqueous phase was pre-warmed to 26°C. The mixture was mechanically agitated at 350 rpm and left to stir for a further 5 minutes. Pluronic® stabilisers explored where F68, F127, P105 and L64. Liquid lipids explored where safflower oil, sunflower oil, castor oil, soybean oil and mineral oil.

7.3.3.2 Liquid lipid and drug compatibility

Liquid lipids used were safflower oil, sunflower oil, castor oil, soybean oil and mineral oil.

For visual compatibility: IND (100 mg) was saturated in the individual liquid lipids (500 mg) at 25 °C and 82 °C. Samples at both temperatures were assessed for their dissolution visually. This was obtained by assessing differences in turbidity, miscibility and for any visual separation between the two excipients.

For DSC measurements: For DSC measurement equipment refer to section 7.2.6. IND and the liquid lipids were mixed in a 50:50 w/w% ratio with a total solid mass of 500 mg. A small amount (5-10 mg) of the physical mixtures were then analysed by DSC measurements. All samples were placed on heat-cool-heat samples from 21 °C to 200 °C, at a heat ratio of 5 °C/min.

7.3.3.3 Liquid lipid and solid lipid compatibility

Liquid lipid used were safflower oil, sunflower oil, castor oil, soybean oil and mineral oil.

For visual compatibility: COMP (100 mg) and the liquid lipids (500 mg) were added together and heated to 82°C. The physical mixtures were heated to assess miscibility of molten COMP with the liquid lipids explored. Miscibility was assessed visually from the homogeneity of the sample, whether it was transparent or turbid and whether there was any evidence of phase separation.

For DSC measurements: COMP and the individual liquid lipids were mixed in a 50:50 w/w% ratio with a total solid mass of 1 g. A small amount (5-10 mg) of the physical mixtures were then analysed by DSC measurements. All samples were placed on heat-cool-heat samples from 21 °C to 200 °C, at a heat ratio of 5 °C/min.

7.3.3.4 Preliminary synthesis of blank-NLCs: assessing the core composition

All NLCs were synthesised as previously described in section 7.3.3.1. The mass of the core (solid and liquid lipid) was standardised at 18 mg. The composition was altered, with solid: liquid lipid w/w% ratios explored as 50:50 w/w% and 70:30 w/w% with respect to the total core mass. Pluronic® F68 was used at a concentration of 0.8 mg/mL for all preliminary experiments.

7.3.3.5 Fluorescence spectroscopy of NLC lipid cores

NLCs were synthesised as per the general synthetic method highlighted in section 7.3.3.1. The solid lipid to liquid lipids were mixed in a 50:50 w/w% with a total solid mass of 18 mg. Immediately after synthesis the samples were analysed for their fluorescence behaviour using the method as described in section 7.2.9.

7.3.3.6 Incorporation of IND into NLC lipid cores

All NLCs were synthesised as demonstrated in section 7.3.3.1. IND was incorporated at 1 wt% and 10 wt% with respect to the total solid mass. The generic compositions are shown below in Table 7.6

Table 7.6: Compositions of IND-NLCs containing 1 wt% and 10 wt% active. The composition of the lipid core was investigated.

Solid lipid: liquid lipid (w/w% ratio)	Solid lipid mass (mg)	Liquid lipid mass (mg)	Pluronic® F68 (mg)	IND (wt%)	IND (mg)
70:30	12.6	5.4	16	1	0.34
70:30	12.6	5.4	16	10	3.4
50:50	9	9	16	1	0.34
50:50	9	9	16	10	3.4

7.3.3.7 Exploration of alternative Pluronic stabilisers for IND-NLC synthesis

NLC synthesis containing 10 wt% IND was carried out using the method in section 7.3.3.1. In addition to Pluronic® F68, addition stabilisers F127, P105 and L74 were explored. The concentration of stabiliser remained at 0.8 mg/mL.

7.3.3.8 Removal of 1-propanol

Freeze drying: The 10 wt% IND-NLC dispersion (1 mL) was added to a cryoprotectant solution (1 mL) at two different concentrations of 5 or 10 mg/mL. The cryoprotectants trialled where polyethylene glycol (PEG) with average M_n's = 400, 2000, 5000 and 10, 0000 g/mol.

Spiral evaporation: The 10 wt% IND-NLC dispersion (10 mL) were placed in a 40 mL vial, heated to 40°C and attached to a spiral evaporating apparatus to remove 1-propanol. The spiral evaporator was an Asynt DrySyn spiral evaporator.

7.3.3.9 Synthesis of indomethacin nanoemulsions (IND-NEs)

Indomethacin nanoemulsions (IND-NEs) were synthesised at 5 and 10 wt% IND. A stock solution of IND and the liquid lipids (mineral oil, safflower oil, sunflower oil, soybean oil and castor oil) collectively at 4.5 mg/mL in analytical acetone were rolled overnight. Their compositions of IND: liquid lipid was dependent on the drug loading. The IND: liquid lipid solutions in analytical acetone (1 mL) was aspirated through an 18 gauge needle (exit width = 1.25 mm), and injected into 5 mL of DI water containing using a 21 gauge needle (exit width = 0.9 mm). The DI water contained 0.8 mg/mL of the appropriate Pluronic® (P105 or F127) stabiliser. The dispersions are left overnight with mechanical

agitation at 500 rpm to remove all residual acetone prior to analysis. The compositions of generic excipients are shown in Table 7.7.

Table 7.7: Compositions of excipients in IND-NE formulations at 5 wt% and 10 wt% drug loading

Pluronic® (P105/ F127) mass (mg)	**Liquid lipid mass (mg)**	**IND loading (wt%)**	**IND mass (mg)**
4	4.075	0.425	5
4	3.65	0.85	10

7.3.3.10 Release studies

IND-NE dispersions (1 mL) at 5 wt% were placed in a biodialyser chamber containing a 1 kDa MWCO membrane. The dialyser was placed in 100 mL of DI water which was incubated at 37.5 °C. An aliquot was taken from the reservoir at 0, 1, 2, 4, 8, 24 and 48 hours. At each time point the reservoir was changed for fresh DI water. The aliquot taken from the sample reservoir was filtered through a 0.2 μm filter and analysed by HPLC (refer to section 7.2.8).

7.3.4 Chapter 5

7.3.4.1 Generic method for the esterification of IND

IND (3 g, 0.008 mol, 1 eq) was dissolved in the minimum amount of anhydrous DCM required (~60 mL) to form a bright yellow solution that was degassed with N_2 for 10 minutes. DMAP (0.15 g, 0.0167 mol, 0.15 eq) and the chosen alcohol for esterification (2 eq) was dissolved in anhydrous DCM. The DMAP/ alcohol for esterification were added under N_2 to the IND/DCM mixture. Following this, DCC (2.59 g, 0.0126 mol, 1.5 eq) was dissolved in DCM (20 mL) and added slowly to the mixture at 0°C and under N_2 whilst stirring. Upon the addition of DCC the solution turned from transparent yellow to a cloudy suspension. Following the complete addition of DCC, the reaction mixture was warmed to room temperature and left for 48-72 hours. The completion of the reaction was determined through TLC. After reaction completion white precipitate of the side product DCU was filtered by gravity. The solvent from the resultant filtrate was removed *in vaccuo* and the crude solid was re-suspended in the minimum amount of cold EtoAc. Residual DCU precipitated and the reaction was filtered by gravity again. The crude product was washed with $NaHSO_4$ (2 x 50 mL) to remove excess DMAP, Na_2CO_3 (2

x 50 mL) to remove unreacted drug, followed by DI water (1 x 100 mL) and brine (1 x 100 mL). The crude product was then loaded onto silica before purification by flash chromatography using EtOAc: Hexane binary eluent systems. The solvent system used was dependent on the different esters synthesised.

7.3.4.3 Generic method for the purification of IND esters using column purification and TLC

Thin layer chromatography was performed using Merck Kieselgel 60 F254 aluminium backed silica plates. Visualization was achieved by UV fluorescence or a basic $KMnO_4$ solution and heat. Flash column chromatography (FCC) was performed using silica gel (Aldrich 40-63 µm, 230-400 mesh). The crude material was pre-adsorbed onto silica prior to application to the column. All purified products were eluted and analysed by ^{1}H NMR, ^{13}C NMR, IR, elemental analysis, mass spectrometry and DSC.

7.3.4.3.1: Ethyl ester:

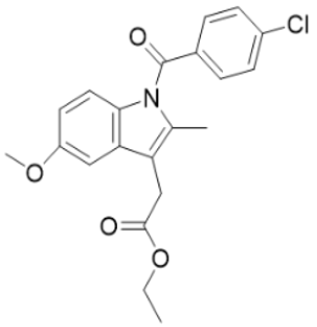

Ethanol (0.77 g, 0.0167 mol, 2 eq) was used. The final product was presented as an off white solid (1.91g, 59 % yield). TLC analysis in 20: 80 EtOAc: Hexane obtained an RF value of 0.3.

^{1}H-NMR (400 MHz, $CDCl_3$): δ ppm =1.26 (T, 3H), 2.38 (S, 3H), 3.65 (S, 2H), 3.84 (S, 3H), 4.15 (Q, 2H), 6.65 (D of D, 1 H), 6.86 (D. 1H), 6.97 (D, 1H), 7.46 (D, 2H), 7.65 (D, 2H). ^{13}C NMR (100 MHz, $CDCl_3$): All ppm shifts correspond to 1 carbon environment unless otherwise stated: δ ppm= 13.40, 14.26, 30.49, 55.71, 61.17, 101.48, 111.81, 112.86, 115.09, 129.26 (2C), 130.85, 130.97, 131.33 (2C), 134.10, 136.03, 139.37, 159.19, 168.46, 171.02. IR (cm^{-1}) = 1673 (C=O, amide), 1725 (C=O ester), 2836-3107 (C-H, C=C, C-C). ESI-MS $[M+Na]^+$ = 408.1 m/z. Elemental analysis = calculated: C (65.38), H (5.25), N (3.63), obtained: C (65.37), H (5.22), N (3.53).

7.3.4.3.2: nButyl ester:

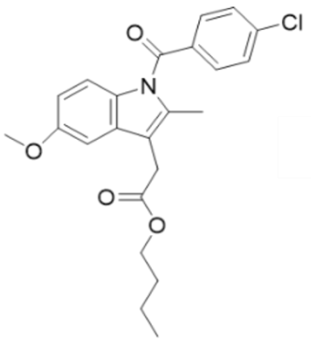

nButyl alcohol (1.24 g, 0.0167 mol, 2 eq) was used. The final product was presented as an off white solid (2.58 g, 74 % yield). TLC analysis in 20: 80 EtOAc: Hexane obtained an RF value of 0.4. ^{1}H-NMR (400 MHz, $CDCl_3$): δ ppm =0.90 (T, 3H), 1.33 (M, 2H), 1.61 (M, 2H), 2.38 (S, 3 H), 3.65 (S, 2H), 3.84 (S, 3 H), 4.10 (T, 2H), 6.65 (D ofD, 1H), 6.86 (D, 1 H), 6.97 (D, 1H), 7.46 (D 2H), 7.65 D, 2H). ^{13}C NMR (100 MHz, $CDCl_3$): All ppm shifts correspond to 1 carbon environment unless otherwise stated: δ ppm=13.49, 13.80, 19.25, 30.57, 30.77, 55.83, 65.06, 101.43, 111.84, 112.90, 115.08, 129.25 (2C), 130.83, 130.95, 131.31 (2C), 134.10, 136.04, 139.8, 159.19, 168.44, 171.07. IR (cm^{-1}) = 1668 (C=O, amide), 1724 (C=O, ester), 2386-3003 (C-H, C=C, C-C). ESI-MS $[M+Na]^+$ = 413.1 m/z. Elemental analysis = calculated: C (66.74), H (5.84), N (3.38), obtained: C (66.95), H (5.88), N (3.38).

7.3.4.3.3: nHexyl ester:

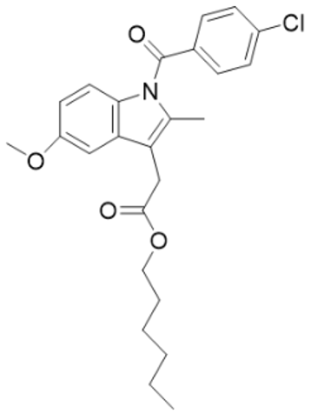

Hexyl alcohol (1.72 g, 0.0167 mol, 2 eq) was used. The final product was presented as a pale yellow solid (2.81 g, 76 % yield). TLC analysis in 20: 80 EtOAc: Hexane obtained an RF value of 0.2. ^{1}H-NMR (400 MHz, $CDCl_3$): δ ppm = 0.86 (T, 3H), 1.26 (M, 6 H), 1.61 (M, 2H), 2.39 (S, 3H), 3.65 (S,

2H), 3.83 (S, 3H), 4.09 (T, 2H), 6.65 (D of D, 1H), 6.86 (D, 1H), 6.97 (D, 1H), 7.46 (D, 2H), 7.65 (D, 2H). ^{13}C NMR (100 MHz, $CDCl_3$): All ppm shifts correspond to 1 carbon environment unless otherwise stated: δ ppm=13.48, 14.09, 22.63, 25.67, 28.70, 30.58, 31.50, 55.81, 65.32, 101.45, 111.78, 112.91, 115.06, 129.24 (2C), 130.82, 130.94, 131.30 (2C), 134.09, 135.99, 139.36, 156.17, 168.42, 171.09. IR (cm^{-1}) = 1689 (C=O, amide), 1722 (C=O, ester), 2834-3093 (C-H, C=C, C-C). ESI-MS $[M+Na]^+$ = 441.2 m/z. Elemental analysis = calculated: C (67.94), H (6.39), N (3.17), obtained: C (68.29), H (6.50), N (3.16).

7.3.4.2 Generic method for emulsion templated freeze drying (ETFD)

Into separate 14 mL glass sample vials, polymer and surfactants were weighed out and dissolved to a final concentration of 22.5 mg/mL in distilled water. These solutions were left overnight on a rolling mixer to ensure thorough dissolution. The active used (IND or an IND ester) was dissolved to a final concentration of 30mgmL^{-1} in chloroform and left on a rolling mixer for 1 hour to ensure thorough dissolution. For the preparation of each SDN sample, 103 µL of surfactant, 207 µL of polymer, and 100 µL of prodrug were added to a 4 mL glass sample vial. This was repeated for all 42 combinations of polymer and surfactant (7×6) and for each IND ester. The final composition yielded SDNs containing 3 mg IND ester (30 wt%), 2.3 mg surfactant (23 wt%), and 4.7 mg polymer (47 wt%). To produce an emulsion the 1:4 ratio of chloroform to aqueous phase was sonicated for 30s with the following protocol: 20% duty cycle; 250 intensity; 500 cycles/burst; frequency sweeping mode (giving an average output of 70W). Samples were sonicated in a temperature-controlled water bath set to 4°C. Immediately after sonication, emulsion samples were frozen in liquid nitrogen, prior to freeze drying using a VirTis BenchTop K freeze dryer (SP Scientific, Ipswich, UK) with condenser temperature set to −100°C and vacuum of <40 µbar. Sample remained in the freezer dryer for 48 hours, after which they were sealed air-tight and stored in a desiccator at ambient temperature, prior to analysis.

7.3.4.3.4: nDodecyl ester:

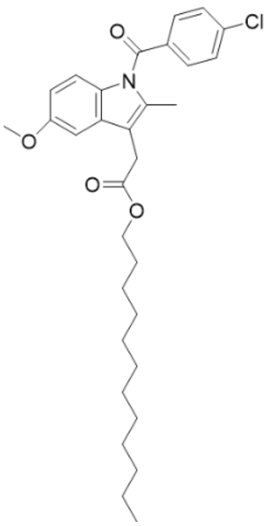

Dodecanol (3.13 g, 0.0167 mol, 2 eq) was used. The final product was presented as a viscous yellow oil (2.73 g, 65 % yield). TLC analysis in 10: 90 EtOAc: Hexane obtained an RF value of 0.4. ^{1}H-NMR (400 MHz, $CDCl_3$): δ ppm = 0.88 (T, 3H), 1.25 (M, 18 H), 1.59 (M, 2H), 2.39 (S, 3H), 3.65 (S, 2H), 3.83 (S, 3H), 4.09 (T, 2H), 6.65 (D of D, 1H), 6.86 (D, 1H), 6.97 (D, 1H), 7.46 (D, 2H), 7.65 (D, 2H). ^{13}C NMR (100 MHz, $CDCl_3$): All ppm shifts correspond to 1 carbon environment unless otherwise stated: δ ppm=13.49, 14.26, 22.83, 26.04, 28.76, 29.37, 29.49, 29.66, 29.71, 29.76, 29.79, 30.59, 32.05, 55.82, 65.35, 101.45, 111.81, 112.91, 115.07, 129.25 (2C), 130.83, 130.95, 131.32 (2C), 134.09, 136.00, 139.38, 156.18, 168.43, 171.10. IR (cm^{-1}) = 1668 (C=O, amide), 1726 (C=O, ester), 2838-3005 (C-H, C=C, C-C). ESI-MS $[M+Na]^+$ = 548.3 m/z. Elemental analysis = calculated: C (70.77), H (7.66), N (2.66), obtained: C (70.95), H (7.68), N (2.69).

7.3.4.3.5: nStearyl ester:

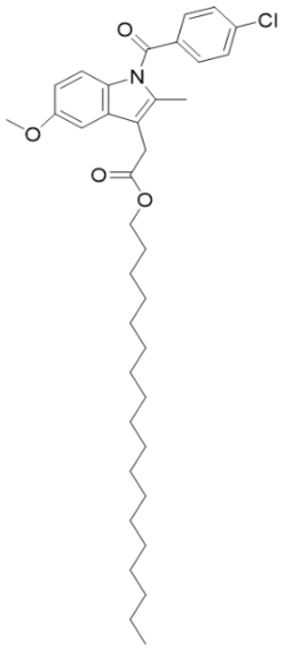

Stearyl alcohol (4.54 g, 0.0167 mol, 2 eq) was used. The final product was presented as a pale yellow solid (4.24 g, 83 % yield). TLC analysis in 30: 70 EtOAc: Hexane obtained an RF value of 0.7. ^{1}H-NMR (400 MHz, $CDCl_3$): δ ppm = 0.88 (T, 3H), 1.25 (M, 30H), 1.61 (Q, 2H), 2.39 (S, 3H), 3.65 (S, 2H), 3.83 (S, 3H), 4.09 (T, 2H), 6.65 (D of D, 1H), 6.86 (D, 1H), 6.69 (D, 1H), 7.46 (D, 2H), 7.65 (D, 2H). ^{13}C NMR (100 MHz, $CDCl_3$): All ppm shifts correspond to 1 carbon environment unless otherwise stated: δ ppm= 13.82, 14.59, 23.16, 26.36, 29.09, 29.70, 29.83, 30.00, 30.05, 30.13, 30.14 (5C), 30.17, 30.92, 32.39, 56.15, 65.67, 101.78, 112.13, 113.24, 115.40, 129.58 (2C), 131.16, 131.28, 131.64 (2C), 134.42, 136.33, 139.71, 156.51, 168.75, 171.42. IR (cm^{-1}) = 1673 (C=O, amide), 1736 (C=O, ester), 2848-2956 (C-H, C=C, C-C). ESI-MS $[M+Na]^+$ = 632.3 m/z. Elemental analysis = calculated: C (72.82), H (8.59), N (2.30), obtained: C (72.69), H (8.66), N (2.32).

7.3.4.3.6: tButyl ester:

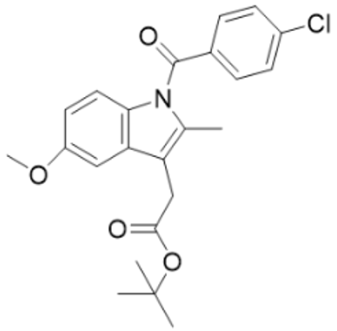

tButyl alcohol (1.24 g, 0.0167 mol, 2eq) was used. The final product was presented as an off white solid (2.20 g, 63 % yield). TLC analysis in 20: 80 EtOAc: Hexane obtained an RF value of 0.5. ^{1}H-NMR (400 MHz, $CDCl_3$): δ ppm = 1.45 (S, 9H), 2.37 (S, 3H), 3.56 (S, 2H), 3.84 (S, 3H), 6.65 (D of D, 1H), 6.87 (D, 1H), 6.96 (D, 1H), 7.46 D, 2H), 7.65 (D, 2H). ^{13}C NMR (100 MHz, $CDCl_3$): All ppm shifts correspond to 1 carbon environment unless otherwise stated: δ ppm= 13.54, 28.24 (3C), 31.88, 55.85, 81.29, 101.51, 111.77, 113.50, 115.07, 129.24 (2C), 130.96, 131.00, 131.30 (2C), 134.19, 135.85, 139.32, 156.15, 168.47, 170.31. IR (cm^{-1}) = 1685 (C=O, amide), 1732 (C=O, ester), 2840-3007 (C-H, C=C, C-C). ESI-MS $[M+Na]^+$ = 436.1 m/z. Elemental analysis = calculated: C (66.74), H (5.84), N (3.38), obtained: C (66.73), H (5.86), N (3.40).

7.3.4.3.7: Benzyl ester:

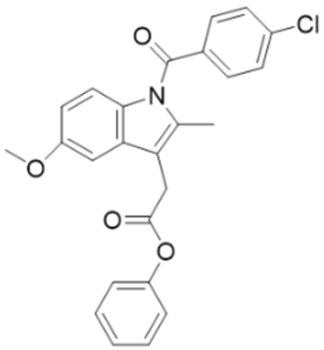

Benzyl alcohol (1.82 g, 0.0167 mol, 2 eq) was used. The final product was presented as an off white solid (2.68 g, 74 % yield). TLC analysis in 20: 80 EtOAc: Hexane obtained an RF value of 0.3. ^{1}H-NMR (400 MHz, $CDCl_3$): δ ppm = 2.36 (S, 3H), 3.71 (S, 2H), 3.76 (S, 3H), 5.14 (S, 2H), 6.65 (D of D,

1H), 6.87 (D, 1H), 6.93 (D, 1H), 7.32 (M, 5H), 7.45 (D, 2H), 7.63 (D, 2H). ^{13}C NMR (100 MHz, $CDCl_3$): All ppm shifts correspond to 1 carbon environment unless otherwise stated: δ ppm= 13.35, 30.58, 55.78, 66.94, 101.33, 112.02, 112.64, 115.11, 128.31 (2C), 128.45, 128.70 (2C), 129.27 (2C), 130.72, 130.95, 131.32 (2C), 134.05, 135.90, 136.08, 139.41, 156.20, 168.44, 170.80. IR (cm^{-1}) = 1660 (C=O, amide), 1720 (C=O, ester), 2846-3113 (C-H, C=C, C-C). ESI-MS $[M+Na]^+$ = 470.1 m/z. Elemental analysis = calculated: C (69.72), H (4.95), N (3.13), obtained: C (69.81), H (4.92), N (3.12).